DOCTOR OF PHILOSOPHY

Temporal and spatial variations of suspended sediments in the Irish Sea determined from AVHRR visible band and in-situ data.

Boudjelas, Souyad

Award date:
1994

Awarding institution:
Bangor University

Title: Temporal and spatial variations of suspended sediments in the Irish Sea determined from AVHRR visible band and in-situ data.

A thesis submitted in accordance with the requirements of the University of Wales for the degree of Doctor of Philosophy.

By Souyad Boudjelas

University of Wales, Bangor,
School of Ocean Sciences,
Menai Bridge,
Gwynedd,
LL59 5EY U.K.

October 1994

ABSTRACT

An observational study of suspended particulate matter (SPM) in the Irish Sea was carried out using AVHRR visible band and beam attenuation data. The satellite data consisted of a total of 165 AVHRR images covering the period between January 1982 to August 1988. The beam attenuation data were obtained from a summer and a winter mooring deployments at two sites in Liverpool Bay.

The satellite imagery has shown that the surface reflectance due to suspended sediments varies throughout the Irish sea. The imagery has also shown that the reflectance undergoes a seasonal variation. The magnitude of this variation was assessed throughout the Irish Sea using a statistical model. The maximum reflectances occur early in the year and the minimum in the summer.

The spatial distributions of the mean and amplitude of the annual variation have been shown to exhibit similar patterns. In some parts of the Irish Sea the surface reflectance was clearly seen to respond to the spring-neap tidal cycle.

The spatial distribution of the annual mean is controlled by the availability of tidal turbulent kinetic energy (TKE). It was also shown that the availability of tidal TKE exerts a control on the seasonal variation and its spatial distribution. It is suggested that a further control is needed to explain the dependency of the seasonal variation on tidal TKE: a possibility is the seasonal availability of sediments.

The beam attenuation data have provided further evidence of the seasonal variation of SPM concentrations at two sites in Liverpool Bay. An important finding from the in-situ data was the contribution of the wind to the seasonality of SPM concentrations in shallow waters.

ACKNOWLEDGEMENTS

I would like to thank Dave Bowers for being my supervisor. Thanks to John Simpson for helpful discussions on several aspects of the work.

Bill Slade worked hard, and succeeded, to provide a faultless service of the I^2S. He gave freely lots of help and time. Thanks Bill. The Institute of Terrestrial Ecology (Bangor) are thanked for allowing the use of the I^2S. Steve Groom of NERC Image Analysis Unit at Plymouth provided the image processing software and many helpful comments regarding the processing of the images. The AVHRR data were provided by Peter Baylis of NERC Dundee satellite receiving station.

Graham Allen gave much help with the computing and many other aspects of the work. His help and contribution is much appreciated. The in-situ data were collected as part of a larger study of Liverpool Bay conducted by Jonathan Sharples. He is thanked for kindly providing the current meter data and for incorporating the transmissometers onto the moorings. Thanks to Tom Rippeth for his help with the deployment and recovery of the moorings and his moral support throughout this work. The transmissometers were provided by Sarah Jones. Many thanks to her for the instruments, introducing me to the processing of transmissometer data and, for proof reading chapter seven and the many constructive comments. I would also like to thank A.J. Elliott for the tidal amplitudes and water depths for the Irish Sea and Toby Sherwin for the tidal analysis software. Thanks to Alex Souza for typing the references.

During this work I was supported by a postgraduate grant from the Algerian Government. They are thanked for the opportunity and financial support.

My family and friends gave continual support throughout the work and I am grateful to them for standing by me to the end.

TABLE OF CONTENTS

LIST OF FIGURES

Chapter 7

CHAPTER 1

Introduction

Suspended particulate matter (SPM) plays an essential role in the biological and chemical processes occurring in shelf seas. Suspended particles increase the attenuation of light and hence reduce the availability of light energy available for plankton growth (Tett *et al*, 1993). Through this mechanism SPM may contribute to the control of biological populations. Pollutants, both dissolved and particulate, may become attached to the surface of suspended particles (Eisma and Irion, 1988). When this process occurs the subsequent transport and, hence, distribution of the chemicals becomes dependent upon the suspended sediment dynamics. Therefore, as well as horizontal and vertical advection due to water movement, the pollutants may also become incorporated into the seabed during deposition and consolidation of the sediments. Conversely, sediment resuspension will bring the pollutants back into the water column from the seabed. Therefore, an understanding of sediment dynamics and resuspension, in particular, is necessary in the efforts to understand the ultimate fate of pollutants such as heavy metals in shelf seas. Sediment suspensions also give rise to engineering problems in many estuaries and harbours, such as maintenance dredging.

A number of techniques have been used to measure SPM concentrations in seawater. Some of these techniques involve the direct collection, and subsequent analysis, of samples of SPM, e.g. filtration and sediment traps. These methods are labour intensive and not well suited for sampling over large areas and over long timescales. Other techniques are indirect, and include those based on optical phenomena, such as light absorption and scattering. An example of a widely used optical technique is transmissometry, which involves measuring the attenuation of a collimated light beam through a fixed pathlength of water. The attenuation has been shown to be proportional to the concentration of particles in the water (Baker *et al*, 1983; Lavelle *et al*, 1984).

SPM concentrations can be calculated from attenuation data via an empirical calibration equation constructed by regressing beam attenuation against a number of SPM concentrations measured by traditional methods. This method has increased the duration of in-situ measurements and hence, has allowed the study of the variations of SPM concentrations on different timescales (Weeks, 1989). However, the spatial coverage remains confined to a few single points. This is a severe constraint on the study of SPM concentrations. Suspended sediments are subject to considerable variability on spatial scales down to the order of meters. Hence, to successfully resolve concentration patterns it is to this spatial resolution that observations must be made. The synoptic coverage provided by satellites goes some way towards satisfying this demand. The remote sensing of SPM is based on the principle that the interaction of incident solar radiation with sub-surface water material results in an increase in the radiance/reflectance measured by the sensor.

Satellite remote sensing is being increasingly used to study the distribution and transport of suspended sediments in many coastal and estuarine environments. For example, sediment algorithms and calibrations of satellite imagery for coastal regions have been derived for: the North Sea (Prangsma and Roozekrans, 1989, Sündermann, 1993); the Solent estuary (MacFarlane and Robinson, 1984) the Adriatic Sea (Tassan and Sturm, 1986); the Bay of Fundy (Topliss, 1986); Delaware Bay (Stumpf and Pennock, 1989) and in Moon Lake, Mississippi (Ritchie *et al*, 1987). In general the form of the relationship between the reflectance measured by the satellite and SPM concentration has been derived statistically using in-situ concentrations and co-located reflectances. The algorithms reported in the literature are diverse and mostly site specific. A review of optical remote sensing in the ocean is presented in chapter 3.

In the Irish Sea fine suspended sediments are known to make a significant contribution to optical conditions (Heathershaw and Simpson, 1974). Visible band imagery shows well defined and persistent patterns of reflectance in the northern Irish Sea which have been attributed to variations in SPM concentrations (Mitchelson, 1984). The imagery

has also indicated a seasonal cycle of reflectance with higher values occurring in winter.

Studies of suspended sediments from in-situ observations have revealed spatial and temporal variations of SPM concentrations in the northern Irish Sea. Mitchelson (1984) observed a strong seasonal cycle in SPM concentrations with high values occurring in spring and autumn and low values in the summer. Time-series of SPM concentrations obtained at 5 m below the surface at a station north-west of Anglesey showed a minimum of the order 1 mg/l in August compared to values of 9 mg/l in April and 6 mg/l in September 1986 Weeks (1989). The same author also observed a strong seasonal cycle in beam attenuation measured by a moored transmissometer deployed 20 m below the surface in mixed waters north-west of Anglesey. The lowest values occurred during the summer months and the highest in April. The beam attenuation started increasing again in September. The sections of the beam attenuation record from 6 April to 12 May and from 12 September to 20 October showed a strong spring-neap cycle with springs being associated with higher values. Superimposed on the spring-neap cycle were a quarter and semidiurnal signals which were attributed to local resuspension and advection of a west-east gradient in SPM concentrations.

Previous spatial surveys of SPM concentrations have been confined to Liverpool Bay, the area between Isle of Man and Anglesey and the area to the north-west of Anglesey (Agnew, 1983; Jacob, 1982; Mitchelson, 1984 and Weeks 1989). These studies have shown the distribution to be far from homogeneous. The mouths of the rivers feeding into Liverpool Bay are associated with relatively high values (>11 mg/l) of SPM concentrations. Further areas of high concentrations were found off the north-west and the eastern coast of Anglesey. Mitchelson (1984) reported concentrations in excess of 12 mg/l in the waters to the north-west of Anglesey. Marked horizontal gradients were evident throughout the areas studied. Most notably, a general decrease in concentration away from the coasts and a strong negative gradient from the local maximum values off the north-west of Anglesey into the lower values (2 mg/l) of the western Irish Sea.

Figure 1.1 Spatial distribution of surface SPM concentration (mg/l) during (a) 26-30 April 1982 (from Mitchelson, 1984) and (b) 30 March - 4 April 1987 (from Weeks, 1989)

These features are common to all of the spatial surveys and can be seen in the example distributions of Fig 1.1a (Mitchelson, 1984) and 1.1b (Weeks, 1989).

Objectives

The broad objective of this work was to carry out an observational study of suspended sediments in the Irish Sea using visible remote sensing and transmissometry. The extensive archive of AVHRR visible band imagery provided an ideal data base, largely untouched in this context, for studying spatial and temporal trends. Implicit in this central objective were several specific aims which are listed below:

• To assess the feasibility of using AVHRR visible data to study surface suspended sediments in a mid-latitude shelf sea.

• To use the remotely sensed data to study the spatial and temporal variations of SPM throughout the Irish Sea, and assess the importance of seasonal and spring-neap cycles. Using the satellite data has enabled the study of SPM to be extended to the whole of the Irish Sea and into periods of the year previously not sampled i.e. winter months.

• To use the in-situ observations of beam attenuation to assess vertical variations of SPM concentrations. The information recorded by the remote sensor originates from the top few metres of the water column. By making simultaneous surface and near-bed measurements of beam attenuation it is possible to assess whether the satellite information is representative of the whole water column.

• To obtain another view of the seasonal cycle by deploying transmissometers in winter and summer, and resolve shorter timescales variations due to tidal and wind effects.

CHAPTER 2

The Irish Sea

2.1 Introduction

This chapter introduces the Irish Sea and outlines the important aspects of the physical oceanography of the area. The Irish Sea is the semi-enclosed sea bounded by latitudes 52^0 and 55^0 N. It is connected to the Atlantic Ocean via St George's Channel in the south and the narrower North Channel to the north. A deep channel (> 80 m) runs northwards from St George's Channel, west of the Isle of Man to the North Channel (Fig. 2.1). To the east, the depths are shallower and seldom exceed 50 m.

2.2 Tides

The dynamics of the Irish Sea are governed by the tides with the semidiurnal constituents being dominant. The amplitude of the M_2 tidal currents exhibits large spatial variations (Fig. 2.2). High amplitudes of the order 1.0 ms^{-1} are found north of St George's Channel, off Anglesey and in the North Channel, compared to less than 0.4 ms^{-1} in Cardigan Bay and to the east and south-west of the Isle of Man. The maximum tidal range occurs on the Lancashire and Cumbrian coasts where the mean spring range is 8 m.

Results from a 3-d model of the Irish Sea by Davies and Jones (1992) in the form of the major and minor axes of the M_2 tidal currents are shown in Fig. 2.3. The bottom currents (Fig. 2.3b) are strong (> 60 cm s^{-1}) and rectilinear throughout the Irish Sea except in the areas to the east and west of the Isle of Man and Cardigan Bay. In the southern Irish Sea and the North Channel the currents are parallel to the coast. In

Figure 2.1 Bathymetry in meters of the Irish Sea (after Elliott, 1991).

Figure 2.2 Amplitude in cm s^{-1} of M_2 depth-mean tidal currents (from Pingree and Griffiths, 1978).

Liverpool Bay and to the north of the Isle of Man the orientation is east-west. The surface M_2 tidal currents (Fig. 2.3a) exhibit the same patterns as the bottom currents but with increased magnitudes.

2.3 Non-tidal circulation

The residual circulation of the Irish Sea is weak with currents typically an order of magnitude smaller than the tidal streams and is thought to be driven mainly by horizontal density gradients and meteorological effects. Observations have shown that the circulation of the Irish Sea consists of a net northward flow which runs from St George's Channel to the North Channel (Bowden, 1955). However, there is no general agreement whether the main northward flow passes east or west of the Isle of Man. There is also evidence of a persistent southward residual flow along the Irish coast. In Fig. 2.4 are shown the near-surface and near-bottom residual circulations in the northern Irish Sea based on current meters and drifters results made by Ramster and Hill (1969). The surface and bottom flow patterns are similar for the western Irish Sea and consist of a northward flow which branches to the east and west of the Isle of Man. In the eastern Irish Sea the near-surface circulation has an anticlockwise motion near the coasts, whereas the bottom flow moves eastward towards the coast. However, other observations by Bowden and Sharaf El Din (1966) have indicated that the surface circulation in the eastern Irish Sea is in fact clockwise.

The density-driven circulation of the Irish Sea was investigated by Heaps and Jones (1977) using a 3-d numerical model. Their results confirmed the existence of the northward flow through St George's Channel into the Irish Sea and out through the North Channel. The modelled flow passed to the west of the Isle of Man. For the two density distributions used to drive the model the mean density currents over the Dublin-Holyhead section were 0.28 and 0.36 cm s^{-1}, agreeing well with observations. Their results indicated the gyre in the eastern Irish Sea to rotate in a clockwise sense. The

Figure 2.3 Distribution of major and minor axes of M_2 current ellipses (a) at the surface and (b) at the seabed (from Davies and Jones, 1992).

Figure 2.4 (a) Near-surface and (b) near-bottom residual circulation in the northern Irish Sea (from Ramster and Hill, 1969).

estuarine circulation in Liverpool Bay, as mentioned below, was also predicted by the model.

Heaps and Jones (1977) also investigated the wind-driven currents in the Irish Sea. A north flowing current of the same magnitude as the density current was induced by a uniform southerly wind speed of the order of 5 m s^{-1}. They concluded that for wind speeds below 5 m s^{-1} the density currents were more significant than the wind-induced currents. However, for wind speeds in excess of 10 m s^{-1} the wind currents become predominant. Driving the model with the prevailing winds of the area, i.e. southwesterlies, resulted in the formation of an anticlockwise gyre in the eastern Irish Sea.

Davies and Jones (1992) developed a 3-d wind-induced circulation model of the Irish and Celtic Sea region to investigate the effect of storms on the circulation. The model used a spectral representation in the vertical giving a continuous current profile throughout the depth. Results for a storm event in 1977 indicate that the Irish Sea responds quickly to meteorological forcing which can create large currents, comparable in magnitude to the tidal currents.

2.4 Stratification

Because of the strong tidal currents most of the Irish Sea remains vertically well mixed throughout the year. The main exception is the area south-west of the Isle of Man which stratifies in the summer when the surface buoyancy flux due to solar heating overcomes tidal stirring. The seasonal thermocline is established to a depth of 20 to 30 m between April and October. The area to the east of the Isle of Man and Cardigan Bay are also stratified in the summer. These two areas are shallower compared to that south-west of the Isle of Man. These stratified regions are well predicted by the parameter $Log_{10}(h / U^3)$ which differentiate between waters which are always mixed

Figure 2.5 Spatial distribution of $LOG_{10}(h/U^3)$ in the Irish Sea.

and those where thermal stratification develops during the summer (Simpson and Hunter, 1974). A plot of the distribution of this parameter for the Irish Sea is shown in Fig. 2.5. The distribution was calculated using the depths in Fig 2.1 and the M_2 current amplitudes of Fig 2.2. Water is stratified for values greater than 2.7.

In Liverpool Bay density stratification occurs as a result of freshwater discharges from the rivers Mersey, Dee, Ribble, Wyre and Lune. The freshwater inputs induce an east-west density gradient which drives an estuarine circulation with a net offshore flow in the surface and an onshore flow below. The density stratification in Liverpool Bay has been shown to vary periodically on semidiurnal and spring-neap timescales (Simpson *et al*, 1990).

2.5 Seabed sediment distribution

Fig. 2.6 shows the distribution of fine-grained sediments on the seabed in the Irish Sea. Two main areas of muddy sediments are found south-west of the Isle of Man and south of St. Bees Head. Both areas are characterised by weak tidal currents. Two much smaller areas of muddy sediments occur in Liverpool Bay and north off Anglesey. Coarser sands and gravels are found north and south of the Isle of Man reflecting the strong tidal currents.

The sources and sinks of fine sediments in the Irish Sea are still not well identified. Nunny (1978) postulated that rivers, coastal erosion, sub-tidal erosion and primary production were possible sources of fine sediments in the Irish Sea. He also suggested that the intertidal mud flats and salt marshes of the coastal bays and estuaries and the sub-tidal mud areas west of the Isle of Man and off Cumbria were possible sinks for fine sediments. Belderson (1964) suggested that the muddy area south-west of the Isle of Man is depositional. He further suggested that the deposited material may have originated from the south or indeed from beyond the southern end of the Irish Sea

Figure 2.6 Distribution of fine-grained sediments in the Irish Sea (from Ministry of Agriculture, Fisheries and Foods, Aquatic Environmental Monotoring Report No. 17, 1987).

transported by the residual flow. It was concluded by Pantin (1978) that the clay seabed sediments exposed off the Solway-Firth and Wigtown were a major source of fine sediments to the Cumbrian coast.

Kirby *et al* (1983) argued that there was no direct evidence of deposition or erosion occurring in the muddy area south-west of the Isle of Man. They also argued against the rivers being sources of fine sediments, instead they suggested that the rivers are in fact sinks.

The principal bedload transport paths in the Irish Sea are shown in Fig. 2.7 (Stride, 1973). These paths were found to agree well with the distributions of the mean and maximum bottom stresses due to M_2 and M_4 tidal currents (Fig. 2.8) derived from the results of a non-linear numerical model by Pingree and Griffiths (1979). The finer particles are transported as suspended sediment in the water column rather than as bedload.

Figure 2.7 Sand transport paths around the British Isles (from Stride, 1973).

Figure 2.8 (a) Mean and (b) maximum bottom stress vectors due to M_2 and M_4 tidal currents (from Pingree and Griffiths, 1979).

CHAPTER 3

Remote sensing of the oceans in the visible band

3.1 Introduction

This chapter is a review of optical remote sensing of the ocean. It begins with a list of definitions of the fundamental parameters. Electromagnetic radiation is discussed in section 3.3, followed by the measurements made by a remote sensor in section 3.4. Surface reflection and atmospheric effects are outlined in sections 3.5 and 3.6, respectively. Section 3.7 establishes the relationship between the sea surface reflectance and the optical properties of the water and in the final section, existing work on suspended sediments using AVHRR visible band imagery is reviewed.

3.2 Definitions

The following definitions are given to introduce the reader to some of the terminology used in optical remote sensing and to the symbols used in this work. The definitions are taken from Jerlov (1976). Each quantity defined is a function of the wavelength of the radiation.

Q Radiant energy. The amount of energy transferred by radiation. Units of Joules (J).

Φ Radiant flux. The amount of radiant energy per unit time. Units of Watts or Joules per second (W or Js^{-1}).

I Radiant intensity. The radiant flux emitted by a source in a given direction per

unit solid angle dω.

$$I = \frac{d\Phi}{d\omega} \quad (Wsr^{-1})$$

E Irradiance. The radiant flux incident on a surface per unit area, ds, of a surface.

$$E = \frac{d\Phi}{ds} \quad (Wm^{-2})$$

The flux incident on the upper face of a horizontal surface per unit area is referred to as the downwelling irradiance, E_d. Whilst that incident on the lower face is referred to as upwelling irradiance, E_u.

S Insolation. The total solar radiant energy received daily per unit horizontal area during a day. It is calculated by integrating E(t) throughout the day.

L Radiance. The radiant flux emitted in a given direction per unit solid angle, dω, per unit projected area, dS, of a surface (Figure 3.1).

$$L = \frac{d^2\Phi}{dS \cos\theta \, d\omega} \quad (Wm^{-2}Sr^{-1})$$

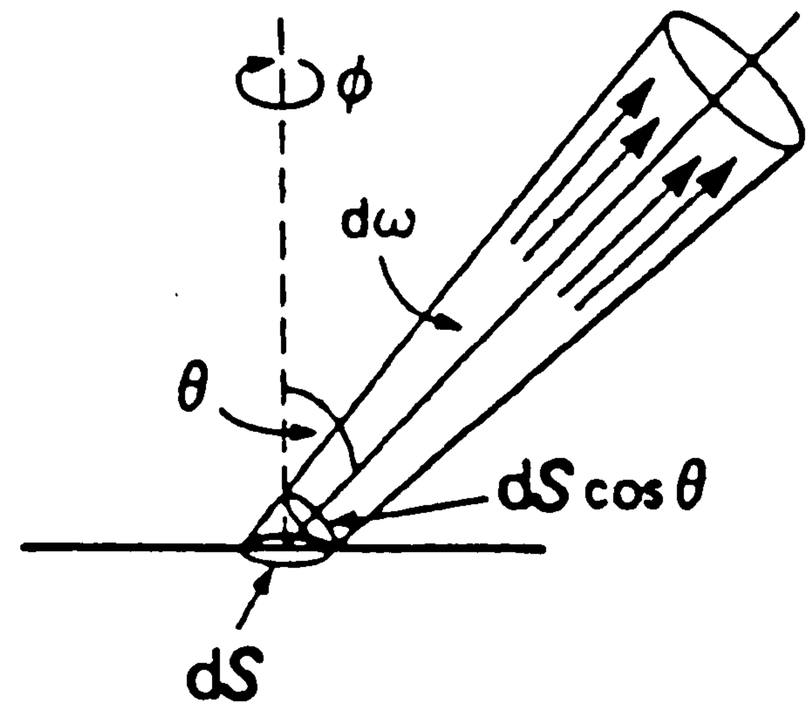

Figure 3.1 Definition sketch of the radiance, L.

R Reflectance. The ratio of the upwelling to the downwelling irradiance at a given depth.

$$R(z) = \frac{E_u(z)}{E_d(z)}$$

3.3 Electromagnetic radiation

Electromagnetic radiation is made up of a continuum of wavelengths ranging from gamma rays to radio waves (Figure 3.2, from Mather, 1987). The portion of the spectrum between 0.4 μm and 0.7 μm constitutes visible/photosynthetic light. The visible light constitutes 38% of the extraterrestrial solar irradiance. Variations in the Earth-Sun distance introduce an annual fluctuation of ± 3.4% around the mean extraterrestrial solar irradiance.

The total irradiance reaching the ocean surface varies throughout the day: it increases gradually from zero at dawn to a maximum at noon when the sun is at the zenith, and then it decreases in a symmetrical manner to zero at dusk. As a consequence, images recorded around noon benefit from a better illumination than images recorded in the morning or late afternoon. The magnitude of the diurnal variation is dependent on the local time, the latitude and the time of year. Figure 3.3 shows an example of the daily variation of total solar irradiance at different times of year and under different atmospheric conditions.

Figure 3.4 shows the seasonal variation of the total daily insolation at different latitudes. Generally, the higher the latitude, the lower is the daily insolation. An exception is observed in midsummer when the increase in day length results in slightly greater daily insolation for high latitude regions.

Third Party Material excluded from digitised copy.
Please refer to original text to see this material.

Figure 3.2 Spectral variation of atmospheric transmission. Also shown are the various spectral bands (from Mather, 1987).

Figure 3.3 The diurnal variation of the total solar irradiance at different times of the year and under different atmospheric conditions at a site in Australia. Line styles are:- solid: clear sky; dotted line intermittent cloud and dashed: generally overcast. (From Kirk, 1983).

Third Party material excluded from digitised copy.
Please refer to original text to see this material.

Figure 3.4 Change in calculated daily insolation throughout the year at different northern latitudes. (From Kirk, 1983).

The solar radiation is reduced during its passage through the atmosphere (Figure 3.5). This reduction is due to both scattering by air molecules and aerosol particles and absorption by gases including ozone, carbon dioxide and water vapour. As shown in Figure 3.2 the transmission through the atmosphere of the incoming radiation is wavelength dependent. There are regions of the electromagnetic spectrum where the effects of scattering and absorption are relatively small : the electromagnetic radiation is less modified in these regions than radiation at other wavelengths. These regions are called atmospheric windows. These include the visible/near-infrared region and certain bands within the infrared.

As a result of atmospheric scattering, a fraction of the solar flux is reflected back to space and the remaining is scattered in the direction of the Earth's surface. The total flux reaching the ocean surface is a combination of direct sunlight and diffuse skylight. The ratio of diffuse to direct radiation received at the surface is dependent on the solar elevation : low solar elevations result in an increase in scattering caused by longer pathlengths. Hence, the diffuse component of the radiation increases (Figure 3.6). When we combine the two components (direct and diffuse) together, up to 50% of the total radiation at the ocean surface is visible light.

Absorption by different gases occurs at particular wavelengths. In the visible, absorption due to ozone is the most important with lesser contributions from oxygen and water vapour.

The effect of clouds on the incoming radiation is variable: a small amount of cloud can increase total irradiance by 5 - 10%, whereas, a thick layer of cloud may transmit only 10% of the solar irradiance (Kirk, 1983).

Figure 3.5 Effect of the atmosphere on the solar irradiance (from Mather, 1987).

Figure 3.6 Time variation of the ratio of diffuse skylight to direct sunlight at the Equator on a clear day. $I_s(0)$ is diffuse skylight and $I_d(0)$ is direct sunlight at the sea surface (adapted from Sathyendranath and Platt, 1990).

3.4 Measurements made by a remote sensor

The total radiance, L_T, measured by a remote sensor in a given wavelength is due to the combined effects of: the water column, the water surface and the atmosphere. This radiance can be expressed as:

$$L_T(\lambda) = [L_w(\lambda) + L_g(\lambda)]\, T(\lambda) + L_p(\lambda) \qquad (3.1)$$

where L_w is the water leaving radiance, L_g is the radiance reflected by the water surface, L_p, is the radiance due to atmospheric effects also referred to as path radiance, T is the atmospheric beam transmittance and λ is the wavelength.

In equation 3.1 only L_w contains information about the water and its components (particulate and dissolved). Table 3.1 shows the relative contributions from TL_w, TL_g and L_p to the total signal, L_T, in the case of clear water and turbid water. More than 80% of the total radiance is due to atmospheric effects which can totally mask the signal originating from within the water column. The term TL_g in this example is due to skyglitter because the sun elevation is low.

For a flat surface, the water leaving radiance just above the water surface, L_w, is related to the radiance just below, L_u, by the equation (Austin, 1974)

$$L_w = \frac{(1-\rho)}{n_w^2} L_u \qquad (3.2)$$

where ρ is the Fresnel reflectivity expressing the amount of the incident radiation which has been reflected back at the water/air interface, n_w is the refractive index for seawater. The factor $(1/n_w^2)$ accounts for the amount by which the radiance emerging from the water is reduced by refraction.

	clear water			turbid water		
wavelength (nm)	TL_w	TL_g	L_p	TL_w	TL_g	L_p
440	14.4	1.2	84.4	18.1	1.1	80.8
520	17.5	1.3	81.2	32.3	1.1	66.6
550	14.5	1.3	84.2	34.9	1.0	64.1
670	2.2	1.5	96.3	16.4	1.2	82.4
750	1.1	1.9	97.0	1.1	1.5	97.4

Table 3.1 Percentage contributions to the total signal received by a remote sensor for a sun elevation of 36^0 (i.e. only sky glitter contributed to L_g (after Robinson (1985)).

The upwelled radiance, L_u, just below the surface is related to the upwelling irradiance just below the surface, $E_u(0^-)$ by the equation

$$L_u = \frac{E_u(0^-)}{Q} \tag{3.3}$$

For a Lambertian surface Q has a value of π and was suggested (Austin, 1980) to take a value around 5 for nadir sightings.

The downwelling irradiances just below and just above the surface $E_d(0^-)$ and $E_d(0^+)$ respectively are related by:

$$E_d(0^-) = (1 - \rho_s) E_d(0^+) \tag{3.4}$$

where ρ_s is the Fresnel reflectance of the sea surface for downwelling irradiance.

Hence, combining equations (3.2), (3.3) and (3.4) and using the definition of the subsurface reflectance just below the surface (i.e. $R_- = E_u(0^-)/E_d(0^-)$), the water leaving radiance can be written

$$L_w = \frac{[(1-\rho)(1-\rho_s)]}{Qn_w^2} E_d(0^+) R_- \qquad (3.5)$$

Where $E_d(0^+)$ is a function of the extraterrestrial solar irradiance, E_0, the solar zenith angle, θ_s, and the atmospheric transmittance, T:

$$E_d(0^+) = E_0(D) \cos\theta_s T \qquad (3.6)$$

The solar extraterestrial solar irradiance can be approximated by (Sturm, 1981)

$$E_0(D) = \bar{E}_0[1 + 0.0167 \cos\frac{2\pi}{365}(D-3)]^2 \qquad (3.7)$$

where E_0 is the mean solar constant and D is Julian day.

After Austin (1974), the subsurface reflectance just below the surface, R_-, is related to that just above the surface, R_+, by

$$R_+ = \frac{(1-\rho)(1-\rho_s)Q}{n_w^2 Q_-} R_- \qquad (3.8)$$

where Q_- is the coefficient of proportionality between the upwelling irradiance and the radiance just below the surface.

With $(1 - \rho)/n_w^2 = 0.544$, $(1 - \rho_s) = 0.955$, $Q_- = 5.1$ and $Q = \pi$ (Austin, 1974), the following relationship is obtained from equation (3.8):

$$R_+ = 0.32\, R_- \tag{3.9}$$

3.5 Surface reflection effects

Reflection at the sea surface of direct sunlight and diffuse skylight give rise to sun and sky glitter respectively. Their sum is equal to the reflected radiance at the sea surface, L_g, in equation (3.1). A smooth sea surface would appear relatively dark compared to those brighter regions where sunglint occurs. Sea surface roughness leads to an enlargement of the area of brightness by wave facets that produce reflection from different angles.

The intensity of sunglint depends on the wind speed and varies considerably throughout a scene, and cannot be adequately approximated. Therefore, the simplest solution to the sunglint problem is to avoid regions which are significantly contaminated with this effect.

3.6 Atmospheric effects

The atmosphere has a masking effect on the water leaving radiance: the magnitude of the signal originating from within the water is of the order of a few percent compared to the signal due to the atmospheric path radiance which can account for more than 80% of the total radiance received by a remote sensor (Quenzel and Kaestener, 1980; Sturm, 1981). When travelling through the atmosphere, the radiation is attenuated

because of the scattering and absorption by the different constituents of the atmosphere. The atmospheric effects must be removed from the total radiance to enable the extraction of the signal which carries information on the underwater properties. The removal of atmospheric effects is usually referred to as atmospheric correction. Different methods to solve this problem have been proposed by many workers (Viollier *et al*, 1980; Sturm, 1981; Arnone and La Violette, 1984; Gordon and Clark, 1981; Robinson, 1985; Singh and Cracknell, 1986).

In the visible part of the spectrum (0.4 μm - 0.8 μm), scattering is due to air molecules and aerosol particles. Molecular or Rayleigh scattering occurs when the diameters of the air molecules are small relative to the wavelength of the radiation. Aerosol or Mie scattering occurs when the particle diameter is of the same order of magnitude as the wavelength. A third type of scattering which also affects visible light is nonselective scattering which, unlike the first two, is not wavelength dependent. This type of scattering is due to particles with radii larger than 10 μm; these include water droplets.

The only important contribution to atmospheric absorption in the visible is due to ozone which has a broad absorption band ranging from 0.45 to 0.8 μm (water vapour has a weak absorption band between 0.7 and 0.74 μm).

Atmospheric attenuation

The atmospheric beam transmittance is defined as (Robinson, 1985)

$$T(\lambda) = \exp\left(-\frac{1}{\cos\theta_v} \int_0^z K(\lambda, z)\, dz \right) \qquad (3.10)$$

where θ_v is the viewing angle, K is the attenuation coefficient and z is the height.

The optical thickness is given by

$$\tau(\lambda, z) = \int_0^z K(\lambda, z)\, dz \tag{3.11}$$

The effects from the different atmospheric constituents are additive, hence

$$\tau(\lambda, z) = \tau_R(\lambda, z) + \tau_A(\lambda, z) + \tau_{oz}(\lambda, z) \tag{3.12}$$

where the subscripts R, A and oz denote Rayleigh, aerosol and ozone, respectively.

For Rayleigh scattering, the optical thickness is given by

$$\tau_R(\lambda, z) = 0.00879\ \lambda^{-4.09}\ \frac{p(0) - p(z)}{p_n(0)} \tag{3.13}$$

where p(z), p(0) are the atmospheric pressures at height z and sea level, respectively, and $p_n(0)$ is the atmospheric pressure at sea level for temperature T = 15°C.

Aerosol particles found in the atmosphere include dust, salt and smoke particles. The type of aerosol found over coastal areas can be very different from that over areas further offshore. Aerosol scattering is also wavelength dependent: it decreases with increasing wavelength. The aerosol optical thickness is given by

$$\tau_A(\lambda, z) = A(z)\ \lambda^{-\eta} \tag{3.14}$$

where η is the Angstrom coefficient and A(z) is proportional to the total number of aerosol particles found between height 0 and z. Measurements made over land showed

that η was in the range within 0.8 to 1.5.

The ozone optical thickness can be calculated from measurements of the ozone content in the atmosphere (Sturm, 1981). The amount of ozone in the atmosphere increases with the latitude: the average values encountered at the poles are higher than those at the equator. It has a seasonal variation which increases with latitude (Viollier *et al*, 1980).

Atmospheric correction

It is difficult to calculate the aerosol scattering because of the great variability in the nature and concentration of aerosol particles in the atmosphere. As a result, a semi-empirical method was suggested to remove atmospheric effects from remotely sensed data. This method was originally developed for CZCS and is based on the following assumptions:

(i) the path radiance, L_p, can be expressed as the sum of the path radiance due to Rayleigh scattering, L_R, and that due to aerosol scattering, L_A.

$$L_p(\lambda) = L_R(\lambda) + L_A(\lambda) \tag{3.15}$$

(ii) the water leaving radiance, L_w, is equal to zero at a wavelength λ_0 (i.e. $L_w(\lambda_0) = 0$).

(iii) no sunglint is present in the scene (the sky glitter is accounted for in the path radiance).

It follows that equation (3.1) can be rewritten as

$$L_T(\lambda) = L_R(\lambda) + L_A(\lambda) + T' L_w(\lambda) \tag{3.16}$$

where T' is the diffuse beam transmittance. The mathematical formulae to calculate T' are given in Viollier *et al* (1980) and Sturm (1981). The use of the diffuse beam transmittance allows for pixels emerging from the water outside the field of view and which have been scattered by the atmosphere into the sensor to be included in the water leaving radiance.

The Rayleigh path radiance, L_R, can be accurately calculated if the sun-target-sensor geometry is known. The formulae necessary to derive L_R can be found in Viollier *et al* (1980) and Sturm (1981).

The aerosol path radiance at one wavelength is proportional to that at another i.e.

$$L_A(\lambda) = \alpha(\lambda, \lambda_0) L_A(\lambda_0) \tag{3.17}$$

α is independent of horizontal position if the normalized size frequency distribution and refractive index of the aerosol are assumed to be independent of the position. If the aerosol phase function is not dependent on the wavelength, the single scattering approximation shows that α can be expressed as

$$\alpha(\lambda, \lambda_0) = \frac{\omega_A(\lambda)\tau_A(\lambda)E_0(\lambda)T_{oz}(\lambda)}{\omega_A(\lambda_0)\tau_A(\lambda_0)E_0(\lambda_0)T_{oz}(\lambda_0)} \tag{3.18}$$

where E_0 is the solar irradiance at the top of the atmosphere, T_{oz} is the ozone transmittance, ω_A is the probability that a photon will backscatter on interaction with the aerosol and τ_A is the aerosol optical thickness.

Combining equation (3.16) and (3.17) the following expression for L_w is obtained:

$$L_w(\lambda) = [\,(L_T(\lambda) - L_R(\lambda)) - \alpha(\lambda, \lambda_0)(L_T(\lambda_0) - L_R(\lambda_0))\,] / T'(\lambda)$$

Therefore, if α is known, the water leaving radiance, L_w, at wavelength λ can be determined. The methods used to calculate α are reviewed in Robinson (1985). A detailed account of how it has been determined in this work will be given in Chapter 5.

3.7 Relationship between R and the optical properties of the aquatic medium.

Theoretical modelling has been widely used to establish the relationship between the subsurface reflectance, R_- and certain optical properties of the medium namely: absorption and backscattering. Morel and Prieur (1977) found that for small values of (b_b / a) (< 0.3), R_- can be approximated by

$$R_- = 0.33 \frac{b_b}{a} \qquad (3.19)$$

where a and b_b are the absorption and backscattering coefficients respectively. Both a and b_b are wavelength dependent and have units of inverse distance (i.e. m^{-1}).

Gordon *et al* (1975) proposed that the reflectance should be a function of $(b_b / a + b_b)$. Whitlock *et al* (1981) investigated the relationship between the subsurface reflectance and the absorption and backscattering coefficients for turbid waters with attenuation

coefficients ranging from 8.9 to 18.9 m^{-1} at 550 nm. They found that $R_.$ was not proportional to (b_b /a) but did vary in a polynomial manner with (b_b / a + b_b).

The coefficients a and b_b are inherent properties of the medium i.e. their magnitude does not vary with the radiance distribution and is dependent only on the water components. It follows that the reflectance depends on the ability of the medium to absorb or backscatter the radiation. An increase of the backscattering coefficient will lead to an increase in the reflectance. Whilst, an increase in absorption will decrease the reflectance.

The contributions of the different water components to the absorption and backscattering coefficients are additive i.e.:

$$a(\lambda) = a_w(\lambda) + a_s(\lambda) + a_p(\lambda) + a_d(\lambda) \tag{3.20}$$

$$b_b(\lambda) = b_w(\lambda) + b_{bs}(\lambda) + b_{bp}(\lambda) \tag{3.21}$$

The subscripts w,s,p and d denote respectively water, inorganic particulate matter, phytoplankton and dissolved organic material.

The individual absorption and backscattering coefficients of the water constituents can be expressed as the product of their concentrations and a specific absorption/backscattering coefficients. Hence, equation (3.20) and (3.21) can be rewritten

$$a(\lambda) = a_w(\lambda) + c_s a_s^*(\lambda) + c_p a_p^*(\lambda) + c_d a_d^*(\lambda) \tag{3.22}$$

$$b_b(\lambda) = b_w(\lambda) + c_s b_{bs}^*(\lambda) + c_p b_{bp}^*(\lambda) \qquad (3.23)$$

where * denotes the specific absorption / backscattering coefficient (i.e. absorption / backscattering coefficient per unit concentration of the substance) and c refers to concentration. The subscripts w, s, p and d are as defined before.

The absorption and scattering properties of pure seawater are well known (Smith and Baker, 1981). Water absorbs strongly at longer wavelengths, and scatters strongly at shorter wavelengths (Figure 3.7). Molecular scattering is symmetrical in the forward and backward direction: (b_{bw} /b_w) = 0.5 (b_w is the scattering coefficient for pure seawater). The absorption by dissolved salts is known to be negligible in the visible part of the spectrum.

The optical characteristics of phytoplankton are dependent on the species and age of the population. Prieur and Sathyendranath (1981) showed that phytoplankton absorption can be represented by a normalized spectrum which is independent of the species (Figure 3.8). The absorption maxima are centred at 440 nm (due to chlorophyll a and carotenoids) and at 675 nm (due to chlorophyll *a* and its degradation product pheophytin *a*). Between the two peaks, the absorption reaches a flat minimum at around 560 nm.

Scattering by phytoplankton particles is generally weak. The backscattering fraction is small and fairly uniform (Figure 3.8). The backscattering coefficient decreases at wavelengths close to the absorption peaks.

Dissolved organic material or yellow substances originate from the decomposition of plant matter. It is found separately from a phytoplankton population. The concentration of yellow substances in marine waters is lower than in inland waters, and it diminishes with increasing distance from the land (Kirk, 1983). Its absorption is known to decrease

Figure 3.7 Absorption (a) and scattering (b) coefficients of pure sea water (from Robinson, 1990).

Figure 3.8 (a) Specific absorption coefficient (normalized at 440 nm) and (b) Specific backscattering coefficient (units are typically of the order of 10^{-3} m^{-1} $(mg\ m^{-3})^{-1}$) for chlorophyll-containing water (from Robinson, 1990).

Figure 3.9 Absorption coefficients of yellow substance (from Sathyendranath and Morel, 1983).

Figure 3.10 Absorption coefficients of "non-chlorophyllian" particles (from Sathyendranath and Morel, 1983).

exponentially with wavelength (Figure 3.9).

Inorganic suspended matter found in the water column includes particles which have been resuspended from the sea bed, transported to the sea by river runoff and land drainage, or eroded from coastal areas. The composition and size of these particles are varied: they range from silt particles with diameters less than 4 μm to sand particles with diameters 0.1 mm. Prieur and Sathyendranath (1981) observed a U-shaped absorption spectra for non-chlorophyllous particles (Figure 3.10). Bukata *et al* (1981) calculated the absorption, scattering and backscattering cross sections of inorganic material. Absorption and backscattering spectra for turbid waters are presented in Whitlock *et al*, (1981).

Natural ocean waters are classified according to the influence of the water constituents relative to one another (Table 3.2). The component which dominates in case 1 waters is phytoplankton and its associated products. Oceanic waters are classified as case 1 waters.

If a water body contains particles of non-chlorophyllous origin in addition to, or instead, of phytoplankton then it will belong to case 2 waters. Coastal waters belong to this category. Figure 3.11 (a) shows typical reflectance spectra for case 1 waters. In the blue violet region the reflectance decreases progressively with increasing pigment concentration. A minimum is reached at 440 nm which corresponds to maximum absorption by chlorophyll *a*. A less marked minimum appears at around 665 nm, followed by a peak in reflectance at 685 nm due to *in vivo* fluorescence of chlorophyll *a*.

An example of reflectance spectra for case 2 waters where suspended sediments are the dominant component are shown in Figure 3.11 (b). In general, the R values are higher than those of case 1 waters throughout the spectrum. As the turbidity increases so does the reflectance.

Third Party material excluded from digitised copy.
Please refer to original text to see this material.

Figure 3.11 Examples of observed reflectance spectra for: (a) Case 1 waters with different concentrations of phytoplankton; (b) Case 2 waters dominated by suspended sediments and (c) Case 2 waters dominated by yellow substance. The dotted line indicates the reflectance of clear ocean water. The arrow indicates increasing concentrations (from Sathyendranath and Morel, 1983).

Table 3.2 Classification of natural waters from Sathyendranath and Morel (1983).

For case 2 waters where yellow substances are the dominant constituent, the reflectance decreases with increasing absorption at the blue end of the spectrum (Figure 3.11 c). The reflectance of clear oceanic waters is represented by the dotted line on the three previous figures. The strong absorption and weak scattering at longer wavelengths leads to negligible values of R in the red and near-IR.

3.8 Use of visible band satellite imagery for monitoring suspended sediments in the oceans

Several studies have shown that total suspended seston can be correlated with reflectance (radiance) obtained from a satellite. For example, the Coastal Zone Colour Scanner (CZCS) (Clarke *et al*, 1980; Tassan, 1981; Tassan and Sturm, 1986) and Landsat Multispectral Scanner (MSS) (Topliss, 1986; Ritchie *et al*, 1987; Stumpf, 1988). In general, the algorithms relating total suspended matter to reflectance (radiance) were obtained through statistical analysis of in-situ measurements of suspended sediment concentrations and co-located reflectances (radiances). These algorithms are based on combinations of reflectances (radiances) sensed in different channels.

Until a replacement for the CZCS is made available, the remote sensing community is left without an ocean colour monitoring system operating at present. The next generation of ocean colour sensors will include the Sea-viewing Wide Field of view Sensor (SeaWiFS) and the MERIS instrument planned by ESA for launch in the mid-1990s on board Columbus or Freedom Polar Platforms (Robinson, 1990). Although, the AVHRR channel 1 and 2 are not ideal for ocean colour monitoring, there have been studies which had shown that they were sensitive to changes in the water constituents namely: chlorophyll and total suspended seston.

A study of La Plata River and its interaction with the ocean was carried out using remotely sensed data from Landsat MSS, AVHRR and CZCS (Gagliardini *et al*, 1984). Data from each system were analysed and compared with each other. They concluded that each of these sensors has its own characteristics and that although they provided different kinds of data, they complemented each other. Their concluding remarks concerning the use of the AVHRR for this type of work was that it was a useful tool for a general study of the whole estuary, particularly useful for turbid waters and fronts;

also its high coverage frequency makes it the most adequate sensor for dynamic processes related to tides.

Groom and Holligan (1987) used CZCS and AVHRR data to study coccolithophore blooms in the NE Atlantic. Stumpf (1987) developed new algorithms to estimate chlorophyll and sediment content in estuarine and coastal waters using AVHRR visible and near-IR data. Lyon *et al*, (1988) showed the usefulness of remotely sensed data such as those provided by the AVHRR and Landsat for the study of sediment loadings in lakes. They suggested that such data could be used to improve model simulations and increase the variety of data types used in the evaluations. The movement and distribution of suspended material in the surface waters of Chesapeake and Potomac estuaries during two separate flood events were studied using in-situ and remotely sensed data from Landsat MSS and the AVHRR (Stumpf, 1988). Stumpf and Tyler (1988) showed that the technique described in Stumpf (1987) can identify blooms in turbid estuaries where the reflectance is between 0.01 and 0.07 and has the potential to make estimates of chlorophyll for concentrations greater than 5 μg/l.

Roozekrans and Prangsma (1988) found correlation coefficients ranging between 0.63 - 0.89 for their log-log relationship between the atmospherically corrected reflectances of the AVHRR channel 1 and co-located in-situ sediments concentrations taken along the Dutch coast. Using the same log-log relationship as above, Prangsma and Roozekrans (1989) produced maps of total suspended matter in the southern North Sea. They also investigated the possibility of monitoring floating blue green algae which are usually seen in fresh water lakes in the Netherlands during the summer months. The maps of the Normalized Difference Vegetation Index (NDVI) showed that positive NDVI values seemed indicative of blue green algae patches at the surface.

In-situ and AVHRR derived sediment concentrations from Delaware Bay acquired within 3.5 hours of each other agreed to within 60% at the 95% confidence level (Stumpf and Pennock, 1989). Satellite imagery can be of great help in the design of

sampling programs particularly in highly dynamic areas including estuaries and the coastal zone (Tyler and Stumpf, 1989). It can also be used to improve the interpretation of the in-situ measurements. The signal recorded in the AVHRR band 1 was shown to be sensitive to the variations in the concentration of the total suspended matter in sea water (Spitzer, Laane and Roozekrans, 1990). Darecki and Krężel (1992) used data from the reflected channels of the AVHRR to estimate chlorophyll *a* concentrations. In-situ maps of mean field surface transparency, diffuse light attenuation, and Secchi disk depth taken in the Skagerrak and Kattegat area were compared to processed AVHRR images (Sagan and Kowalczuk, 1992).

All these workers arrived at similar conclusions concerning the use of AVHRR data in estuarine and coastal studies. The two reflected channels have the dynamical range to study highly turbid waters. Its high temporal resolution makes it ideal for investigating phenomena occurring on various time scales.

CHAPTER 4

The Advanced Very High Resolution Radiometer

4.1 Satellites and orbital configuration

The Advanced Very High Resolution Radiometer (AVHRR) is flown on board the NOAA-series of near-polar orbiting sun-synchronous meteorological satellites. A satellite flying in a sun-synchronous orbit always crosses the equator at the same local solar time. It crosses the equatorial plane twice per revolution: first from south to north (ascending) and then from north to south (descending). There are two NOAA spacecrafts in orbit simultaneously; each of them providing one daily and one nightly coverage of any point situated on the equator. There is a difference of about 6 hours between each satellite pass. Their respective daytime overpasses occur at about 07:30 (even numbered satellites, e.g. NOAA-8) and 14:30 (odd numbered satellites, e.g. NOAA-9) local time. The nighttime passes occur at 19:30 and 02:30, respectively. The orbital altitude and period are within the ranges 833 - 870 km and 101 - 102 minutes respectively. Table 4.1 lists the satellites in the NOAA series and their respective launch dates. The two satellites operating at present are NOAA-11 and NOAA-12.

Satellite	Launch dates
TIROS-N	October 1978
NOAA-6	June 1979
NOAA-7	June 1981
NOAA-8	March 1983
NOAA-9	December 1984
NOAA-10	September 1986
NOAA-11	October 1988
NOAA-12	May 1991

Table 4.1 Satellites and launch dates

4.2 Sensor scanning parameters

The sensor scans from right to left in a line orthogonal to the direction of travel. The instantaneous field of view (IFOV) is 1.4 mrad which corresponds to a distance on the ground of 1.1 km and the pixel size is 1.1 km x 1.1 km at nadir. The size of the pixels increases away from the satellite nadir. A scanline includes 2048 pixels covering an angle of $\pm 55.4^0$ from nadir yielding a swath width of approximately 2580 km. The satellite collects 360 scanlines per minute. The data are recorded to 10 bits precision (the signal from each pixel is assigned a value from 1 to 1024 according to its intensity).

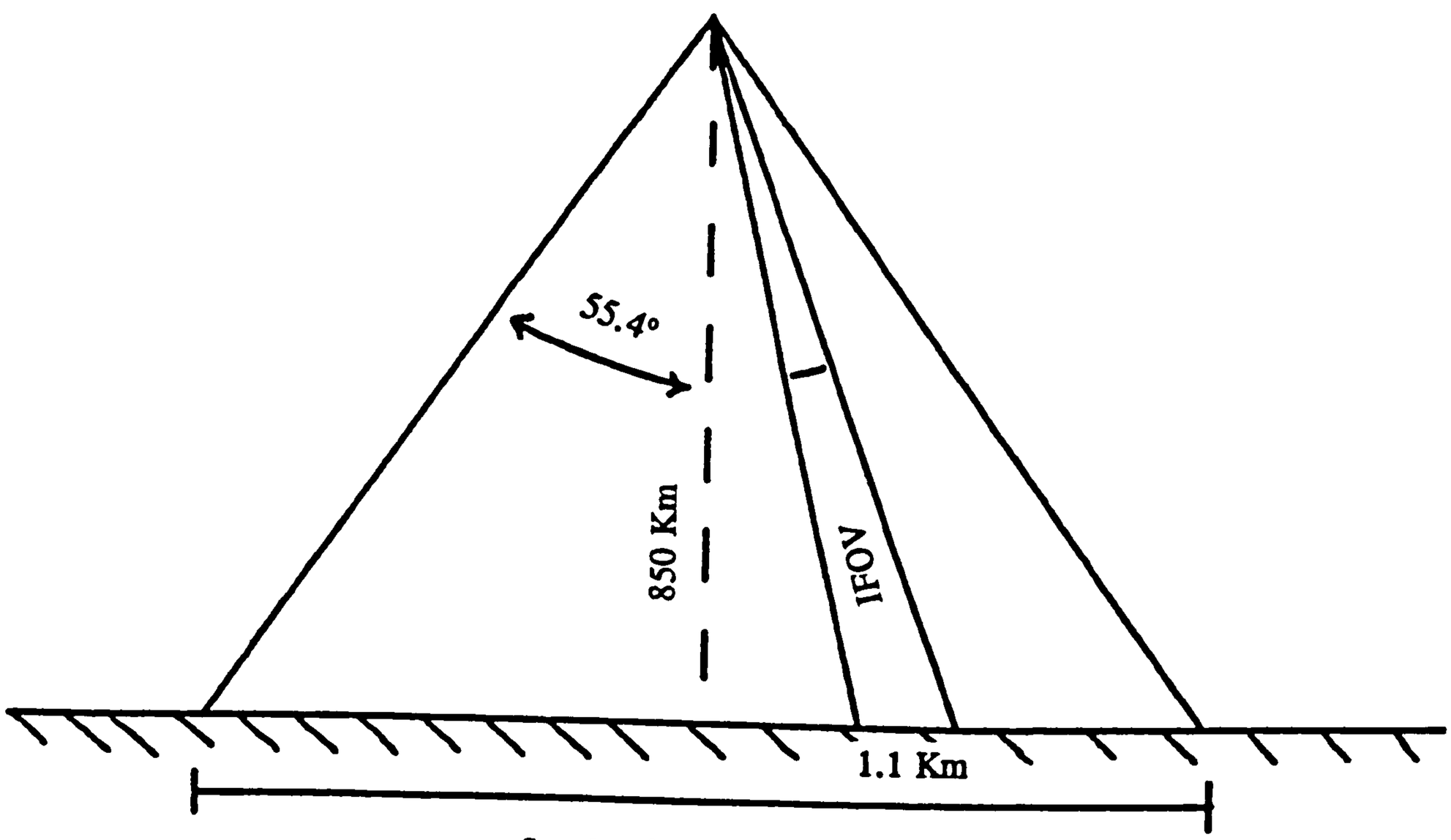

Figure 4.1 AVHRR scanning configuration.

4.3 AVHRR spectral characteristics

The AVHRR has five channels (Table 4.2). The spectral response functions for the visible and near-IR channels are shown in Figure 4.2. Channel 1 (visible) and 2 (near-IR) have been mainly used for the identification of clouds and land/water boundaries, the study of vegetation and crops and viewing ice and snow cover. Data from the thermal infrared channels have been used to calculate sea surface temperatures.

The two reflected channels are only preflight calibrated. There is an internal calibration device on board for thermal infrared channels.

Channel	Description	Bandwidth (μm)		S/N ratio
		AVHRR*	AVHRR/2#	
1	Visible	0.58 - 0.68		3:1 at 0.5% albedo
2	Near-IR	0.72 - 1.10		3:1 at 0.5% albedo
3	Thermal IR	3.55 - 3.93		NEΔT 0.12 K at 300 K
4		10.5 - 11.5	10.3 - 11.3	
5		10.5 - 11.5	11.5 - 12.5	

* AVHRR was flown onboard NOAA-6, 8 and 10.

\# AVHRR/2 was flown onboard NOAA-7, 9 and 11.

Table 4.2 AVHRR sensor characteristics.

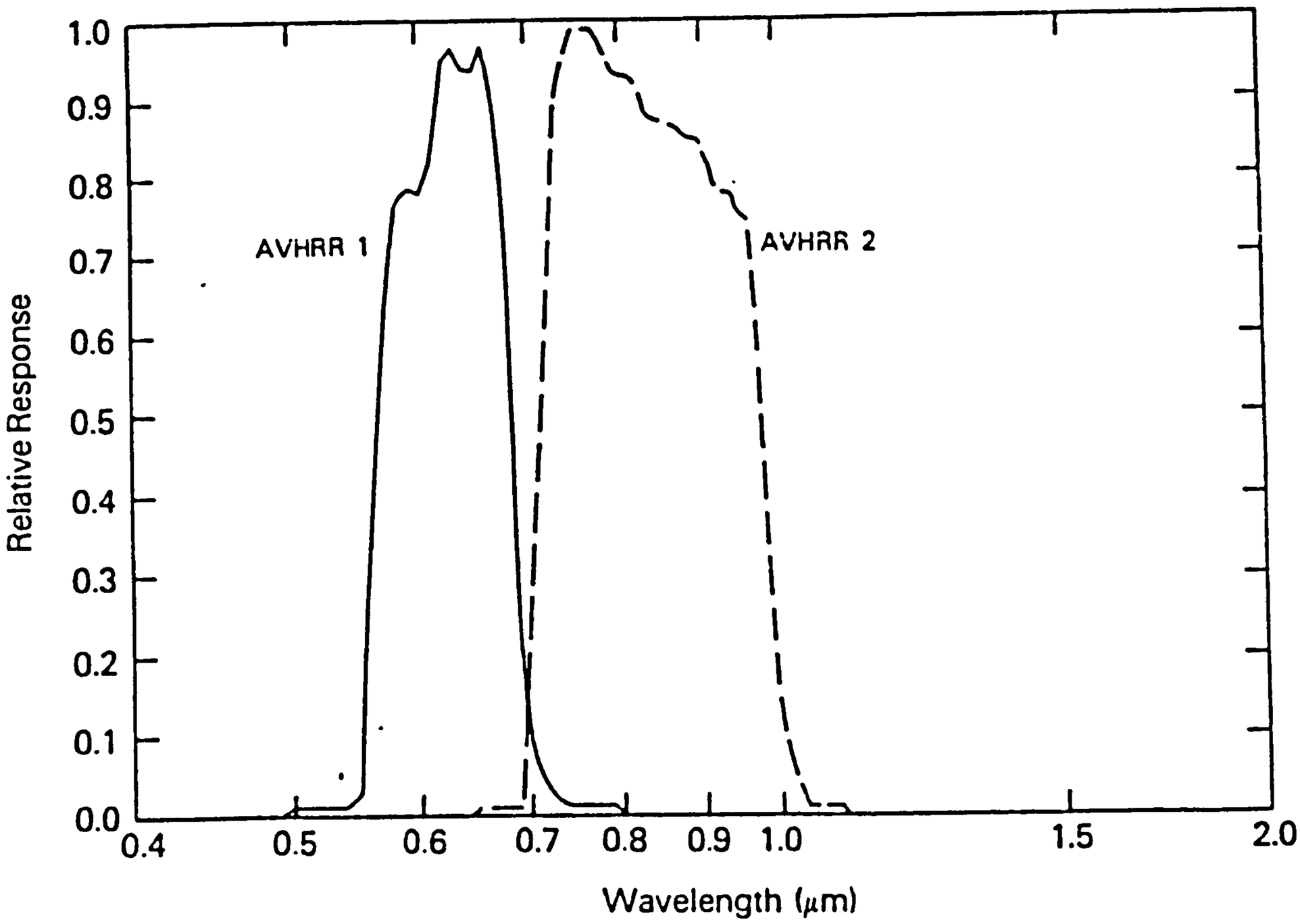

Figure 4.2 Sensor spectral response

4.4 Comparison with other sensors used for monitoring turbidity

For comparison the spectral characteristics of Landsat MSS and CZCS are shown in Table 4.3. MSS bands 5 and 6 and CZCS bands 4 and 5 are compatible with AVHRR bands 1 and 2.

	bandwidth (μm)	
Band	CZCS	MSS
1	0.433 - 0.453	
2	0.510 - 0.530	
3	0.540 - 0.560	
4	0.660 - 0.680	0.50 - 0.60
5	0.700 - 0.800	0.60 - 0.70
6		0.70 - 0.80
7		0.80 - 1.10

Table 4.3 Spectral characteristics of Landsat MSS and CZCS.

As shown in Table 4.4, the AVHRR is able to resolve changes in moderately turbid waters (i.e. radiometric sensitivity). Its high saturation radiances for both reflected channels allows the study of very turbid waters (Stumpf, 1987). Two daytime images are obtainable daily from the two NOAA satellites in orbit simultaneously, which can be useful when studying highly variable areas (e.g. estuaries, rivers and coastal areas). As a consequence of its large swath, one scene can include the whole area under study and therefore, allows for its study during the same dynamic and meteorological conditions.

	AVHRR	CZCS	MSS
Ground resolution (km)	1.1	0.825	0.08
Swath width (km)	2580	1636	185
Repeat interval (days)	1-2	3-5	16
Saturation radiance ($mWcm^{-2}sr^{-1}\mu m^{-1}$)			
visible channel	50.0	2.88*	17.9
near-IR channel	33.0	23.9	14.8
Radiometric sensitivity ($mWcm^{-2}sr^{-1}\mu m^{-1}$ per count)			
visible channel	0.052	0.005	0.131
near-IR channel	0.034	0.093	0.115

* value for minimum gain.

Table 4.4 Comparison of sensor characteristics (Stumpf, 1987).

CHAPTER 5

Processing of the Remote Sensing Data

5.1 Introduction

In this chapter the steps in the initial processing of the satellite data are outlined. The data are initially in terms of raw digital numbers (DN) and need to be converted into physical units. The methods involved in this conversion are described in this chapter.

The remote sensing data used in this work were supplied by the satellite receiving station at Dundee University. The AVHRR archive at Dundee covers the area shown in Figure 5.1 and spans the period from 1978 to the present. The data are transmitted in digital form from the satellite to Earth where they are stored on magnetic tapes. The data are made available to potential users as hardcopy photofacsimile black and white imagery, computer compatible magnetic tapes (CCTs) or floppy disks.

For daytime satellite passes closest to overhead U.K. contact prints are produced for channels 2 and 4; for other passes only one of the above channels is contact printed. Prints of channel 4 are produced for night time passes. These prints are collated to form the browse file.

Each print is photographed onto 35 mm film and contact prints each containing 35 images are developed. These form the contact print browse file.

5.2 Selection of images

The scenes used in this study were selected by screening both the AVHRR browse file

Figure 5.1 The approximate area covered by the AVHRR archive at Dundee is depicted within the circle shown (from NERC Satellite Station, Dundee, 1991).

at Dundee and the contact print browse file at the School of Ocean Sciences (U.C.N.W.). Given the size of the contact prints it is often difficult to estimate the extent of cloud cover over the area of interest. In many instances, images which appeared to be cloud free on the contact prints later turned out to be too contaminated by clouds to be of use in the study. The data were despatched from Dundee on CCTs as requested. Photographs called quicklooks are provided for each file on a CCT. Quicklooks are useful for identifying the area of interest from the whole data set when reading the files. Orbital information on each individual scene are also supplied with the tapes.

5.3 Format of AVHRR data

AVHRR data are made up of minor frames, each containing 11090 10-bit words. One minor frame corresponds to one AVHRR scanline (Satellite receiving station Dundee University, 1986). There are 10240 10-bit words of video data in one minor frame. A scan line of video data consists of 2048 samples, each sample containing five values corresponding to the five AVHRR channels. The remaining 850 10-bit words making up a minor frame are spacecraft telemetry, calibration data and other instrument information.

5.4 Dundee CCTs format

The Dundee CCTs of AVHRR data contain the full scan width and all five channels. The header is also included. The number of scanlines that can be stored on a tape depends on the media and density types. For example, a 1600 bpi 2400' tape may contain up to 2370 scanlines while a 6250 bpi tape will contain 6700 scanlines.

The 10-bit words are stored as 8-bit words. This is achieved by turning three successive 10-bit words starting with the first 10-bit word into 4 8-bit words. The last two bits of the fourth 8-bit word are set to zero. The next three 10-bit words are treated similarly throughout the minor frame.

5.5 Image processing hardware

The data processing was done on an International Imaging Systems (I^2S) Model 75 image processor and a MicroVAX II minicomputer. The latter is operated under VMS and has 16 Mb memory. The CCTs are read from a Cipher M990 tape drive which reads 1600/6250 bpi tapes. The data read are stored on two Fujitsu M2263 disk drives, each providing 1.2 Gb disk space.

The user and the I^2S interact with each other by means of an applications program providing Image Analysis utilities called System 600 which runs on the VAX. The many aspects of System 600 include: (i) providing a common user interface for processing and manipulating images, (ii) controlling the Model 75 (M75) Image Processor, (iii) moving data between the VAX and the M75, and (iv) providing tools for the analysis of images using both the VAX cpu and the M75.

The Model 75 acts as a back end processor for the MicroVAX. It is made up of several boards, each having a specific function:

(i) The I/O boards provide means for image transfer between the VAX and the refresh memories and from the pipeline to the refresh memories.

(ii) Mathematical operations can be performed on images in the refresh memories using the arithmetic unit.

(iii) The refresh memory boards comprise 14 8-bit memory planes, 1 8-bit swapping memory, and 8 1-bit graphics memory planes. They are used to store images which are ready for viewing or manipulation.

(iv) The colour boards control the output to the red, green, and blue guns of the display monitor and contain the main look up tables.

(v) The graphics memory planes are used to control and display the contents of the 8 1-bit graphics or overlay planes. The latter allow graphical information (e.g. text, lines of latitude and longitude, histograms) to be superimposed on the images. They can also be used as a mask, by denoting certain points of the image as *on* or *off* (e.g. land and cloud masking).

(vi) The warper board provides a very fast means by which images can be mapped onto one another, or onto different cartographic projections.

(vii) The videometer gathers the statistics of the images from the pipelines output.

(viii) The trackerball unit reads and controls input from the M75 keypad, and the trackerball.

Figure 5.2 shows the different components of the image analysis equipment at the Institute of Terrestrial Ecology (ITE) at Bangor. The monitor can display images which are up to 512 lines wide by 512 scan lines (samples). Photographic negatives can be produced using the Dunn 633 Microcolour Camera. Colour A4 prints can also be obtained using the D-scan CH5301 which employs a thermal ink transfer method to produce clear printouts.

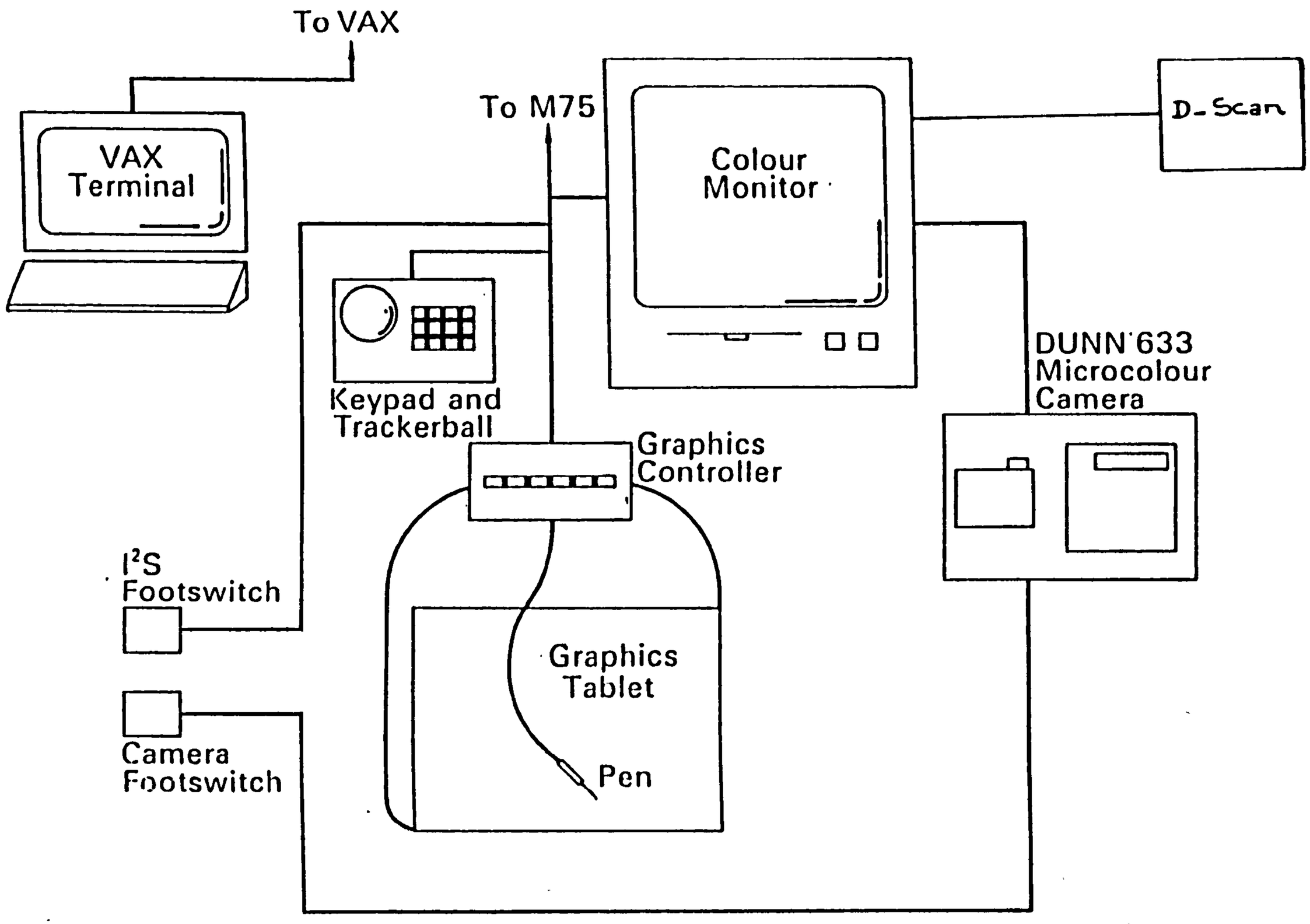

Figure 5.2 Hardware components of the image analysis equipment at ITE, Bangor (I^2S manual).

5.6 Description of the stages of AVHRR image processing.

The software used to analyse the imagery was written by S.B. Groom (Groom and Holligan, 1987). The software involved in the atmospheric correction of the AVHRR data is based on algorithms developed for the Coastal Zone Colour Scanner (CZCS). These algorithms have been modified to accommodate the characteristics of the AVHRR. The Rayleigh and aerosol contributions are considered additive and removed separately. The ocean is assumed to be a blackbody (i.e. zero reflectance) in channel 2 (near-IR) (solar radiation is strongly absorbed by water molecules at longer wavelengths). The method is similar to that described in Chapter 3. A description of each step follows.

5.6.1 Reading the data from the CCTs

The Irish Sea constitutes only a subsection of the whole data file. Using the quicklook photograph corresponding to an image the position of the area is identified, and extracted using the function: TAPE'AVHRR'DUNDEE which is a program that reads CCTs issued by Dundee.

These reduced file images are used in order to minimize redundant storage of data and hence reduce processing time and disk space. It takes between 20 to 30 minutes to read one file.

The image file created by TAPE'AVHRR'DUNDEE contains data for all five AVHRR channels and a header where information including the image identity, the image size, the spacecraft name, the viewing date and time are recorded. The header is also written to a separate file. Each file is named after its identification number. Images from different years are stored in separate subdirectories.

To assess the quality of the image, it is displayed on the colour monitor using the roam function on the M75. Images which are judged too contaminated by clouds are rejected at this stage of the processing.

5.6.2 Image enhancement

Each AVHRR pixel in an image has a value between 0 and 1023. The values of the sea pixels form only a small portion of the full range; in channels 1 and 2 the intensities of the sea pixels are in the range 0 to 255. As the display device resolves 256 grey levels, viewing the full pixel range leads to a low resolution image. To increase the resolution pixels with values greater than 255 (i.e. 256 to 1023) are set to 255. The output is a two band byte image with pixel values ranging between 0 and 255.

5.6.3 Radiometric conversion

For each channel, the recorded digital numbers (DN) are converted into equivalent radiances, L, using the equation:

$$L(chan) = G(chan)\, x\, DN(chan) + I(chan) \tag{5.1}$$

where G and I are the preflight gain and intercept in channel chan, respectively.

5.6.4 Apparent reflectance conversion

The radiances, L, are converted into reflectances, R, using the following equation:

$$R(chan) = \frac{\pi L(chan)}{E_0(chan)\cos\theta} \tag{5.2}$$

Where E_0 is the solar constant, and θ is the solar zenith angle.

Expressed in terms of reflectances equation (3.16) becomes:

$$R_t(chan) = R_r(chan) + R_a(chan) + T^{'}(chan)R_w(chan) \tag{5.3}$$

where subscripts t, r, a and w denote total, Rayleigh, aerosol and water leaving, respectively.

5.6.5 Rayleigh correction

The Rayleigh correction is based on Gordon *et al* (1983), but uses units of reflectance instead of radiance following Viollier *et al* (1980). The Rayleigh reflectances in both channels (visible and near-IR) are calculated using the sun-target-sensor geometry, and then are subtracted from their respective total reflectances in each channel i.e:

$$R_{r\text{-}corr}(chan) = R_t(chan) - R_r(chan) \tag{5.4}$$

where $R_{r\text{-}corr}$ is the Rayleigh corrected reflectance.

After removing the Rayleigh contribution from the total signal in each channel, equation (5.3) is reduced to:

(i) channel 1

$$R_{r\text{-}corr}(chan1) = R_a(chan1) + T'(chan1)\,R_w(chan1) \tag{5.5}$$

(ii) channel 2 (R_w(chan2) = 0)

$$R_{r\text{-}corr}(chan2) = R_a(chan2) \tag{5.6}$$

where subscripts t, r, a and w are as defined previously. The Rayleigh-corrected reflectance in channel 2 contains only the aerosol contribution.

5.6.6 Aerosol correction

The aerosol reflectance in channel 1 is deduced from that in channel 2 using the equation (Viollier *et al*, 1980):

$$R_a(chan1) = \varepsilon\, R_a(chan2) \tag{5.7}$$

where ε is the optical thickness ratio, give by

$$\varepsilon = \frac{\tau_a(chan1)}{\tau_a(chan2)} \tag{5.8}$$

Using equation 3.14, ε can be rewritten as

$$\varepsilon = \left(\frac{\lambda_1}{\lambda_2}\right)^{-\eta} \tag{5.9}$$

where η is the Angström coefficient and the wavelength λ_1 and λ_2 are equal to 628 nm (visible) and 826 nm (near-IR) respectively.

Combining equations (5.5), (5.6) and (5.7), the water leaving reflectance, R_w, in channel 1 is given by

$$R_w(chan1) = \frac{R_{r\text{-}corr}(chan1) - \varepsilon R_{r\text{-}corr}(chan2)}{T'(chan1)} \qquad (5.10)$$

The software uses an interactive method based on Arnone and La Violette (1984) to select the Angström coefficient and hence calculate ε. In this work, ε was estimated using the clear water technique which was first applied to CZCS data (Gordon, 1980; Gordon *et al*, 1983; Sturm, 1981) and has since been applied to AVHRR data (Stumpf, 1987; Stumpf and Pennock, 1989). This technique involves calculating ε for a clear water area in the scene, then using this value of ε to perform a pixel-by-pixel aerosol correction over the whole scene. The method assumes that the optical properties of aerosol are independent of position though time dependent.

Groom and Holligan (1987) computed a statistical equation which relates the AVHRR channel 1 to the CZCS band 3:

$$R_w(AVHRR1) = \frac{1}{3.6} R_w(CZCS3) \qquad (5.11)$$

Gordon and Clark (1981) calculated a value of 0.28 mW/cm^2 μm sr for the clear water radiance (i.e. phytoplankton pigment concentration < 0.25 mg m^{-3}) for the CZCS band 3. The above radiance corresponds to a reflectance value of 0.0048. Therefore, the clear water reflectance for the AVHRR channel 1 is equal to:

$$R_{clearwater}\ (AVHRR1) = \frac{0.0048}{3.6} = 0.0013$$

It follows that ε is given by

$$\varepsilon = \frac{R_{r\text{-}corr}(chan1) - T'(chan1)\,R_{clearwater}(chan1)}{R_{r\text{-}corr}(chan2)} \qquad (5.12)$$

The previous equation is then used to calculate ε for every sea pixel in the image. The lowest value of ε which corresponds to clear water is used in equation (5.10) to calculate R_w for each pixel in the scene. The values of ε obtained for each image used in this study are tabulated in Appendix 1. Prangsma and Roozekrans (1989) used similar approach for removing the aerosol contribution but assumed that the reflectance of clear water was zero in channel 1 of the AVHRR. Spitzer *et al* (1990) using the same method as Prangsma and Roozekrans (1989) obtained an ε equal to 1.3.

It is this final value, R_w, the water leaving reflectance which is the quantity containing information about the water properties and which this study is concerned with. The range of R_w is from 0.13 %, for clear water, to 5 %, for turbid waters. All further references to reflectance are to this parameter and for brevity, the subscript w is dropped.

5.6.7 Land and cloud masking

As the sea reflectance in the near-IR is very small, channel 2 is used to determine the mask value for the land and cloud pixels. This value is obtained interactively using the M75 level slice command on a channel 2 display image. This command is used to

determine the grey level values associated with the sea pixels. The start of the colour slice is fixed to zero by locking the cursor in the x-direction, then the cursor is moved till all the sea areas have been coloured. The value at which this happen is noted. The mask for land and cloud pixels is created by setting to zero all pixels exceeding the threshold value obtained previously.

5.6.8 Geometric correction

Remotely sensed images are distorted as a result of the earth's curvature. This type of distortion affects mainly imagery gathered by sensors with wide angular field of view (e.g. AVHRR and CZCS). Comparison between images sensed at different times is possible only if the images have been rectified. The process of projecting an image onto a plane, and making it conform to a map projection system is called geometric correction. Methods for geometrically correcting satellite imagery are discussed in Robinson (1985) and Mather (1987).

The present software uses an orbital model based on Wilson *et al* (1981) to create a set of ground control points in the input image necessary for the geometric correction. The latter is achieved using a standard warping algorithm available on the M75.

The pixel values of the new grid are obtained by resampling the values of the source pixels. Bilinear interpolation was used to resample the data onto a grid of 512 x 512 elements. The map projection system onto which the images are warped is a Mercator projection.

5.6.9 An example image

As an example of how a satellite image changes with the stages of processing and the spatial patterns emerge a series from one image are shown. The example image is taken from the 7th March 1985. The sea surface appears dark on the raw image from the AVHRR channel 1 (Fig. 5.3a). At this stage the image is a map of the total reflectance that the satellite senses and no structure can be seen. Once the Rayleigh correction has been applied the image starts showing details of the spatial variations (Fig. 5.3b). In the Rayleigh corrected channel 2 there appears little variation throughout the image (Fig. 5.3c). After removing the aerosol effects the faint spatial variations of Fig. 5.3b are sharpened and the final product is the sea surface reflectance (Fig. 5.3d).

5.6.10 Data reduction

When the image analysis was completed the data files were transferred from the MicroVAX II minicomputer at I.T.E. to the VAX mainframe computer at U.C.N.W. where the remaining steps of the data processing were performed. Before any further processing all data files were converted from byte to ASCII format.

Each data file contains 512 x 512 data points with a ground resolution of 1.1 x 1.1 km. The data were spatially averaged over 16 x 16 data points leading to a new grid of 32 x 32 elements (Figure 6.5) with a ground resolution of 18 x 18 km. The purpose of this operation was to reduce the large amount of data points (262144 data points) in each file and to smooth the data.

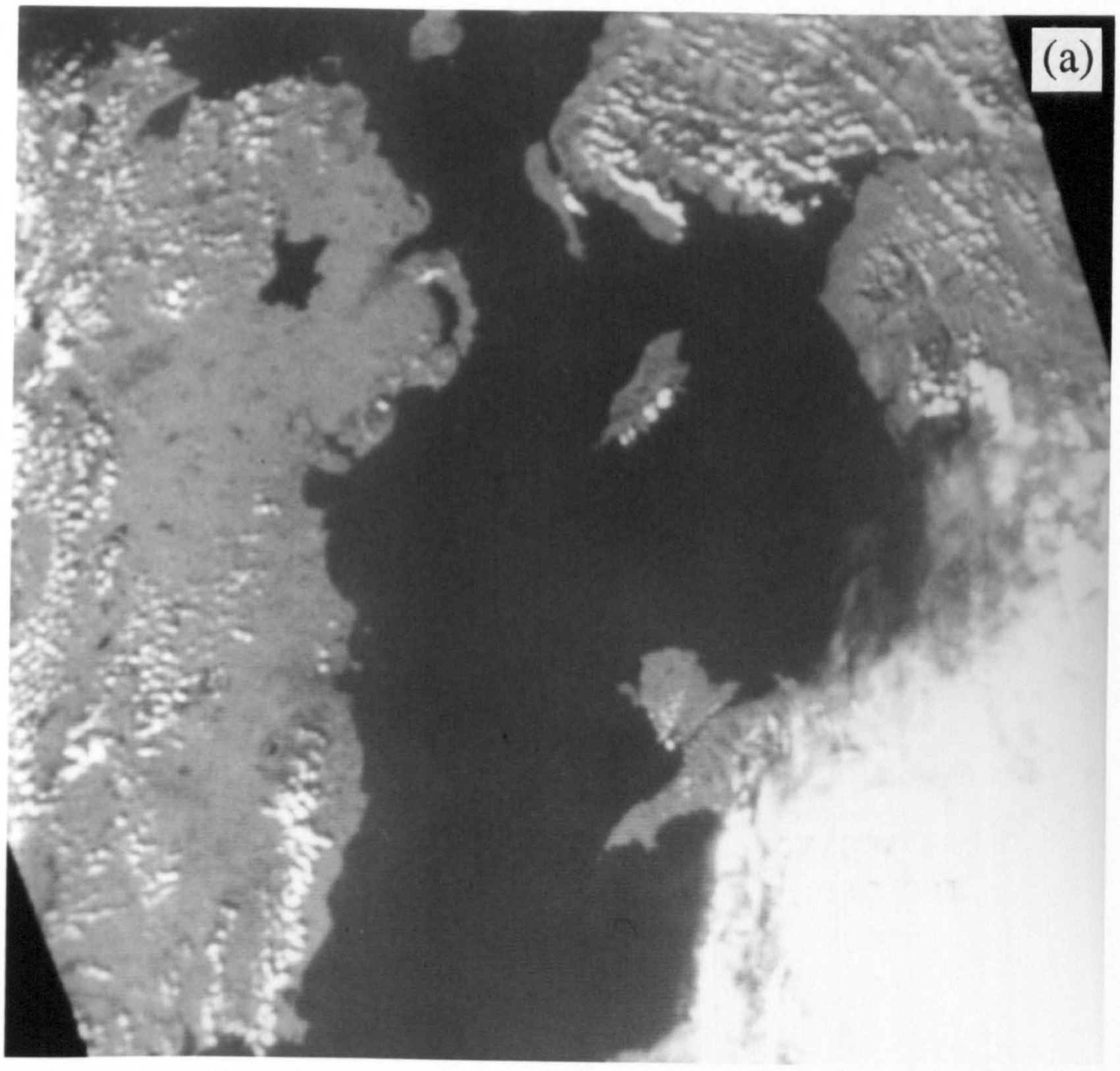

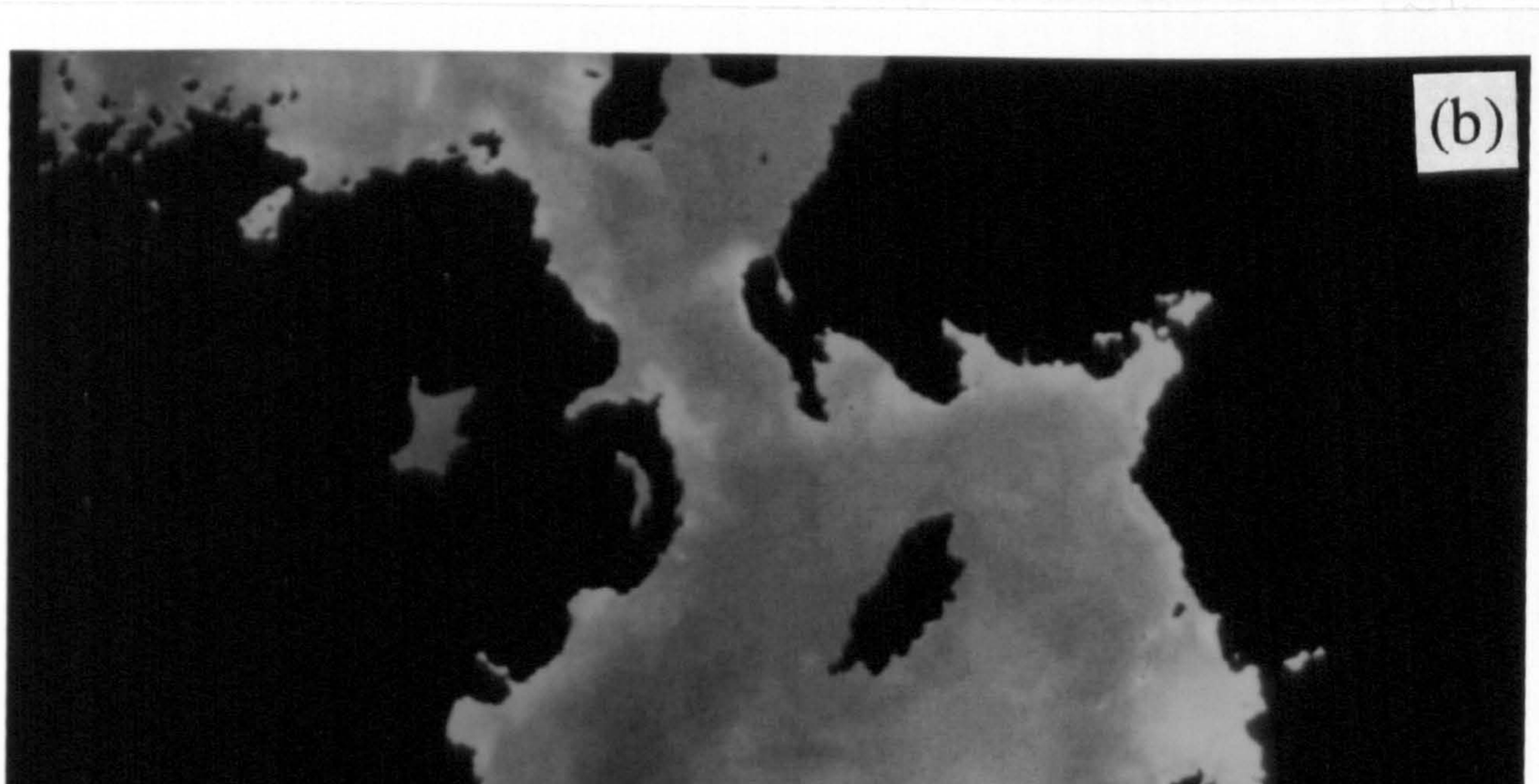

Figure 5.3 Example of an AVHRR image at different stages of processing. (a) Raw image; (b) Channel 1 after Rayleigh correction applied.

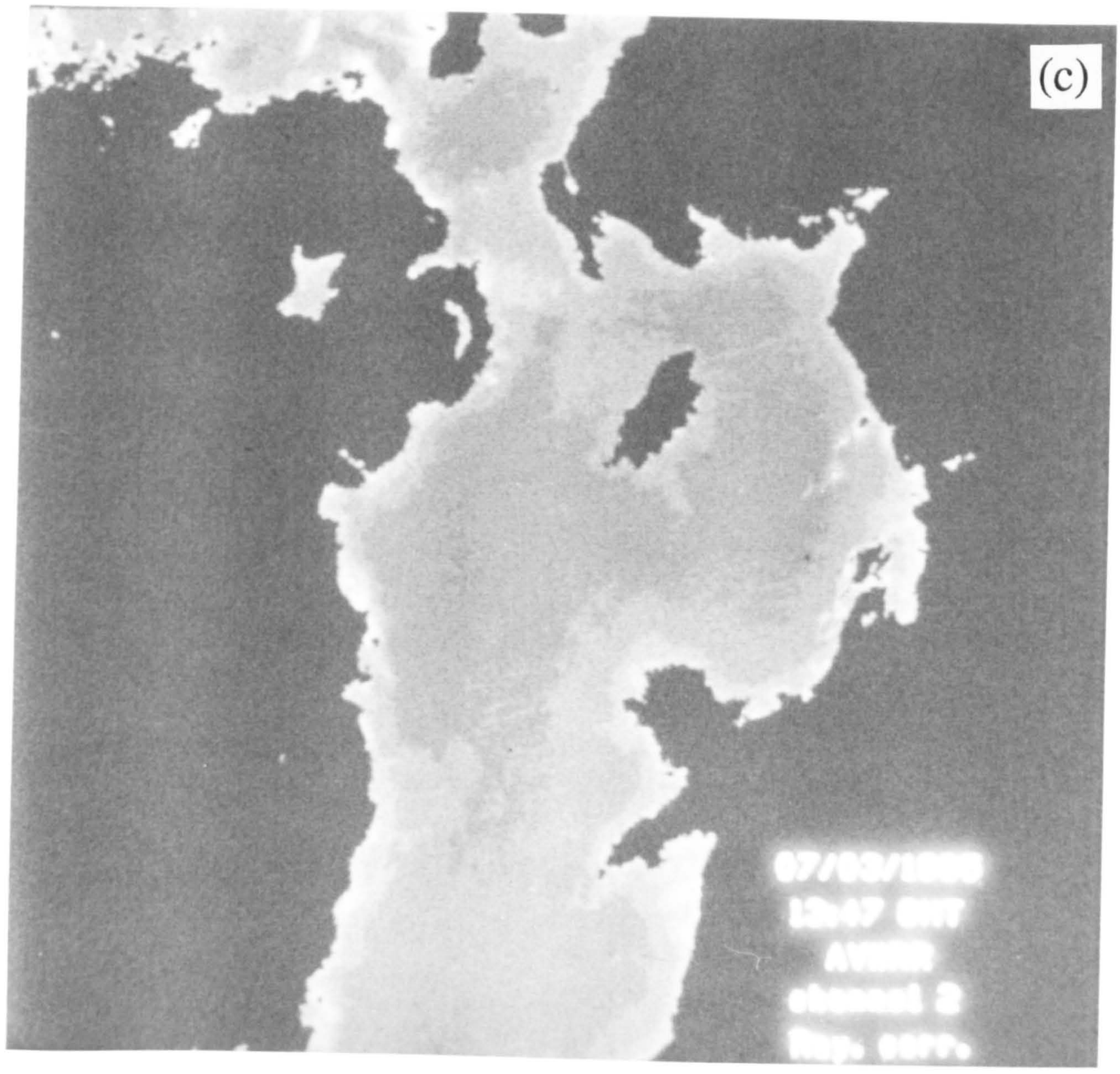

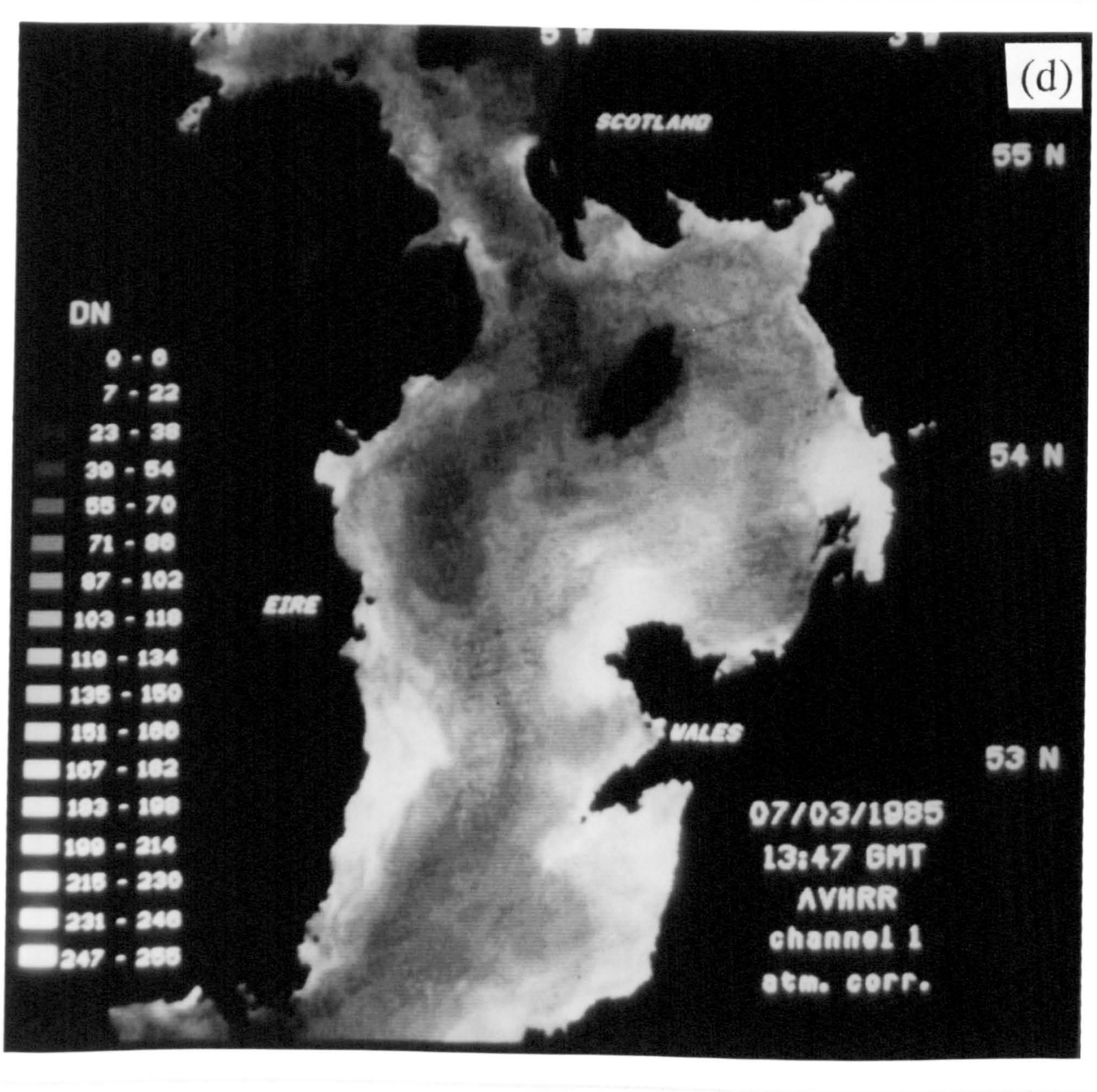

Figure 5.3 (continued) (c) Channel 2 after Rayleigh correction applied and (d) Channel 1 atmospherically corrected.

CHAPTER 6

Remotely sensed data results

6.1 Introduction

In this chapter the results of the analysis of the AVHRR visible band imagery are presented. AVHRR visible data have been used in several regions to study sediment distributions, notably in Chesapeake Bay (Stumpf, 1987), Delaware Bay (Stumpf and Pennock, 1989), the North Sea (Roozekrans and Prangsma, 1988) and the Bay of Biscay (Froidefond *et al*, 1993). However, this technique has previously not been applied to the Irish Sea. It is this omission which this work attempts to resolve.

In previous studies in the Irish Sea, single CZCS images have been used to corroborate spatial distributions of suspended sediments as found from in-situ measurements (e.g. Simpson and Brown, 1987; Weeks and Simpson, 1991). In this sense, satellite data have been used in a supporting role to the in-situ data. No studies have concentrated solely on the satellite imagery to further our understanding of the spatial and temporal variations. In-situ measurements have previously been confined to the northern Irish Sea and from April to October. As satellite data have only been used to compare to in-situ data this is also true of the remotely sensed data. Therefore, there exists significant gaps in the spatial and temporal coverage of sediments in the Irish Sea.

This study uses a large set of AVHRR images which covers a timespan of several years and contains scenes sampled throughout the whole of the year, extending the coverage into the previously unreported winter months. The extensive dataset allows the study of spatial and temporal variations on various timescales over the whole of the Irish Sea.

This chapter continues with a summary of the data used in section 6.2. The seasonal

cycle is examined in section 6.3, in a qualitative sense in section 6.3.1 and then by means of a statistical model in section 6.3.2. How the sediment distribution varies over the spring-neap cycle is next examined in section 6.4. The results of the chapter are summarized and discussed in the final part of the chapter.

6.2 Data summary

A total of 165 images from the daytime passes of the AVHRR between January 1982 and August 1988 were used in this study. Lists of images together with the dates and times they were sensed are given in Appendix 1. The number of images per year ranged from a minimum of 9 in 1988 to a maximum of 36 in 1984, with an average of 23.6. A histogram of the distribution of the number of images per year is given in Fig. 6.1a. Generally, there were more images per year in the first four years than the latter three.

The composite distribution by month, irrespective of year, is shown in Fig. 6.1b. The average number of images per month is 13.8. The months April to July each have more than 20 images with the maximum being 35 in May. For the two periods of August to October and January to March there are between 4 and 16 images per month. There are no images for the other two months of the year ie. November and December.

While Fig. 6.1 shows the distribution by year and month, Fig. 6.2 is a histogram of number of images for the individual seven years. Each year has generally a similar distribution: a larger number of images during April to September and fewer for the remainder of the year. The distribution of the number of images is a reflection of the amount of cloud cover ie. months which are cloudier have fewer images. The percentage of cloudy sea pixels for each of the 165 images used in this work is given in Appendix 1.

As explained in section 5.6.9 each sensed image consists of a 512 x 512 grid. The

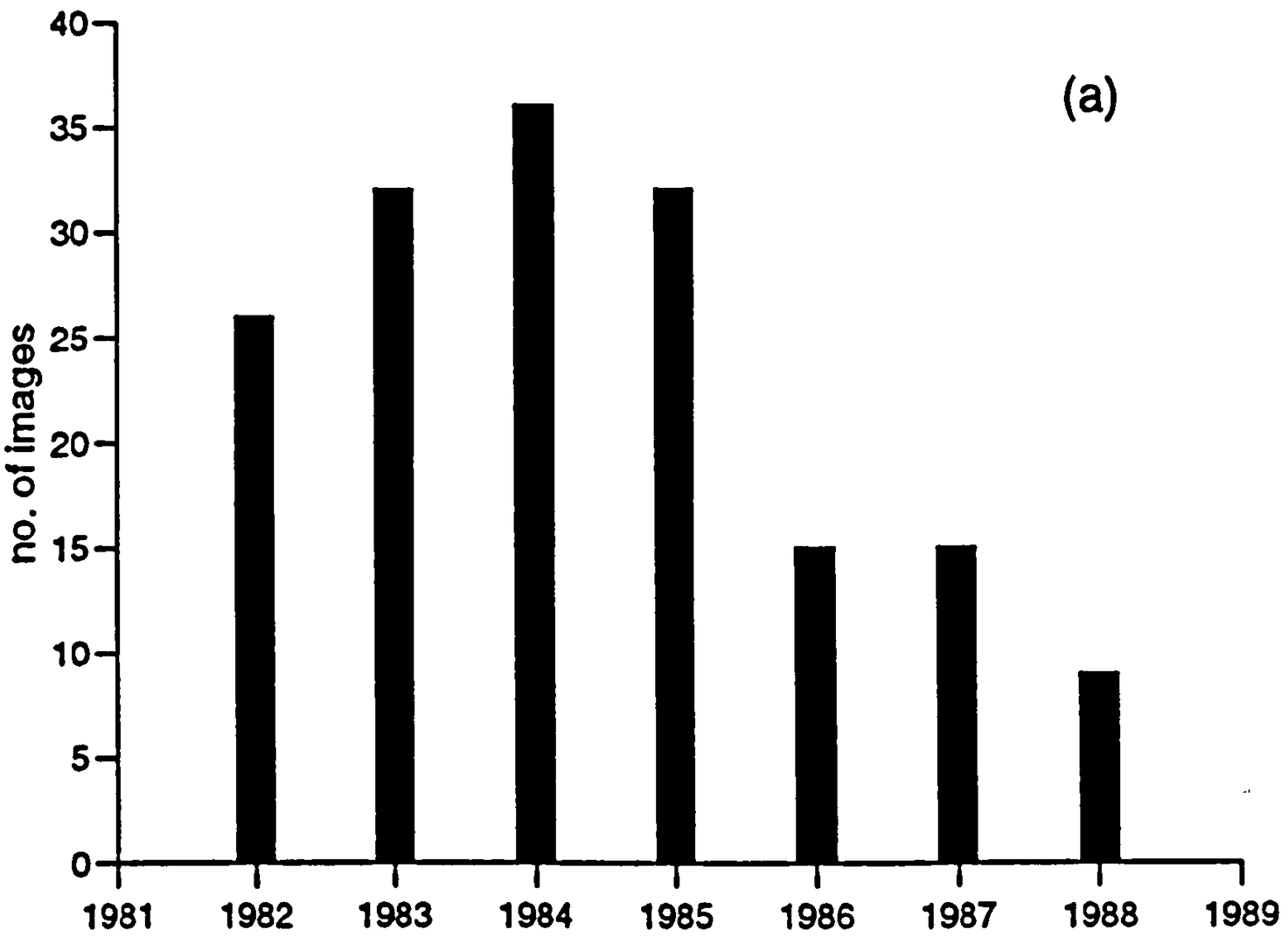

Figure 6.1 Number of satellite images: (a) per year (b) per month.

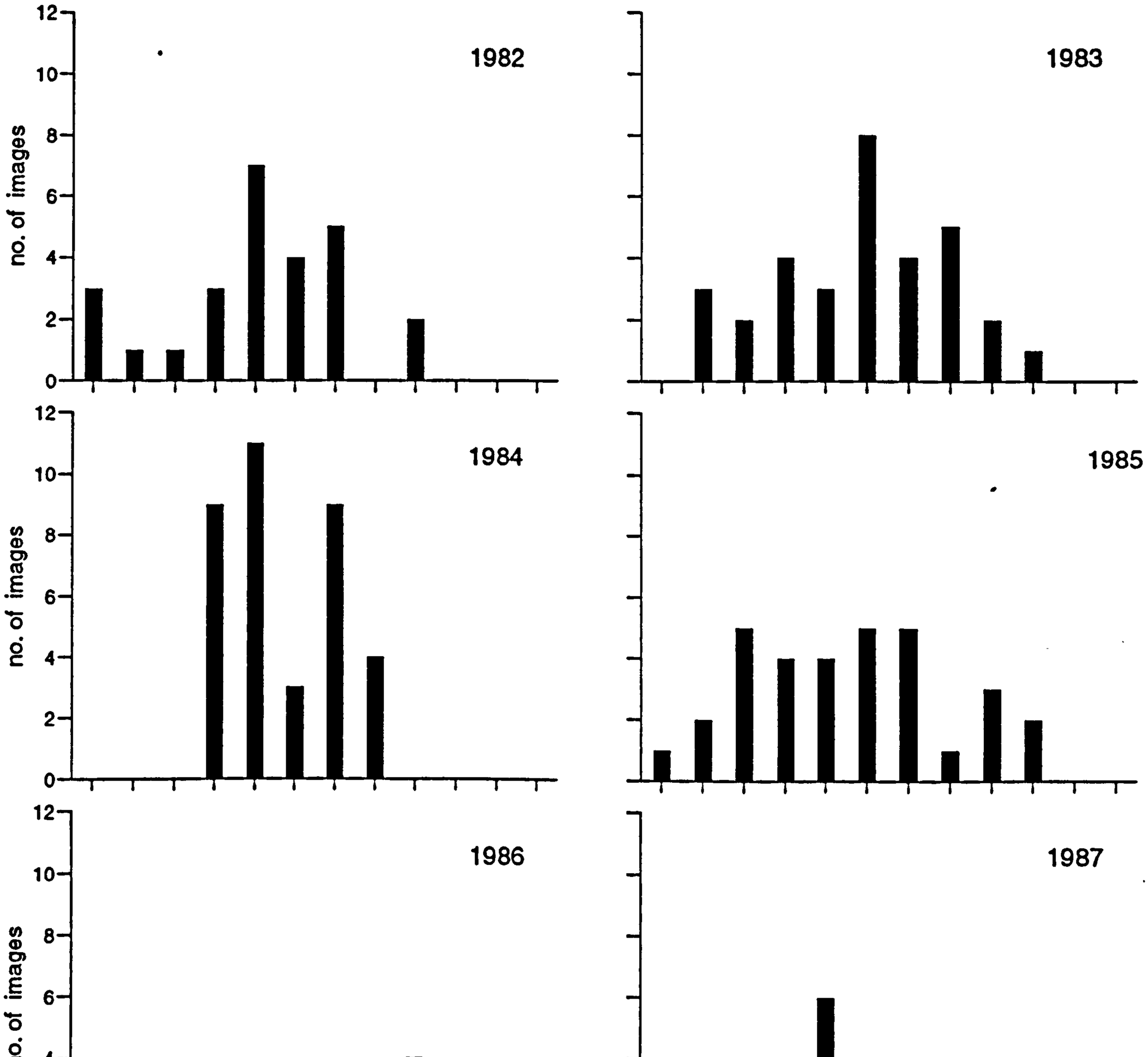

Figure 6.2 Monthly distribution of images for the study period.

analyses presented in this chapter are based on the spatially averaged data, after the original data have been averaged onto a 32 x 32 grid. The actual grid used is shown in Fig. 6.5. Each grid point is defined by its x and y-position in the grid by the subscripts i and j, respectively.

6.3 Seasonal cycle of reflectance in the Irish Sea

6.3.1 Observations

The atmospherically corrected winter images exhibit patterns of surface reflectance which are consistent from year to year; this is also true for the summer images. These patterns are in good agreement with observed in-situ SPM distributions in the Irish Sea. They also show a remarkable similarity to patterns of reflectance of the Irish Sea seen in CZCS imagery. These comparisons and the consistency of the patterns placed confidence in the atmospheric correction and led to the conviction that the reflectance patterns seen in the AVHRR imagery are caused by the surface SPM of the Irish Sea.

Typical examples of the horizontal distribution of reflectance of the Irish Sea in winter and summer from two years are shown in Fig. 6.3. The observed patterns and seasonal changes are consistent from year to year over the study period. The most striking difference between the winter (Figs. 6.3a and c) and the summer (Figs. 6.3b and d) scenes is the much higher reflectance overall in winter. The high reflectances, represented by yellows and reds, cover much of the coastal areas in winter, but in the summer have retreated into a few selected locations. These two scenes illustrate the seasonal variation of reflectance of the Irish Sea which we shall investigate in detail later in this chapter.

Spatially there are similarities between summer and winter. High reflectances are

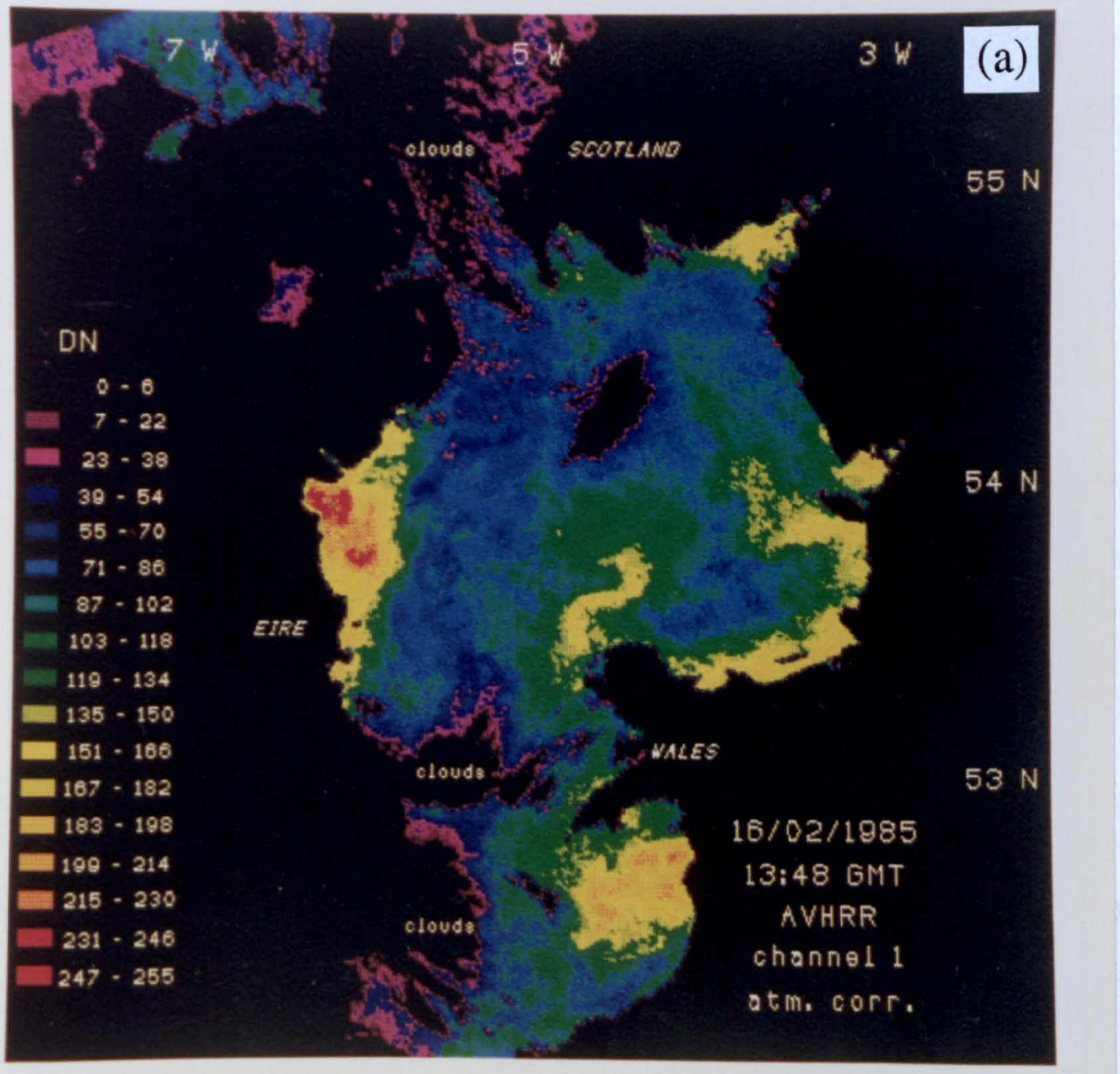

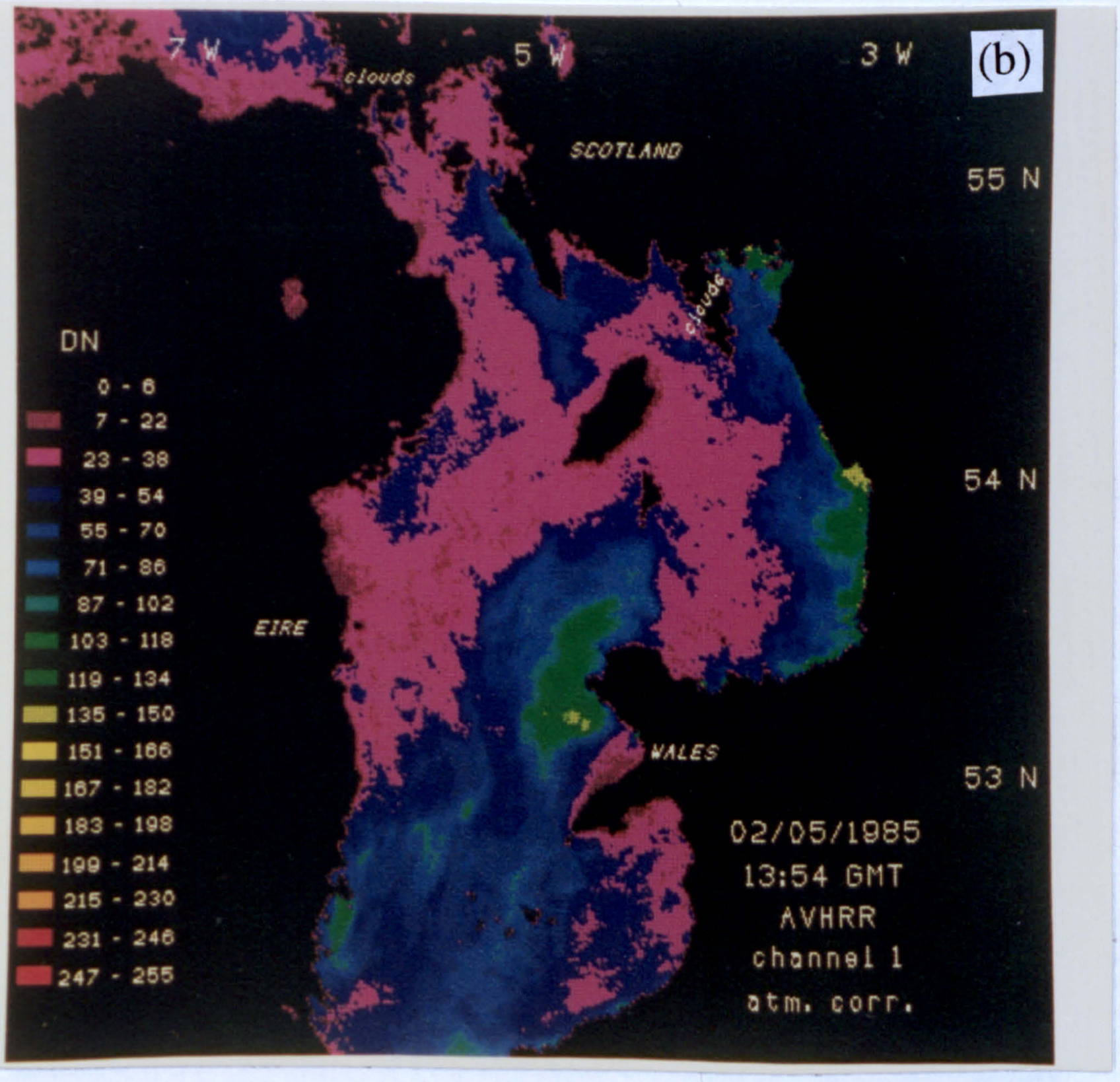

Figure 6.3 Example distributions of surface reflectance in the (a) winter of 1985 and (b) summer of 1985

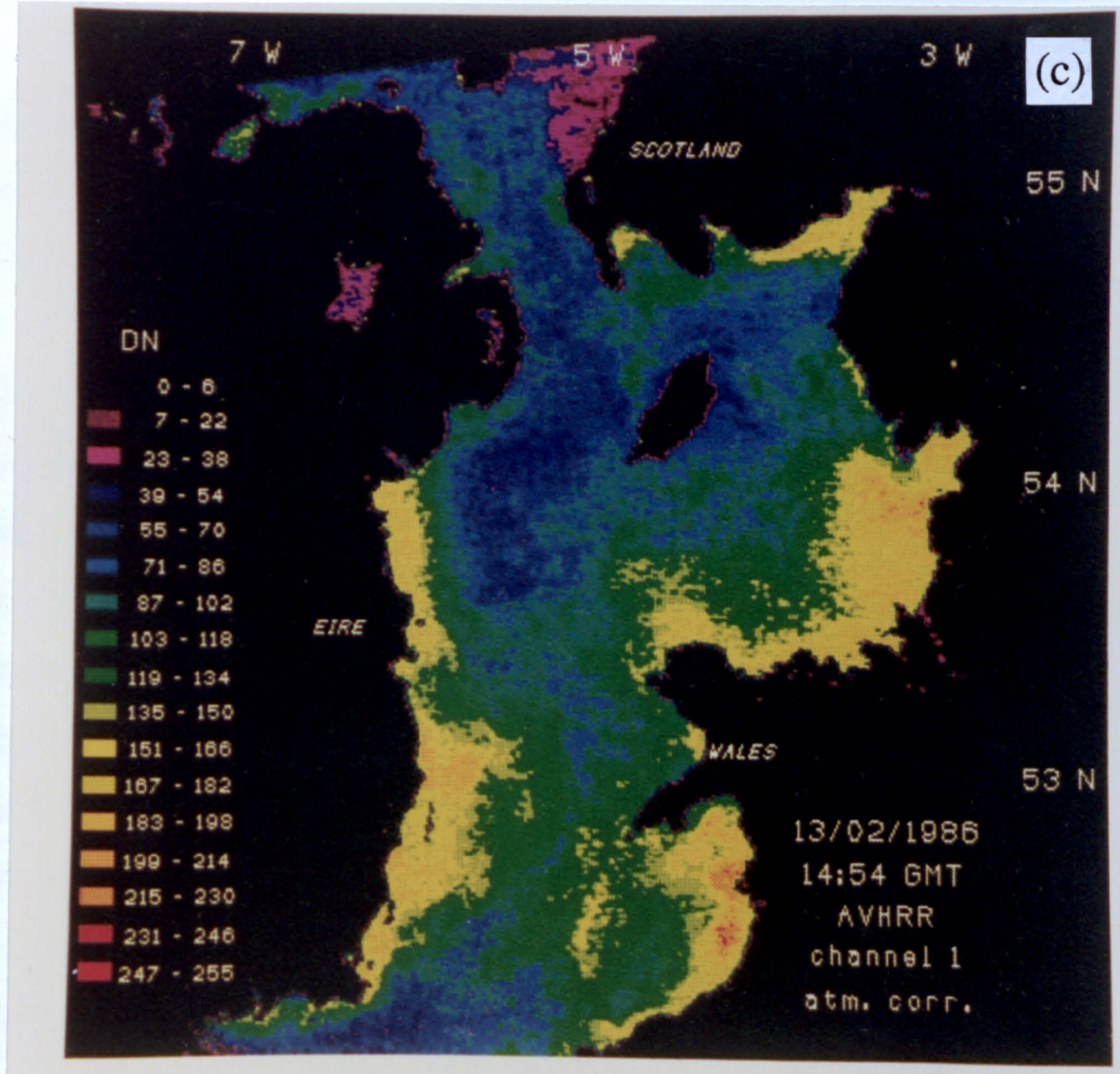

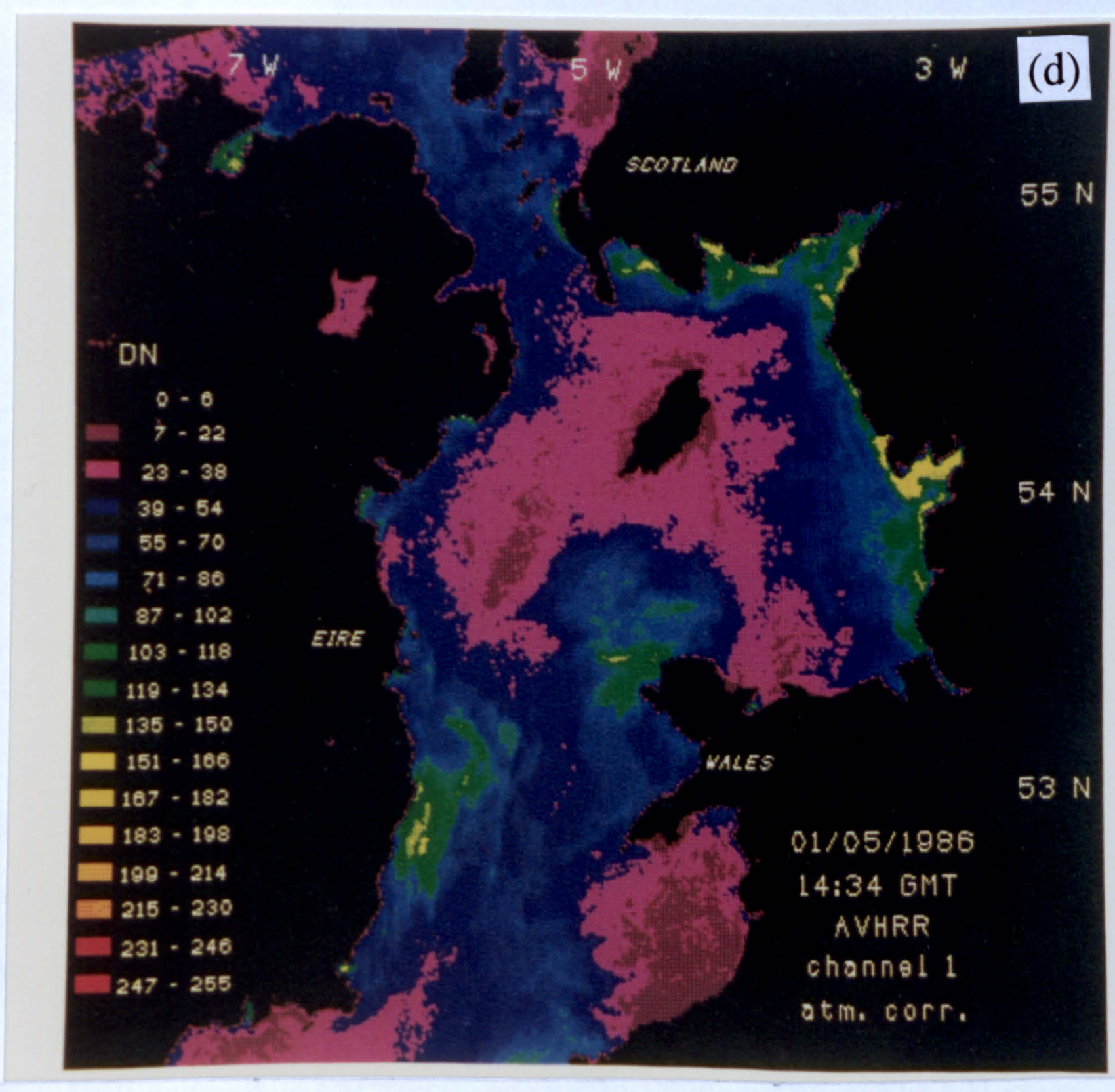

Figure 6.3 (continued) Example distributions of surface reflectance in the (c) winter of 1986 and (d) the summer of 1986.

always found off Anglesey, near Wicklow, and along the English coast. Low values of reflectance occur in the deep channels, the western Irish Sea and the areas north and east of the Isle of Man.

Evidence of a seasonal cycle has been shown by four snapshots of the spatial distribution as seen in the satellite images. To illustrate how the reflectance at a particular site varies throughout the year in more detail composite annual time-series for eight selected sites are shown in Fig. 6.4. The selection of the eight sites is not an attempt at classifying or explaining the different seasonal cycles but to merely emphasize the temporal nature of the signal. Interpretation of the spatial distribution of the seasonal cycle of reflectance is conducted later in this chapter. The positions of the sites are indicated in Fig. 6.5 and the dynamical conditions are presented in Table 6.1. Areas where $\log_{10}(h/ U^3) > 2.7$ become thermally stratified during the summer months (Simpson and Hunter, 1974). It can be clearly seen that the seasonality of reflectance varies considerably from site to site and for each site is consistent over different years.

Sites	M_2 current amplitude U (cm s^{-1})	Depth h (m)	$\log_{10}$ (h / U^3) (m^{-2} s^3)	Bed sediments (Fig. 2.6)
A	111.6	38.4	1.44	sand and gravel
B	109.4	50.5	1.59	sand and gravel
C	56.6	19.8	2.04	sandy
D	27.4	14.9	2.86	sand and gravel
E	19.8	107.8	4.14	mud
F	89.9	132.0	2.26	sandy
G	30.6	21.0	2.87	sand and mud
H	101.8	89.5	1.93	gravelly

Table 6.1 Dynamical characteristics and bed sediments at the eight selected sites. The M_2 tidal current amplitudes are from a model by Pingree and Griffiths (1978).

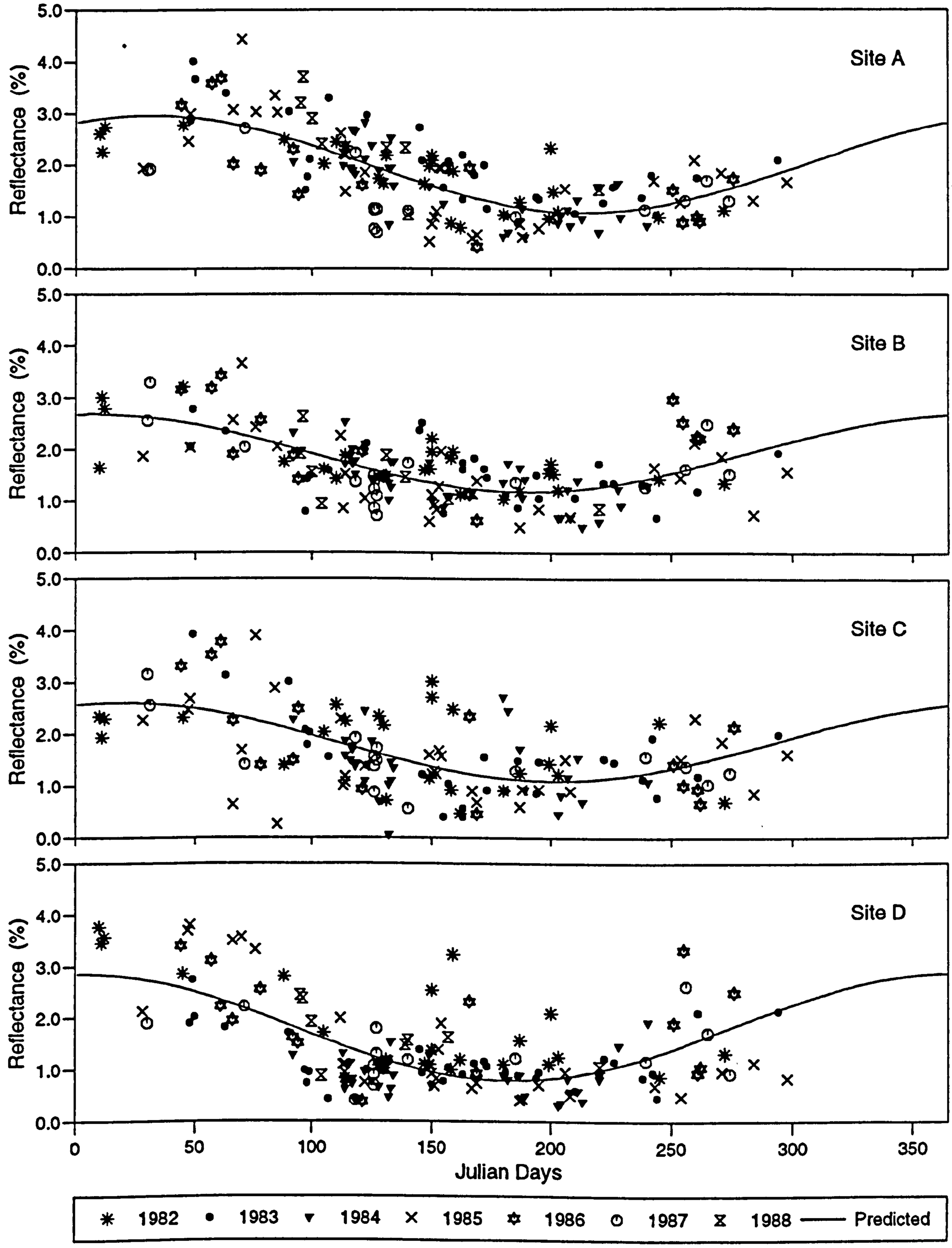

Figure 6.4 Composite annual time-series of reflectance at eight selected sites.

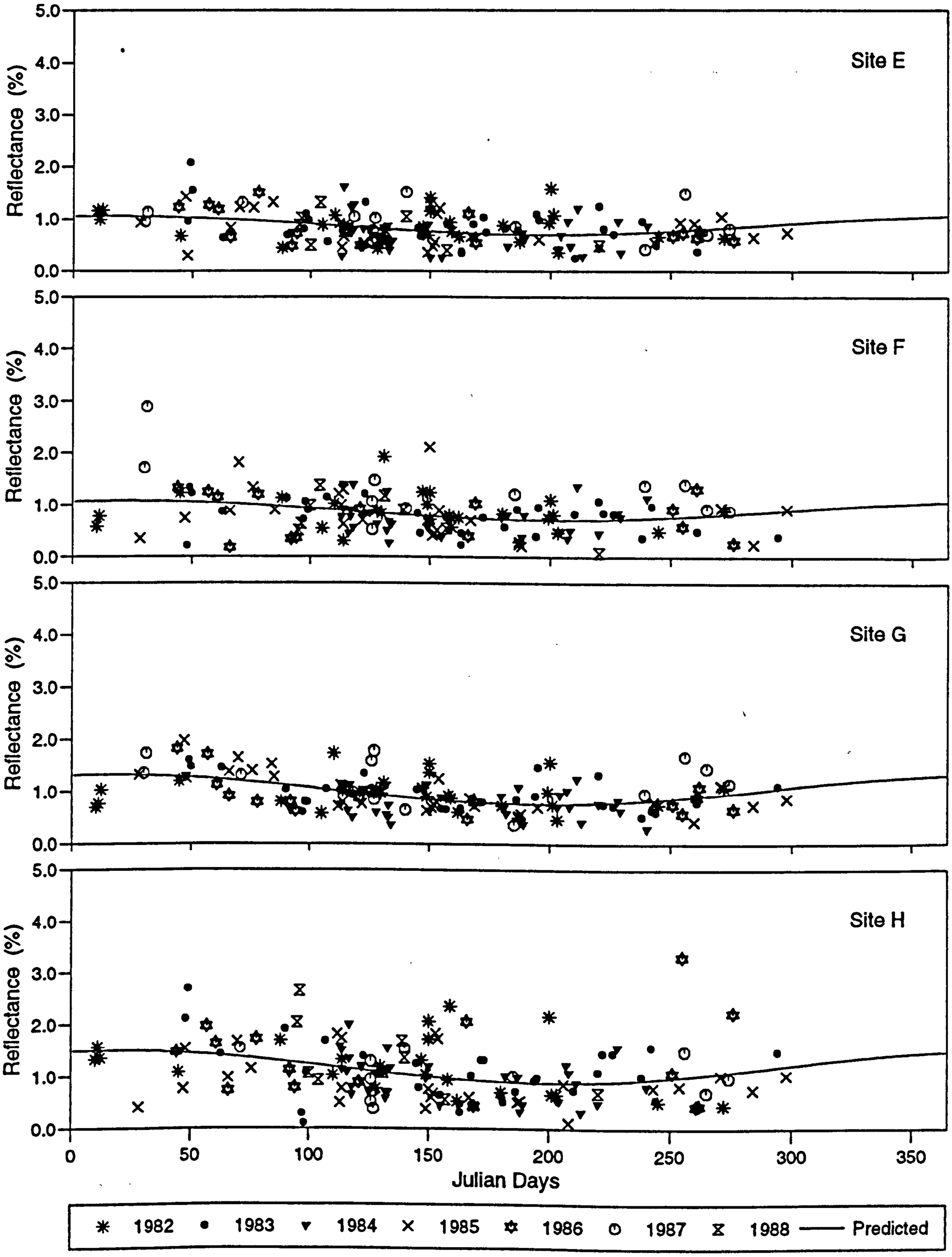

Figure 6.4 (continued) Composite annual time-series of reflectance at eight selected sites.

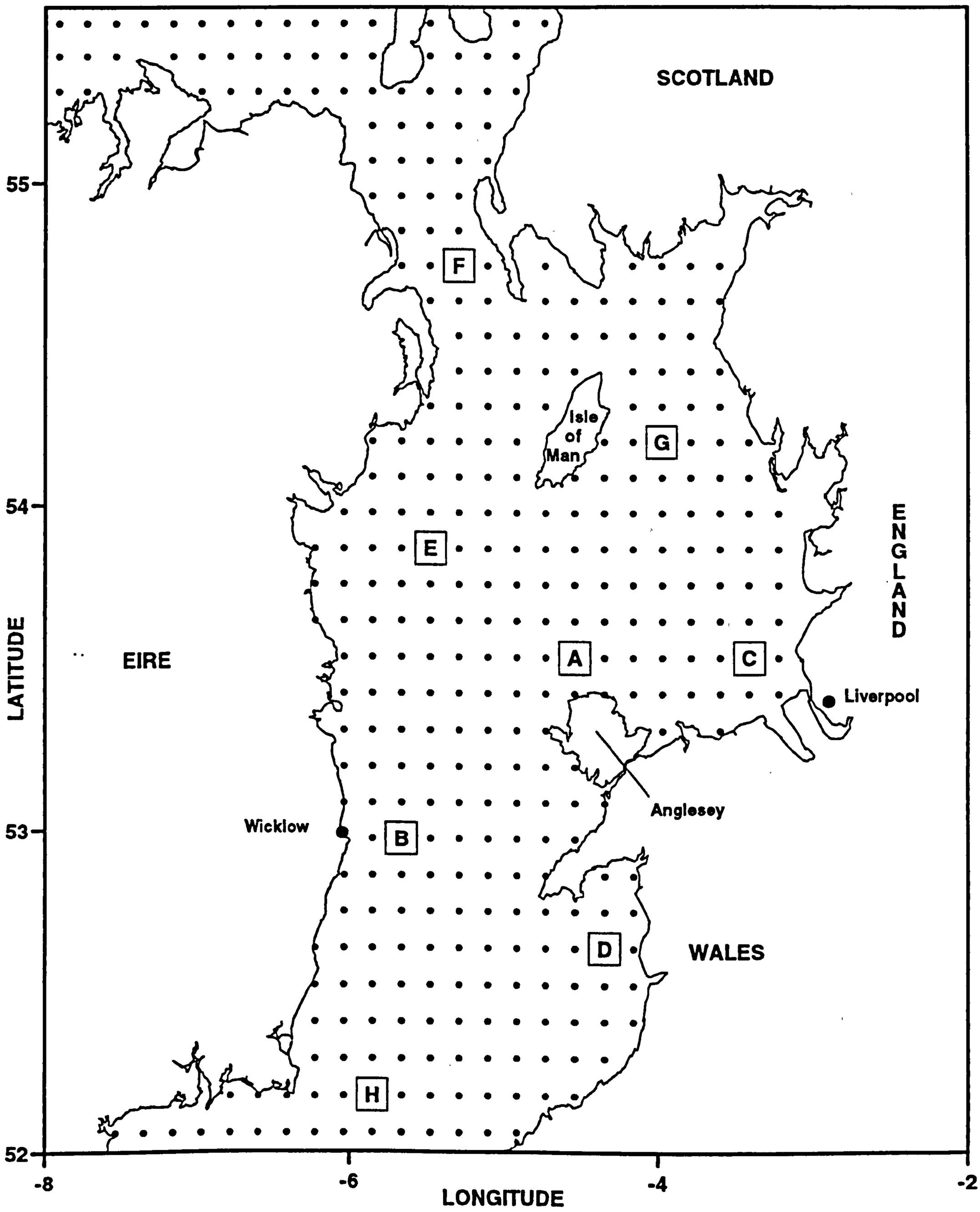

Figure 6.5 Positions of the eight selected sites and the grid used in the analysis of the satellite images.

6.3.2 Statistical model for the composite seasonal cycle

(i) Description

The observations have shown the seasonal cycle of reflectance to be important in certain areas of the Irish Sea but not in others. A statistical model was used to assess the importance of this cycle for the whole of the Irish Sea. The annual cycle parameters were estimated from least squares fits to composite time-series of reflectance at each grid element. The fitted reflectance at a grid point, R_{ij} is given by :

$$R_{ij}(t) = A_{ij} + R_{a_{ij}} \cos(\omega t + \phi_{ij}) \qquad (6.1)$$

where R_{ij} is reflectance (%), ω is the frequency of the annual cycle (radians/day), t is time in days (t = 1 on the 1st January in any year). The parameters A_{ij}, R_{aij}, and ϕ_{ij} are respectively the mean, amplitude, and phase of the annual cycle. The subscripts i (x-direction) and j (y-direction) are the coordinates of a grid point.

For clarity, in the following, the subscripts i and j are dropped. Eq. (6.1) can be rewritten as:

$$R(t) = A + B\cos\ \omega t + C\sin\ \omega t \qquad (6.2)$$

It is this latter form of Eq. (6.1) which was actually fitted to the observations. The coefficients A, B, and C are determined by the least squares fits. The estimated values of B and C are then used to calculate the amplitude and phase of the annual cycle.

The amplitude of the annual cycle is given by:

$$R_a = \sqrt{B^2 + C^2} \qquad (6.3)$$

and the phase is:

$$\phi = \tan^{-1}\left(-\frac{C}{B}\right) \tag{6.4}$$

(ii) Error analysis

To assess the statistical significance of the model for each grid cell the standard deviations of the annual cycle parameters A, R_a and ϕ need to be calculated. The standard deviation of the A's are given directly from the least squares fits, whereas the standard deviations of the R's and ϕ's are determined from those of the B's and C's. Expressions for the standard deviations of the R's and ϕ's are now derived in terms of the standard deviations of the B's and C's. The derivation follows that given by Bevington, 1969.

Given a function z = z(x,y), if x and y are independent then the variance of z is given by:

$$\sigma_z^2 = \left(\frac{\partial z}{\partial x}\right)^2 \sigma_x^2 + \left(\frac{\partial z}{\partial y}\right)^2 \sigma_y^2 \tag{6.5}$$

where σ_x^2 and σ_y^2 are the variances of x and y, respectively.

It follows that the variance, σ_{Ra}^2, of the amplitude at each grid point can be expressed as:

$$\sigma_{R_a}^2 = \left(\frac{\partial R_a}{\partial B}\right)^2 \sigma_B^2 + \left(\frac{\partial R_a}{\partial C}\right)^2 \sigma_C^2 \tag{6.6}$$

where $\frac{\partial R_a}{\partial B} = \frac{B}{\sqrt{(B^2+C^2)}}$ and $\frac{\partial R_a}{\partial C} = \frac{C}{\sqrt{(B^2+C^2)}}$ (derived from Eq. (6.3)). The

quantities σ_B^2 and σ_C^2 are the estimated variances of the coefficients B and C, respectively.

Substituting the partial derivatives in Eq. (6.6) by their actual expressions gives:

$$\sigma_{R_a}^2 = \frac{B^2\sigma_B^2 + C^2\sigma_C^2}{(B^2 + C^2)}$$

Therefore the standard deviation of the amplitude is:

$$\sigma_{R_a} = \sqrt{\frac{B^2\sigma_B^2 + C^2\sigma_C^2}{(B^2 + C^2)}} \qquad (6.7)$$

Similarly the variance, σ_ϕ^2, of the phase can be expressed as:

$$\sigma_\phi^2 = \left(\frac{\partial\phi}{\partial B}\right)^2 \sigma_B^2 + \left(\frac{\partial\phi}{\partial C}\right)^2 \sigma_C^2 \qquad (6.8)$$

where $\frac{\partial\phi}{\partial B} = \frac{C}{(B^2 + C^2)}$ and $\frac{\partial\phi}{\partial C} = \frac{-B}{(B^2 + C^2)}$ (derived from Eq. (6.4)).

Substituting these two terms in Eq. (6.8) gives:

$$\sigma_\phi^2 = \frac{B^2\sigma_C^2 + C^2\sigma_B^2}{(B^2 + C^2)^2}$$

Hence the standard deviation of the phase is:

$$\sigma_{\phi} = \sqrt{\frac{B^2\sigma_C^2 + C^2\sigma_B^2}{(B^2+C^2)^2}} \tag{6.9}$$

The standard deviations of the mean, amplitude and phase were then used to calculate confidence intervals for these parameters. The general formula for a t-confidence interval is:

(quantity) ± (value from t-table) x (estimated standard deviation of quantity)

The term [(value from t-table) x (estimated standard deviation of quantity)] was calculated for each of the annual cycle parameters at each grid cell. This term will be referred to in the text as the confidence range.

6.3.3 Results of the seasonal model

The results of the statistical model of the seasonal variation are presented as contour plots for each of the fitted parameters, i.e. annual mean, amplitude and phase lead. It has been shown in the composite time-series that the annual signal varies over the Irish Sea and, hence, any spatial distribution of these parameters will best be seen in contour plots.

When presenting results of regression models, the statistical significance of each of the regression coefficients must be considered. As explained in the previous section, this refers to the test of the fitted coefficient being significantly different to zero, to a fixed degree of probability. In this study the 99 % confidence level is used throughout. Together with the actual coefficients, contour plots of the confidence ranges are also presented to allow assessment of the significance of the results.

The values of the annual mean, A, are significant throughout the whole of the Irish Sea (Figs. 6.6 and 6.7). Generally, the confidence ranges are much smaller in magnitude than the annual means. The annual means exhibit a well-defined distribution of localized areas of high reflectances separated from areas of low values by strong horizontal gradients. Such high levels are found in an area around the north west coast of Anglesey (and extending into the central Irish Sea); along the Irish coast around Wicklow; in Liverpool Bay and Cardigan Bay. Cardigan Bay differs from the other areas of high means in that the values decrease more slowly into the areas of low mean i.e. it is not marked by a zone of strong horizontal gradients.

The highest means are found close to the coast in Liverpool Bay and are greater than 2.4 %. The values decrease strongly westwards and then increase again into another area of high means off Anglesey. Typical mean reflectances in the identified high reflectance areas are around 2.0 %.

The remainder of the Irish Sea is characterised by low annual means (< 1.3 %) and small horizontal gradients. This is true of the whole of the northern part of the Irish Sea, i.e. the approximate area to the north of latitude 53.5° and outside of Liverpool Bay. The other area of low means is the narrow section that runs northwards from St George's Channel, into central Irish Sea and finally into its northern part. The lowest values of the annual mean are 0.8 % and are found off the west coast of the Isle of Man.

The results for the annual amplitude are also significant throughout the entire area (Figs. 6.8 and 6.9). Again a clear spatial distribution is evident. The distribution pattern of fitted annual amplitudes is similar to the spatial distribution of the annual mean, but of a significantly lower value. High values are found in four separate areas: Liverpool Bay, Cardigan Bay, off the Irish coast around Wicklow and off the north west coast of Anglesey. Annual amplitudes greater than 0.7 % are typical of these areas.

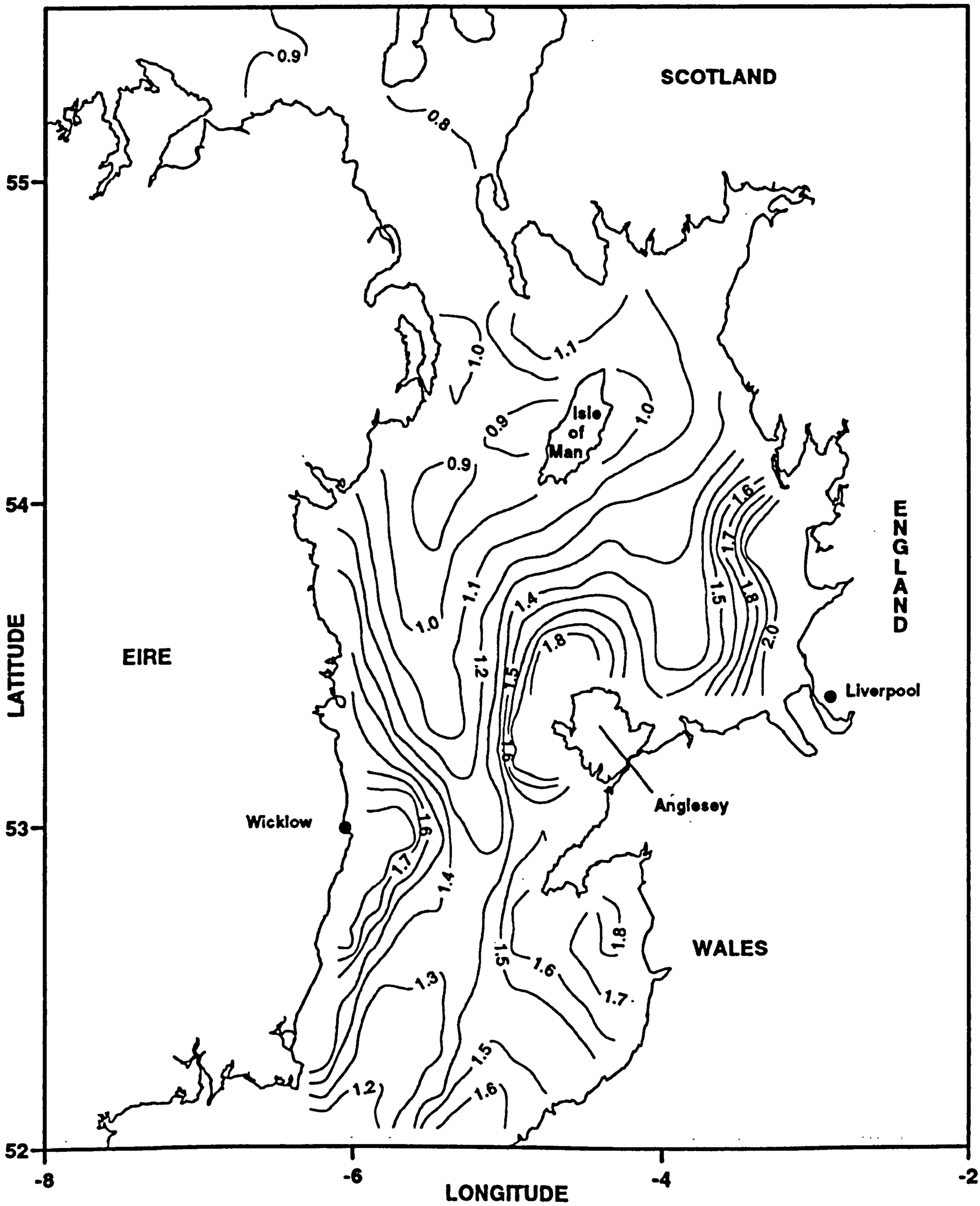

Figure 6.6 Distribution of the annual mean, A (%).

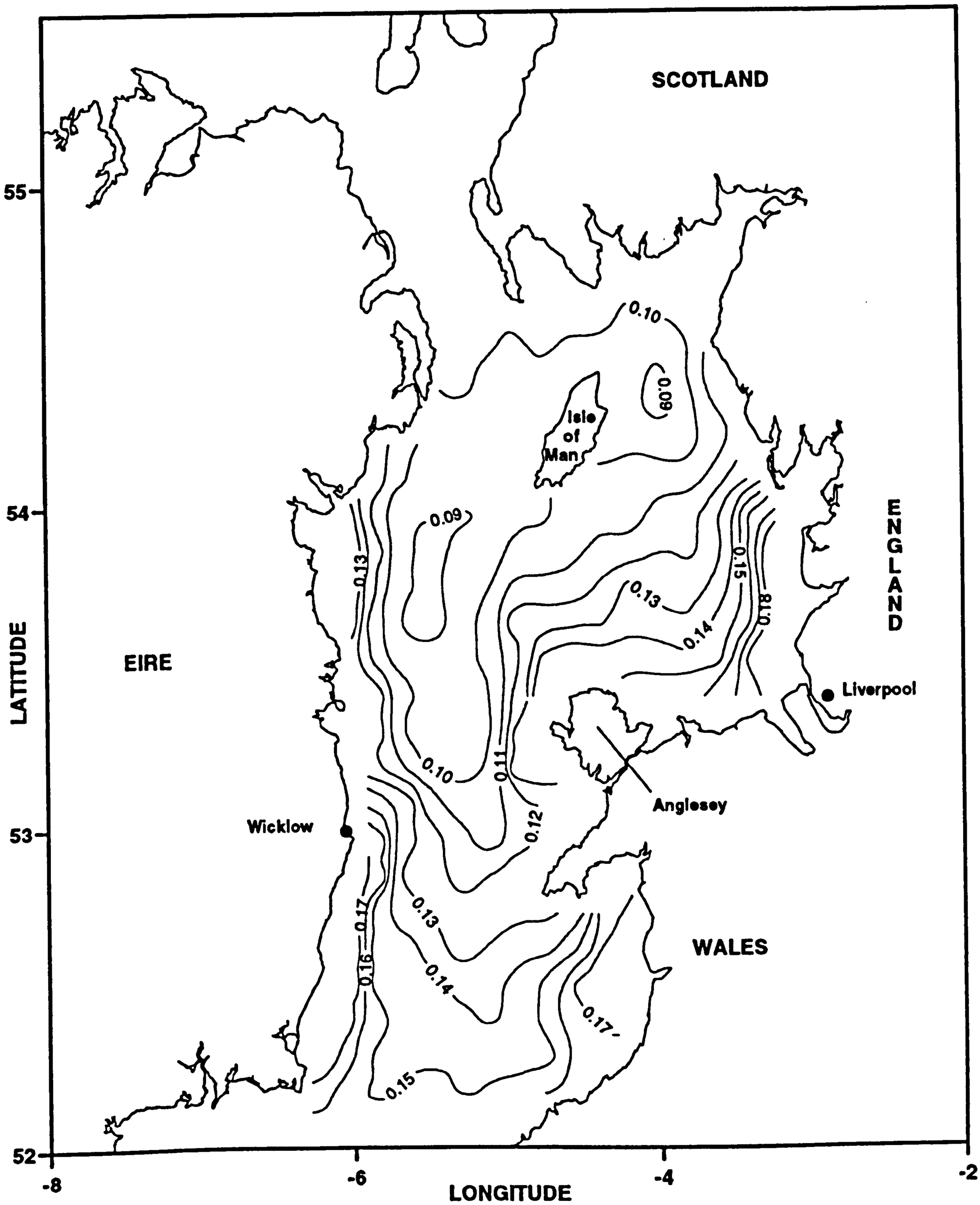

Figure 6.7 Distribution of the confidence range of the annual mean (%).

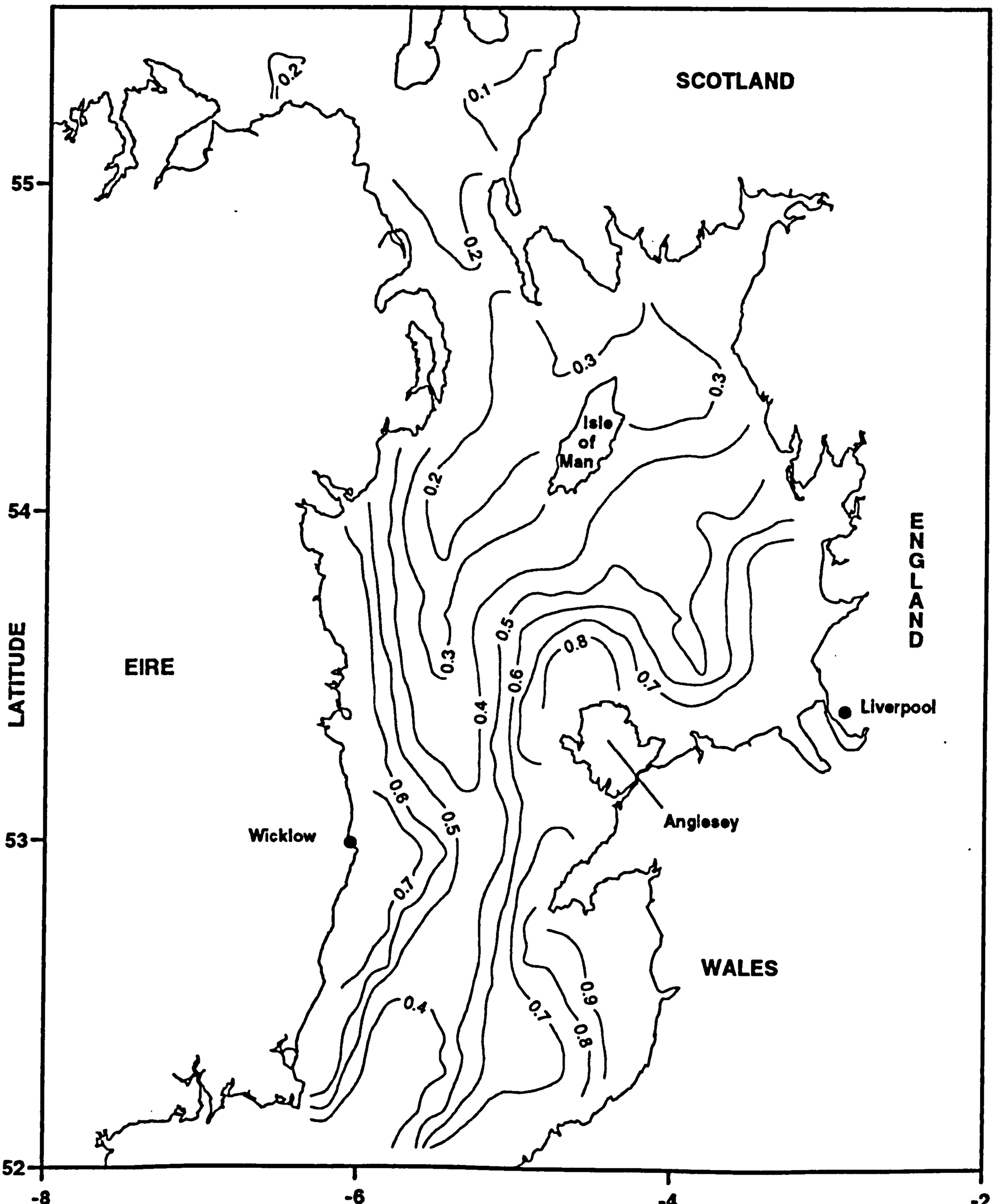

Figure 6.8 Distribution of the seasonal amplitude, R_a (%).

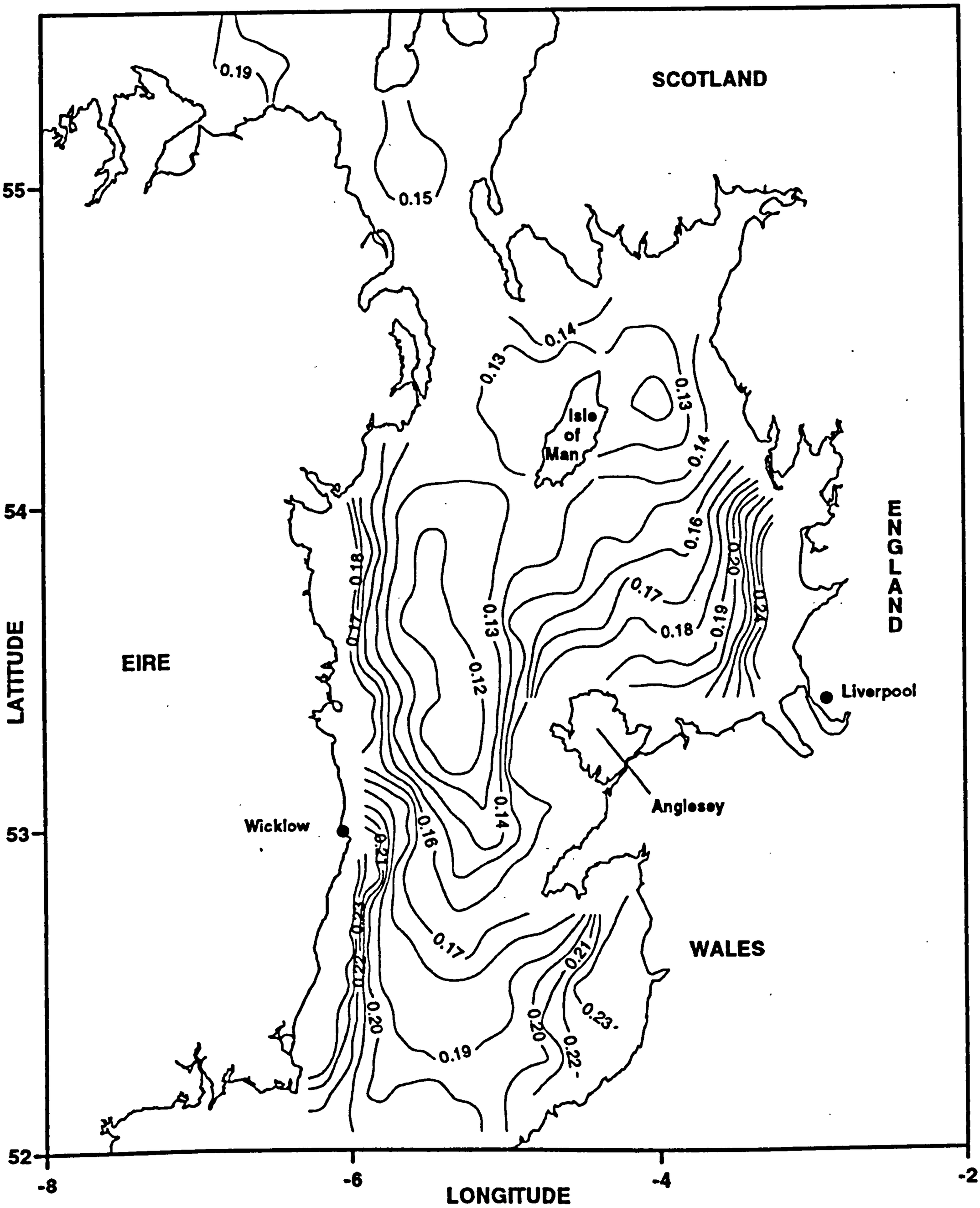

Figure 6.9 Distribution of the confidence range of the seasonal amplitude (%).

The highest annual amplitudes are found in Cardigan Bay and are of the order of 1.1 %. Unlike the distribution of the annual mean, the horizontal gradients to the west of Cardigan Bay are of a similar magnitude to those around other areas of maximum values. The northern part of the Irish Sea and a central section running from the south to the north are, again, characterised by low values (of the order of 0.3 %) and relatively small horizontal gradients. Minimum annual amplitudes are 0.1 % and are located between the Isle of Man and the coast of Northern Ireland.

The spatial distributions of the annual mean and amplitude have been shown to exhibit similar patterns. This similarity implies that the two are related in some fashion. The relationship between the two can be clearly seen to be well defined (Fig. 6.10). A definite linear relationship exists between the two parameters. Low annual amplitudes are associated with low annual means. Amplitudes increase as annual means increase. However, this linearity becomes less evident with larger annual amplitudes when the scatter increases. The scatter plot also shows that no areas of the Irish Sea have high annual means but low annual amplitudes: a situation that is physically possible but evidently does not occur.

The predicted phase leads and their confidence ranges are shown in Figs. 6.11 and 6.12. The times of maximum reflectance occur after the beginning of the year. The largest lags (indicated by negative leads) are 45 days i.e. mid-February and are found north-west of Anglesey. Liverpool Bay and the southern Irish Sea have maximum reflectances sometime in January of each year. In the remainder of the Irish Sea the maximum annual values are predicted to occur at the start of each year.

How well the model fits the observations is expressed in terms of the percentage of the observed variance that the model accounts for; this value is known as the r^2 value of the model. The seasonal cycle accounts for up to 50% of the observed variance of the reflectance in the Irish Sea (Fig. 6.14). The seasonal variation is, as expected, most important where the seasonal amplitude is largest. In these areas a typical value of r^2

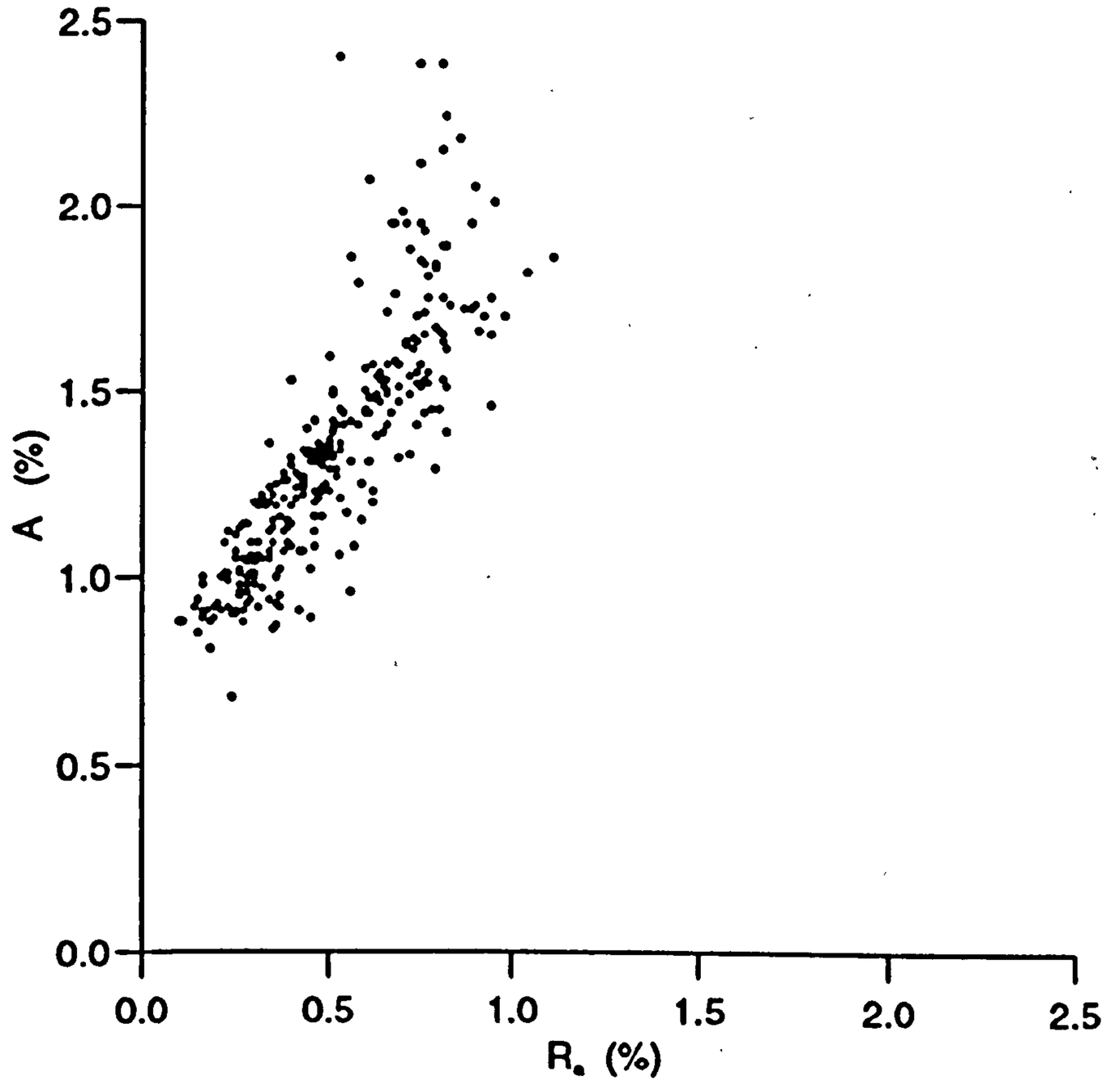

Figure 6.10 Scatter plot of the annual mean against the seasonal amplitude.

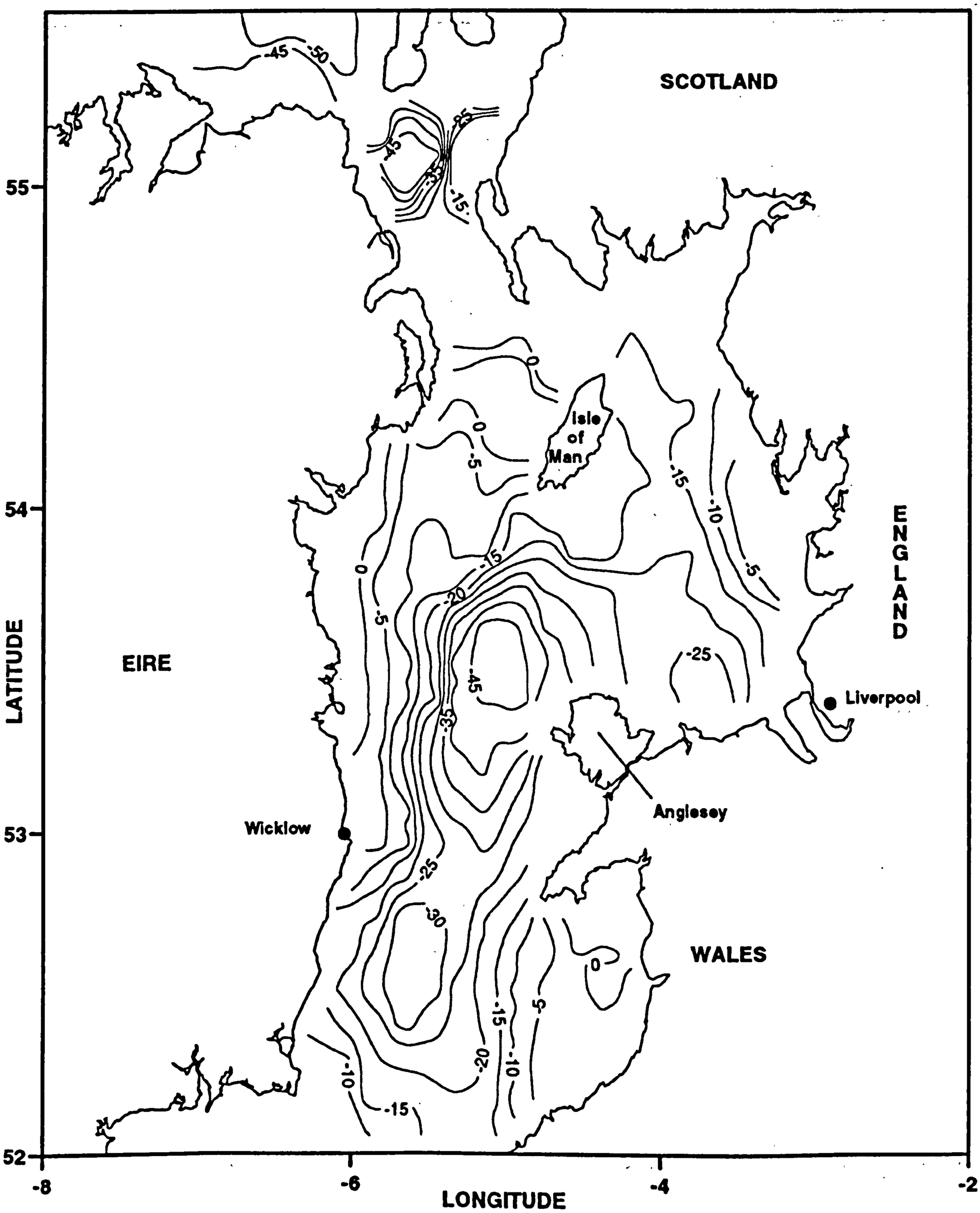

Figure 6.11 Distribution of the phase lead, in days, of the seasonal variation, ϕ.

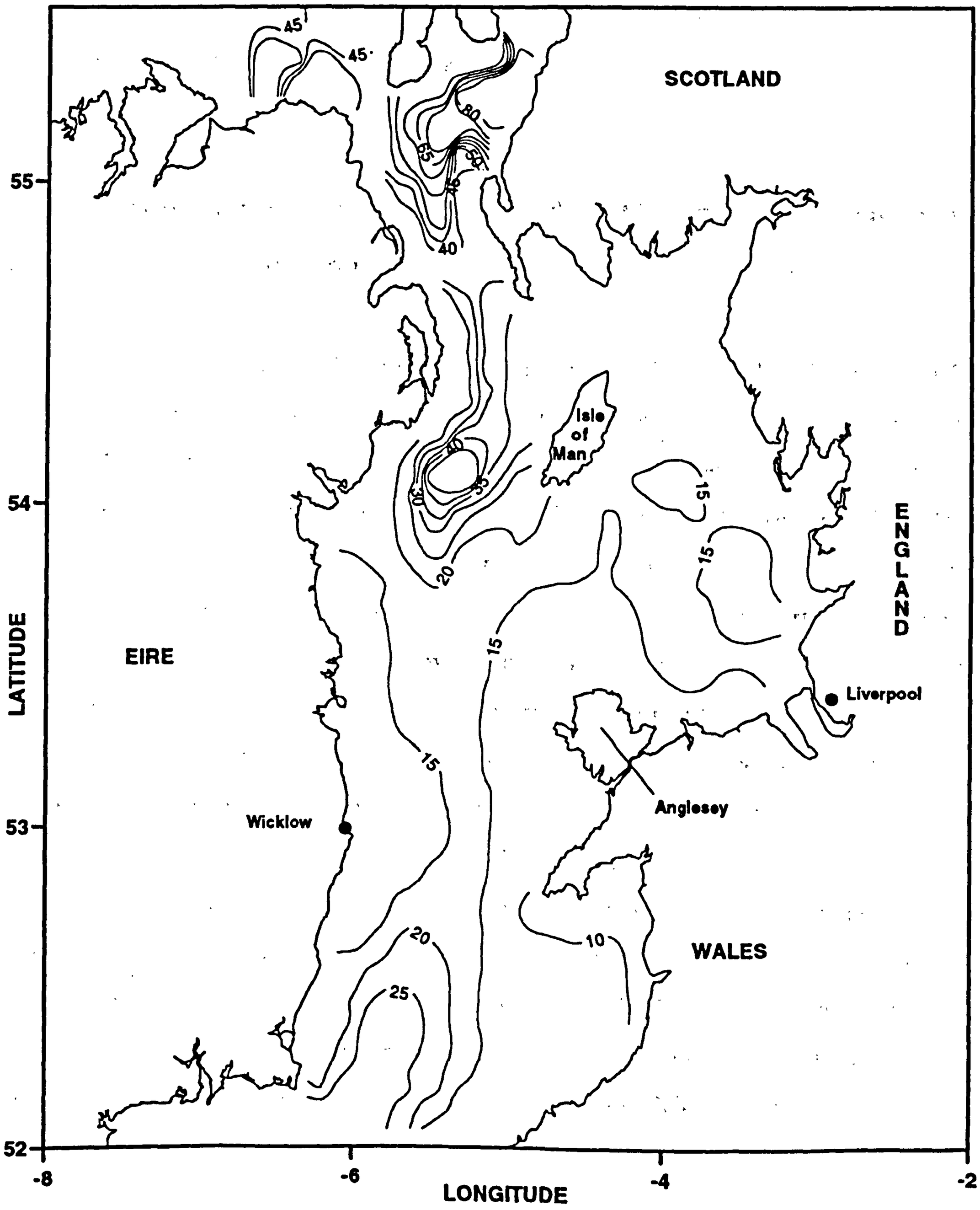

Figure 6.12 Distribution of the confidence range, in days, of the phase of the annual cycle.

is 35-50 %. In some northern areas the seasonal model accounts for very small amounts of the variances. Minimum values of explained variance are almost zero in some parts of northern Irish Sea. In these areas the majority of the observed variance is found at time scales less than seasonal (see Fig. 6.4).

6.3.4 Interpretation of the spatial distributions of the mean and amplitude of the seasonal cycle

The spatial distributions of the mean and amplitude of the annual variation of surface reflectance of the Irish Sea have been established earlier in this section. Simpson and Brown (1987) suggested that SPM concentrations in the northern Irish Sea are strongly dependent on the availability of turbulent kinetic energy (TKE) from the tidal flows. They also suggested that the onset of stratification during the summer months also controls surface SPM concentrations because the vertical flux of particulates into the surface layer is drastically reduced by the presence of the pycnocline. This view has since been supported by Weeks (1989). The role of the pycnocline acting as a barrier to the upward flux of particulates has also been reported by Jones *et al* (1994b) from observations at a seasonally stratified site in the southern North Sea.

The extensive spatial coverage of the present data sets of reflectance, the amplitude of the M_2 tidal currents and the water depth allows some exploration of the processes which may control surface SPM concentrations in the Irish Sea. This was attempted by seeking empirical relationships between the mean and amplitude of the annual cycle and the physical parameters. A simple method for identifying dependency or physical relationships between two different quantities is by plotting scatter diagrams.

First was investigated the relationship between the annual cycle parameters and the amplitude of the M_2 tidal currents, U. No clear relationship has emerged between A and

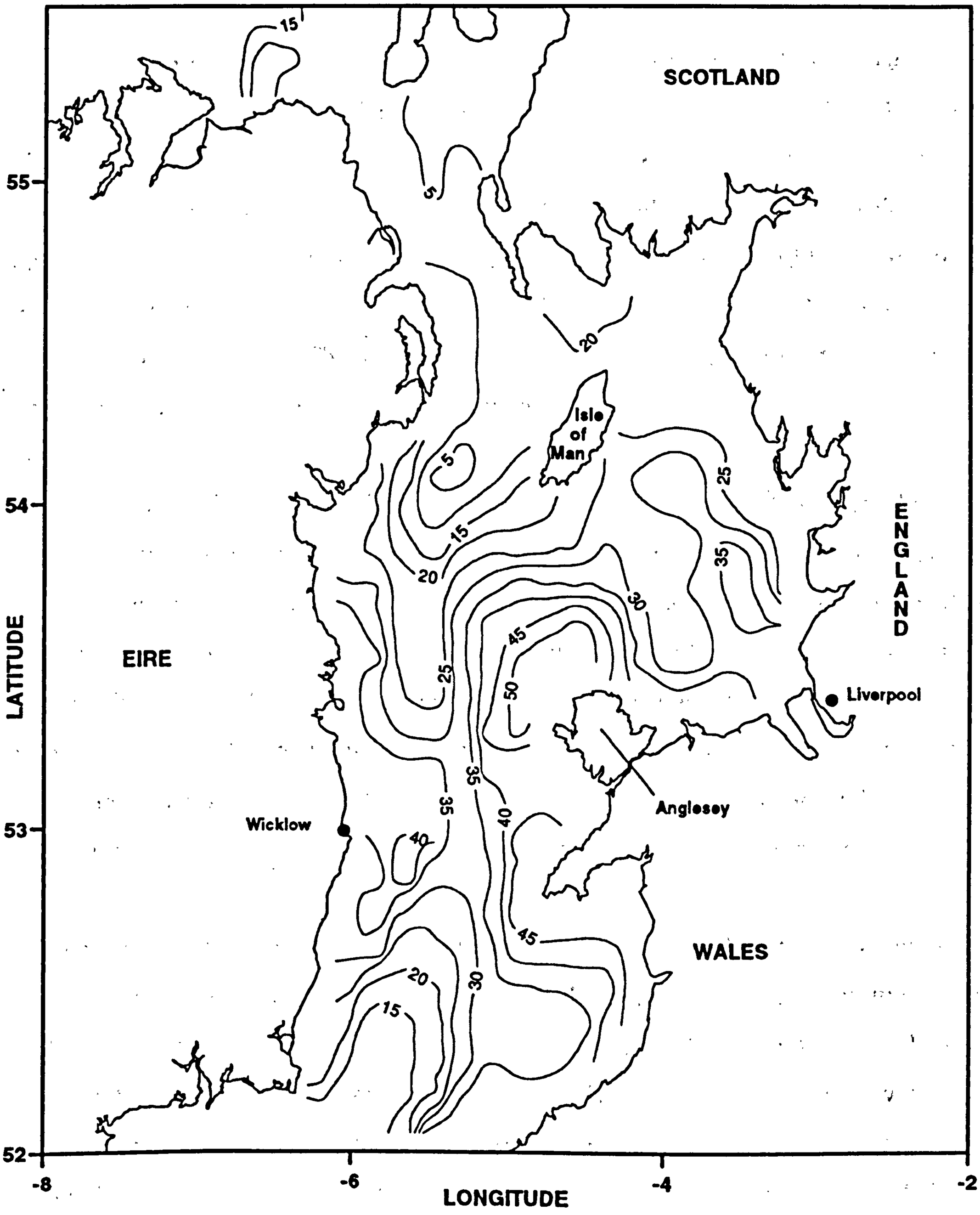

Figure 6.14 Distribution of the percentage of the observed variance explained by the seasonal model, r^2.

U and R_a and U (Fig. 6.15a). It was hypothesised that the relationships between these parameters and U may be dependent on the water depth. To test this hypothesis the data were divided into six depth intervals: 0 to 20 m, 20 to 40 m, 40 to 60 m, 60 to 80 m, 80 to 100 m and > 100 m. The relationships between the annual cycle parameters and U were examined in each depth interval. The scatter plots of A vs U and R_a vs U are shown Figs. 6.16 and 6.17. For h < 20 m the scatter is large for all values of U suggesting that in shallow waters the mean and amplitude of the annual cycle are not dependent on U. As the depth increases a linear trend between A and U and R_a and U becomes apparent. The values of the mean and amplitude for high U's are in general higher in shallower water. This does not hold for depths greater than 100 m. The slope of the linear trend is larger for shallower waters.

The scatter plots of A vs h and R_a vs h in Figs. 6.18 a and b, respectively, exhibit large scatter for low water depths i.e. both low and high values of the mean and amplitude occur in shallow waters. As the depth increases the values of A and R_a tend to decrease. In deep waters only low values of A and R_a are found. To check whether the relationship with the depth was a function of the currents the data were divided into six intervals of U and the relationship between the annual cycle parameters and U was investigated in each interval of U (Figs. 6.19 and 6.20). The mean and amplitude decrease with water depth for all intervals of the tidal current amplitudes.

As mentioned earlier in this section, the availability of turbulent kinetic energy has been suggested as a controlling factor on SPM concentrations. A measure of the available tidal turbulent kinetic energy is the parameter U^3/h (Simpson and Hunter, 1974). If this were the case areas of high tidal TKE would be associated with high annual mean levels of reflectance. Conversely, low tidal TKE would only be able to support low mean levels. This relationship is most evident in Figs. 6.21 and 6.22 for water depths greater than 20 m. This result supports the contention that availability of tidal TKE is a control on the mean SPM concentrations in shelf seas.

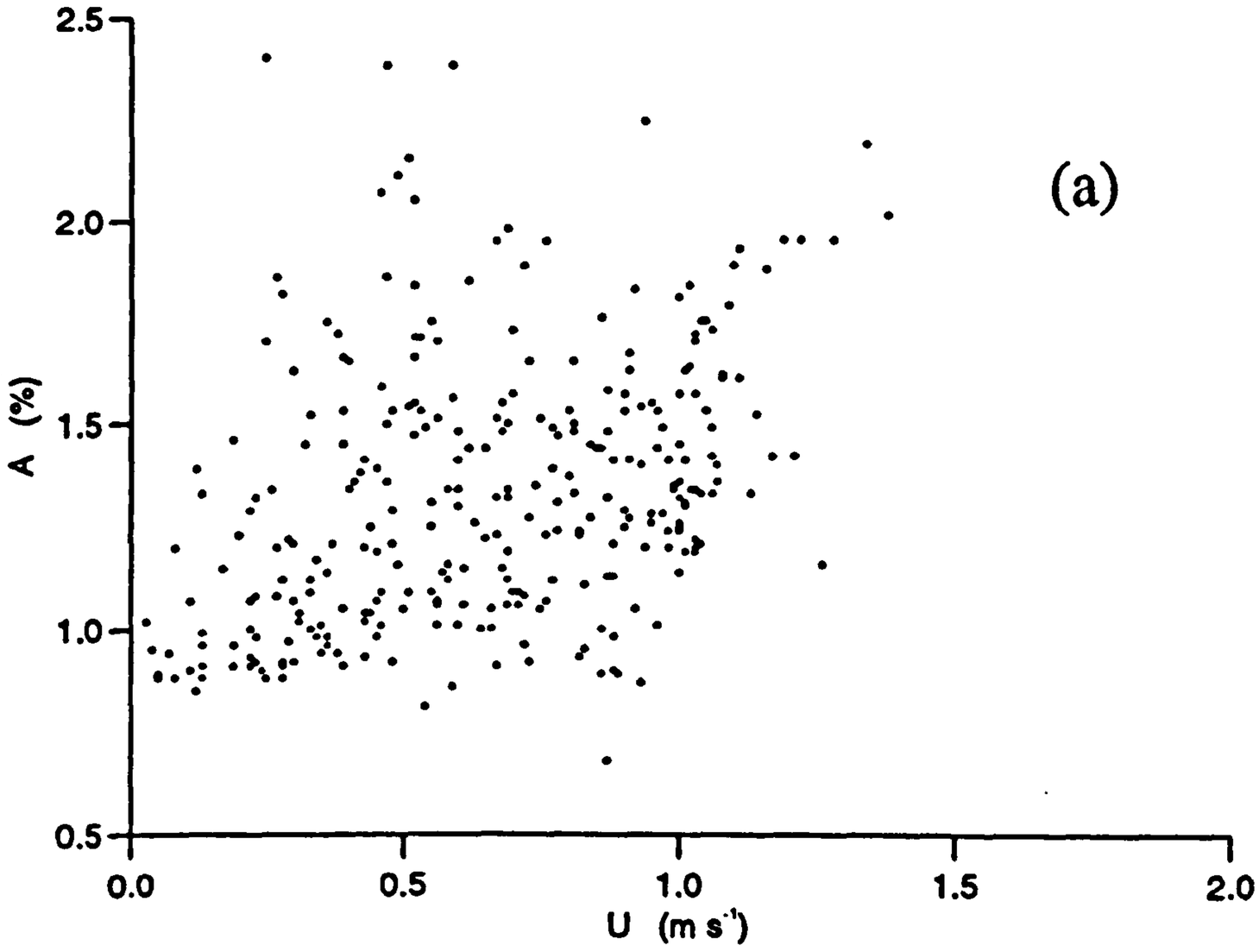

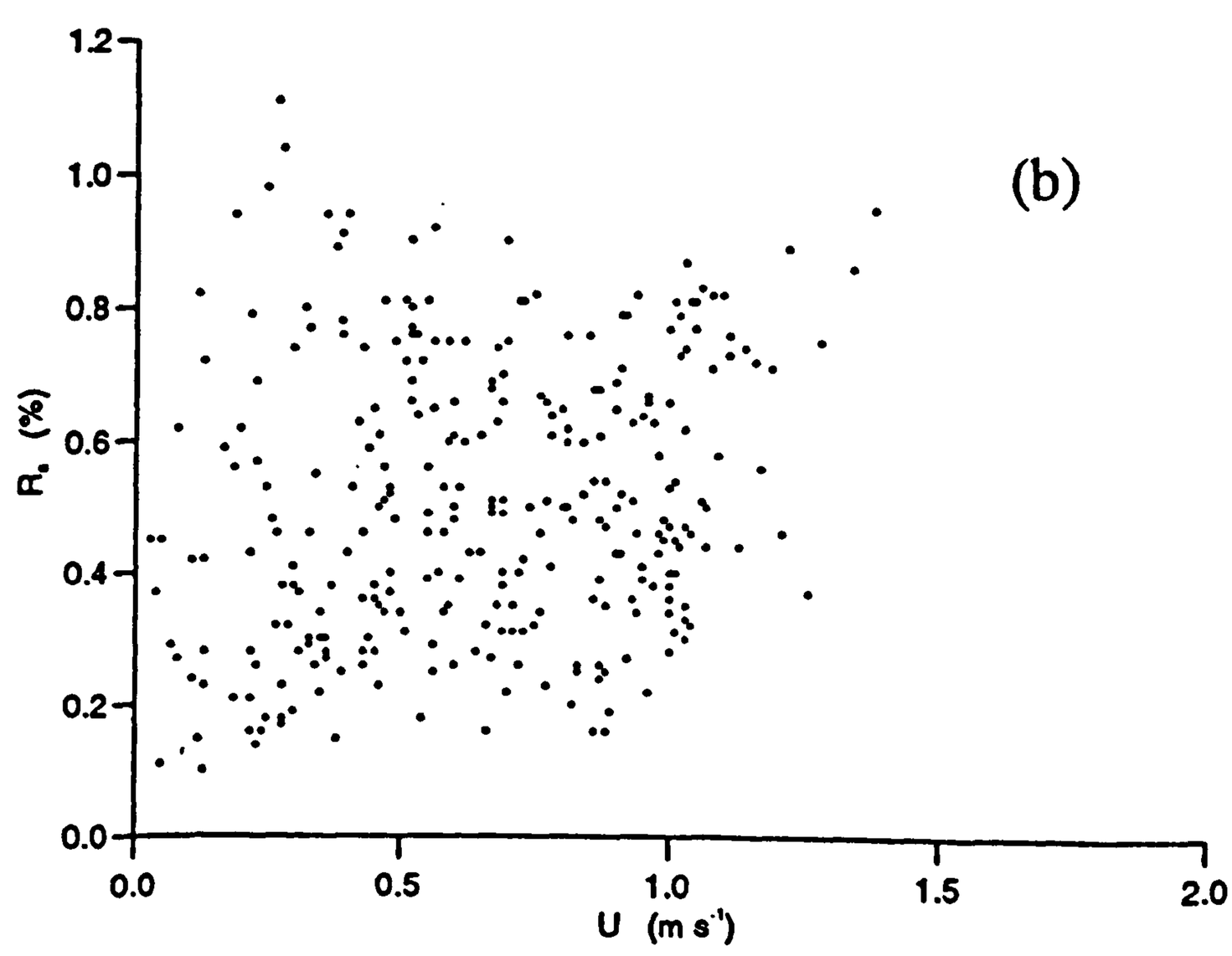

Figure 6.15 Scatter plots of (a) annual mean and (b) amplitude of annual cycle against the M_2 current amplitude.

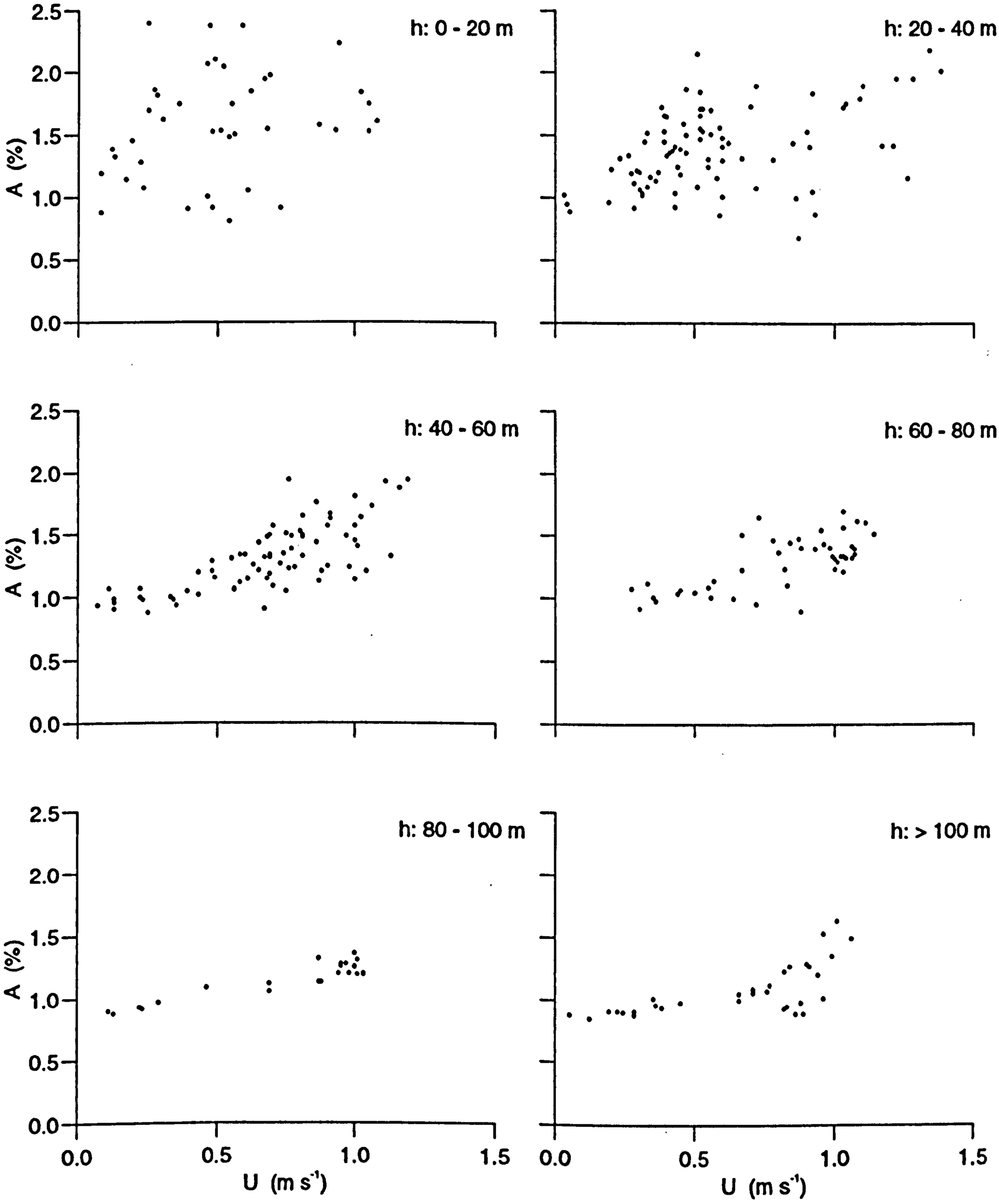

Figure 6.16 Scatter plots of annual mean against M_2 current amplitude for different depth ranges.

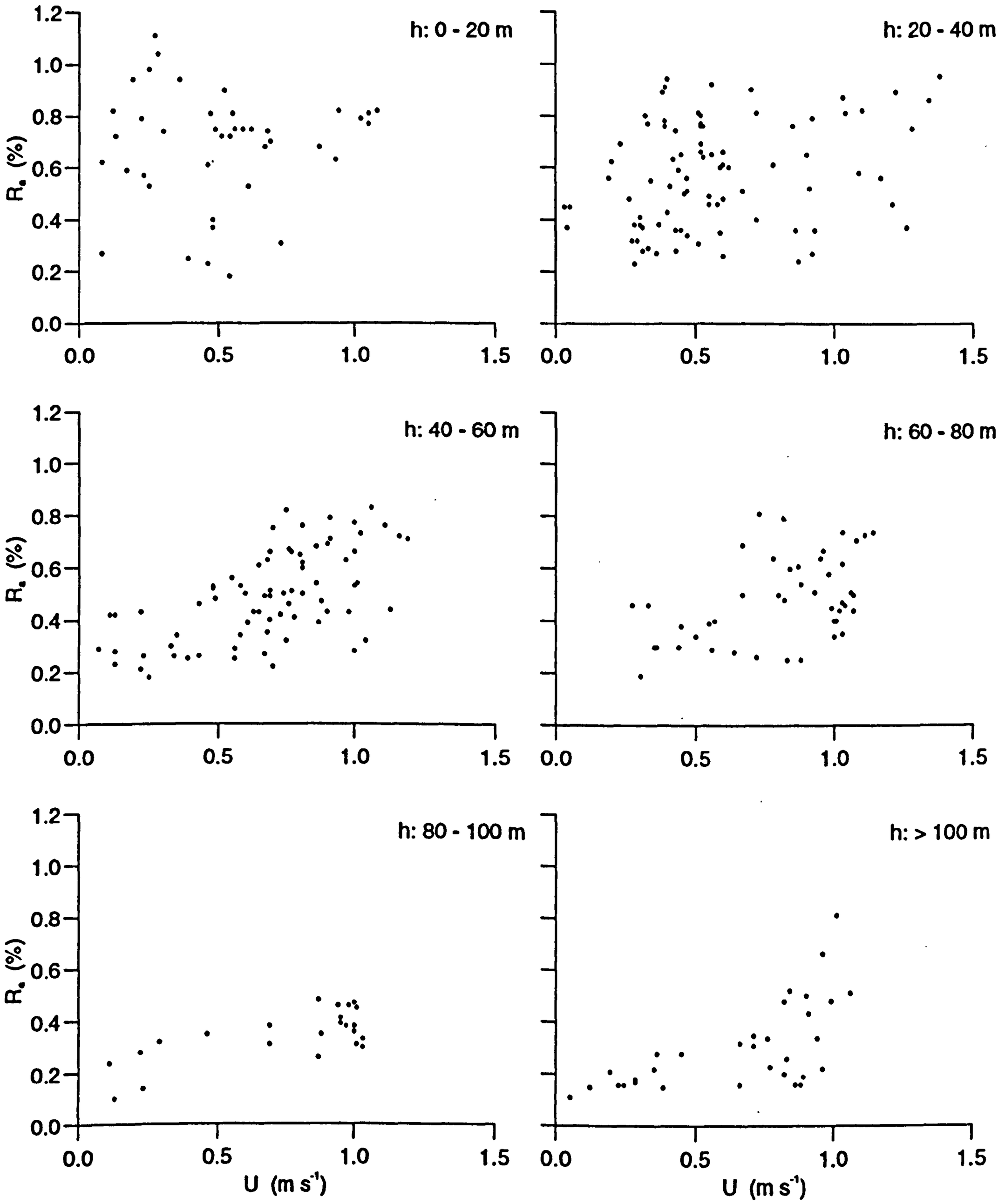

Figure 6.17 Scatter plots of the amplitude of the annual cycle against M_2 current amplitude for different depth ranges.

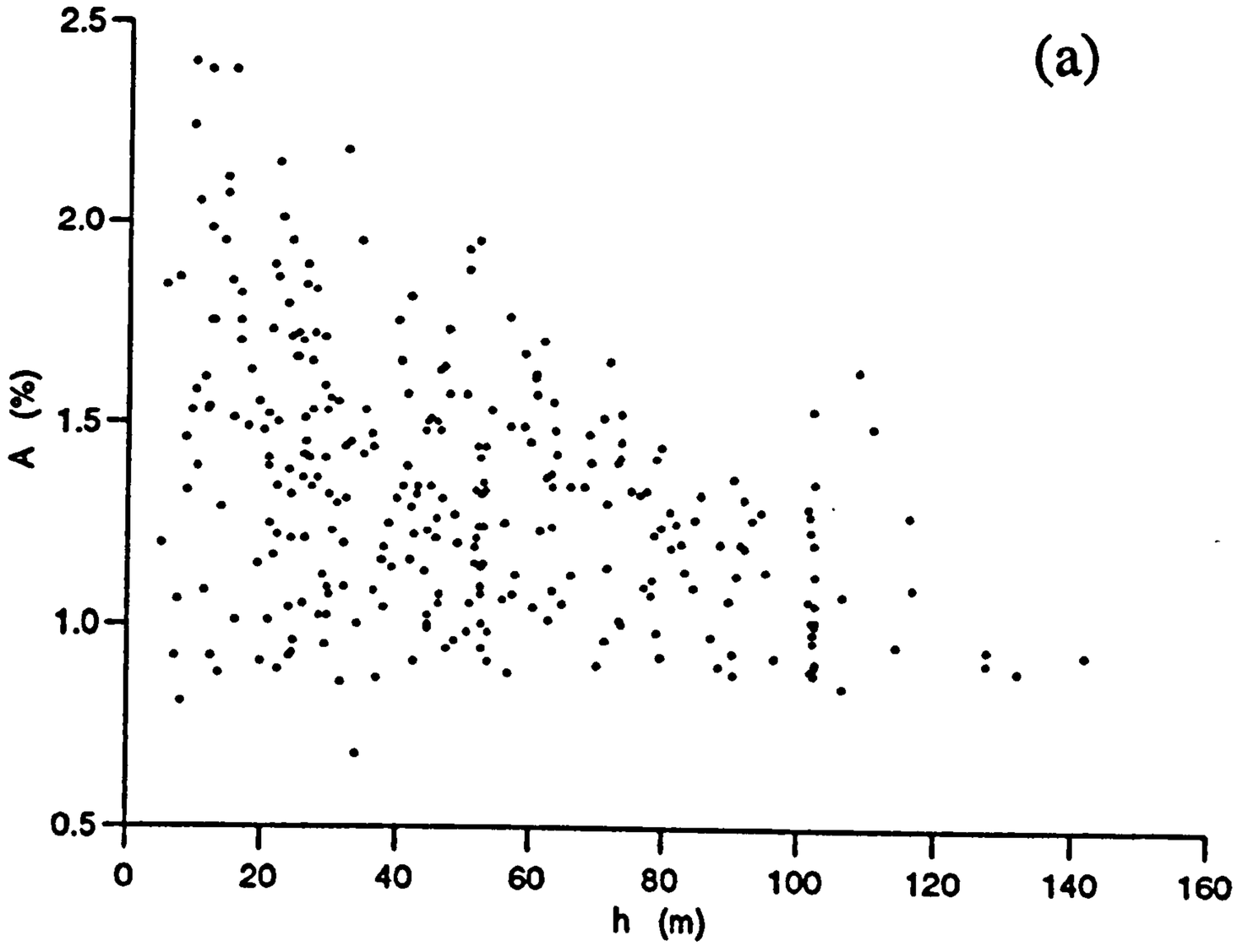

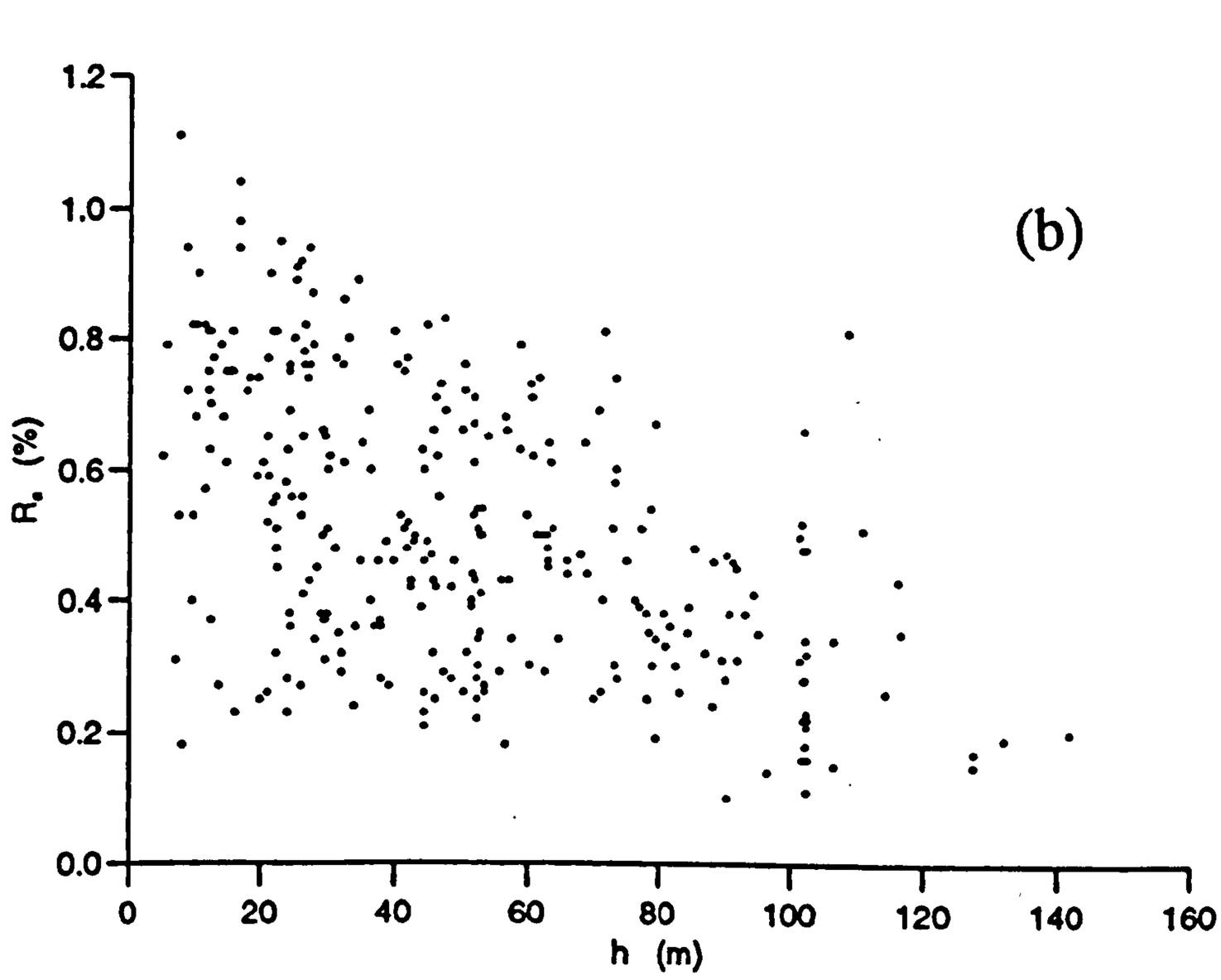

Figure 6.18 Scatter plots of (a) annual mean and (b) amplitude of annual cycle against water depth for all data.

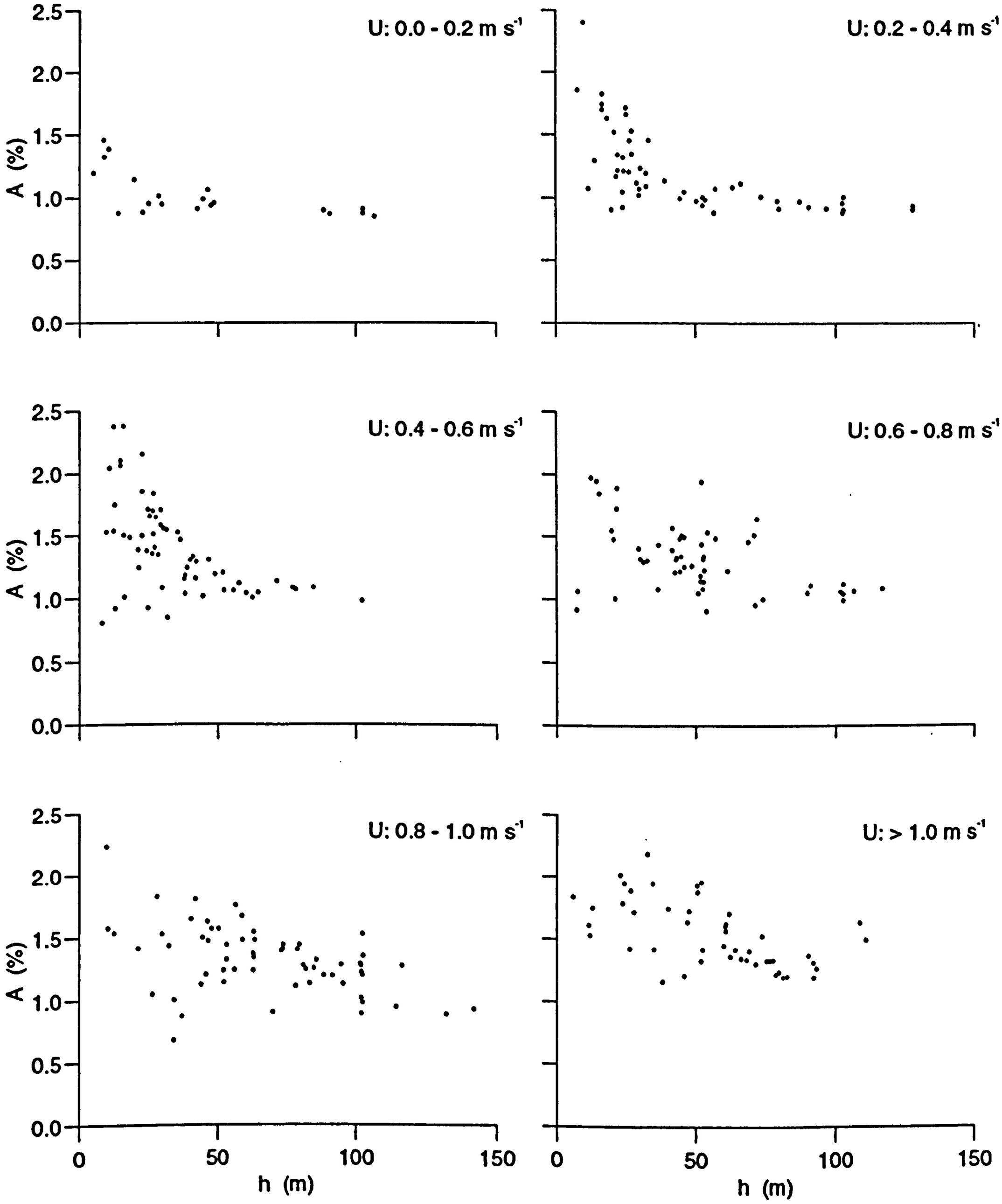

Figure 6.19 Scatter plots of annual mean against water depth for different ranges of M_2 current amplitudes.

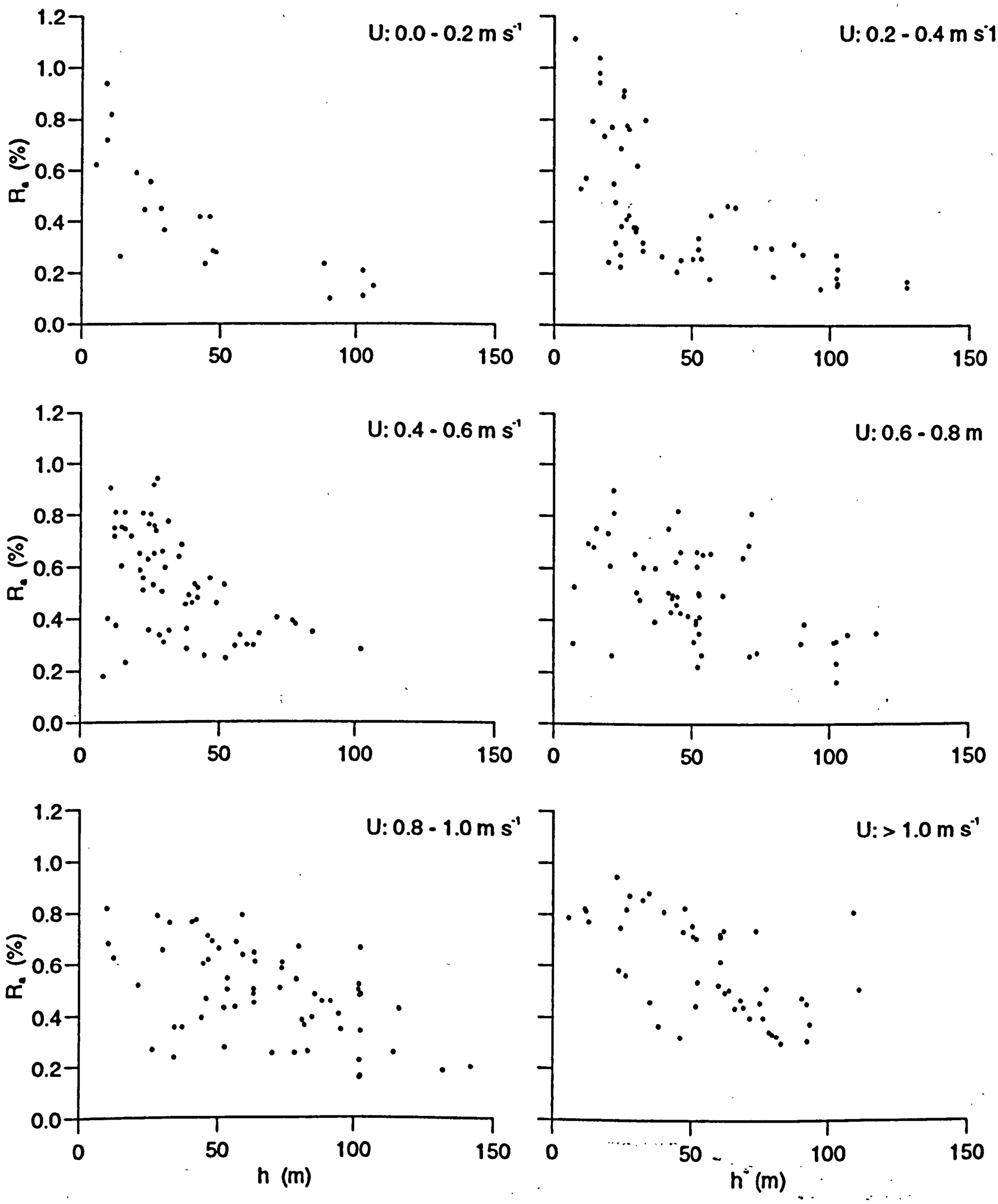

Figure 6.20 Scatter plots of amplitude of the annual cycle against the water depth for different ranges of M_2 current amplitude.

6.4 Spring-neap cycle of surface reflectance in the Irish Sea.

There is some in-situ evidence that suspended sediment concentrations in shelf seas respond to the spring-neap cycle (e.g. Buchan *et al*, 1967; Weeks, 1989). Intuitively, it would be expected that the stronger tidal currents associated with springs would, through enhanced bed shear stress, erode more sediment from the seabed and also, bring sediment already in suspension closer to the surface. This variation may be especially important in a tidally dominated environment such as the Irish Sea.

No evidence of a spring-neap variation in surface reflectances from satellite data has been reported. This is not surprising because the cloud cover means that continuous time-series of imagery are hard to come by. However, with the large data of this study set it may be possible to find evidence of a spring-neap dependency in the surface reflectances. In this section the question asked is: Is the reflectance, on average, higher at spring tides than at neaps?

6.4.1. Statistical model for the spring-neap cycle in reflectance.

A linear statistical model was used to study the spring-neap variation of reflectance. The seasonal cycle of reflectance as predicted in section 6.3 was subtracted from the composite annual time-series at each grid cell. The fitted model was of the form:

$$R_{ij}(t) = \alpha_{ij} + \beta_{ij} F(t) \qquad (6.10)$$

where R' is the reflectance after removing the seasonal variation and F is a tidal range factor. F is defined as the ratio of the tidal range at Liverpool on the day of the image to the tidal range at Liverpool at mean neap tides (taken to be 4.5 m). Therefore, F is 1 at mean neaps and increases to over 2 at large spring tides. The tidal range at

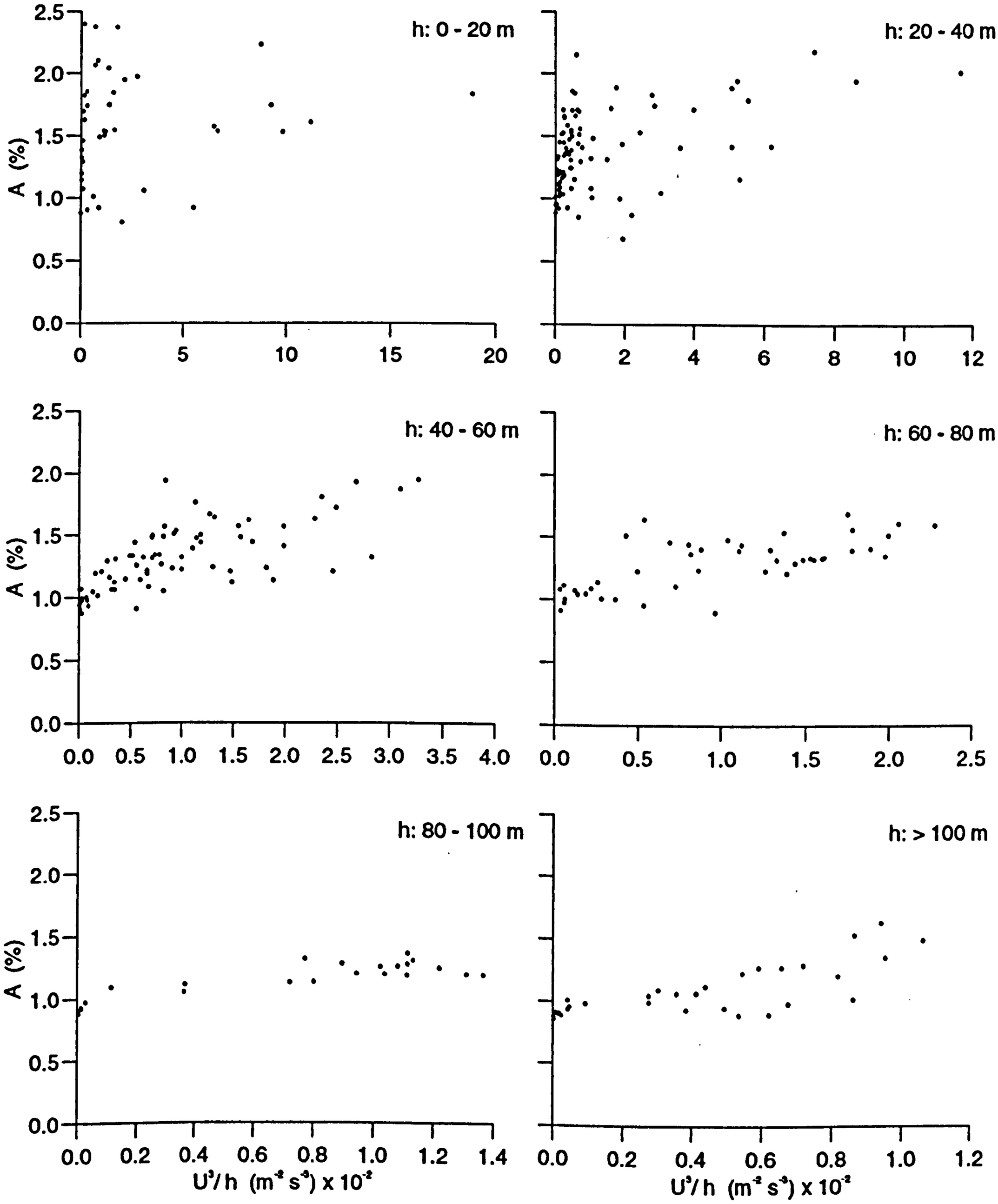

Figure 6.21 Scatter plots of annual mean against U^3/h for different depth ranges.

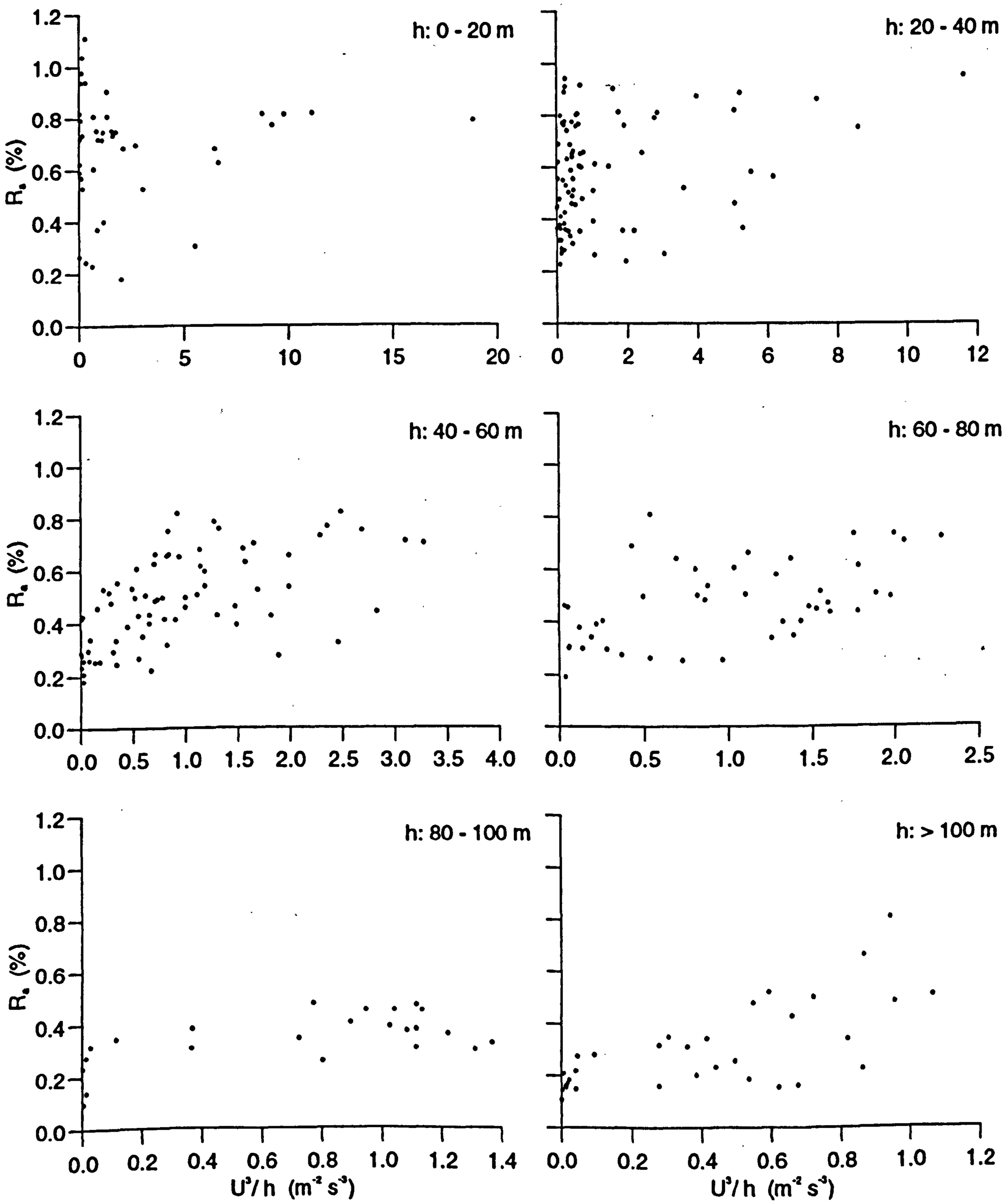

Figure 6.22 Scatter plots of the amplitude of the annual cycle against U^3/h for different depth ranges.

Liverpool on the day of each image was used for the whole Irish Sea as spring and neap tides occur at the same time throughout the region. The tidal ranges were taken from the Admiralty Tide Tables. Here, again, the subscripts i and j are used in the defining equation to indicate the spatial dependency of the parameters, but are dropped in later expressions. For each grid cell the model coefficients, β and α, were determined by least squares fitting.

6.4.2 Results of the spring-neap model.

The fitted values of β and its confidence range are shown in Figs. 6.23 and 6.24, respectively. There is a significant spring-neap cycle over large areas of the Irish Sea, most notably: the central and southern regions; Liverpool Bay and Cardigan Bay (Fig. 6.25). In the significant areas β is positive (indicating higher levels of reflectance at springs) and of the order of 0.4 %. Such a value of β indicates a neap to spring variation in reflectance of 0.64 % (taking F at springs = 2.2 and F at neaps = 0.6). In the other large area of significant spring-neap variation (to the north of the Isle of Man) β is slightly lower at 0.2 % and produces a neap to spring variation of 0.32 %.

No significant spring-neap variation is seen in the remainder of the Irish Sea, most notably the area to the west and south-west of the Isle of Man. The negative values off the Irish coast are not significant and, hence, do not suggest lower reflectances at springs.

The amount of the variance explained by the spring-neap variation is generally low (Fig. 6.26). The highest values of r^2 are 10 % and are found in the central Irish Sea. The low values of r^2 are due to the amount of scatter in the data. The scatter and the differing importance of the spring-neap variation is better seen as plots of reflectance against tidal range. Such plots for the eight selected sites mentioned in the earlier part

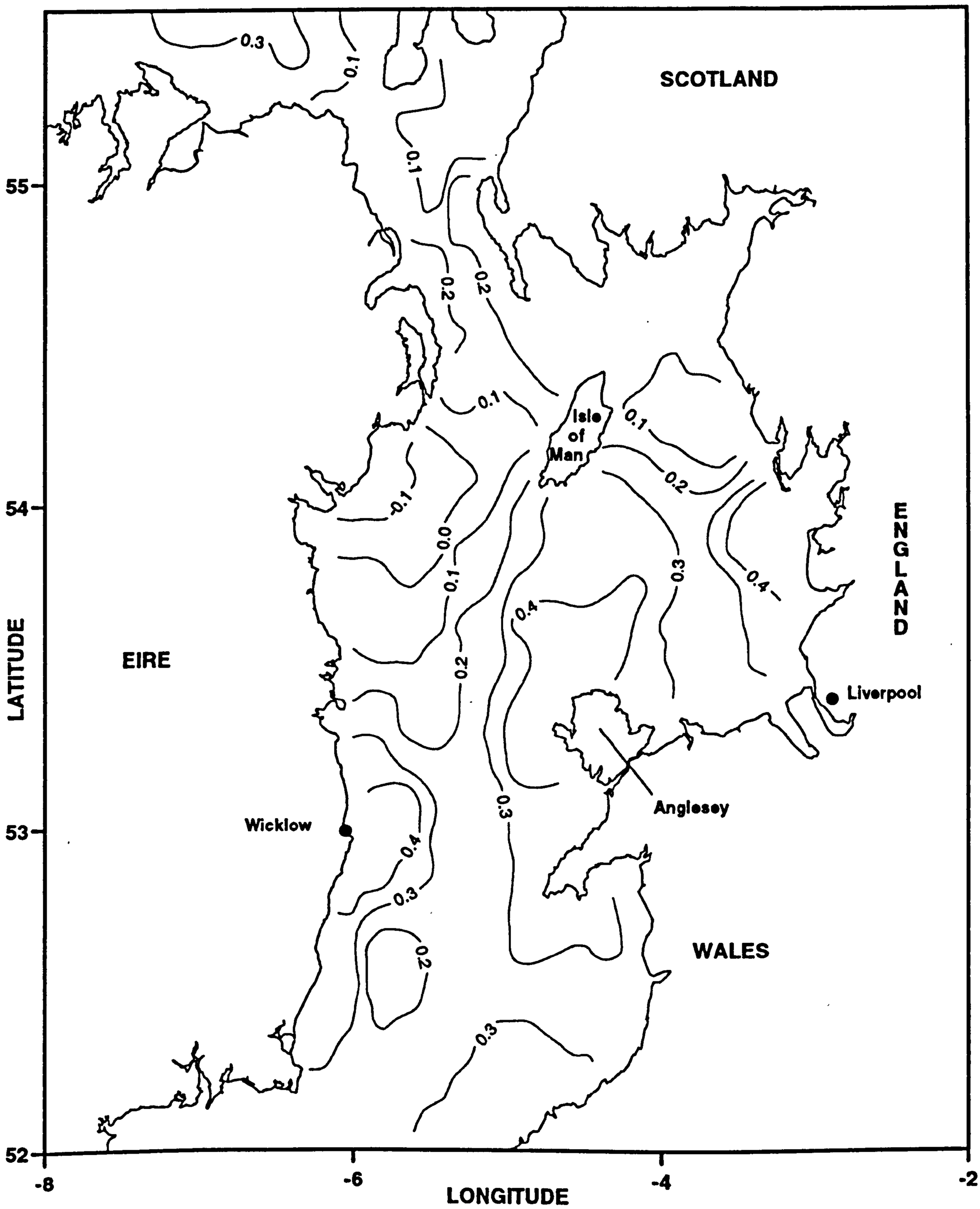

Figure 6.23 Distribution of the regression coefficient, β, in the spring-neap model (%).

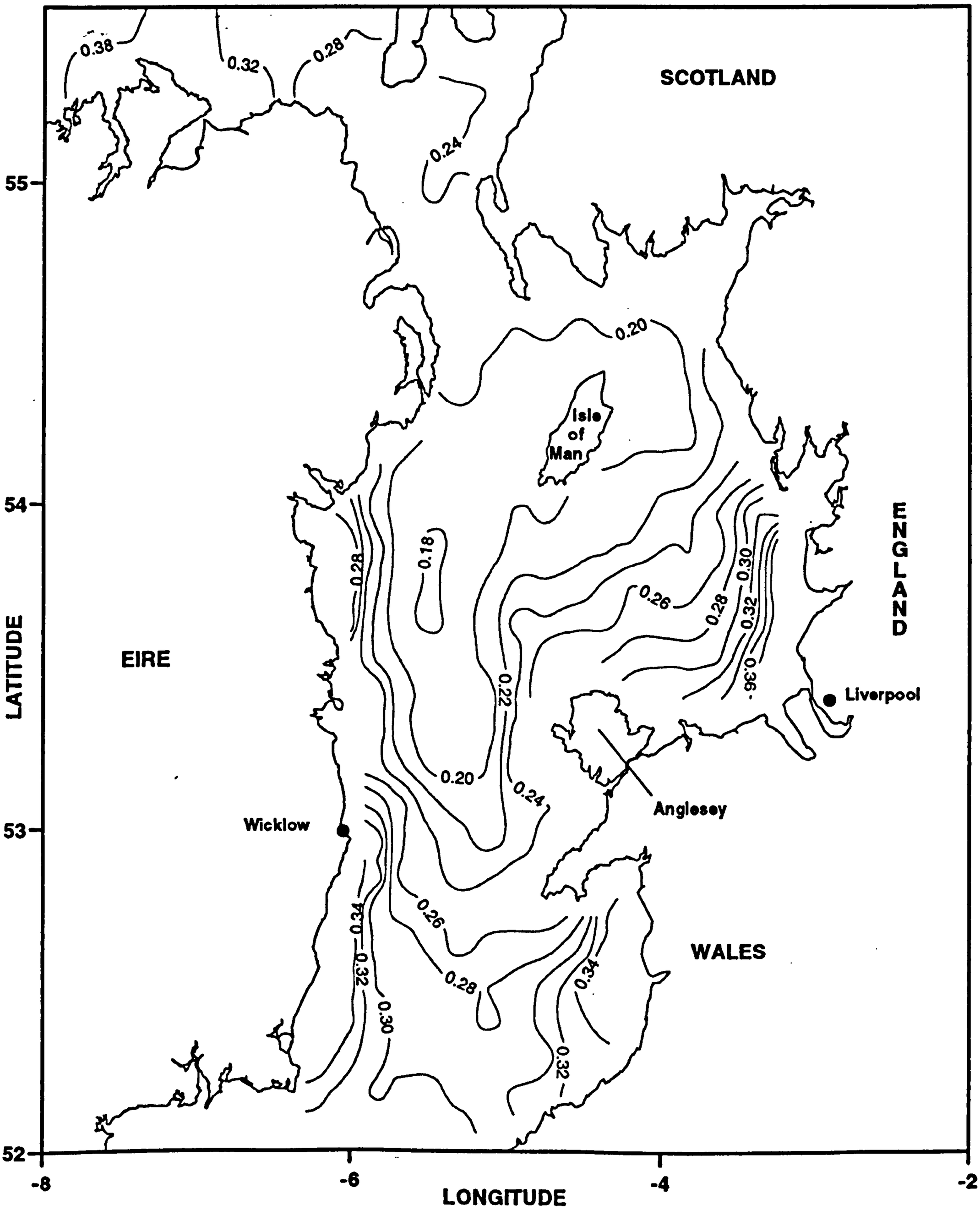

Figure 6.24 Distribution of the confidence range for the spring-neap regression coefficient (%).

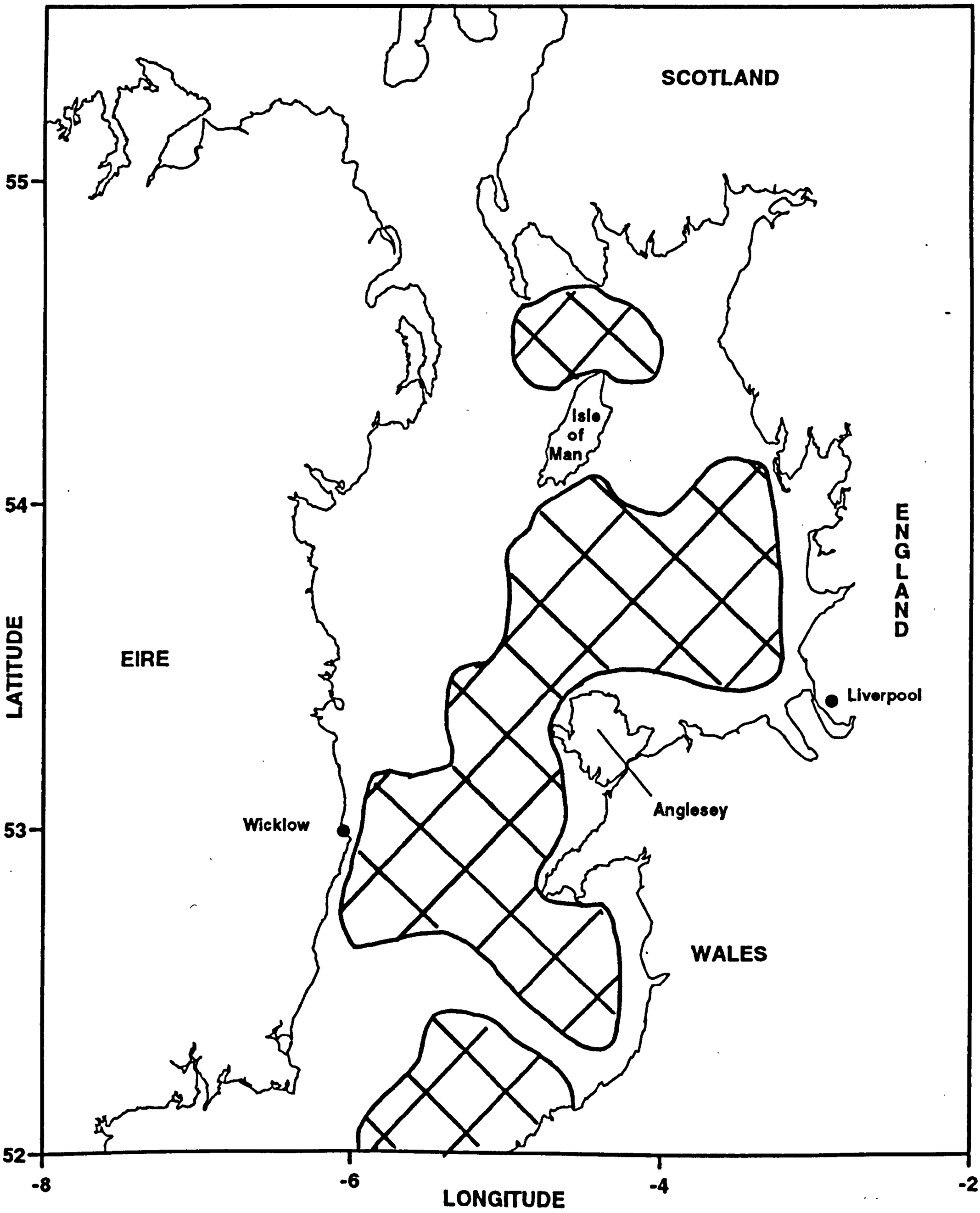

Figure 6.25 Distribution of the significant values of the spring-neap regression coefficient. Significant values are found in the shaded areas.

of this chapter are shown in Fig. 6.27. Even for the sites with significant β's i.e. the gradient, there is a large amount of scatter about the regression line which is of a comparable magnitude to the spring-neap variation. Such scatter is a combination of noise and the presence of other driving processes.

6.5 Discussion

The satellite data have revealed the spatial and temporal variations of the surface reflectance of the Irish Sea. The horizontal distribution is characterised by well defined areas of high and low reflectances throughout the region. The spatial patterns are consistent from year to year over the study period and are similar to known surface SPM distributions.

It has been shown that the surface reflectance of the Irish Sea undergoes a seasonal variation. The spatial distribution of the magnitude of this variation has also been established. The annual means show a well defined distribution of localized areas of high values separated from areas of low values by strong horizontal gradients. However, this is not the case for the high values in Cardigan Bay where there is a gradual transition from the high values of the bay to the lower values in the deeper channel. The distribution of the amplitude of the seasonal cycle is similar to the spatial distribution of the annual mean i.e. areas of high means undergo a stronger seasonal cycle than areas of low means. The horizontal gradients of the amplitude are weaker than those of the annual mean. The maximum reflectances occur early in the year and the minimum in the summer.

In some parts of the Irish Sea the surface reflectance is clearly seen to respond to the spring-neap tidal cycle i.e. spring tides are associated with higher values than neaps. The stronger currents at springs cause enhanced bed shear stresses which in turn cause greater resuspension of sediments. As well as increased bed shear stresses, springs are

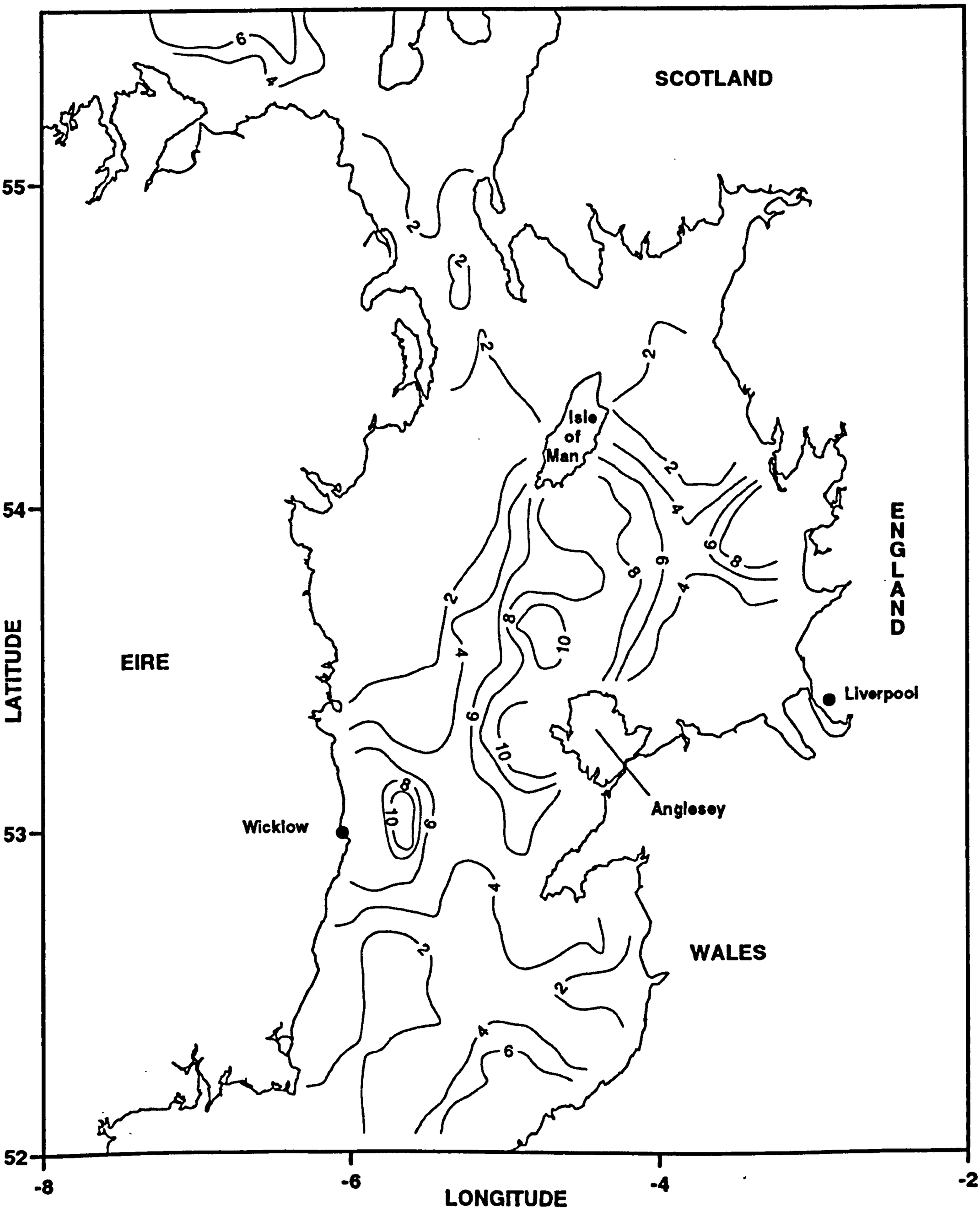

Figure 6.26 Distribution of the percentage of the variance of the observations (after the seaonal cycle has been subtracted) explained by the spring-neap model.

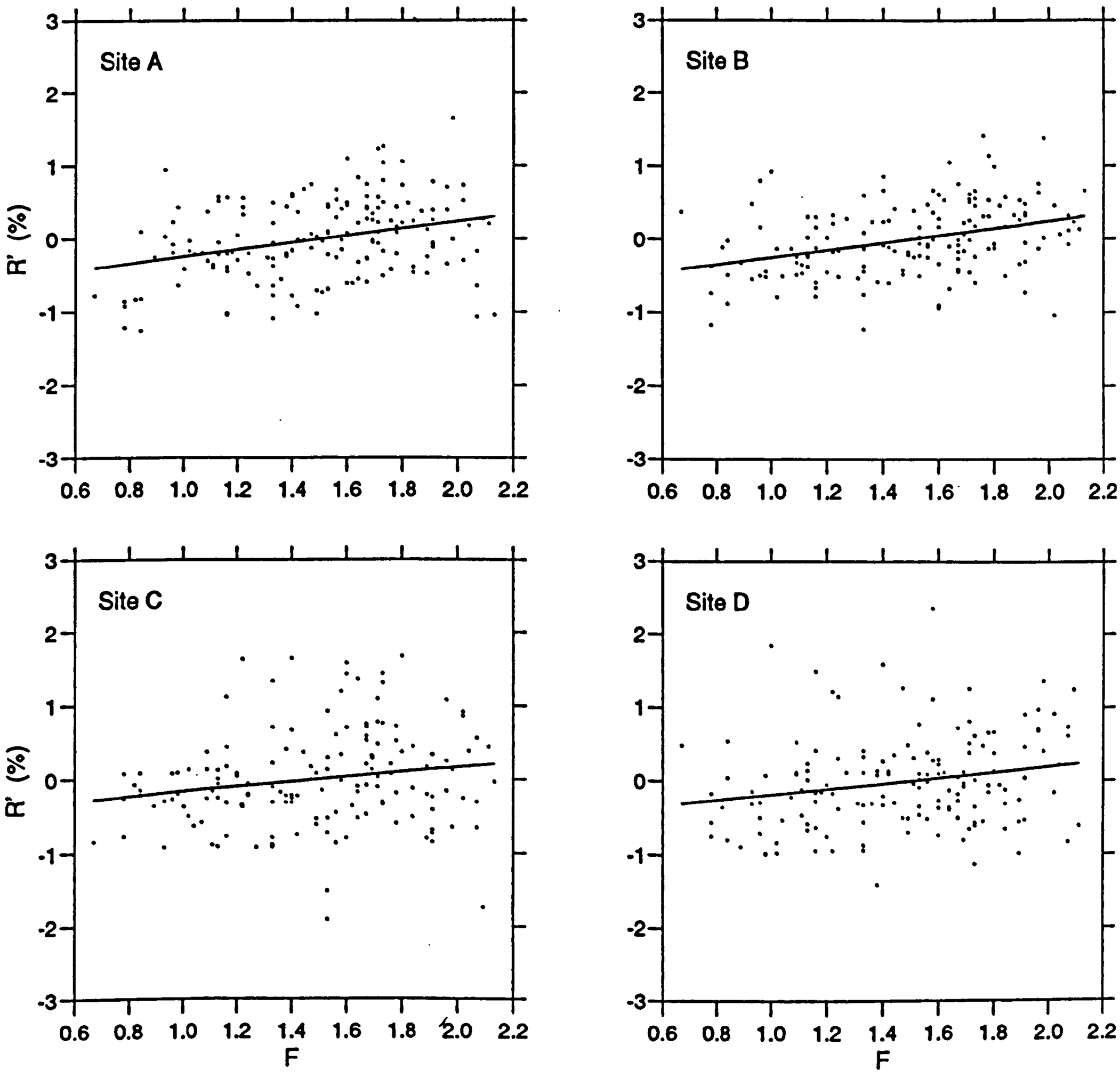

Figure 6.27 Scatter plots of reflectance (annual cycle has been subtracted) against tidal range, F, for selected sites.

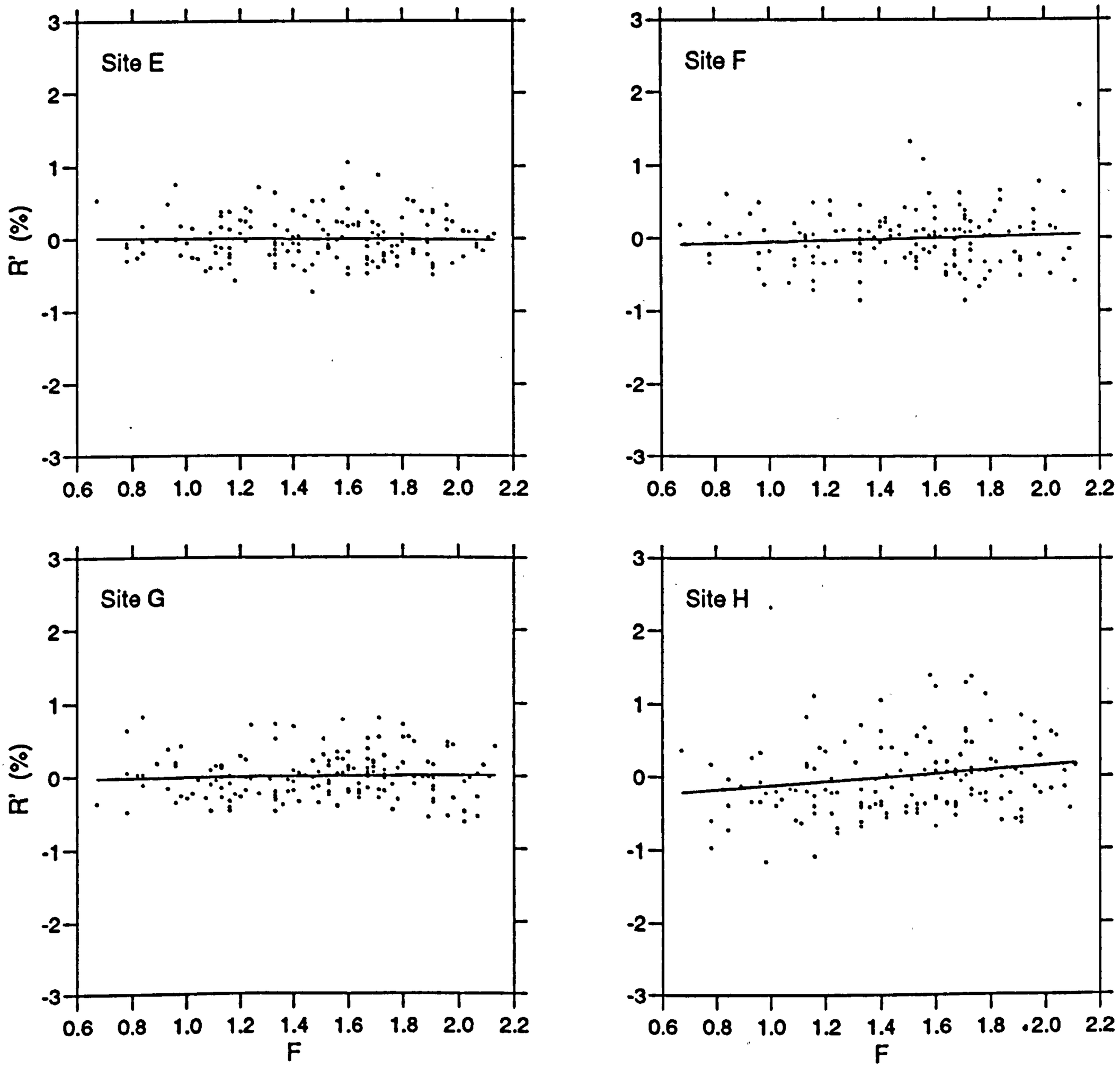

Figure 6.27 (continued) Scatter plots of reflectance (annual cycle has been subtracted) against tidal range, F, for selected sites.

associated with higher levels of turbulent kinetic energy leading to enhanced vertical mixing, throughout the water column. The vertical flux of already suspended sediment may, therefore, be also enhanced, increasing the sediment concentrations higher in the water column.

When the two separate variations are considered together up to 60 % of the observed variance in the surface reflectance can be explained (Fig 6.28). These maximum values are found off the north west coast of Anglesey. Of course, with the seasonal signal accounting for the larger component of variance the r^2 pattern for the combined effect closely resembles the pattern for the seasonal cycle alone. The combined seasonal and spring-neap variations account for the least amount to the east of Isle of Man: as low as 5 % of the variance is accounted for in this area.

The results of this chapter have indicated that the annual mean reflectance is dependent on U^3/h. This suggests that the availability of tidal TKE is a control on the annual mean. The relationship between A and U^3/h is linear for water depths greater than 20 m. This implies that areas where the availability of tidal TKE is high have larger means than areas with lower levels of TKE.

The results have also indicated that the amplitude of the seasonal variation of reflectance is correlated to the availability of tidal TKE. This suggests that in areas where the availability of tidal TKE is high the reflectance undergoes a larger seasonal variation than in areas where the availability tidal TKE is low. This correlation is not as easily understood as the relationship between TKE and the annual mean. The parameter U^3/h is a constant for any position, therefore, it is not immediately obvious why the amplitude of the annual variation should depend on it. This suggests that there is a secondary control or process involved.

The observed correlation between the available M_2 TKE and the seasonal amplitude can be understood if the availability of sediment were to vary over the year. If the total

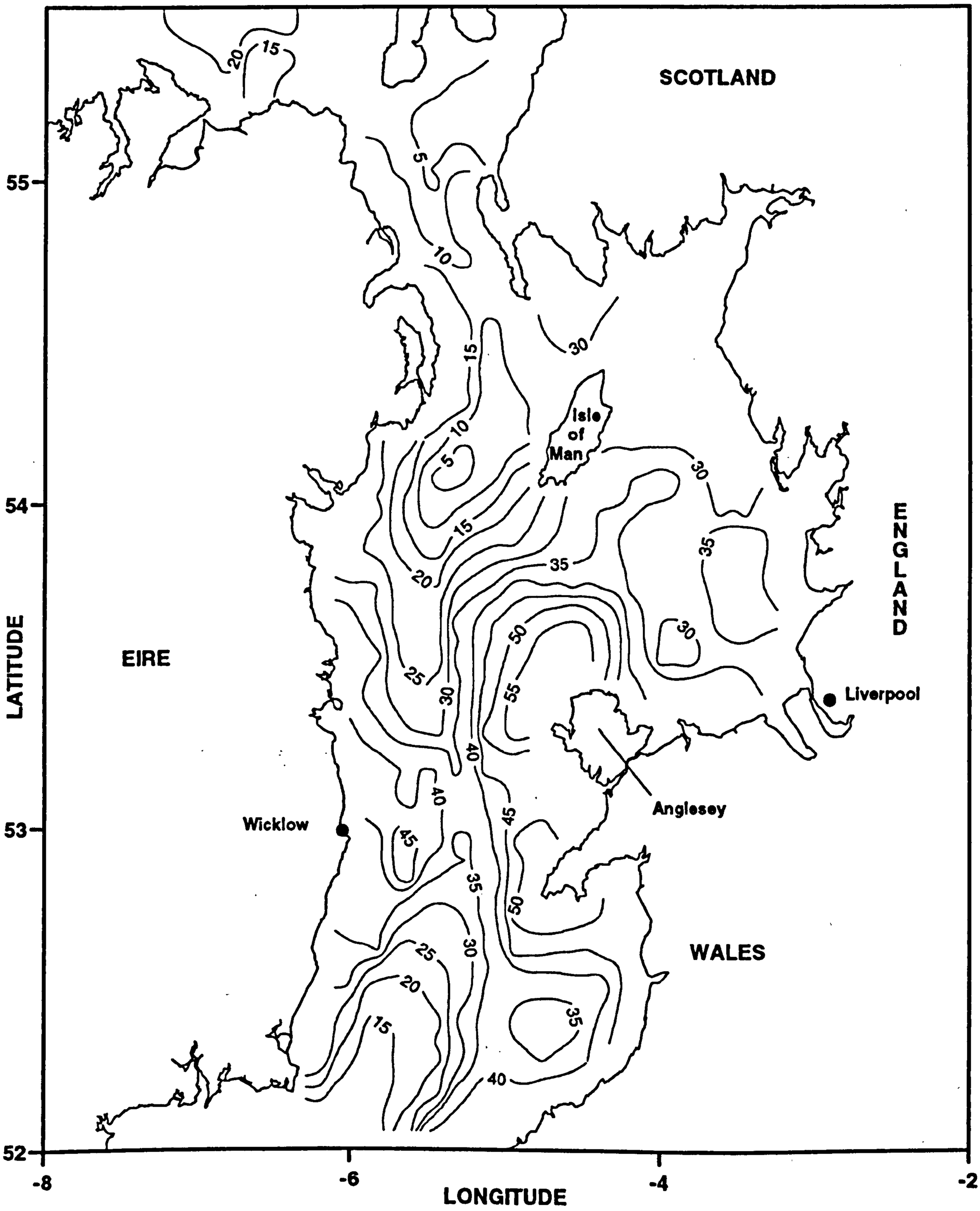

Figure 6.28 Distribution of the explained variance, r^2 (%), for the combined effects of the seasonal and spring-neap cycles.

amount of sediment in suspension and on the seabed was greatly reduced in the summer, then, irrespective of the level of available TKE to drive the resuspension, surface SPM concentrations would be reduced. During the winter, if available sediment levels were large then the concentrations would be related to the level of tidal energy. Hence, in a scenario where availability of sediments controlled surface concentrations in the summer, but availability of tidal TKE was the controlling factor in winter the amplitude of the seasonal cycle would be, as observed in this study, dependent on the parameter U^3/h.

Variations in the amount of available sediment may be due to either a decrease in the total sediment load of the Irish Sea or the sediment present becoming harder to resuspend in the summer. Buchan *et al* (1967) suggested that in the summer microorganisms secrete mucus which increases the binding of particles. If this were so, the sediments would become less readily eroded leading to decreased availability during the summer and hence a larger seasonal signal.

The storm events associated with winter produce periods of high wind speeds. These high wind speeds impart energy to the water column and hence, enhance the bed shear stresses. During these periods SPM concentrations increase as a result of enhanced resuspension. These episodes of high resuspension are more important in winter, hence, contributing to the seasonal variation of SPM concentrations.

If seasonal stratification were to affect surface SPM concentrations, then it would reduce the levels of sediments in the summer. If the trapping of particulates below the pycnocline were important it should be more noticeable in areas which have high winter concentrations. Conversely, in areas of low winter surface SPM concentrations the seasonal cycle is small and so this mechanism would be less noticeable if present. In the Irish Sea the only region which seasonally stratifies and has high values of reflectance in winter is Cardigan Bay. In this case the trapping of particulates below the pycnocline can not be discounted. This process would be less noticeable in the other

seasonally stratified areas because they have low winter values of reflectance.

This study was concerned with identifying the spatial distribution of SPM concentrations and exploring the physical mechanisms responsible. The work was not concerned with establishing the role of seabed sediment types in controlling the spatial distributions of SPM. However, this may be important in controlling SPM patterns and to conclude this chapter a comparison was made between seabed sediment types and the spatial distributions established in this chapter.

The surface suspended particulate matter is either locally resuspended from the seabed or advected into the region where they are observed. If advection processes are assumed to be negligible then the surface SPM values should reflect the type of sediments on the seabed. In general, areas of high means and high amplitudes are seen to be associated with sandy seabed sediments e.g. Liverpool Bay and Cardigan Bay (Fig. 2.6). The large area of mud south-west of the Isle of Man is within the region which exhibits the lowest means and amplitudes. Mud is more cohesive than sand and as such is less readily resuspended as more work needs to be done to overcome the binding forces. This comparison tentatively suggests that indeed seabed sediment type may need to be considered in this problem.

CHAPTER 7

Beam Attenuation Measurements in Liverpool Bay

7.1 Introduction

The satellite data have shown a significant seasonal cycle in the surface reflectance of the Irish Sea. A spring-neap variation was also evident in parts of the Irish Sea. In Liverpool Bay strong horizontal gradients were consistently seen in the images: surface reflectance values increased eastward. In order to corroborate these findings time-series of beam attenuation were collected at two sites in Liverpool Bay. The collection of beam attenuation at different depths allows the assessment of how representative the surface reflectance is of the whole water column.

Transmissometers have been widely used for monitoring particle distributions in the water column (Heathershaw and Simpson, 1974; Spinrad *et al*, 1983; Baker *et al*, 1983; Lavelle *et al*, 1984; Halper and McGrail, 1988; Grabemann and Krause, 1989; Weeks, 1989; Gardner and Walsh, 1990). They provide continuous measurements of beam attenuation which can be converted into mass or volume concentration of suspended particulate matter (SPM). The linear relationship between beam attenuation and particle concentration is derived empirically and is usually site specific. This results from the fact that the beam attenuation depends not only on particle concentration but also on the particle population characteristics, namely: size, shape, and refractive index (Baker and Lavelle, 1984; Moody *et al*, 1987; Jonasz, 1987).

The concentration of suspended particulate matter in coastal waters generally exhibits significant spatial and temporal variations which are determined by a variety of physical and biological processes. Many investigations have shown that SPM concentrations in

estuarine and coastal waters exhibit tidal variations which were characterised by a time lag between the concentration and the current speed. Data collected off the North Yorkshire shelf showed that on spring tides the highest concentrations near the bottom occurred at peak currents whereas on neaps the concentrations lagged 30 min behind the currents (Jago, 1981). In contrast, neither the surface nor the mid-depth concentrations exhibited significant tidal variations. Lavelle *et al* (1984) observed a 15 min time lag between SPM concentrations and current speed at 5 m from the bed in the main basin of Puget Sound, Washington. The near simultaneity of concentration and current speed maxima was attributed to local erosion. Observations made by Nichols (1984) in Rappahannock estuary revealed semidiurnal fluctuations in SPM concentrations near the bed with maxima in concentrations occurring near, or slightly after, peak flood and ebb current. Postma (1967) suggested that the time lag between SPM concentrations and currents can be explained by scour (a certain time is required for accelerating flow to stir up sediment and carry it higher in the water column) and settling (time taken for suspended particles to settle after the current speed has decreased to that required for settling to occur) lag effects.

Fortnightly variations in SPM concentrations in the Menai Straits have been reported by Buchan *et al* (1967). During springs SPM concentrations were of the order of 50 mgl^{-1} compared to 5 mgl^{-1} during neaps. Similar variations in SPM concentrations were also observed in the Dover Strait (Jones *et al*, 1994a), at a well-mixed site in the southern North Sea (Jago and Jones, 1994), and in the Rhine ROFI (Simpson *et al*, 1993). Beam attenuation time-series from a well-mixed site in the Irish Sea exhibited a springs-neaps variation in the spring and autumn but not in the summer (Weeks, 1989).

Superimposed on the tidal variations are seasonal variations of SPM concentrations which are not universally present. Buchan *et al* (1967) attributed the seasonal variation of SPM concentrations in the Menai Straits to bioproductivity. High concentrations in winter and low ones in summer were observed by Newton and Gray (1972) off the

coast of North Yorkshire. These differences were attributed to changes in wave activity between winter and summer. The onset and disruption of thermal stratification may cause a seasonal cycle in SPM concentrations by trapping sediments below the pycnocline during the summer months (Weeks, 1989). Concentrations of SPM in Eastern Long Island Sound showed a seasonal variation which was partly attributed to seasonal variations in Connecticut river discharge and partly to wind stress (Bohlen, 1975). Measurements in the Irish Sea showed that SPM concentrations in mixed and frontal regions decreased by as much as 50 % from late May to August 1982 (Agnew, 1983; Mitchelson, 1984). Weeks (1989) observed a strong seasonal cycle of beam attenuation and SPM concentrations in the northern Irish Sea, particularly in mixed water.

During storms, resuspension of bottom sediments and transport of suspended matter over continental shelves are greatly intensified (Rodolfo *et al,* 1971; Lavelle *et al,* 1978, Butman *et al,* 1979; Cacchione and Drake, 1982). Gabrielson and Lukatelich (1985) related the rate of sediment resuspension to a function of wind velocity and direction in an estuarine system. Pejrup (1986) found that SPM concentrations in a shallow estuary were affected by the wind speed, the origin of the water, and the wind direction. Jago *et al* (1993) found that resuspension increased under combined wave/current flows during storms at three sites in the North Sea. Modelling studies by Sündermann and Puls (1990) revealed that wind waves significantly influence the transport of suspended sediment in the North Sea, especially in shallow water.

Variations in SPM concentration can be determined by biological activity. Buchan *et al* (1967) proposed two possible explanations for the seasonal cycle observed in SPM concentrations in the Menai Straits: (i) during the summer the rate of erosion and dispersion of particulate matter is reduced because of the mucus secreted by microorganisms increased the binding between the sediment grains; (ii) removal of suspended particles from the water column in the summer by filter feeding organisms. Phytoplankton production caused variability in SPM concentration and composition

during cycles of growth, decline, and settlement (Jones *et al*, 1994b). The same authors identified bloom flocculation as an important process which resulted in an increase of the settling rate and removal via scavenging of fine-grained particles from the water column as the flocs settle out.

7.2 Study area and data acquisition

7.2.1 Study area

In Liverpool Bay the tides may be described in terms of a standing wave (Bowden, 1955) with mean tidal flows running in an E-W direction. Mean tidal ranges at Liverpool are 8.3 m at springs and 4.5 m at neaps. There is asymmetry in the tides causing the ebb tide to be slower than the flood. Maximum velocities occur about 3 hours before and after high water and attain values between 0.75 and 1 ms^{-1} on springs. Observations of currents and salinity made by Bowden and Sharaf El Din (1966) showed an estuarine-type circulation in Liverpool Bay, with a net offshore flow at the surface and an onshore flow at the bottom. This circulation is driven by the horizontal density gradient which is maintained throughout the Bay by the freshwater discharge from the rivers Dee, Mersey, Ribble, Wyre and Lune (Fig. 7.1). The area exhibits marked periodic stratification as the density-driven transport resulting from the horizontal density gradient is acted on by varying levels of tidal mixing (Simpson *et al*, 1990; Sharples, 1992).

Bottom sediments in Liverpool Bay are predominantly medium to fine sands, with muddy patches near the Mersey and near the Lancashire coast. Gravels occur between Anglesey and the Isle of Man (Fig. 2.6).

Figure 7.1 Example surface isopycnals for Liverpool Bay showing the horizontal density gradient maintained by freshwater input from the rivers. (after Miller, 1985)

7.2.2 Data acquisition

Measurements of beam attenuation, temperature, conductivity, and currents were made in Liverpool Bay at sites LB2 (53° 33.69'N, 3° 38.72'W) and LB3 (53° 34.92'N, 3° 44.38'W) (Fig. 7.2) using moored self-recording transmissometers and current meters. The water depth at LB2 was 35 m and at LB3 was 41 m. The moorings were separated by a distance of 6.7 km, with LB2 lying to the east of LB3.

The sampling strategy consisted of two mooring deployments which were conducted during the summer 1990 from the 13th June to the 25th July and during the winter from the 14th November 1990 to the 20th February 1991. In the following text these deployments will be respectively referred to as: summer and winter deployment. One mooring was deployed at LB3 during the summer deployment and was equipped with a transmissometer and two current meters. During the winter deployment, moorings were deployed at LB2 and LB3. Each of the moorings comprised: two transmissometers and three current meters. The spacing of the moorings and the positioning of the instruments on each mooring was selected to resolve the horizontal and vertical variations in beam attenuation and to identify the controlling factors. Depths, instrument types, and periods of the recovered data are given in Table 7.1.

Meteorological data in the form of hourly wind speed and direction from the station at Valley (Anglesey) were provided by the Meteorological Office, Bracknell. These were used to check whether the suspended matter in the water column at the study sites has a component due to wind.

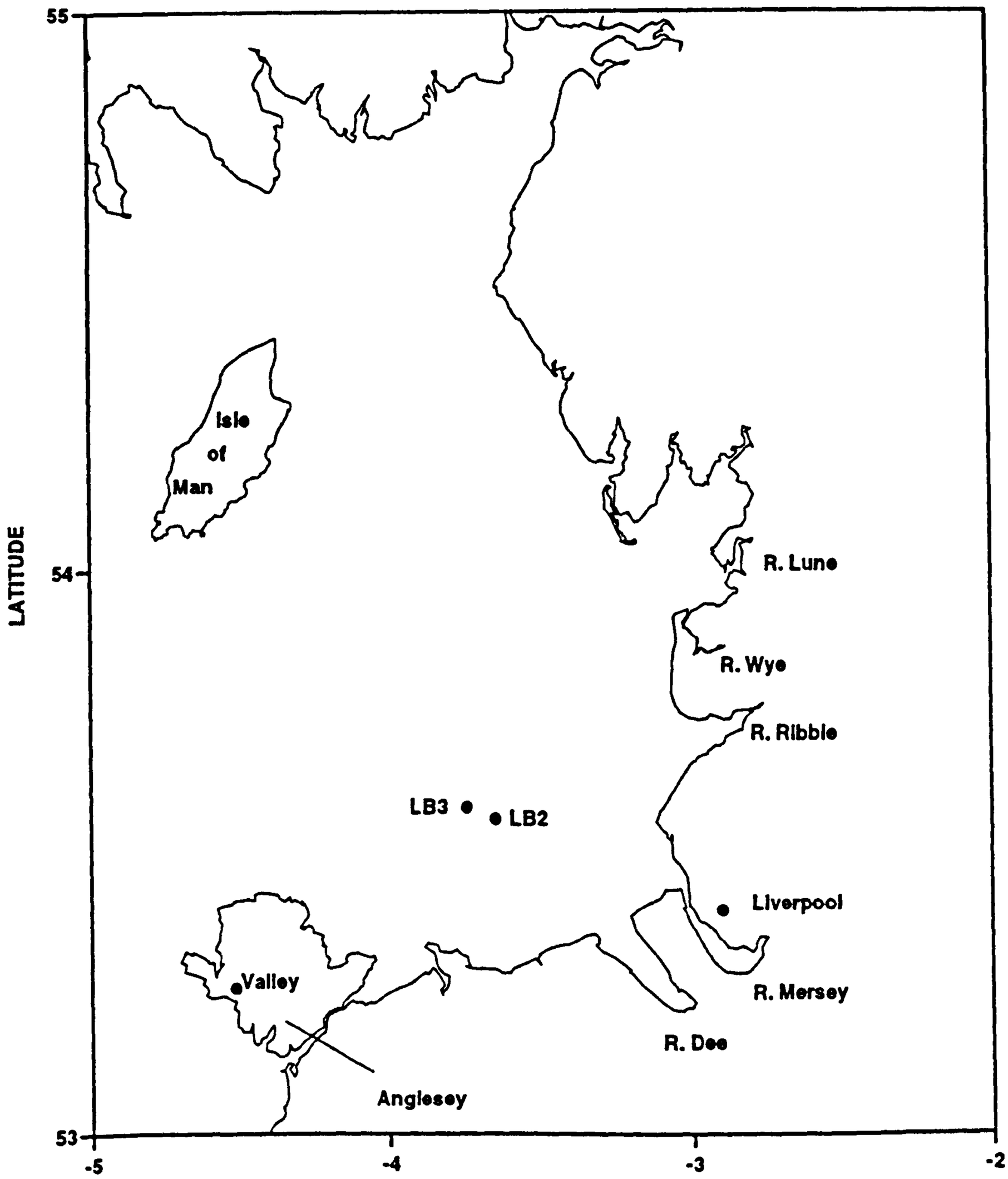

Figure 7.2 Location of the moorings

					Recovered Data			
Site	**Instrument**	**Type**	**Height above seabed (m)**	**Sampling interval (mins)**	**Start** Time (GMT)	Date	**End** Time (GMT)	Date
LB3 (winter)	9070	RCM7	Surface	20	13:40	14/11/90	22:00	10/02/91
	Transmissometer	UCNW	Surface	1	13:26	14/11/90	09:40	09/02/91
	3257	RCM4	23.0	20	13:40	14/11/90	20:40	16/02/91
	6941	RCM4	9.0	20	13:40	14/11/90	20:40	16/02/91
	Transmissometer	Sea Tech	3.0	1	13:26	14/11/90	09:50	19/12/90
LB2 (winter)	9069	RCM7	Surface	20		record	too noisy	
	Transmissometer	UCNW	Surface	1	10:16	14/11/90	09:30	09/02/91
	3308	RCM4	23.0	20	10:20	14/11/90	02:40	12/02/91
	3261	RCM4	9.0	20	10:20	14/11/90	13:40	19/02/91
	Transmissometer	UCNW	3.0	1		Instrument	failure	
LB3 (summer)	6456	RCM4	Surface	10		record	too noisy	
	Transmissometer	UCNW	32.0	1	13:50	13/06/90	09:20	25/07/90
	9070	RCM7	31.0	10	14:00	13/06/90	09:20	25/07/90

Table 7.1 Summary of the deployments at LB2 and LB3.

Transmissometers

Four of the transmissometers used in this study were designed and built at the Marine Laboratories at UCNW. They measure beam transmittance in a 25 cm water path using a Light Emitting Diode (LED) with a wavelength of 665 nm. The choice of a red light is made to minimise the influence of yellow substance on the beam transmittance. The design is similar to that of the commercially available Sea Tech instrument (Bartz *et al*, 1978). Instantaneous values (not affected by ambient light) are logged onto a solid state memory card at 1 minute intervals for up to 3 months.

The bottom transmissometer at site LB3 during the winter deployment was a Sea Tech instrument with a 660 nm LED and a pathlength of 25 cm (it was fitted with the same logger as the UCNW transmissometers). The Sea Tech and the UCNW transmissometers have been shown to record similar beam attenuation for the same water parcel (S. Jones personal communication). Therefore beam attenuation records from these instruments are comparable.

Current meters

The current meters used were Aanderaa RCM model 4 and 7 (Table 7.1) which recorded temperature, conductivity, current speed and direction. The RCM4 measures current speed by counting the total number of rotor revolutions during the sampling interval. The current direction is read at the end of the sampling period. For the RCM7, the number of rotor revolutions and the direction of the compass are sampled every 12 seconds (for sampling intervals longer than 10 minutes, speed and direction are recorded every 1/50 of the sampling interval) during the sampling interval and decomposed into East-West and North-South components. Successive components are added and intermediately stored. At the end of the sampling interval the resultant vector is calculated and stored (Aanderaa Instruments Operating Manuals). The manufacturer's specifications for the RCMs and the calculated resolutions for the selected temperature

and conductivity ranges are given in Table 7.2. The salinity resolution was 0.034 (psu) for constant temperature and 0.024 (psu) for constant conductivity over the ranges sampled in this work.

The meters at the surface measured only temperature and conductivity. The sampling intervals were 10 and 20 minutes for the summer and winter deployments, respectively.

	RCM4	RCM7
Accuracy Temperature	± 0.050 °C	± 0.050 °C
Resolution	0.023 °C	0.023 °C
Accuracy Conductivity	± 0.025 $mmhocm^{-1}$	± 0.025 $mmhocm^{-1}$
Resolution	0.030 $mmhocm^{-1}$	0.030 $mmhocm^{-1}$
Range Speed	2.5 to 250 cms^{-1}	2.0 to 250 cms^{-1}
Accuracy	± 1 cms^{-1} or ± 2% of actual speed which ever is greater	± 1 cms^{-1} or ± 2% of actual speed which ever is greater
Accuracy Direction	For speeds of 2.5 - 5 and 100 - 200 cms^{-1}: ± 7.5 ° For speeds from 5 - 100 cms^{-1}: ± 5.0 °	For speeds of 2.5 - 5 and 100 - 200 cms^{-1}: ± 7.5 ° For speeds from 5 - 100 cms^{-1}: ± 5.0 °
Resolution	0.35 °	0.35 °

Table 7.2 RCMs specifications (Aanderaa, 1987)

7.3 Data processing

7.3.1 Transmissometer data

Time-series of the raw transmissometer data sampled every minute were plotted to check their quality. A complete record was recovered during the summer deployment. During the winter deployment the surface instruments at both moorings operated successfully from deployment until 9th February 1991 when the batteries ran out. The bottom instrument at LB3 failed on the 19th December 1990. No data were recovered from the bottom meter at LB2 due to instrument failure. Spikes were identified with the help of the graphs and replaced by linear interpolation.

The despiked voltages were converted into beam transmittance, T, as follows:

$$T = \frac{V - V_0}{V_{100} - V_0} \qquad (\%) \qquad (7.1)$$

where V is the measured voltage, V_0 is the voltage at 0% transmittance, V_{100} is the voltage at 100% transmittance. V_0 is the voltage recorded when the light path is completely blocked and V_{100} is the voltage reading in air and is taken after a thorough cleaning of the lenses.

The relationship between beam transmittance and beam attenuation, c, is given by:

$$c = \frac{1}{L} Ln\left[\frac{1}{T}\right] \qquad (m^{-1}) \qquad (7.2)$$

where L is the instrument pathlength (m).

Combining Eqs. (7.1) and (7.2) gives the following expression for the beam attenuation:

$$c = \frac{1}{L} Ln \left[\frac{V_{100} - V_0}{V - V_0} \right] \qquad (m^{-1}) \qquad (7.3)$$

The resulting beam attenuation time-series were then averaged by a running mean and decimated to hourly values. It is these hourly values which are used in the following analyses.

For any water parcel the total beam attenuation is due to the combined attenuations of: (i) the water when pure, (ii) any particles present and (iii) dissolved yellow substance. For wavelengths larger than 600nm the attenuation due to yellow substance is considered to be negligible. Therefore, c, can be written as:

$$c = c_w + c_p \qquad (m^{-1}) \qquad (7.4)$$

where the subscripts w and p denote pure water and particles, respectively. As c_w is a constant, the variations in the observed values of c are a measure of the variations in c_p, ie the attenuation due to particulate matter.

7.3.2 Current meter data

The raw binary current meter records were checked for spikes. Time-series judged too noisy were not processed further and are not included in this work (Table 7.2). Individual spikes and spikes occurring over periods less than 3 hours were replaced by linear interpolation. The despiked data were then converted into physical parameters namely: temperature (°C), conductivity ($mmhocm^{-1}$), speed (cms^{-1}) and direction (°). The salinity was calculated from the temperature and conductivity using the Practical

Salinity Scale 1978 (UNESCO, 1981). The speed and direction were resolved into east-west (u) and north-south (v) velocity components. The temperature and conductivity measurements from the RCMs were calibrated against the CTD, before and after deployment. The CTD was calibrated against SIS reversing thermometers and water samples analysed on an Autosal salinometer, respectively.

7.3.3 Low pass filtered data

The low frequency signal of the beam attenuation, salinity, velocity components, and wind speed were calculated by low pass filtering the relevant time-series of observed hourly values. The 72 hours filter (Pugh, 1987) was used for the longer time-series. This filter causes a data loss of 3 days at the beginning and end of each record. For the shorter records (less than 50 days long) this 6-day data loss was felt to be too much considering the length of the records. In this case a Doodson X_0 was used and the resulting time-series were smoothed using a five-hour running mean.

7.4 Mooring time-series results

7.4.1 Observations

The current meter results from both deployments are presented in the form of time-series plots of hourly data and filtered data of the velocity components u (east-west) and v (north-south) and salinity, s, in Figs. 7.3 to 7.6.

Both sites were characterised by strong currents with speeds of the order of 0.8 ms^{-1} at springs and 0.4 ms^{-1} at neaps. The variance in the east-west direction was up to 55 times larger than the variance in the north-south direction indicating a near rectilinear

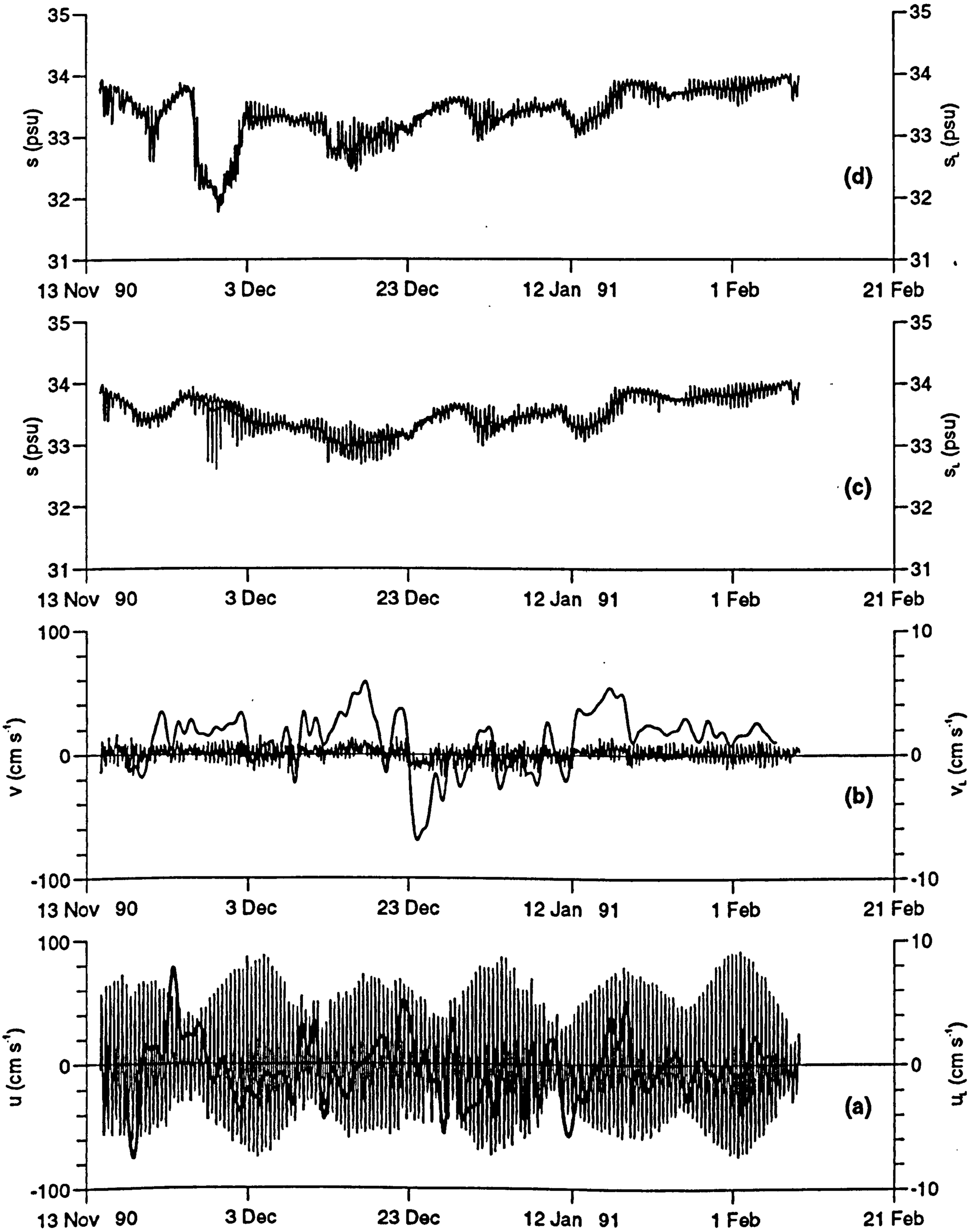

Figure 7.3 Time-series from LB3 23 mab for the winter deployment of:
(a) observed and low-frequency east-west current component,
(b) observed and low-frequency north-south current component and
(c) observed and low-frequency salinity.
(d) Observed and low-frequency salinity at LB3 surface for winter deployment.

(Scales for low-frequency signals on the right)

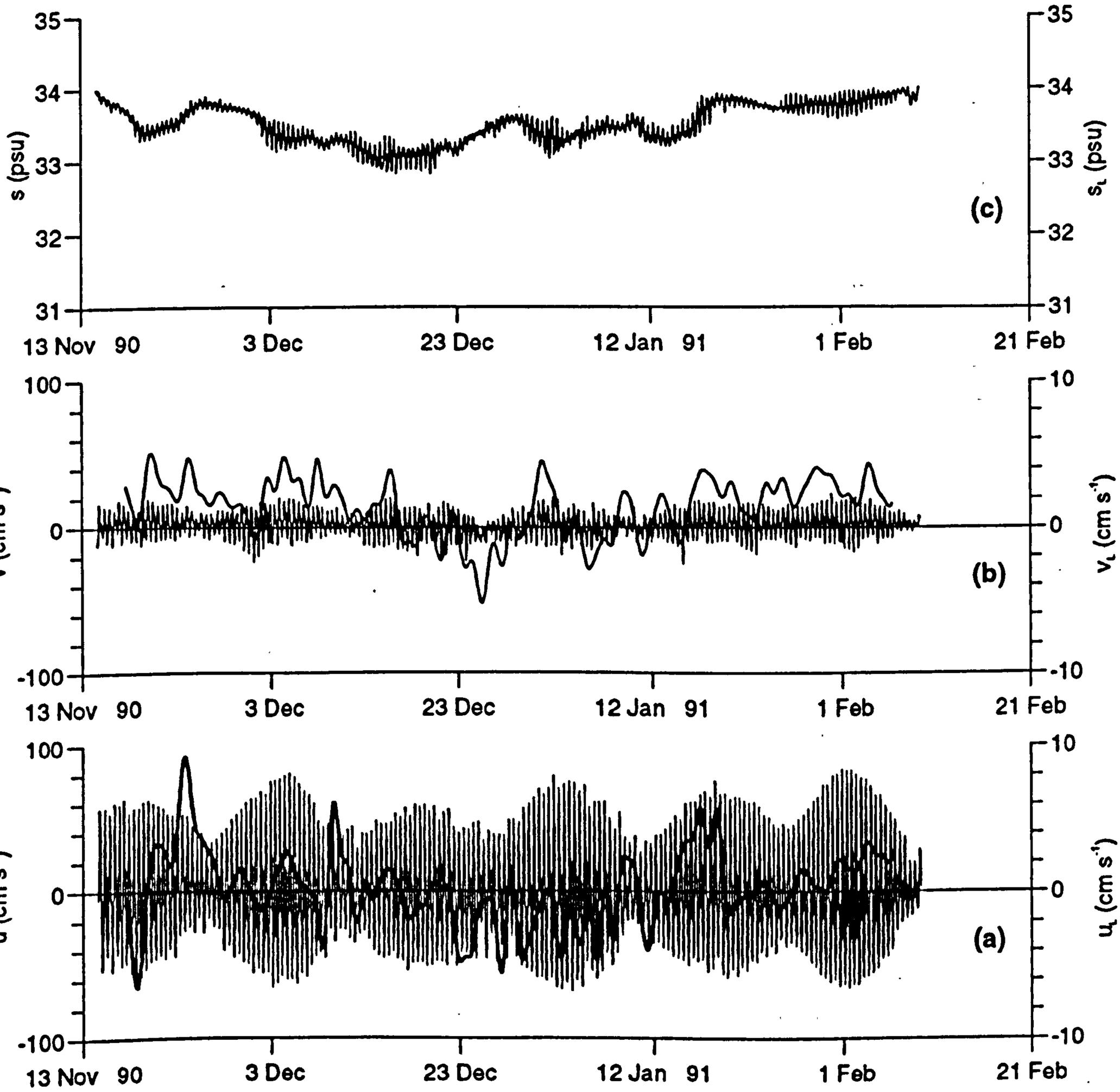

Figure 7.4 Time-series from LB3 9 mab for the winter deployment of:
(a) observed and low-frequency east-west current component,
(b) observed and low-frequency north-south current component and
(c) observed and low-frequency salinity.

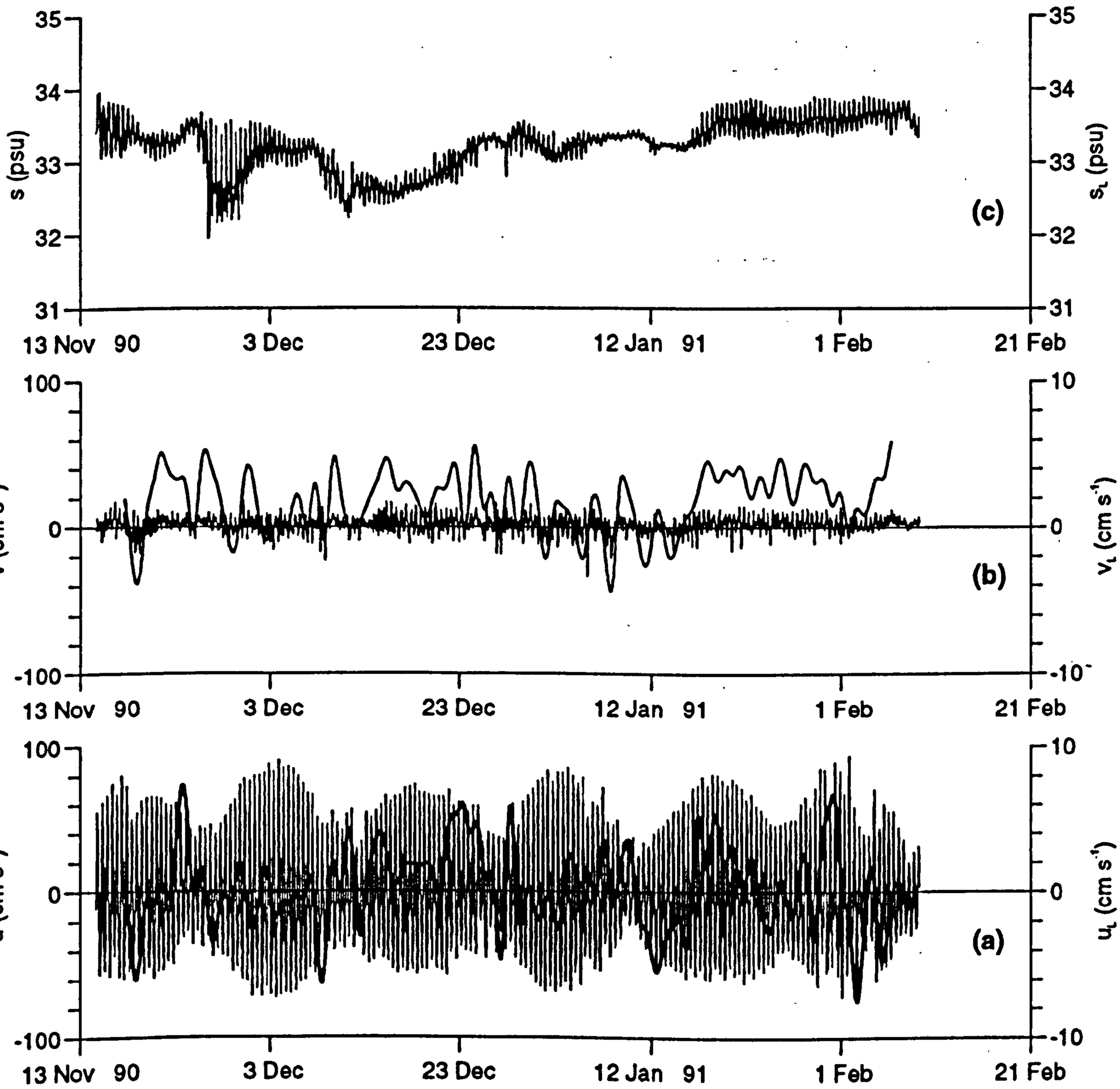

Figure 7.5 Time-series from LB2 23 mab for the winter deployment of:
(a) observed and low-frequency east-west current component,
(b) observed and low-frequency north-south current component and
(c) observed and low-frequency salinity.

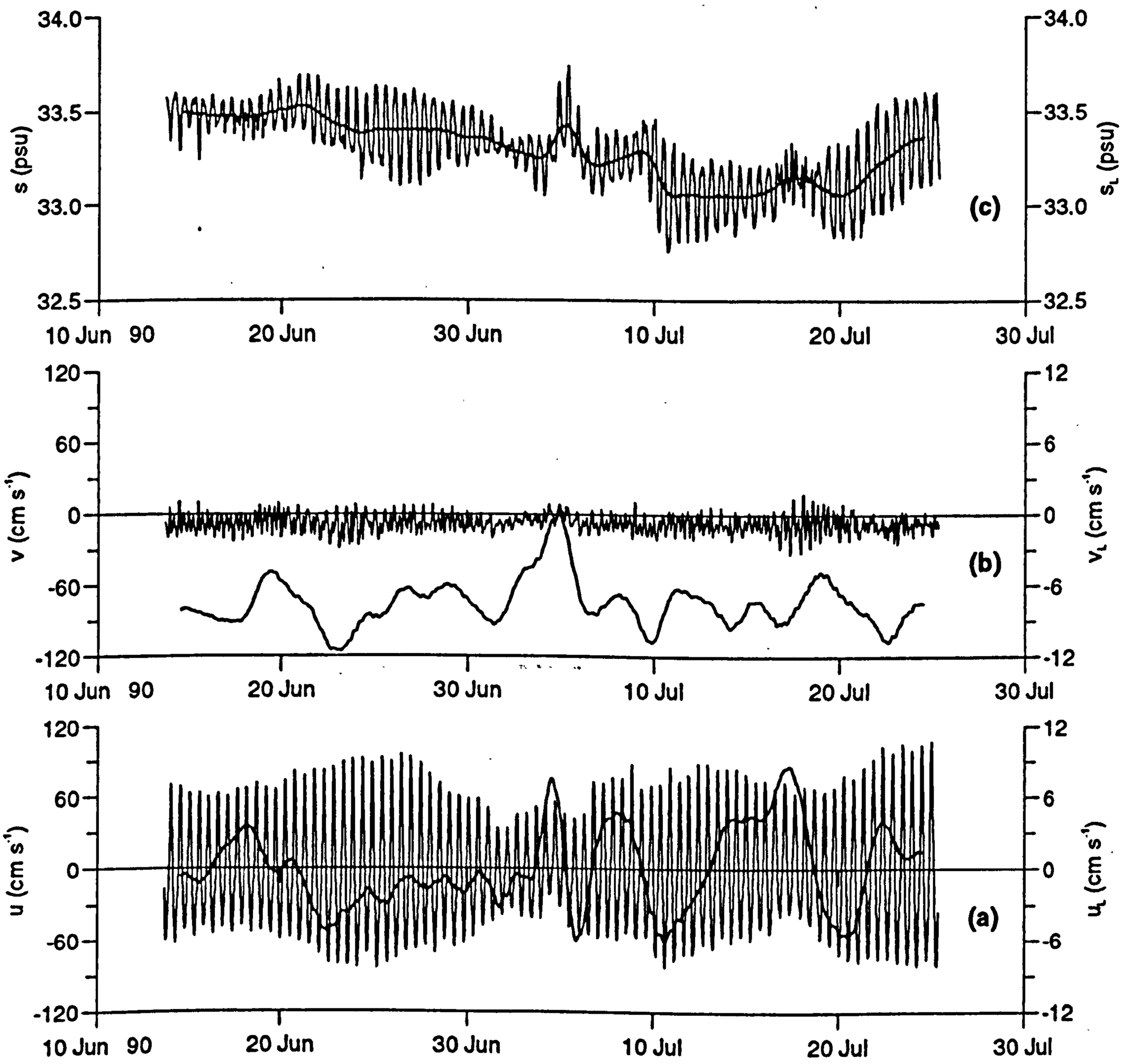

Figure 7.6 Time-series from LB3 32 mab for the summer deployment of:
(a) observed and low-frequency east-west current component,
(b) observed and low-frequency north-south current component and
(c) observed and low-frequency salinity.

east-west flow at the study sites.

Tidal analyses were carried out on the east-west velocity component using a programme developed at the Unit of Coastal and Estuarine Studies (UCES). A total of 27 tidal constituents were resolved including 5 related constituents which were inferred from the equilibrium tide (Appendix 2). Table 7.3 shows these results for the 5 major constituents. The predominance of the M_2 constituent is clearly evident in Table 7.3. Next largest are the other major semidiurnal constituents S_2 and N_2 with amplitudes ~ one-third and one-fifth that of M_2. These results, confirm the semidiurnal nature of the tides at the moorings sites.

Site	Height above bed	Deploy ment	Amplitude (cm s^{-1})					Phase lag (°)				
			M_2	S_2	N_2	K_2	M_4	M_2	S_2	N_2	K_2	M_4
LB2	23 m	winter	52.0	19.0	9.9	5.1	4.8	241	278	219	278	124
LB3	09 m	winter	47.7	16.6	9.9	4.5	4.3	236	280	213	280	121
LB3	23 m	winter	52.0	18.4	9.9	5.3	5.0	241	281	219	281	120
LB3	31 m	summer	62.9	21.4	14.2	5.8	5.6	243	289	223	289	126

Table 7.3 Amplitude and phase lag for the 5 largest constituents of the east-west component of current. Phase Lags are relative to midnight on the 1st January 1900. Note K_2 has been inferred from S_2 using the equilibrium tide.

Average wind speeds were 6.0 and 4.3 ms^{-1} for the winter and summer deployments, respectively. During the winter wind direction and speed were highly variable (Fig. 7.7) except for the period between the 21st December and the 12th January. Throughout this

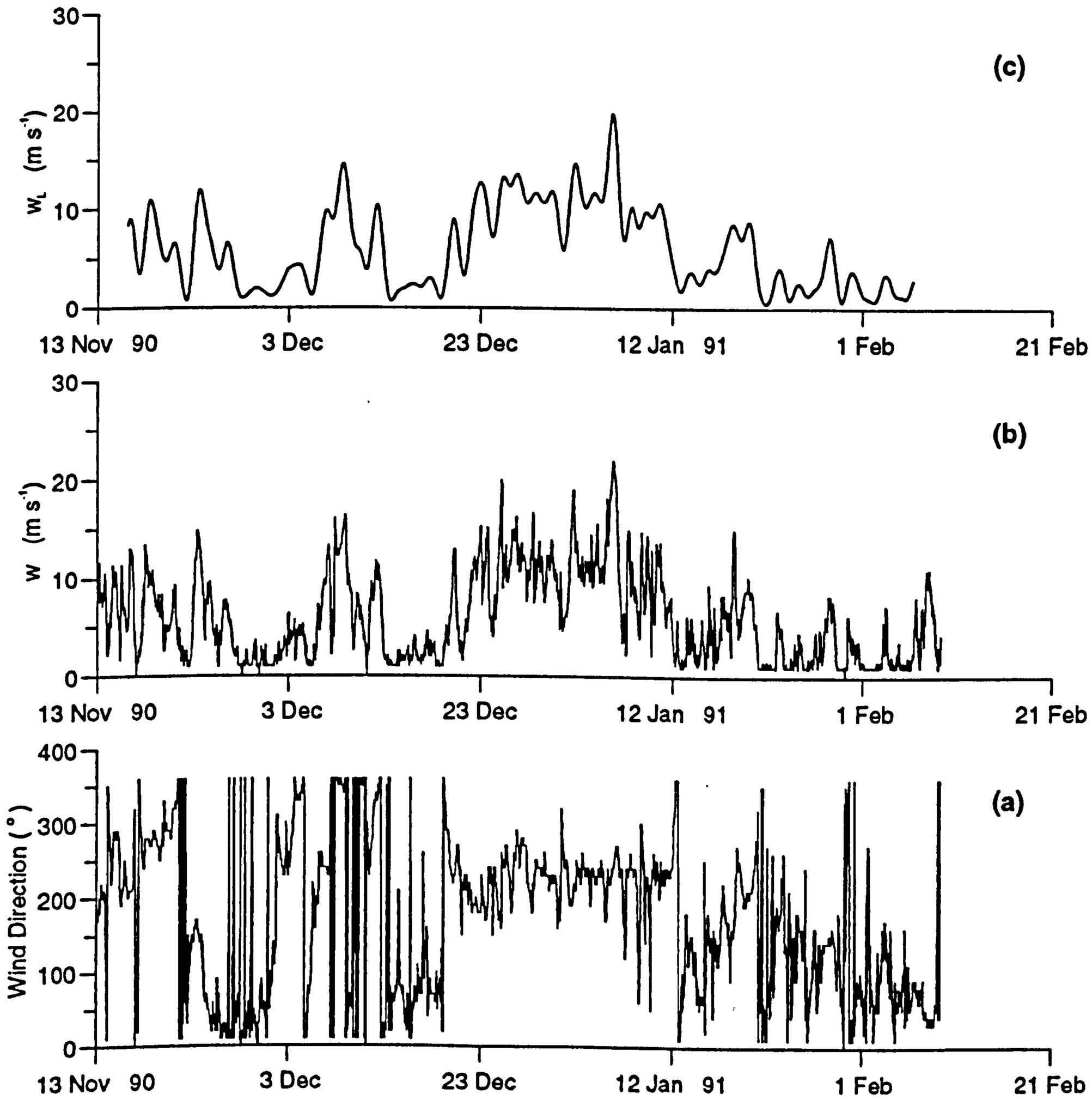

Figure 7.7 Hourly values of (a) wind direction, (b) wind speed, and (c) low frequency wind speed from the Met station at Valley, Anglesey for the winter deployment

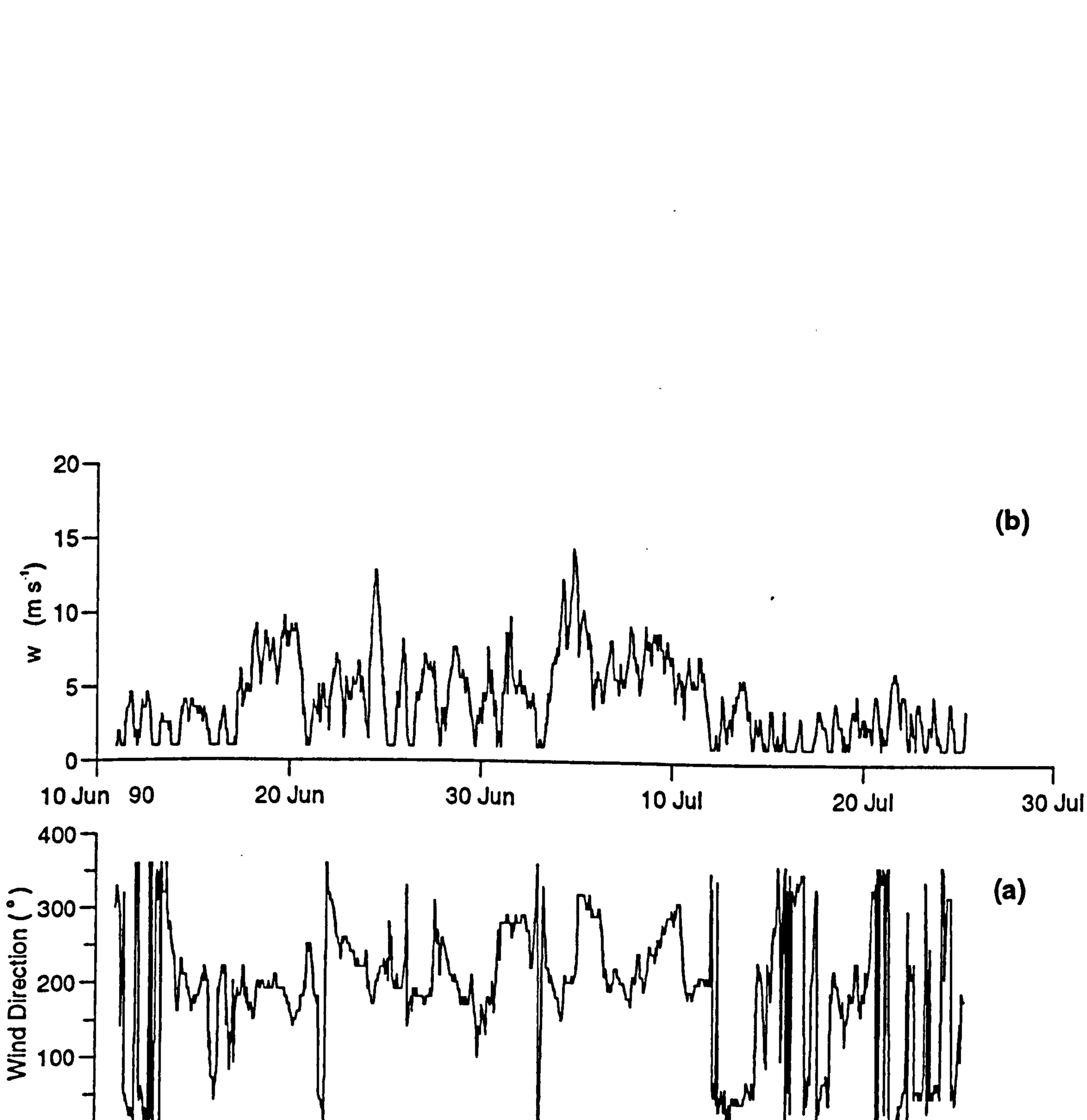

Figure 7.8 Hourly values of (a) wind direction, (b) wind speed from the Met station at Valley, Anglesey for the summer deployment

period winds were stronger than average, having a mean of 10.7 ms^{-1}, and persistently to the east. The summer wind speeds were less variable than during the winter (Fig. 7.8): winter variance = 19.8 ms^{-1} and summer variance = 7.0 ms^{-1}.

Time-series of the salinity difference between 9 mab and the surface at LB3 during the winter deployment (Fig. 7.13a) showed that there was a period of strong and sustained stratification ($\Delta s > 1.25$ psu) between the 26th November and the 2nd December. The water became vertically mixed by the following spring tide on the 3rd December.

The temporal variations of the surface beam attenuation at LB2 and LB3 during the winter deployment exhibited similar features (Figs. 7.9a and 7.11a). They were characterised by a persistent background beam attenuation of the order of 1.0 m^{-1} and intermittent periods of higher attenuation levels. Surface beam attenuation values ranged from 0.5 to 13.5 m^{-1} at LB2 and 0.6 to 11.3 m^{-1} at LB3. The mean values at LB2 and LB3 were 2.5 and 2.1 m^{-1}, respectively. The surface attenuation records from the two moorings indicated that the water was generally more turbid at LB2 than at LB3. This was confirmed by the observed horizontal gradients of beam attenuation between LB2 and LB3 (Fig. 7.13b) which in general were positive (i.e. the values increased to the east) throughout the deployment.

The beam attenuation records were dominated by the low frequency signal which accounted for over 88 % of the variance in the beam attenuation at both sites (Figs. 7.9b and 7.11b). Superimposed on the low frequency variation was a high frequency signal which was coherent with the latter: larger oscillations were observed at times of high beam attenuation levels (Figs. 7.9c and 7.11c).

One event which dominated these two time-series occurred between the 25th December 1990 and 21st January 1991, during which the highest values of beam attenuation were recorded. This event followed the onset and duration of strong westerly winds over the area. Another interesting event was the sharp increase and subsequently higher levels

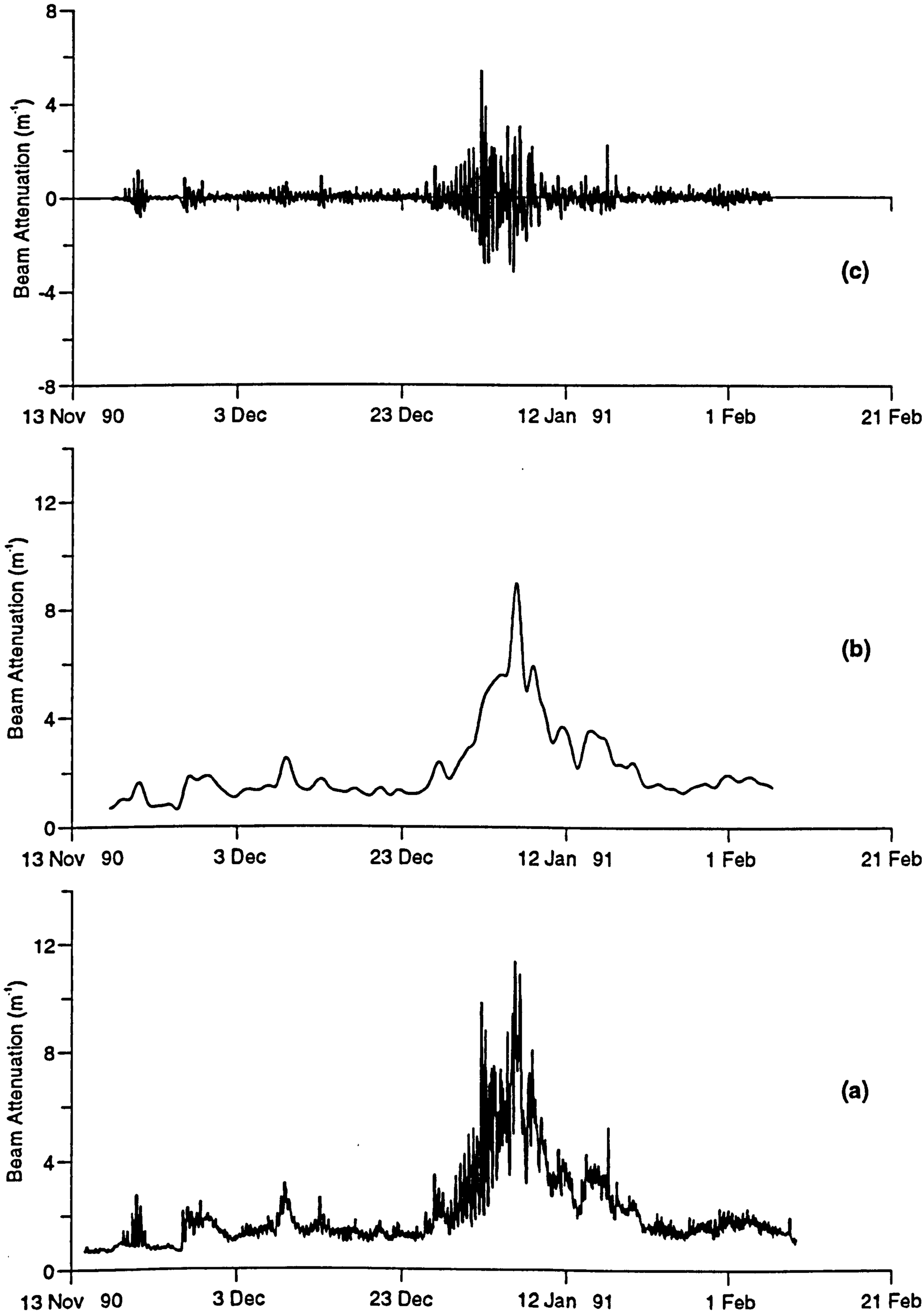

Figure 7.9 Hourly values of beam attenuation at the surface at LB3 during the winter deployment:
(a) observed
(b) low pass filtered
(c) (observed - low pass filtered)

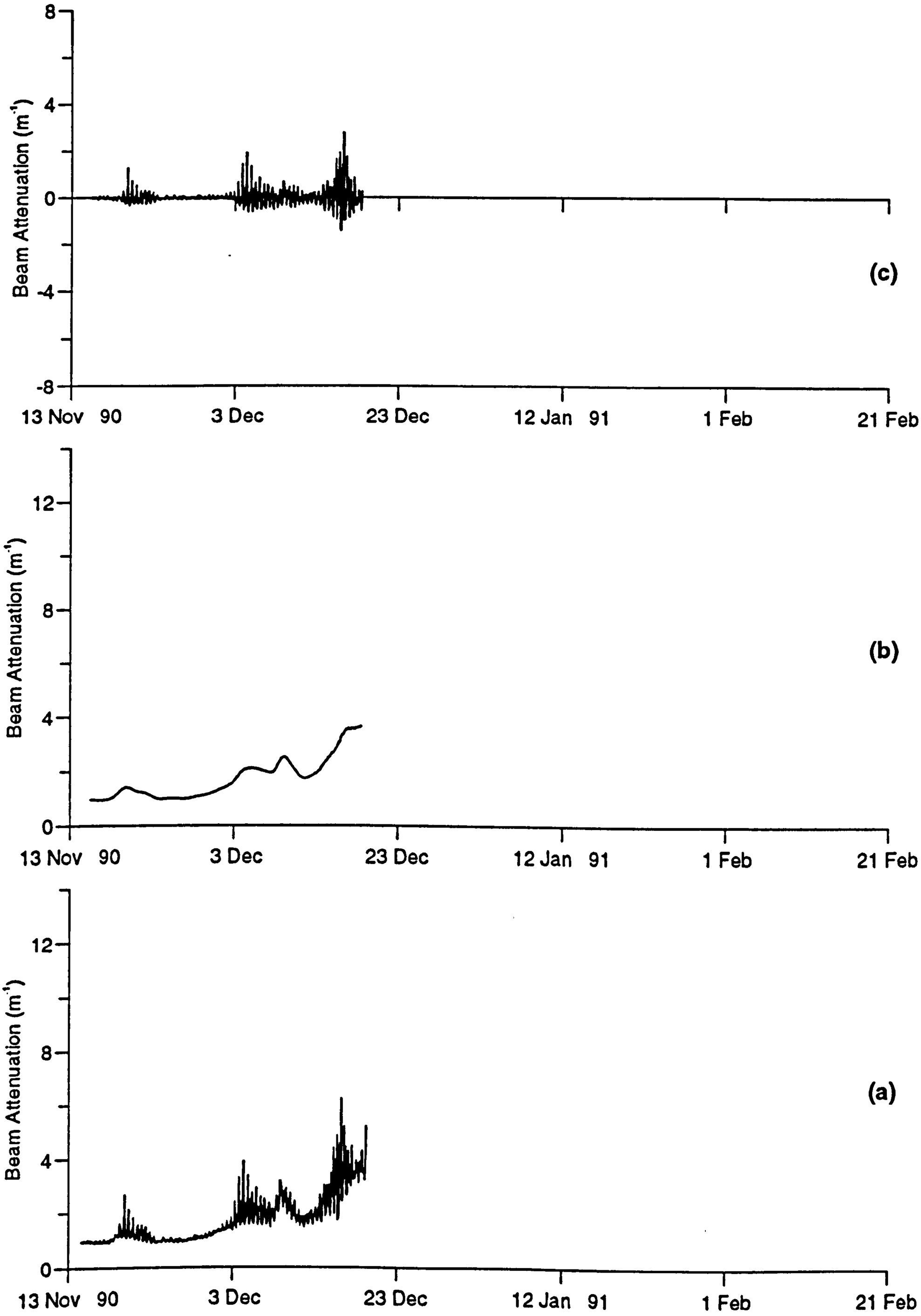

Figure 7.10 Hourly values of beam attenuation at 3 mab at LB3 during the winter deployment:
(a) observed
(b) low pass filtered
(c) (observed - low pass filtered)

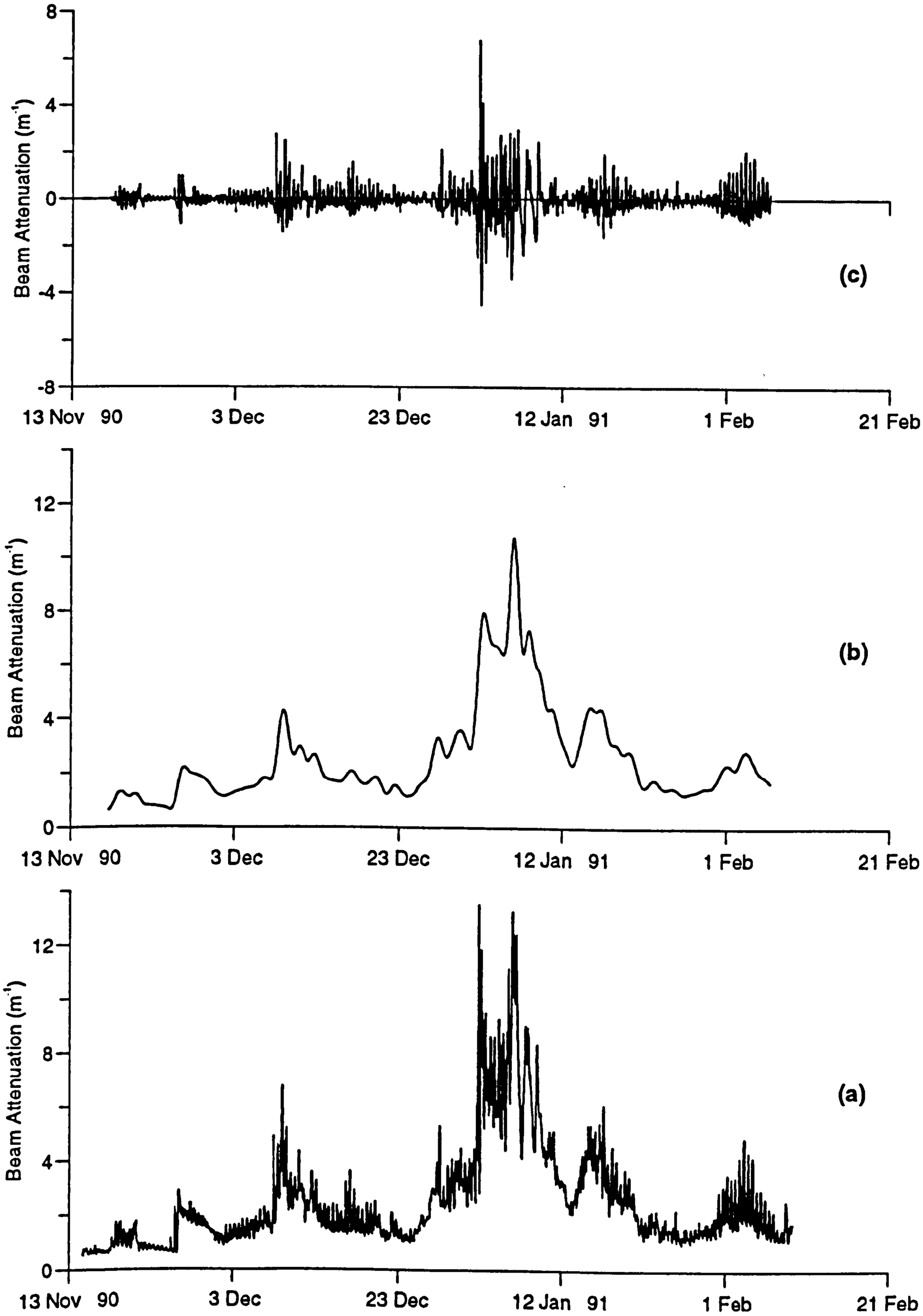

Figure 7.11 Hourly values of beam attenuation at the surface at LB2 during the winter deployment:
(a) observed
(b) low pass filtered
(c) (observed - low pass filtered)

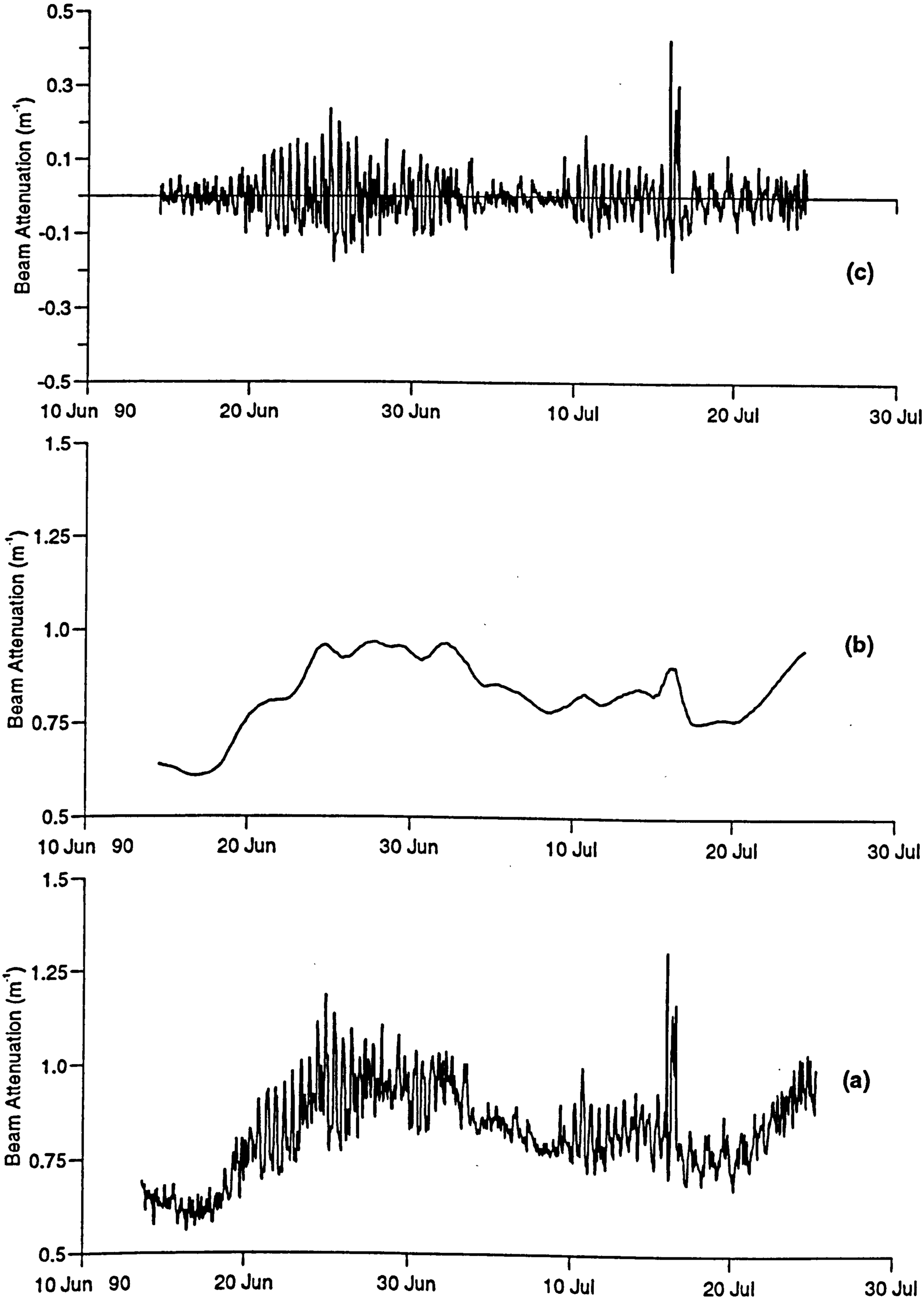

Figure 7.12 Hourly values of beam attenuation at 32 mab at LB3 during the summer deployment:
(a) observed
(b) low pass filtered
(c) (observed - low pass filtered)

of beam attenuation which coincided with the period of stratification mentioned above. The loss of particles (hence a decrease in beam attenuation) from the surface plume is caused by settling and mixing. One significant difference between these data records was the marked semidiurnal oscillations seen at LB2 but not at LB3 towards the end of the deployment. This was thought to be caused by the tidal advection of fresher, more turbid water from onshore passing LB2 which does not reach LB3.

The beam attenuation record at 3 mab at LB3 during the winter deployment is shown in Fig. 7.10a; it covers only a portion of the deployment from the 14th November to the 19th December 1990. The values ranged from 0.9 to 6.2 m^{-1} with a mean of 1.7 m^{-1}. The beam attenuation increased steadily over the period of observation. Superimposed on this steady increase were semidiurnal oscillations with variable ranges. The observed vertical gradients in beam attenuation between 3 mab and the surface at LB3 (Fig. 7.13c) were in general always positive throughout the deployment. This indicates levels of suspended sediments at 3 mab which were higher than those at the surface. One significant exception occurred during the period of stratification, when the gradient was negative ie. the surface water was more turbid than that at 3 mab.

During the summer deployment the mean value of beam attenuation at 32 mab at LB3 was 0.8 m^{-1} (Fig. 7.12a). This is significantly less than the values at both 3 mab and the surface at LB3 during the winter (cf 1.7 m^{-1} and 2.1 m^{-1}, respectively).

There was some indication of a spring-neap variation in the beam attenuation, with larger mean values occurring at springs. As well as increased mean levels, spring tides were also periods of marked semidiurnal oscillations. This is particularly evident around the springs of the 24th June. At neaps these oscillations tend to be considerably reduced. However, the high values observed on the 16th July are an exception. These semidiurnal variations observed during the summer were of a significantly smaller magnitude to those observed in the winter.

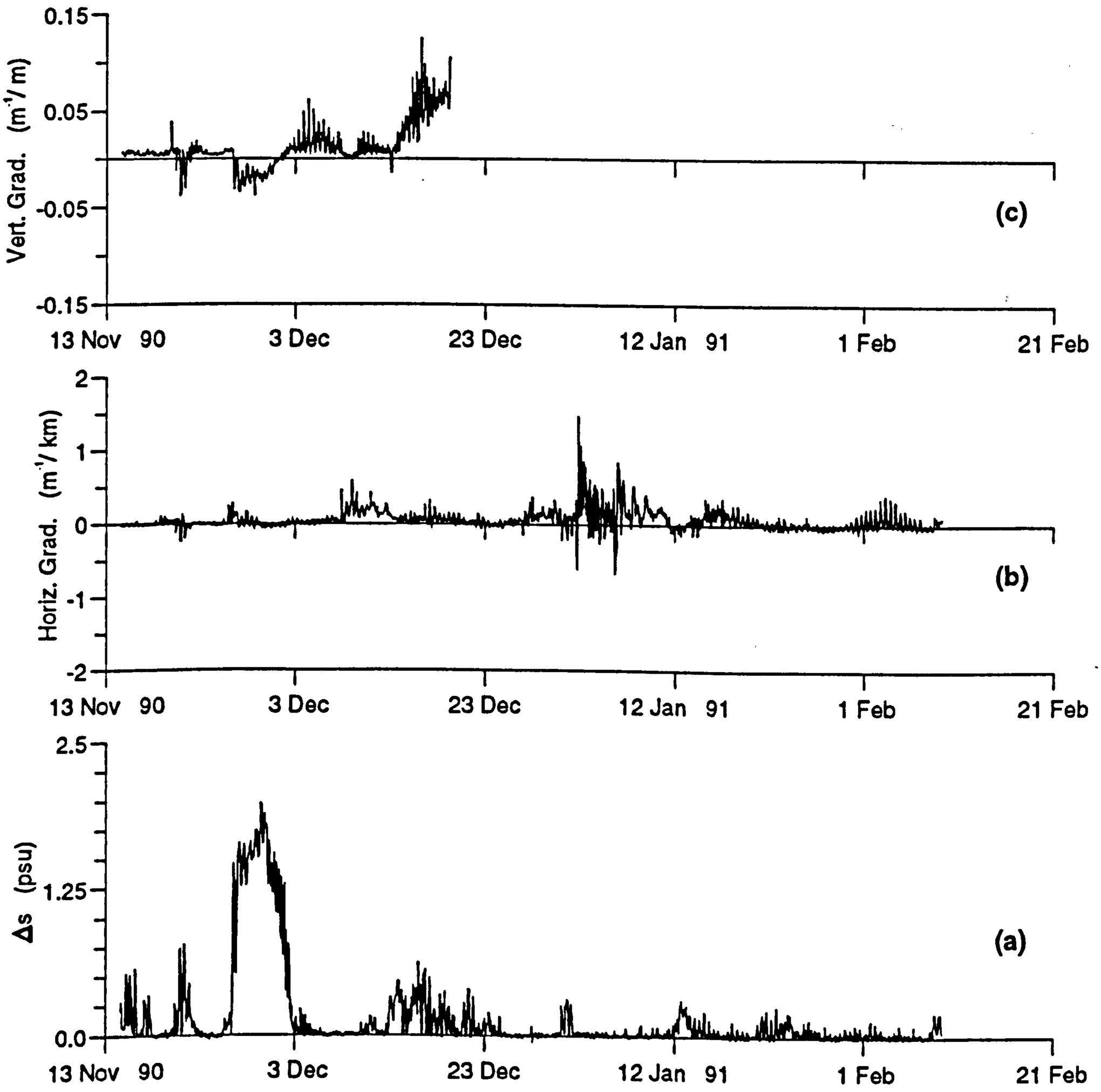

Figure 7.13 (a) salinity difference between 9 mab and surface at LB3
(b) surface horizontal gradient of beam attenuation between LB2 and LB3
(c) vertical gradient in beam attenuation between 3 mab and surface at LB3

7.4.2 Multiple regression analysis

In this section it is attempted to explain some of the variability in beam attenuation in terms of changes in the environment. Visual inspection of the data records strongly suggests that the wind plays an important role in controlling SPM concentrations at these sites, especially in winter. Advection of water parcels past the moorings, both tidal and long term is also likely to be important. This can be estimated either by integrating the velocity record or by using the salinity as a tracer for the water type. Finally it was necessary to establish whether there was a springs-neaps cycle of beam attenuation at the study sites. Multiple regression analyses were used to examine the link between beam attenuation and certain environmental variables. The low and high frequency variations of beam attenuation at the surface at LB2 and LB3 from the winter deployment were studied separately. For the summer deployment at LB3 32 mab and the winter deployment at LB3 3 mab the low frequency signals were not examined due to the short length of the data records.

(i) Low frequency variation in beam attenuation

The low frequency variations were studied using the low pass filtered data (section 7.3.3). The fitted equations were of the form:

$$c_L(t) = c_0 + \alpha W_L(t)^m + \beta F(t) + \gamma x_L(t) \qquad (7.5)$$

$$c_L(t) = c_0' + \alpha' W_L(t)^m + \beta' F(t) + \gamma' s_L(t) \qquad (7.6)$$

where c_L = beam attenuation (m^{-1}), W_L = wind speed ($m\ s^{-1}$), F = tidal range (m), x_L = displacement (km), s_L = salinity and the subscript L indicates low pass filtered.

The constants c_0, α, β, γ, c_0', α', β', γ', and the exponent m are to be determined by the regression analyses. Eqs. (7.5) and (7.6) were repeatedly fitted for m = 1, 2, and 3. The optimum value for the exponent m was that which produced the largest percentage variance explained by the fit (r^2).

Lagged correlations carried out between W_L and c_L produced correlation coefficients of 0.61 and 0.58 at the surface at LB2 and LB3, respectively. These coefficients were significant at the 97.5 % level. The correlations also revealed the existence of a lag between W_L and c_L: beam attenuation lagged wind speeds by 10 hours at both sites. Therefore the time-series of W_L used in the regression analyses was adjusted to start 10 hours before the time-series of c_L.

The tidal range, F, is given by:

$$F(t) = 1 + \frac{1}{3}\cos\left(\frac{2\pi}{T}t + \phi\right) \qquad (7.7)$$

where t is time in days measured relative to start of the data, T = 14.7 days is the period of the springs-neaps cycle. ϕ represents where in the springs-neaps cycle the observations start and was determined by a least squares fit of a cosine curve with a period, T, to the observed currents. The resulting value for ϕ was - 3.47 radians. Time-series of F covering the winter deployment were then created using Eq. (7.7) (Fig. 7.14b).

The low frequency displacement, x_L, was calculated by integrating the low pass east-west velocity component, u_L, over time (Fig. 7.14a). In the analysis of LB3 surface the advection term was determined from the current at LB2 23 mab (rather than LB3 23 mab). Being at a depth of 12 m it was considered that the currents at LB2 23 mab were more representative of the surface flow than LB3 23 mab which is 19 m below the surface i.e. 7 m deeper than LB2 23 mab.

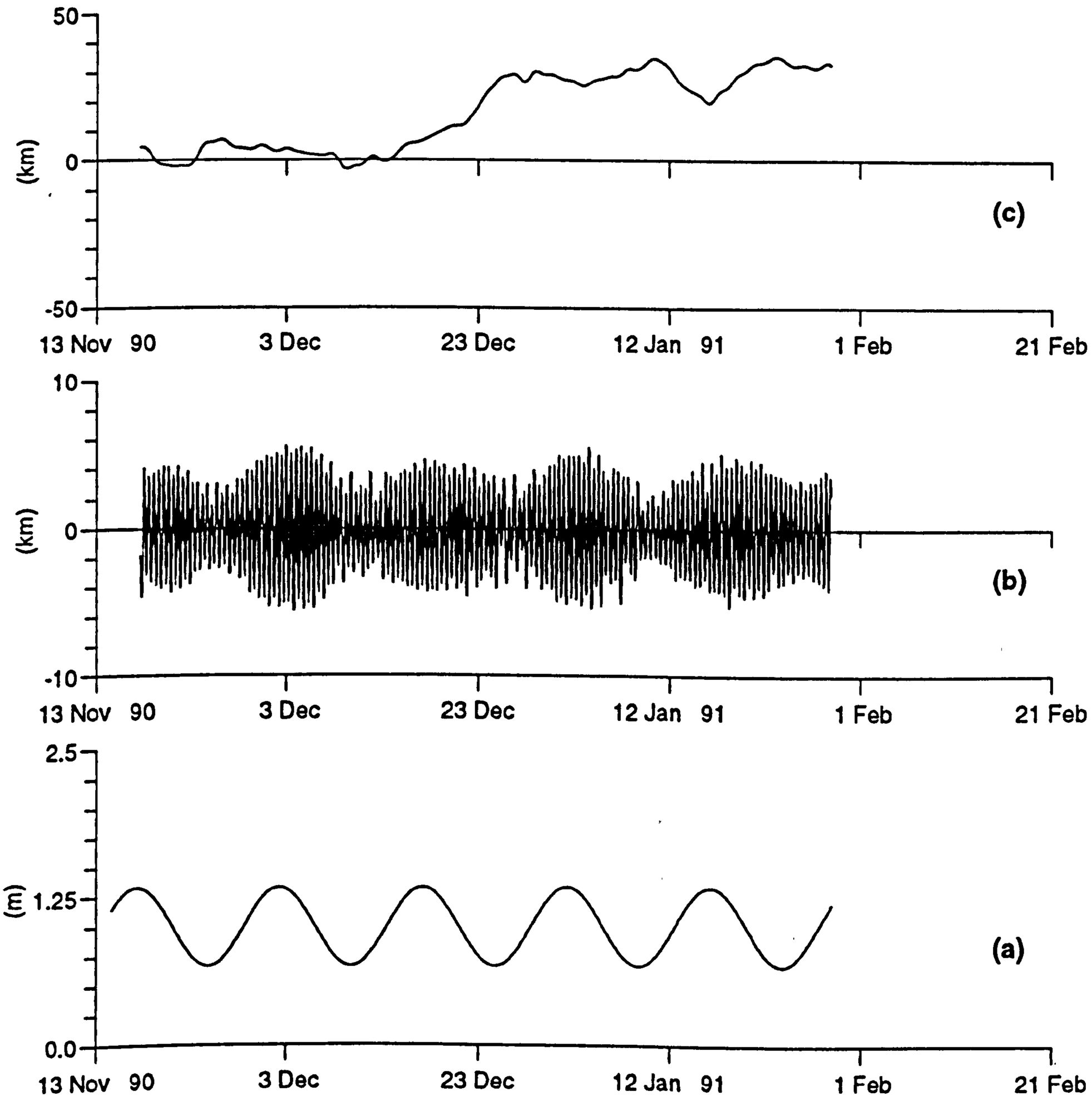

Figure 7.14 (a) Tidal range, (b) Tidal displacement, and (c) Low frequency displacement

The low frequency variation of salinity, s_L, at LB3 surface was used in the analysis of both LB2 and LB3 data. The salinity was used as a flag for the water type. Low salinities are associated with water from the rivers.

(ii) High frequency variations in beam attenuation

Because the high frequency signals of beam attenuation from the winter and summer were highly variant in time the time-series were split into 3-day sections which were used in the regression analyses. The prediction equations were of the form:

$$c(t) = k_0 + k_1 U(t)^n + k_2 W(t)^m + k_3 x(t) \tag{7.8}$$

$$c(t) = k_0' + k_1' U(t)^n + k_2' W(t)^m + k_3' s(t) \tag{7.9}$$

where c = beam attenuation (m^{-1}), U = current speed ($U = (u^2 + v^2)^{1/2}$) ($m\ s^{-1}$), W = wind speed ($m\ s^{-1}$), x = tidal displacement (km), s = salinity and k_0, k_1, k_2, k_3, k_0', k_1', k_2', k_3', n and m are constants to be inferred from the regression analyses. The data fittings were repeated for n and m equal 1, 2, and 3. This resulted in 9 different combinations of Eqs. (7.8) and (7.9).

The tidal displacement, x, was calculated by integrating the east-west tidal current over time (Fig. 7.14c). The constant k_3 in Eq. (7.8) is an estimate of the horizontal gradient of beam attenuation over a 3-day period. A negative k_3 means the beam attenuation increases to the east.

7.4.3 Results of regression analysis

(i) Low frequency variation

The regression constants resulting from fitting Eqs. (7.5) and (7.6) to the low frequency beam attenuation at LB2 and LB3 for m = 1, 2, and 3 are presented in Tables 7.4 and 7.5, respectively. Also are given the percentages variance explained (r^2) by the fit and the 95 % confidence intervals of the constants.

The best fit to the low frequency signal was obtained with Eq. (7.5) when m was equal to 3 (Table 7.4). This fit accounted for 48 and 49 % of the variability of c_L at LB2 and LB3, respectively. In Fig. (7.15) are shown for each mooring the time-series of the low frequency beam attenuation predicted for the deployment using the constants of the best fit. The analyses with Eq. (7.6) produced r^2 which were up to 13 % smaller (Table 7.5) than those obtained with Eq. (7.5).

It can be seen from Table 7.4 that for the best fit the constants α, β, and γ were significant at the 95 % level. Whereas c_0 was barely significant at LB2 and nonsignificant at LB3. The low frequency beam attenuation at both sites increased with the wind speed cubed ($\alpha > 0$). The wind effects appeared to be stronger at LB2 than at LB3 as indicated by the values of α: 1.08×10^{-3} and 0.76×10^{-3} m^{-4} s^3, respectively. This is consistent with wind-induced wave activity being stronger in shallower water.

A positive γ implies that c_L increased when the low frequency displacement was eastward and decreased when it was westward. This suggests a negative mean gradient in beam attenuation (represented by $-\gamma$) over the deployment. This was contrary to the observed deployment mean gradient which was equal to 0.0643 m^{-1}/km, ie. positive. Therefore, the relationship between c_L and x_L, although statistically significant, was not consistent with the observations.

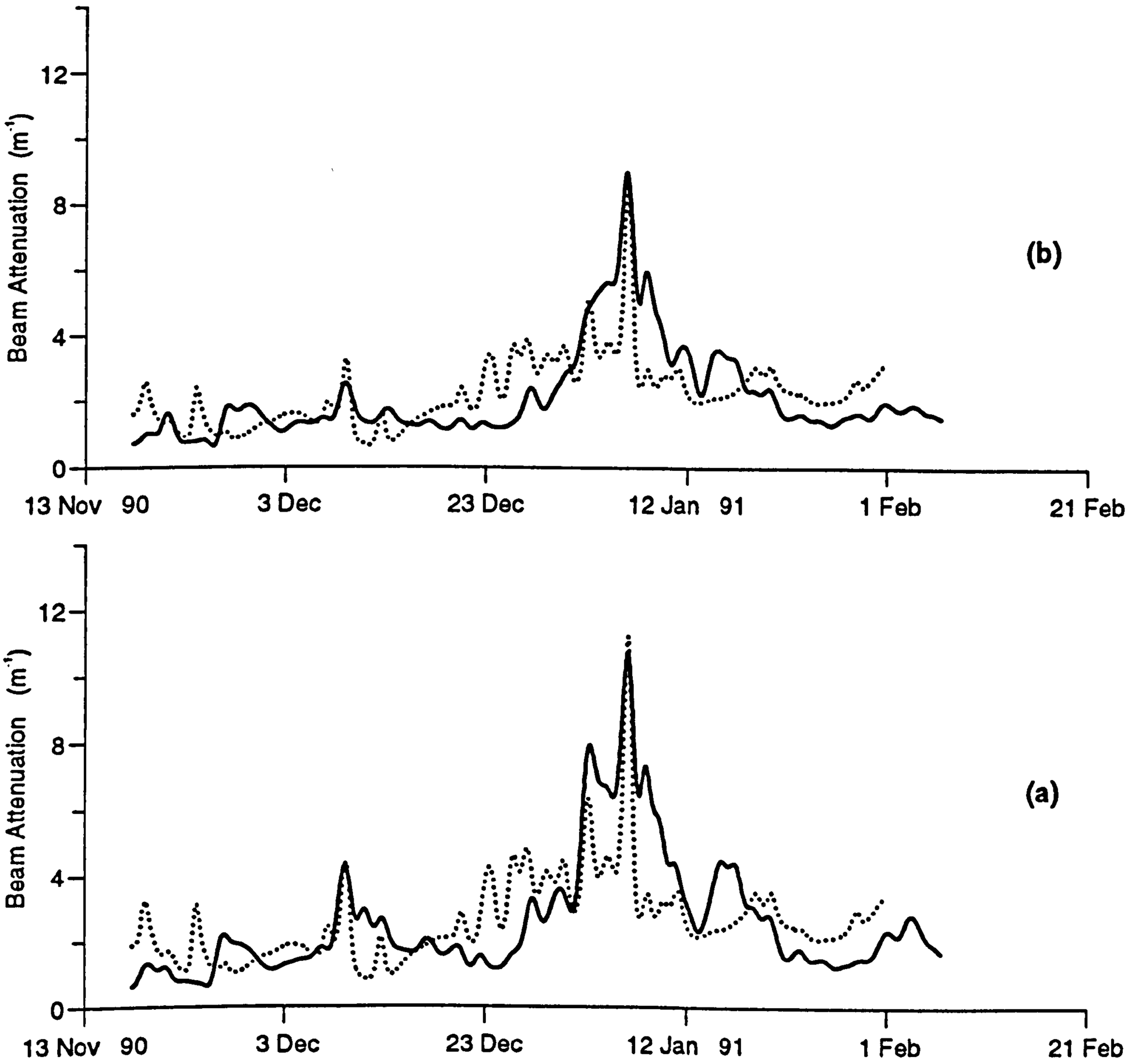

Figure 7.15 Observed (solid line) and predicted (dotted line) time-series of the low frequency beam attenuation at the surface: (a) LB2 and (b) LB3

	m	c_0	α	β	γ	R^2
	1	(-4.48 ± 3.17) x10^{-1}	(223.14 ± 16.80) x10^{-3}	(11.34 ± 2.91) x10^{-1}	(4.33 ± 0.51) x10^{-2}	41.2
LB2	2	(0.57 ± 3.00) x10^{-1} ns	(16.00 ± 1.04) x10^{-3}	(11.55 ± 2.78) x10^{-1}	(4.14 ± 0.49) x10^{-2}	46.0
	3	(2.97 ± 2.95) x10^{-1}	(1.08 ± 0.07) x10^{-3}	(11.53 ± 2.74) x10^{-1}	(4.22 ± 0.48) x10^{-2}	47.7
	1	(-3.52 ± 2.46) x10^{-1}	(148.40 ± 13.02) x10^{-3}	(10.52 ± 2.26) x10^{-1}	(4.34 ± 0.40) x10^{-2}	41.8
LB3	2	(-0.20 ± 2.33) x10^{-1} ns	(10.93 ± 0.81) x10^{-3}	(10.56 ± 2.16) x10^{-1}	(4.18 ± 0.38) x10^{-2}	46.5
	3	(1.47 ± 2.27) x10^{-1} ns	(0.76 ± 0.05) x10^{-3}	(10.44 ± 2.10) x10^{-1}	(4.20 ± 0.37) x10^{-2}	49.1

Table 7.4 Results of the regression analyses on the low frequency beam attenuation using Eq. (7.5). Nonsignificant values at 95 % level are shown by ns.

	m	c_0'	α'	β'	γ'	R^2
	1	(4.62 ± 5.83) ns	(246.40 ± 16.43) x10^{-3}	(9.16 ± 2.91) x10^{-1}	(-13.24 ± 17.72) x10^{-2} ns	31.9
LB2	2	(3.27 ± 5.56) ns	(17.72 ± 1.03) x10^{-3}	(8.81 ± 2.78) x10^{-1}	(-7.47 ± 16.87) x10^{-2} ns	37.8
	3	(0.51 ± 5.48) ns	(1.20 ± 0.07) x10^{-3}	(7.73 ± 2.75) x10^{-1}	(1.92 ± 13.93) x10^{-2} ns	39.3
	1	(4.73 ± 4.70)	(178.32 ± 13.22) x10^{-3}	(7.01 ± 2.35) x10^{-1}	(-13.07 ± 14.26) x10^{-2} ns	27.5
LB3	2	(3.84 ± 4.49) ns	(12.98 ± 0.83) x10^{-3}	(6.76 ± 2.25) x10^{-1}	(-9.18 ± 13.62) x10^{-2} ns	33.3
	3	(1.90 ± 4.40) ns	(0.89 ± 0.05) x10^{-3}	(5.96 ± 2.21) x10^{-1}	(-2.56 ± 13.33) x10^{-2} ns	35.2

Table 7.5 Results of the regression analyses on the low frequency beam attenuation using Eq. (7.6).

The relationship between c_L and F was positive ($\beta > 0$) indicating that springs are associated with periods of greater turbidity than neap tides. The values of β showed that a 1 m change in the tidal range would cause an estimated change in beam attenuation of 1.15 and 1.04 m^{-1} at LB2 and LB3, respectively. This springs-neaps variation in the low frequency beam attenuation was not apparent in the observations, perhaps because it was masked by changes due to other processes.

(ii) High frequency variations

The constants and the r^2 resulting from the analyses on the 3-day time-series of beam attenuation for the winter and summer deployments are tabulated in Appendix 3. Comparison between 3-day averages of the observed horizontal gradients and those estimated (only significant estimates were included) by the regression analyses using Eq. (7.8) are shown in Fig. 7.16.

Average values of the constants tabulated in Appendix 3 are shown together with the average r^2 in Tables 7.6 (using tidal displacement) and 7.7 (using salinity) for each combination of the exponents n and m.

Tables 7.6 and 7.7 clearly show that Eq. (7.9) provided the best fit to the variance in the data from both the winter and summer deployments, resulting in r^2 which were up to 15 % higher than those obtained with Eq. (7.8). As the only difference between these two equations resides in the use of either the tidal displacement (Eq. (7.8)) or the salinity (Eq. (7.9)) as independent variable, the above result indicates that the high frequency variations in beam attenuation are more related to changes in water type (represented by salinity) than to tidal advection. Following the observations made above, Eq. (7.9) was selected as the best fit to both the winter and summer data and consequently no further reference is made to Eq. (7.8).

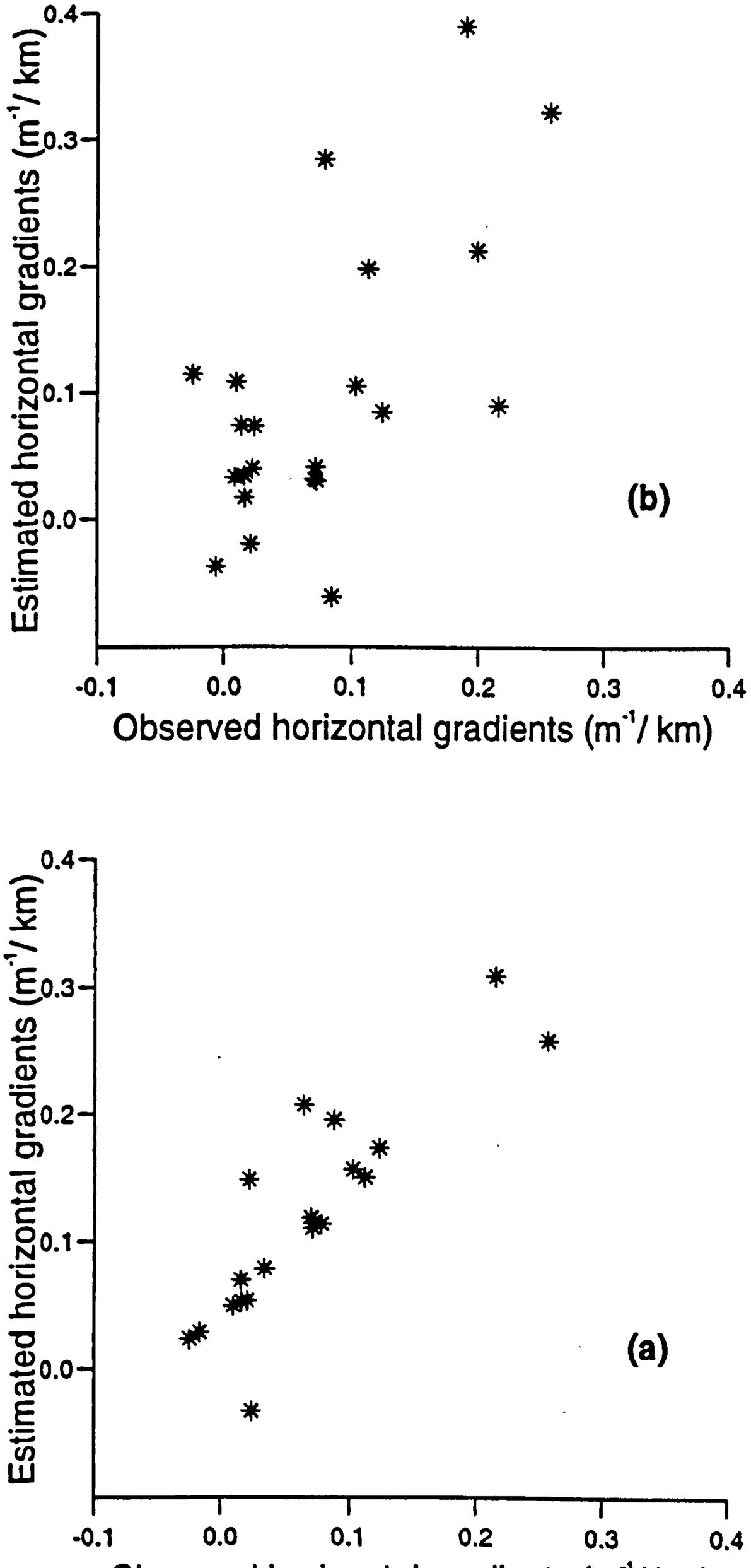

Figure 7.16 Comparison between observed and estimated horizontal gradients of beam attenuation at the surface: (a) LB2 and (b) LB3

Increasing the exponent m from 1 to 3 resulted in a small but consistent decrease in r^2 for both the winter and summer data (Tables 7.7). Therefore, changes in beam attenuation are associated with variations in the wind speed (m = 1) as opposed to the wind speed squared (m = 2) or cubed (m = 3).

There is a less clear relationship between n and the variance accounted for by the fit. In some cases, incrementing n from 1 to 3 induced a slight (less than 1 %) decrease in r^2 for the winter data at the surface at LB2 and LB3 and the summer data at LB3 32 mab. For the winter data at LB3 3 mab, an increase in r^2 of the order 1.5 % occurred when n was varied from 1 to 3. In this last case, because the same amount of variance explained by the fit was obtained for n = 2 and n = 3, the exponent n in Eq. (7.9) was set to 2.

In summary, Eq. (7.9) with n = 1 and m = 1 was the best fit to the variance in the data at: LB2 and LB3 surface (winter) and LB3 32 mab (summer). In this case, the fit accounted respectively for 46.0, 51.3, and 36.2 % of the variance in the data. For the winter data at LB3 3 mab, the best fit was obtained with Eq. (7.9) for n = 2 and m = 1 and described nearly 64 % of the variability in the data.

The standard deviations of the average values of the constants for the best fit were calculated for each data set to check whether the mean values were statistically significant (Table 7.7). The standard deviations were determined from the estimated standard deviations of the individual values tabulated in Appendix 3 using Eq. (6.5). These calculations revealed that for the winter data at the surface at LB2 and LB3, the averages of k_0', k_2', and k_3' were much larger than their respective standard deviations. This indicates that the average values were statistically significant. The standard deviations of the mean of k_1' at LB2 and LB3 were of the same order of magnitude as their actual values. Also, it can be seen from Appendix 3 that over 66% of the individual values of k_1' were nonsignificant. Therefore, beam attenuation variations at the surface at LB2 and LB3 during the winter deployment were not determined by the

current speed. At both sites, the average of k_2' is positive which means that an increase in wind speed would result in an increase in beam attenuation. The mean value of k_2' at LB2 is ~ 1.6 times larger than its value at LB3, indicating stronger wind effects at the shallower site LB2. The average value of k_3' being negative means that high beam attenuation values were associated with low salinities and vice versa. This suggests that fresher water recently input to Liverpool Bay from the rivers is more turbid.

For the winter data at LB3 32 mab, the mean values of k_0', k_1', and k_3' for the best fit were significant (Table 7.7). In this case, the beam attenuation increased with the current speed squared ($k_1' > 0$) and decreased with the salinity ($k_3' < 0$). As for the surface data, high beam attenuation values were associated with fresher water. Eight out of the ten individual values of k_2' were nonsignificant (Appendix 3), suggesting that wind speed did not affect the beam attenuation variations at LB3 3 mab during the winter deployment.

The results for the summer data at LB3 32 mab revealed that both current and wind speeds had little bearing on the beam attenuation variations (Appendix 3 and Table 7.7). Examination of the individual values of k_3' showed that most of them were significant. However, the average of k_3' was nonsignificant. The values of k_3' which were used to calculate its mean were in general positive between the 14th and the 26th June and negative between the 26th June and the end of the deployment (Appendix 3).

7.5 Discussion

The summer and winter observations at LB3 showed a strong seasonal cycle in beam attenuation. The mean value at the surface during the winter deployment was 2.1 m^{-1}, whereas, for the summer deployment at 9 m below the surface the mean was 0.8 m^{-1}. These observations agree well with other beam attenuation measurements made in other

	n	m	k_0	k_1	k_2	k_3	R^2 (%)
	1	1	1.30	0.97	29.75 x10^{-3}	-6.42 x10^{-2}	47.9
	1	2	1.34	0.98	7.60 x10^{-3}	-6.38 x10^{-2}	47.3
	1	3	1.35	0.99	1.80 x10^{-3}	-6.37 x10^{-2}	46.7
	2	1	1.43	1.67	21.44 x10^{-3}	-6.47 x10^{-2}	49.7
LB3 3 mab	2	2	1.46	1.70	5.60 x10^{-3}	-6.43 x10^{-2}	49.2
	2	3	1.47	1.73	1.23 x10^{-3}	-6.42 x10^{-2}	48.7
	3	1	1.48	3.30	13.06 x10^{-3}	-6.48 x10^{-2}	50.2
	3	2	1.51	3.38	3.53 x10^{-3}	-6.43 x10^{-2}	49.8
	3	3	1.52	3.44	0.67 x10^{-3}	-6.40 x10^{-2}	49.2
	1	1	2.01	-0.11	24.02 x10^{-3}	-8.03 x10^{-2}	37.7
	1	2	2.10	-0.11	1.91 x10^{-3}	-7.97 x10^{-2}	36.3
	1	3	2.13	-0.12	0.40 x10^{-3}	-7.94 x10^{-2}	34.8
	2	1	2.00	-0.12	24.01 x10^{-3}	-8.03 x10^{-2}	37.4
LB3 sfc	2	2	2.08	-0.14	1.92 x10^{-3}	-7.99 x10^{-2}	36.0
	2	3	2.11	-0.15	0.40 x10^{-3}	-7.96 x10^{-2}	34.5
	3	1	1.99	-0.10	24.19 x10^{-3}	-8.04 x10^{-2}	37.0
	3	2	2.07	-0.15	1.94 x10^{-3}	-8.00 x10^{-2}	35.7
	3	3	2.10	-0.17	0.40 x10^{-3}	-7.97 x10^{-2}	34.2
	1	1	2.30	-0.21	55.30 x10^{-3}	-9.57 x10^{-2}	41.3
	1	2	2.46	-0.21	4.90 x10^{-3}	-9.52 x10^{-2}	40.5
	1	3	2.52	-0.21	0.80 x10^{-3}	-9.51 x10^{-2}	39.3
	2	1	2.28	-0.29	55.78 x10^{-3}	-9.59 x10^{-2}	41.4
LB2 sfc	2	2	2.44	-0.30	4.96 x10^{-3}	-9.54 x10^{-2}	40.7
	2	3	2.50	-0.32	0.81 x10^{-3}	-9.53 x10^{-2}	39.6
	3	1	2.26	-0.41	56.34 x10^{-3}	-9.59 x10^{-2}	41.3
	3	2	2.42	-0.44	5.03 x10^{-3}	-9.54 x10^{-2}	40.6
	3	3	2.49	-0.48	0.82 x10^{-3}	-9.54 x10^{-2}	39.4
	1	1	0.84	-29.63 x10^{-3}	2.91 x10^{-3}	-1.75 x10^{-3}	34.2
	1	2	0.84	-29.67 x10^{-3}	0.76 x10^{-3}	-1.64 x10^{-3}	33.9
	1	3	0.85	-29.73 x10^{-3}	0.12 x10^{-3}	-1.60 x10^{-3}	33.0
	2	1	0.84	-34.58 x10^{-3}	2.77 x10^{-3}	-1.79 x10^{-3}	34.8
LB3 32 mab	2	2	0.84	-34.60 x10^{-3}	0.75 x10^{-3}	-1.67 x10^{-3}	34.5
	2	3	0.84	-35.02 x10^{-3}	0.12 x10^{-3}	-1.64 x10^{-3}	33.5
	3	1	0.83	-40.87 x10^{-3}	2.75 x10^{-3}	-1.80 x10^{-3}	34.4
	3	2	0.84	-41.03 x10^{-3}	0.74 x10^{-3}	-1.69 x10^{-3}	34.1
	3	3	0.84	-42.30 x10^{-3}	0.12 x10^{-3}	-1.66 x10^{-3}	33.2

Table 7.6 Average values of the constants resulting from the regression analyses on the 3-day time-series of beam attenuation using Eq. (7.8).

	n	m	k_0'	k_1'	k_2'	k_3'	R^2 (%)
	1	1	57.83	0.87	18.89 $x10^{-3}$	-1.70	62.5
	1	2	57.68	0.87	3.34 $x10^{-3}$	-1.69	61.6
	1	3	57.87	0.88	0.98 $x10^{-3}$	-1.69	60.9
	2	1	57.88	1.46	17.68 $x10^{-3}$	-1.70	63.9
			(2.74)*	(0.11)*	(12.55 $x10^{-3}$)*	(0.08)*	
LB3 3 mab	2	2	57.67	1.47	3.13 $x10^{-3}$	-1.69	63.1
	2	3	57.86	1.49	0.94 $x10^{-3}$	-1.69	62.5
	3	1	57.68	2.75	16.38 $x10^{-3}$	-1.68	63.9
	3	2	57.42	2.78	2.95 $x10^{-3}$	-1.68	63.1
	3	3	57.61	2.81	0.91 $x10^{-3}$	-1.68	62.4
	1	1	66.96	-0.17	39.08 $x10^{-3}$	-1.95	51.3
			(3.25)*	(0.06)*	(3.49 $x10^{-3}$)*	(0.10)*	
	1	2	65.60	-0.17	3.14 $x10^{-3}$	-1.91	49.6
	1	3	64.74	-0.18	0.37 $x10^{-3}$	-1.88	47.9
	2	1	67.04	-0.20	39.04 $x10^{-3}$	-1.95	51.0
LB3 sfc	2	2	65.74	-0.21	3.16 $x10^{-3}$	-1.91	49.4
	2	3	64.91	-0.22	0.37 $x10^{-3}$	-1.88	47.6
	3	1	67.20	-0.22	39.13 $x10^{-3}$	-1.96	50.6
	3	2	65.96	-0.26	3.17 $x10^{-3}$	-1.92	49.0
	3	3	65.12	-0.29	0.37 $x10^{-3}$	-1.89	47.3
	1	1	65.86	-0.17	62.72 $x10^{-3}$	-1.90	46.0
			(4.88)*	(0.09)*	(6.19 $x10^{-3}$)*	(0.15)*	
	1	2	65.04	-0.17	5.20 $x10^{-3}$	-1.87	45.0
	1	3	64.00	-0.18	0.73 $x10^{-3}$	-1.84	43.7
	2	1	65.98	-0.22	63.18 $x10^{-3}$	-1.90	46.0
LB2 sfc	2	2	65.15	-0.23	5.28 $x10^{-3}$	-1.87	45.1
	2	3	64.06	-0.24	0.74 $x10^{-3}$	-1.84	43.7
	3	1	66.14	-0.28	63.74 $x10^{-3}$	-1.91	45.7
	3	2	65.25	-0.31	5.31 $x10^{-3}$	-1.88	44.8
	3	3	64.32	-0.34	0.75 $x10^{-3}$	-1.85	43.5
	1	1	1.40	-15.79 $x10^{-3}$	3.11 $x10^{-3}$	-17.96 $x10^{-3}$	36.2
			(0.50)*	(7.80 $x10^{-3}$)*	(1.54 $x10^{-3}$)*	(15.08 $x10^{-3}$)*	
	1	2	1.34	-16.09 $x10^{-3}$	0.50 $x10^{-3}$	-15.70 $x10^{-3}$	35.8
	1	3	1.35	-16.38 $x10^{-3}$	0.08 $x10^{-3}$	-16.20 $x10^{-3}$	34.8
	2	1	1.42	-19.30 $x10^{-3}$	2.96 $x10^{-3}$	-18.59 $x10^{-3}$	36.3
LB3 32 mab	2	2	1.36	-19.50 $x10^{-3}$	0.48 $x10^{-3}$	-16.41 $x10^{-3}$	36.0
	2	3	1.37	-20.17 $x10^{-3}$	0.08 $x10^{-3}$	-16.81 $x10^{-3}$	35.0
	3	1	1.43	-23.18 $x10^{-3}$	2.91 $x10^{-3}$	-18.86 $x10^{-3}$	35.9
	3	2	1.37	-23.51 $x10^{-3}$	0.47 $x10^{-3}$	-16.75 $x10^{-3}$	35.5
	3	3	1.38	-25.00 $x10^{-3}$	0.07 $x10^{-3}$	-17.21 $x10^{-3}$	34.6

Table 7.7 Average values of the constants resulting from the regression analyses on the 3-day time-series of beam attenuation using Eq.(7.9). * standard deviations for the best fit.

parts of the Irish Sea (Mitchelson, 1984 and Weeks, 1989)

There was no apparent spring-neap cycle in the observed time-series from the winter deployment at both moorings. However, during the summer deployment the mean values were slightly higher at springs than at neap tides. The measurements made by Weeks (1989) revealed a strong tidal response in spring and autumn which was not present in the summer records.

The observed horizontal gradients of beam attenuation between LB2 and LB3 during the winter deployment were always positive: the beam attenuation increased onshore. This agrees with measurements of SPM concentrations in Liverpool Bay (Jacob, 1982 and Weeks, 1989).

At LB3 during the winter deployment the beam attenuation values were higher at 3 mab than at the surface. The mean value of the vertical gradient between 3 mab and the surface was 0.0118 m^{-1}/m. One significant exception occurred during the period of strong stratification when these gradient became negative: the surface values were higher that those at 3 mab. This suggests that either SPM has been input from the rivers or has been resuspended very near to the shore then carried out by the fresher water.

The regression analyses on the low frequency beam attenuation from the winter deployment at the surface at LB2 and LB3 showed that approximately 50 % of the variance in the time-series can be explained in terms of changes in the windstress, the low frequency displacement, and the tidal range. At both sites the beam attenuation lagged the wind speed by 10 hours. The wind effects were found to be stronger at the shallower site LB2.

The estimated horizontal mean gradient in beam attenuation was negative, whereas the observed mean was positive. This lack of agreement could be due to extrapolating the

low frequency displacement a long way (up to 40 km, see Fig 7.14c) from the moorings. In effect, it is assumed that the currents at the moorings are representative of the currents throughout Liverpool Bay, but this may not be the case. The source of the water parcels estimated by integrating the current meter record may therefore be very different from their real source (for example there may be a re-circulating eddy that the current meter is not picking up). This is an illustration of the problem of estimating low frequency displacements from a single mooring.

The regression analyses on the 3-day time-series indicated that the high frequency variations in beam attenuation from the winter and summer deployments were more related to salinity changes than to tidal advection. The beam attenuation at the surface at LB2 and LB3 during the winter increased with the wind speed. The wind response at LB2 was approximately twice that at LB3. The correlation between beam attenuation and salinity was negative at both sites: fresher water was more turbid. The current speed did not appear to have any bearing on the surface beam attenuation.

The beam attenuation at 3 mab at LB3 during the winter deployment was determined by changes in the current speed squared and the salinity. It increased with the current speed squared because the amount of particles in the water column had been increased by local resuspension. There was no evidence of local resuspension in the surface time-series at this site. This suggests that the resuspended material did not reach the height of the instrument and hence, was not detected. Similarly, as for the surface data, there was a negative correlation between the beam attenuation and the salinity. The wind speed did not apparently contribute to changes in beam attenuation. However, it must be stressed that the record at 3 mab did not include the period of very strong winds.

During the summer deployment at LB3, the contributions of both the current and wind speeds to the variations in beam attenuation were nonsignificant. However, beam attenuation was correlated with salinity. The correlation between these two parameters was positive between the 14th and the 26th June and negative for most of the remaining

3-day periods.

A major result from the in-situ data was the importance of windstress, and its episodic nature, on the level of beam attenuation. The results from the winter deployment clearly show how quickly the SPM concentrations respond to storms: within hours of the wind speed increasing the concentrations have markedly increased. Conversely, as the wind abates the sediment levels rapidly decrease due to settling and/or horizontal advection. This wind generated event dominates the beam attenuation record and emphasises the role of windstress in the dynamics of sediments, particularly in shallow waters.

CHAPTER 8

Summary

There is an ever growing interest in the study of SPM distributions in shelf seas which is driven by concern over water quality and the effects of pollution on fisheries. The high temporal and spatial variability of SPM distributions in shelf seas makes their monitoring in-situ difficult. Self recording optical sensors have increased the temporal coverage but the spatial coverage is still limited. However, remote sensing with its extensive synoptic and frequent sampling can make a major contribution to this field.

For the first time an extensive data set of AVHRR visible band imagery was used to study the variations of surface suspended sediments in the Irish Sea. The imagery has shown that the surface reflectance due to suspended sediments undergoes a seasonal variation. The magnitude of this variation was assessed throughout the Irish Sea using a statistical model. The maximum reflectances have been seen to occur early in the year and the minimum in the summer.

The results from the model have also shown that the annual mean reflectance varies widely throughout the Irish Sea. High annual means are found in areas around the north west coast of Anglesey, along the Irish coast near Wicklow, in Liverpool Bay and Cardigan Bay. In these areas the annual means are typically of the order of 2.0 %.

Low annual means (< 1.3 %) are found in the northern part of Irish Sea, i.e. the area to the north of latitude 53.5° and outside Liverpool Bay. The other area of low values is the narrow section that runs northwards from St George's Channel, into the central Irish Sea and finally into its northern part.

The amplitude of the annual variation exhibits a spatial distribution which is similar to that of the annual mean. These parameters were found to be highly correlated i.e. small amplitudes are associated with low means and high amplitudes with high means. High amplitudes occur in Cardigan Bay, Liverpool Bay, off Wicklow and off the north west coast of Anglesey. Typically the values are greater than 0.7 % in these areas.

Low amplitudes of the order of 0.3 % occur in the northern part of the Irish Sea and in a central section running from the south to the north. The lowest amplitudes ~ 0.1 % are found in the area between the Isle of Man and the coast of Northern Ireland.

The spring-neap variation of surface reflectance was investigated using a statistical model. The results of the model have shown that there is a significant spring-neap cycle of reflectance in: the central and southern parts of the Irish Sea; Liverpool Bay and Cardigan Bay. In these areas the reflectance varies by as much as 0.64 % from springs to neaps. The other area of significant spring-neap variation is north of the Isle of Man where the spring to neap variation is ~ 0.32 %. In the remainder of the Irish Sea, most notably the area to the west and south-west of the Isle of Man there is not a significant spring-neap variation.

The combined effects of the seasonal and spring-neap cycles explain as much as 60 % of the total variance of the observed surface reflectance. Individually the seasonal cycle accounts for up to 50 % of the total variance.

The spatial variation of the annual mean can be understood in terms of the distribution of the availability of tidal turbulent kinetic energy. Areas where the availability of tidal TKE is high have larger annual means than areas where the availability of tidal TKE is low.

The seasonal variation and its spatial distribution can be explained by the availability of tidal TKE in winter and the availability of sediments in the summer. The amplitude

of the seasonal variation was shown to be correlated to U^3/h i.e. to the availability of tidal TKE. It is not at first obvious why the amplitude should be dependent on the level of TKE as the latter is constant throughout the year. If the availability of sediments was large in winter, then, surface SPM concentrations would be controlled by the availability of tidal TKE. In the summer, if the availability of sediments is greatly diminished, then, irrespective of the level of tidal TKE, the surface SPM concentrations would be reduced. These conditions would explain the seasonal variation of surface reflectance in the Irish Sea and the correlation of the amplitude with U^3/h. Variations in sediments availability can result either from a reduction of the total sediment load in the Irish Sea and/or the sediments present become harder to erode in the summer.

It can not be ascertained that the summer pycnocline regulates the surface SPM concentrations in the seasonally stratified waters but it cannot either be discounted, particularly, in Cardigan Bay where a strong seasonal cycle was observed. Heathershaw and Simpson (1974) found the distribution of transmittance in the seasonally stratified region south-west of the Isle of Man to be strongly related to the temperature structure. Evidence of this process was also reported by Weeks (1989).

This work also suggests that the type of seabed sediments may play a role in the distribution of SPM in the Irish Sea. In general, areas of high annual mean and high amplitudes were seen to be associated with sandy seabeds e.g. Liverpool Bay and Cardigan Bay. Areas of cohesive seabed sediments such as south-west of the Isle of Man are associated with the lowest means and amplitudes.

The beam attenuation data from the winter and summer deployments have shown further evidence of a pronounced seasonal variation in SPM concentrations at two sites in Liverpool Bay. The mean level and variability of beam attenuation was higher in winter than in summer.

At the surface during the winter deployment horizontal gradients of beam attenuation were maintained between the two moorings throughout the deployment. The values increased towards the coast. The near-bottom values of beam attenuation were higher than those at the surface (the difference between bottom and surface values did not exceed 5.0 m^{-1} over the period of the near-bottom observations). However, there was a period during which the vertical gradients became negative. This period coincided with a time of sustained stratification. The observed increase in surface particulates is accounted for by the freshwater plume being horizontally advected offshore. As the period of stratification progressed the values of beam attenuation decreased as a result of settling and/or dilution of particles.

The results showed that up to 50 % of the low frequency variations of surface beam attenuation during the winter deployment were associated with changes in windstress, the low frequency displacement and tidal range. The levels of SPM showed a fast response ~10 hours to changes in windstress at both sites with the effects of wind being stronger at the shallower site. The regression analyses showed that there was a significant spring-neap variation of beam attenuation. However, this variation was not apparent in the time-series as the latter were dominated by the variations due to windstress.

During the winter the high frequency variations of beam attenuation at the surface can be understood in terms of variations in salinity and wind speed. The correlation between beam attenuation and salinity was negative i.e. fresher water was associated with higher levels of particulates. Beam attenuation values increased with wind speed. The high frequency variations of beam attenuation at the bottom can be explained in terms of changes in salinity and current speed squared. Similarly as for the surface data there was a negative correlation between the salinity and beam attenuation. The local resuspension signal indicated by the correlation with the current speed squared was not observed in the surface data. This is indicative either of a lack of turbulent kinetic energy to mix the suspended sediments up to the surface or the suspended particles

have a fast settling rate or the suspended material was advected away from the point where it was resuspended. The high frequency variations of beam attenuation in the summer did not appear to respond to either current or wind speeds. However, the levels of beam attenuation changed with water type but unlike the winter data the sign of the correlation with salinity is not consistent throughout the deployment.

The strong correlation between beam attenuation and salinity suggests either that rivers are sources of suspended sediments or particles are resuspended near to the shore and horizontally advected offshore with the fresher water.

An important finding from the in-situ data was the effects of wind on SPM concentrations, particularly, during periods of high windstress associated with winter. Enhancement of bed stresses during these events result in greater resuspension and hence, to increased concentrations. During the summer deployment the mean wind speeds were lower than those in winter and no periods of strong winds occurred. Hence, the summer deployment was absent of any wind-induced periods of increased concentrations. If this difference between winter and summer conditions is representative it would suggest that wind does contribute to the seasonal variation. Its effect is to produce periods of high resuspension which are more intense and more frequent in the winter. Thereby increasing the difference between winter and summer levels of suspended sediments.

The results presented in this thesis are based on observations from two independent data types. The insights gained from the two data sets complement each other and have led to a more complete understanding of the nature of the variations of SPM in the Irish Sea and their controls. The satellite data results have shown that the surface reflectance in the Irish Sea undergoes seasonal and springs-neaps variations; similar variations are also evident in the beam attenuation at the two mooring sites. Such agreement indicates that the two signals have a common cause i.e. variations in SPM concentrations.

The satellite results have shown that the seasonal variation of surface reflectance in the Irish Sea is controlled by the availibility of tidal TKE. It was suggested that a further control was needed to explain this dependency: a possibility is the seasonal availability of sediment. The in-situ data have indicated that the wind may also contribute to the seasonal variation of SPM concentrations. However, time-series of beam attenuation from a site of 75 m depth, off the north coast of Anglesey, did not exhibit any correlation with windstress (Weeks, 1989). This supports the contention that wind effects are most important in shallow waters. Therefore, the contribution of the wind to the variations of surface reflectance must be considered particularly in the shallower parts of the Irish Sea. The wind effects may also explain some of the scatter around the seasonal variation of surface reflectance seen in Fig. 6.4.

Although the in-situ data are limited spatially, they have provided added information on the high frequency variations of SPM concentrations. The real strenght of the satellite data is its extensive spatial coverage, which means maps of the annual mean and the amplitude of the seasonal and springs-neaps variations can be drawn.

This work has established the important parameters which must be included in future attempts to model SPM distributions in shelf seas. The essential components of such model are: resuspension by wind and tides, advection, settling and availibility of sediment. This latter term will be hard to quantify and will depend on biological and chemical, as well as physical factors. It may be possible to determine the sources and sinks of sediment in coastal areas by establishing a sediment budget.

REFERENCES AND BIBLIOGRAPHY

* indicates publications used in this thesis but not cited in the text.

Aanderaa (1978). *RCM 4 operating manual,* technical description no. 119. Aanderaa, Bergen, Norway.

Aanderaa (1987). *RCM 7 & 8 operating manual,* technical description no. 159, Aanderaa, Bergen, Norway.

Agnew, M.M. (1983). A study of the use of sea colour for determining phytoplankton pigment and seston concentrations in coastal waters. MSc Thesis, University of Wales.

Arnone, R.A. and P.E. La Violette (1984). A method of selecting optimal Angstrom coefficients to obtain quantitative ocean color data from Nimbus-7 CZCS. *Proceedings of the Society of Photo-Optical Instrumentation Engineers* **489**, 187-194.

Austin, R.W. (1974). The remote sensing of spectral radiance from below the ocean surface, In: *Optical aspects of Oceanography.* Eds Jerlov, N.G. and B. Neilson. Academic Press, New York, p 317-345.

Austin, R.W. (1980). Gulf of Mexico ocean-colour surface-truth measurements. *Boundary-layer Meteorology,* **18,** 269-285.

Baker, E.T., G.A Cannon and H.C. Curl Jr. (1983). Particle transport processes in a small marine bay. *J. Geophys. Res.,* **88**, 9661-9669.

Baker, E.T. and J.W. Lavelle (1984). The effect of particle size on the light attenuation coefficient of natural suspensions. *J. Geophys. Res.,* **89**, 8197-8203.

Bartz, R., J.R.V. Zanevel and H. Pak (1978). A transmissometer for profiling and moored observations in water. SPIE, *Ocean Optics V,* **160**, 102-108.

Belderson, R.H. (1964). Holocene sedimentation in the western half of the Irish Sea. *Mar. Geol.*, **2,** 147-163.

Bevington, P.R. (1969). *Data reduction and error analysis for the physical sciences.* McGraw-Hill Book Company, USA.

Bishop J.K.B, (1986). The correction and suspended particulate matter calibration of Sea Tech transmissometer data. *Deep Sea Res.,* **33,** 121-134.*

Bohlen, W.F. (1975). An investigation of suspended material concentrations in eastern Long Island Sound. *J. Geophys. Res.*, **80**, 5089-5100.

Bowden, K.F. (1955). Physical oceanography of the Irish Sea. *Fishery Invest.*, Lond., Ser. 2, **18 (8).**

Bowden, K.F. and S.H. Sharaf El Din (1966). Circulation and mixing processes in the Liverpool Bay area of the Irish Sea. *Geophys. J. R. astr. Soc.*, **11,** 279-292.

Buchan, S., G.D. Floodgate and D.J. Crisp (1967). Studies on the seasonal variation of the suspended matter in the Menai Straits. I the inorganic fraction. *Limnology and Oceanography,* **12**, 419-431.

Buchan, S., G.D. Floodgate and D.J. Crisp (1973). Studies of the seasonal variation of the suspended matter of the Menai Straits. II. Mid stream data. *Deut. Hydro. Zeit.* **2**, 74-83.*

Bukata, R.P., J.H. Jerome, J.E. Bruton, S.C. Jain and H.H. Zwick (1981). Optical water quality model of Lake Ontario. 1: Determination of the optical cross sections of organic and inorganic particulates in Lake Ontario. *Applied Optics,* **20**, 1696-1703.

Butman, B., M. Noble and D.W. Folger (1979). Long-term observations of bottom current and bottom sediment movement on the Mid-Atlantic continental shelf. *J. Geophys. Res.*, **84**, 1187-1205.

Cacchione, D.A. and D.E. Drake (1982). Measurements of storm-generated bottom stresses on the continental shelf. *J. Geophys. Res.*, **87**, 1952-1960.

Clark D.K., E.T. Baker and A.E. Strong (1980). Upwelled spectral radiance distribution in relation to particulate matter in sea water. *Bound. Layer Met.* **18,** 287-298.

Cox, C. and W. Munk (1955). Some problems in optical oceanography. *J. Mar. Res.*, **14**, 63-70.*

Cracknell, A.P. (1981). *Remote Sensing in Meteorology, Oceanography and Hydrology.* Ellis Horwood Limited, U.K. 541pp.*

Curran, O.J. and E.M.M. Novo (1988). The relationship between suspended sediment concentration and remotely sensed spectral radiance: A review. *J. Coast. Res.*, **4**, 351-368.*

Darecki, M. and A. Krężel (1992). Chlorophyll vs AVHRR satellite data during SKAGEX experiment (abstract). *Annales Geophysicae*, Supplement II to volume 10

Davies, A.M. and J.E. Jones (1992). A three-dimensional wind driven circulation model of the Celtic and Irish Sea. *Cont. Shelf Res.*, **12,** 159-188.

Eisma, D.and G. Irion (1988). Suspended matter and sediment transport. In: *Pollution of the North Sea: An Assessment.* Eds. W. Salamons, B.L. Bayne, E.K. Duursma and U. Förstner. Springer-Verlag, Berlin.

Elliott, A.J. (1991). EUROSPILL: Oceanographic processes and NW European databases. *Marine Pollution Bulletin,* **22,** 548-553.

Froidefond, J.M., P. Castaing, J.M. Jouanneau, R. Prud'Homme and A. Dinet (1993). Method for the qualification of suspended sediments from AVHRR NOAA-11 satellite data. *Int. J. Remote Sensing,* **14**, 885-894.

Gabrielson, J.O. and R.J. Lukatelich (1985). Wind-related resuspension of sediments in the Peel-Harvey estuarine system. *Estuarine, Coast. Shelf Sci.*, **20**, 135-145.

Gagliardini, D.A., H. Karszenbaum, R. Legeckis and V. Klemas. (1984). Application of Landsat MSS, NOAA/TIROS AVHRR, and Nimbus CZCS to study the La Plata River and its interaction with the ocean. *Remote Sens. Environ.*, **15**, 21-36.

Gardner, W.D. and I.D. Walsh (1990). Distribution of macroaggregates and fine-grained particles across a continental margin and their potential role in fluxes. *Deep-Sea Res.*, **37**, 401-411.

Gordon, H.R. (1976). Radiative transfer: a technique for simulating the ocean in satellite remote sensing calculations. *Applied Optics,* **15**, 1974-1979.*

Gordon, H.R. (1980). A preliminary assessment of the Nimbus-7 CZCS atmospheric correction algorithm in a horizontally inhomogeneous atmosphere. *Oceanography from Space*. Ed by J.F.R. Gower. Plenum Press. New York.

Gordon, H.R. and W.R. McCluney (1975). Estimation of the depth of sunlight penetration in the sea for remote sensing. *Applied Optics,* **14**, 413-416.*

Gordon, H.R., O.B. Brown and M.M. Jacobs (1975). Computed relationships between the inherent and apparent optical propeties of a flat homogeneous ocean. *Applied Optics,* **14**, 417-427.

Gordon, H.R. and D.K. Clark (1981). Clear water radiances for atmospheric correction of coastal zone color scanner imagery. *Applied Optics,* **20**, 4175-4180.

Gordon, H.R., D.K. Clark, J.W. Brown, O.B. Brown, R.H. Evans and W.W. Broenkow (1983). Phytoplankton pigment concentrations in the Middle Atlantic Bight: comparison of ship determinations and CZCS estimates. *Applied Optics,* **22,** 20-36.

Gordon, H.R., O.B. Brown, R.H. Evans, J.W. Brown, R.C. Smith, K.S. Baker and D.K. Clark (1988). A semianalytic radiance model of ocean color. *J. Geophys. Res.*, **93 C10,** 10909-10924.*

Grabemann, I. and G. Krause (1989). Transport processes of suspended matter derived from time series in a tidal estuary. *J. Geophys. Res.*, **94 C10,** 14373-14379.

Groom, S.B. and P.M. Holligan (1987). Remote sensing of Coccolithophore blooms. *Adv. Space Res.*, **7,** 73-78.

Halper, F.B and D.W. McGrail (1988). Long-term measurements of near-bottom currents and suspended sediment concentration on the outer Texas-Louisianan continental shelf. *Cont. Shelf Res.*, **8,** 23-36.

Hamblin, P.F. (1989). Observations and model of sediment transport near the turbidity maximum of the upper Saint Lawrence Estuary. *J. Geophys. Res.*, **94 C10,** 14419-14428.*

Heaps, N.S. (1972). Estimation of density currents in the Liverpool Bay area of the Irish Sea. *Geophys. J. R. Astr. Soc.*, **30,** 415-432.*

Heaps, N.S. and J.E. Jones (1977). Density currents in the Irish Sea. *Geophys. J. R. astr. Soc.*, **51,** 393-429.

Heathershaw D.C and J.H. Simpson (1974). Fine structure of light attenuation and its relation to temperature in the Irish Sea. *Estuarine and Coast. Mar. Sci.,* **2,** 91-103.

Holyer, R.J. (1978). Toward universal multispectral suspended sediment algorithms. *Remote Sens. Environ.*, **7,** 323-338.*

Jacob, N.J. (1982). Multispectral irradiance algorithms for the determination of chlorophyll an inorganic seston in the Irish Sea. MSc Thesis, University of Wales.

Jago, C.F. (1981). Sediment response to waves and currents, North Yorkshire Shelf, North Sea. *Spec. Publs. Int. Ass. Sediment,* **5,** 283-301.

Jago, C.F., A.J. Bale, M.O. Green, M.J. Howarth, S.E. Jones, I.N. McCave, G.E. Millward, A.W. Morris, A.A. Rowden and J.J. Williams (1993). Resuspension processes and seston dynamics, southern North Sea. *Phil. Trans. R. Soc. Lond.*, **A343,** 475-491.

Jago, C.F., and S.E. Jones (1994). Dynamics of suspended particulate matter in the Southern North Sea: I. Tidally mixed waters. *Cont. Shelf Res.* (in press).

Jerlov, N.G. (1976). *Marine Optics.* Elesevier, Amsterdam.

Jonasz, M. (1987). The effect of nonsphericity of marine particles on light attenuation. *J. Geophys. Res.*, **92 C13**, 14637-14640.

Jones, S.E., C.F. Jago and J.H. Simpson (1992). Simulation of suspended particulate dynamics in the southern North Sea. *In: Mixing Processes in Estuaries and Coastal Seas.* 6th International Biennial Conference on Physics of Estuaries and Coastal Seas, Margaret River, Centre for Water Research, Uni. of Western Australia, Perth. p51-55.*

Jones, S.E., C.F. Jago, D. Prandle and D. Flatt (1994a). Suspended sediment dynamics: Measurement and Modelling in the Dover Strait. In: *Mixing and Transport in the Environment.* Ed. By K.J. Beven, P.C. Chatwin and J.H. Millbank, John Wiley and Sons Ltd, U.K. 183-201.

Jones, S.E., C.F. Jago, A.J. Bale, D. Chapman, R. Howland and J. Jackson (1994b). Dynamics of suspended particulate matter in the Southern North Sea. II. Seasonally stratified waters. *Cont. Shelf Res.* (in press).

Jumars P.A., A.R.M. Nowell and R.F.L. Self (1981). A simple model of flow-sediment-organism interaction. *Mar. Geol.*, **42**, 155-172.*

Kirby, R. and W.R. Parker (1983). Distribution and behavior of fine sediment in the Severn Estuary and Inner Bristol Channel, U.K. *Can. J. Fish. Aquatic Sci.*, **40**, 83-95.

Kirk, J.T.O. (1983). *Light and photosynthesis in aquatic ecosystems.* Cambridge University Press, UK, 401pp.

Kitchen, J.C., J.R.V. Zaneveld and H. Pak (1982). Effect of particle size distribution and chlorophyll content on beam attenuation spectra. *Applied Optics*, **21**, 3913-3918.*

La Viollete, P.E., D.R. Johnson and D.A. Brooks (1990). Sun-glitter photographs of Georges Bank and the Gulf of Maine from the space shuttle. *Oceanography*, April 1990.*

Lavelle, J.W., R.A. Young, D.P Swift and T.L. Clarke (1978). Near-bottom sediment concentration and fluid velocity measurements on the inner continental shelf, New York. *J. Geophys. Res.*, **83**, 6052-6062.

Lavelle, J.W., H.O. Mofjeld and E.T Baker (1984). An in-situ erosion rate for a fine-grained marine sediment. *J. Geophys. Res.*, **89**, 6543-6552.

Lyon, J.G., K.W. Bedford, C-C.J. Yen, D.H. Lee and D.J. Mark (1988). Determinations of suspended sediment concentrations from multiple day Landsat and AVHRR data. *Remote Sens. Environ.*, **25**, 107-115.

MacFarlane, N and I.S. Robinson (1984). Atmospheric correction of Landsat MSS data for a multidate suspended sediment algorithm. *Int. J. Remote Sensing*, **5**, 561-576.

Madsen, O.S., L.D. Wright, J.D. Boon and T.A. Chisholm (1993). Wind stress, bed roughness and sediment suspension on the inner shelf during an extreme storm event. *Cont. Shelf. Res.*, **13**, 1303-1324.*

Mather, P.M. (1987). *Computer processing of remotely-sensed images.* John Wiley and Sons, UK, 352pp.

McCave, I.N. (1983). Particulate size spectra, behavior, and origin of Nepheloid layers over the Nova Scotian Continental Rise. *J. Geophys. Res.*, **88**, 7647-7666.*

McCave, I.N. (1984). Erosion, transport and deposition of fine-grained marine sediments. *Geol. Soc. London Spec. Pub.*, **15**, 35-69.*

Mehta A.J., T.M. Parchure, J.G. Dixit and R. Ariathurai (1982). Resuspension potential of deposited cohesive sediment beds. In: *Estuarine comparisons.* Ed. V.S. Kennedy. Academic Press, London, pp 591-609.*

Miller, I. (1985). Nutrient dynamics in relation to a thermohaline discontinuity in the NE Irish Sea. Ph.D. Thesis, University of Wales.

Mitchelson, E.G. (1984). Phytoplankton and suspended sediment distributions in relation to physical structure and water-leaving signals. Ph.D. Thesis, University of Wales Bangor, 126pp.

Mitchelson, E.G., N.J. Jacob and J.H. Simpson (1986). Ocean colour algorithms from the case 2 waters of the Irish Sea in comparison to algorithms from Case 1 waters. *Cont. Shelf Res.*, **5**, 403-415.*

Moody, J.A., B. Butman and H.H. Bothner (1987). Near-bottom suspended matter concentration on the Continental shelf during stoems: estimates based on in situ observations of light transmission and a particle size dependent transmissometer calibration. *Cont. Shelf Res.*, **7**, 609-628.

Morel, A. (1986). Chlorophyll-specific scattering coefficient of phytoplankton. A simplified theoretical approach. *Deep-Sea Res.*, 1093-1105.*

Morel, A. and L. Prieur (1977). Analysis of variations in ocean color. *Limnol. Oceanogr.*, **22**, 709-722.

Muir, A.S. (1991). Satellite Image Products. NERC Satellite Station Dundee University, U.K., 24pp.

Newton, A.J. and J.S. Gray (1972). Seasonal variation of suspended solid matter, off the coast of North Yorkshire. *J. Mar. Biol. Ass. U.K.*, **52**, 33-47.

Nichols, M.M. (1986). Effects of fine sediment resuspension in estuaries. In: *Estuarine cohesive sediment dynamics.* (Ed. A.J. Mehta). Springer-Verlag, Berlin.

Novo, E.M.M., J.D. Hansom and P.J. Curran (1989a). The effect of viewing geometry and wavelength on the relationship between reflectance and suspended sediment concentration. *Int. J. Remote Sensing,* **10**, 1357-1372.*

Novo, E.M.M., J.D. Hansom and P.J. Curran (1989b). The effect of sediment type on the relationship between reflectance and suspended sediment concentration. *Int. J. Remote Sensing,* **10,** 1283-1289.*

Nowell, A.R.M, P.A. Jumars and J.E. Eckman (1981). Effects of biological activity on the entrainment of marine sediments. *Mar. Geol.*, **42,** 133-153.*

Nunny, R.S. (1978). A desk-top study of the nature and dynamics of fine particulate matter in the northern Irish Sea in relation to the Windscale discharge. Ministry of Agriculture, Fisheries and Food, Marine Environment Protection, **2,** 40pp.

Nykjaer, L. (1988). Remote sensing applied to the Northwest African upwelling area. Ph.D. Thesis, University of Copenhagen 144pp.*

Pantin, H.M. (1978). Quaternary sediments from the north-east Irish Sea: Isle of Man to Cumbria. *Bull. Geol. Surv. G.B.* **64.**

Pejrup, M. (1986). Parameters affecting fine-grained suspended sediment concentrations in a shallow micro-tidal estuary, Ho Bugt, Denmark. *Estuarine, Coast. Shelf Sci.*, **22,** 241-254.

Pingree, R.D. and D.K. Griffiths (1978). Tidal fronts on the shelf seas around the British Isles. *J. Geophys. Res.*, **83 C9**, 4615-4622.

Pingree, R.D. and D.K. Griffiths (1979). Sand transport paths around the British Isles resulting from M_2 and M_4 tidal interactions. *J. mar. bio. Ass. U.K.*, **59**, 497-513.

Plass, G.N., T.J. Humphreys and G.W. Kattawar (1978). Color of the ocean. *Applied Optics,* **17**, 1432-1446.*

Postma, H. (1967). Sediment transport and sedimentation in the estuarine environment. In: *Estauries.* Ed. G.H. Lauff, Am. Assoc. Adv. Sci., Washington DC. 158-179.

Postma, H. (1980). Sediment transport and sedimentation. In: *Chemistry and Biogeochemistry of Estuaries.* Ed. E. Olausson and I. Cato, John Wiley ans Sons Ltd, UK.*

Prangsma, G.J. and J.N. Roozekrans (1989). Using NOAA AVHRR imagery in assessing water quality parameters. *Int. J. Remote Sensing,* **10**, 811-818.

Prieur, L. and S. Sathyendranath (1981). An optical classification of coastal and oceanic waters based on the specific spectral absorption curves of phytoplankton pigments, dissolved organic matter, and other particulate materials. *Limnol. Oceanogr.,* **26**, 671-689.

Pugh, D. (1987). *Tides, surges and mean sea-levels.* John Wiley and Sons, Chichester, 472pp.

Quenzel, H. and M. Kaestner (1980). Masking effects of the atmosphere on remote sensing of chlorophyll. In: *Oceanography from space*, Ed. by J.F.R. Gower. Plenum Press, New York.

Quibell, G. (1991). The effect of suspended sediment on reflectance from freshwater algae. *Int. J. Remote Sensing,* **12**, 177-182.*

Ramster, J.W. and H.W. Hill (1969). Current system in the Northern Irish Sea. *Nature,* **224**, 59-61.

Rimmer, J.C, M.B. Collins and C.B. Pattiaratchi (1987). Mapping of water quality coastal waters using Airborne Thematic Mapper data. *Int. J. Remote Sensing,* **8**, 85-102.*

Ritchie, J.C., C.M. Cooper and J. Yongqing (1987). Using Landsat multispectral scanner data to estimate suspended sediments in Moon Lake, Mississippi. *Remote Sens. Environ.,* **23**, 65-81.

Robinson, I.S. (1979). The tidal dynamics of the Irish and Celtic Seas. *Geophys. J. R. Astro. Soc.,* **56**, 159-197.*

Robinson, I.S. (1983). Satellite observations of ocean colour. *Phil. Trans. R. Soc. Lond.,* **A309**, 415-432.*

Robinson, I.S. (1985). Satellite Oceanography. Ellis Horwood Limited, UK, 455pp.

Robinson, I.S. (1990). Remote sensing - information from the colour of the seas. In: *Light and Life in the Sea.* Ed. P.J. Herring, A.K. Campbell, M. whitfield and L. Maddock, CUP, Cambridge, U.K., 19-38.

Rodolfo, K.S., B.A. Buss and O.H. Pilkey (1971). Suspended sediment increase due to Hurricane Gerda in continental shelf waters off Cape Lookout, North Carolina. *J. Sediment. Petrol.,* **41,** 1121-1125.

Roozekrans, J.N. and G.J. Prangsma (1988). Processing and application of digital AVHRR-imagery for land and ses surfaces. Final report of BCRS project no. TO-3.1, K.M.N.I., Netherlands.

Sagan, S. and P. Kowalczuk (1992). Some optical properties of Skageraak waters vs AVHRR satellite data (Abstract). *Annales Geophysicae*, supplement II to volume 10

Satellite Receiving Station Dundee University (1986), Satellite Image products available from Dundee University. Dundee University, UK.

Sathyendranath, S. and A. Morel (1983). Light emerging from the sea - Interpretation and uses in remote sensing. In: *Remote Sensing Applications in Marine Science and Technology.* Ed by A.P. Crcknell. 323-357.

Sathyendranath, S., L Prieur and A. Morel (1989). A three-component model of ocean colour and its application to remote sensing of phytoplankton pigments in coastal waters. *Int. J. Remote Sensing,* **10**, 1373-1394.

Sathyendranath, S. and T. Platt (1990). The light field in the ocean: its modification and exploitation by the pelagic biota. In: *Light and Life in the Sea.* Ed. P.J. Herring, A.K. Campbell, M. whitfield and L. Maddock, CUP, Cambridge, U.K., 3-18.

Sharples, J. (1992). Time dependent stratification in regions of large horizontal gradient. Ph.D. Thesis, University of Wales.

Simpson, J.H. and J.R. Hunter (1974). Fronts in the Irish Sea. *Nature,* **250,** 404-406.

Simpson, J.H. and J. Brown (1987). The interpretation of visible band imagery of turbid shallow seas in terms of distribution of suspended particles. *Cont. Shelf. Res.*, **7**, 1307-1313.

Simpson, J.H., J. Brown, J. Matthews and G. Allen (1990). Tidal straining, density currents, and stirring in the control of estuarine stratification. *Estuaries,* **13**, 125-132.

Simpson, J.H., W.G. Bos, F. Schirmer, A.J. Souza, T.P. Rippeth, S.E. Jones and D. Hydes (1993). Periodic stratification in the Rhine ROFI in the North Sea. *Oceanologica Acta,* **16**, 23-32.

Singh, S.M. and A.P. Cracknell (1986). The estimation of atmospheric effects for SPOT using AVHRR channel-1 data. *Int. J. Remote Sensing,* **7**, 361-377.

Smith, R.C. and K.S. Baker (1981). Optical properties of the clearest natural waters 200-800 nm). *Applied Optics,* **20**, 177-184.

Spinrad, R.W., J.R.V. Zaneveld and J.C. Kitchen (1983). A study of the optical characteristics of the suspended particles in the benthic Nepheloid layer of the Scotian Rise. *J. Geophys. Res.*, **88**, 7641-7645.

Spitzer, D., R. Laane and J.N. Roozekrans (1990). Pollution monitoring of the North Sea using NOAA/AVHRR imagery. *Int. J. Remote Sensing,* **11**, 967-977.

Stride, A.H. (1973). Sediment transport by the North Sea. In: *North Sea Science,* Ed. E.D. Goldberg, MIT Press, Camb., M.A., 101-130.

Stumpf, R.P. (1987). Application of AVHRR satellite data to the study of sediment and chlorophyll in turbid coastal water. A NOAA Technical Memorandum NESDIS AISC 7 pp50.

Stumpf, R.P. and J.R. Pennock (1989). Calibration of a general optical equation for remote sensing of suspended sediments in a moderately turbid estuary. *J. Geophys. Res.*, **94 (C10)**, 14363-14371.

Stumpf, R.P. and M.A. Tyler (1988). Satellite detection of bloom and pigment distributions in estuaries. *Remote Sens. Environ.*, **24**, 385-404.

Stumpf, R.P., G. Gelfenbaum and J.R. Pennock (1993). Wind and tidal forcing of a buoyant plume, Mobile Bay, Alabama. *Cont. Shelf Res.*, **13**, 1281-1301.

Stumpf, R.P. (1988). Sediment transport in Chesapeake Bay during floods: Analysis using satallite and surface observations. *J. Coast. Res.*, **4**, 1-15.

Sturm, B. (1981). The atmospheric correction of remotely sensed data and the quantitative determination of suspended matter in marine water surface layers. In: *Remote sensing in meteorology, oceanography and hydrology.* Ed. A.P. Cracknell. Ellis Horwood, Chichester, 163-197.

Sündermann, J. and R. Klöcker (1983). Sediment transport modelling with applications to the North Sea. In: *North Sea Dynamics.* Ed. J. Sündermann and Lenz. Springer-Verlag, Berlin.*

Sündermann, J. and W. Puls (1990). Modelling of suspended sediment deispersion and related transport of lead in the North Sea. *Mitt. Geol.-Paläont. Insitut Univ, Hamburg,* **69,** 143-155.

Sündermann, J. (1993). Suspended particulate matter in the North Sea: field observations and model simulations. *Phil. Trans. R. Soc. Lond.,* **A343,** 423-430.

Tassan, S. (1981). A method for the retrieval of phytoplankton and suspended sediment concentrations from remote measurements of water colour. *Proceedings of the Fifteenth International Symposium on Remote Sensing of Environment,* Ann Arbor, Mi, May 1981. 577-586.

Tassan, S. (1988). The effect of dissolved 'yellow substance' on the quantitative retrieval of chlorophyll and total suspended sediment concentrations from remote measurements of water colour. *Int. J. Remote Sensing,* **9,** 787-797.*

Tassan, S. and B. Sturm (1986). An algorithm for the retrival of sediment content in turbid coastal waters from CZCS data. *Int. J Remote Sensing,* **7,** 643-655.

Tett, P.B, I.R. Joint, D.A. Purdie, M. Baars, S. Oosterhuis, G. Daneri, F. Hannah, D.K. Mills, D. Plummer, A.J. Pomroy, A.W. Walne and H.J. Witte (1993). Biological consequences of tidal stirring gradients in the North Sea. *Phil. Trans. R. Soc. Lond.,* **343,** 493-508.

Topliss, B.J. (1986). Spectral variations in upwelling radiant intensity in turbid coastal waters. *Estuarine, Coast. Shelf. Sci.,* **22,** 395-414.

Topliss, B.J., C.L. Almos and P.R. Hill (1990). Algorithms for remote sensing of high concentration, inorganic suspended sediment. *Int. J. Remote Sensing,* **11,** 947-966.*

Tyler, M.A. and R.P. Stumpf (1989). Feasibility of using satellites for detection of kinetics of small phytoplankton blooms in estuaries: Tidal and migrational effects. *Remote Sens. Environ.,* **25,** 233-249.

UNESCO (1981). UNESCO technical paper in Marine Science, no. 36.

Viollier, M., D. Tanré, P.Y. Deschamps (1980). An algorithm for remote sensing of water color from space. *Boundary-Layer Meteorology,* **18,** 247-267.

Walker N.D, G.S. Fagion, L.J. Rouse and D.C.Biggs (1994). The great flood of summer 1993: Mississippi river discharge studied. *EOS 2 August 1994, 75,* **31.***

Weeks, A.R. (1989). Spatial and time dependent variations in suspended particulate material concentrations in the shelf seas. Ph.D. Thesis, University of Wales, Bangor.

Weeks, A.R. and J.H. Simpson (1991). The measurement of suspended particulate concentrations from remotely-sensed data. *Int. J. Remote Sensing,* **12**, 725-737.

Weeks, A.R., J.H. Simpson and D. Bowers (1993). The relationship between concentrations of suspended particulate material and tidal processes in the Irish Sea. *Cont. Shelf. Res.,* **13**, 1325-1334.*

Whitlock, C.H., L.R. Poole, J.W. Usry, W.M. Houghton, W.G. Witte, W.D. Morris and E.A. Gurganus (1981). Comparison of reflectance with backscatter and absorption parameters fror turbid waters. *Applied Optics,* **20**, 517-522.

Wilson, W.H., R.C. Smith J.W. Notten (1981). The CZCS geolocation algorithms. Scripps Institution of Oceanography. SIO Ref. 81-32.

APPENDIX 1

A catalogue of all the 165 satellites images used in this study. Together with the date and time each image was sensed is listed the cloud cover and the value of the optical thickness ratio,ε, used in the atmospheric correction.

Image id	Date	Time (GMT)	ε	% clouds
332/03A	10/01/82	13:47	0.79	13.4
332/04B	11/01/82	13:58	0.81	2.1
332/06A	12/01/82	13:47	0.96	20.2
337/03A	14/02/82	14:03	1.02	5.3
343/08B	29/03/82	13:59	1.25	14.8
346/04B	15/04/82	13:58	1.24	25.5
346/14B	20/04/82	09:00	0.88	14.2
347/11B	24/04/82	13:53	1.18	16.0
349/14B	08/05/82	14:27	1.13	6.8
350/04B	10/05/82	14:04	1.08	3.0
350/06A	11/05/82	13:52	1.16	16.6
352/10B	27/05/82	14:03	1.00	21.4
352/13B	29/05/82	13:39	1.09	14.5
353/01A	30/05/82	08:23	0.20	0.0
353/01B	30/05/82	13:27	1.13	5.0
354/02B	07/06/82	13:33	1.08	3.6
354/04A	08/06/82	13:21	1.00	10.7
354/10B	11/06/82	14:26	0.98	13.6
357/04B	29/06/82	14:13	1.03	4.7
358/03A	06/07/82	14:30	0.88	23.7
359/13A	18/07/82	13:48	0.98	7.7
360/01A	19/07/82	13:36	0.98	3.9
360/02B	20/07/82	13:24	1.28	20.5
360/07B	22/07/82	14:41	0.90	3.0
367/12A	02/09/82	14:42	0.95	0.3
369/04B	29/09/82	14:21	0.97	8.0

Image id	Date	Time (GMT)	ε	% clouds
387/03A	17/02/83	14:30	1.30	10.7
387/05A	18/02/83	14:17	1.20	5.0
387/06B	19/02/83	14:05	1.30	28.8
389/02A	04/03/83	14:49	1.35	9.5
392/08A	31/03/83	14:23	1.20	17.2
393/06B	07/04/83	14:38	1.20	8.3
393/08A	08/04/83	14:26	1.20	4.5
393/09B	09/04/83	14:14	1.20	7.1
394/09B	17/04/83	14:17	1.10	11.6
396/09A	03/05/83	14:24	1.10	2.4
400/02B	25/05/83	14:58	1.20	15.1
400/05A	26/05/83	14:46	1.26	11.0
401/11B	04/06/83	14:37	1.11	47.5
402/02A	06/06/83	14:12	1.05	22.3
403/01A	12/06/83	08:32	1.18	14.5
403/02A	12/06/83	14:40	1.20	16.6
403/12A	17/06/83	08:24	1.18	35.6
404/08A	21/06/83	08:38	1.00	0.0
404/10B	22/06/83	08:16	1.53	36.2
406/02A	30/06/83	14:22	1.08	12.5
406/13A	05/07/83	15:02	1.00	15.7
408/04B	13/07/83	15:05	1.55	4.5
408/07A	14/07/83	14:53	1.38	26.4
410/13A	29/07/83	15:11	1.06	45.7
412/08B	08/08/83	14:50	1.21	4.5
412/13A	10/08/83	14:35	1.19	0.9
413/07B	14/08/83	15:17	1.17	0.0
415/07B	26/08/83	14:31	1.36	3.0
416/01A	30/08/83	08:32	1.00	29.1
416/07A	01/09/83	14:59	0.84	23.4
419/03A	18/09/83	08:23	1.18	8.0
424/06B	21/10/83	14:51	1.00	10.7

Image id	Date	Time (GMT)	ε	% clouds
452/05A	01/04/84	15:06	1.10	15.1
455/10A	22/04/84	08:43	0.60	16.3
455/12B	23/04/84	08:22	1.08	10.1
455/13B	23/04/84	15:37	1.23	1.2
456/04B	25/04/84	15:12	1.07	0.0
456/06A	26/04/84	08:57	0.78	17.5
456/07A	26/04/84	15:00	0.88	3.0
456/08B	27/04/84	08:36	0.57	4.7
456/09A	27/04/84	14:48	1.11	0.0
457/03A	01/05/84	08:49	1.20	9.5
457/04A	01/05/84	15:40	1.30	14.8
457/11B	04/05/84	15:02	1.22	7.4
458/03A	07/05/84	08:20	0.92	13.9
458/12A	11/05/84	08:33	0.80	16.6
458/13A	11/05/84	15:17	0.89	3.0
458/14B	12/05/84	08:12	0.60	1.8
459/01B	12/05/84	15:04	0.79	0.9
459/03B	13/05/84	14:51	0.95	2.1
461/09B	28/05/84	15:09	0.85	6.5
461/11A	29/05/84	14:56	0.40	23.7
462/08B	02/06/84	15:35	0.93	24.0
466/05B	28/06/84	15:29	0.80	15.1
466/10B	30/06/84	15:04	0.79	8.6
467/07B	05/07/84	15:43	0.64	21.1
467/10A	06/07/84	15:30	0.97	33.5
467/11B	07/07/84	15:18	0.97	10.1
470/01B	21/07/84	15:46	0.83	22.8
470/04A	22/07/84	15:33	0.70	9.8
470/11A	25/07/84	14:57	1.05	8.6
470/12B	26/07/84	08:29	1.35	13.6
471/06A	29/07/84	15:48	1.12	9.5
471/11A	31/07/84	15:23	0.97	22.3
473/01A	07/08/84	15:37	0.84	15.1
474/08B	15/08/84	15:39	0.82	9.2
474/11B	16/08/84	15:27	0.82	16.0
476/13B	27/08/84	14:51	0.95	18.4

Image id	Date	Time (GMT)	ε	% clouds
505/02B	28/01/85	13:49	1.00	23.7
508/03A	16/02/85	13:48	1.55	8.0
508/05A	17/02/85	13:37	1.46	29.1
511/04B	07/03/85	13:47	1.61	1.2
511/11B	11/03/85	13:04	1.38	0.6
512/13A	17/03/85	13:41	1.00	3.6
514/13B	25/03/85	13:56	1.00	41.2
515/04B	26/03/85	13:46	1.57	27.3
520/10A	22/04/85	14:00	1.16	3.0
520/12B	23/04/85	13:49	1.38	4.2
520/14A	24/04/85	08:05	1.44	9.5
520/14B	24/04/85	13:39	1.33	15.1
524/06B	02/05/85	13:54	1.19	2.7
528/13B	29/05/85	14:09	0.94	0.0
529/02A	30/05/85	13:57	0.98	0.9
529/04B	31/05/85	13:48	1.03	0.3
529/06B	01/06/85	13:36	1.03	0.0
529/08B	02/06/85	13:26	0.91	1.2
529/10B	03/06/85	13:16	0.94	8.9
531/12B	16/06/85	14:19	1.00	5.6
532/03B	18/06/85	13:57	1.03	24.3
535/02B	06/07/85	14:06	1.18	20.2
535/04A	07/07/85	08:02	0.92	19.6
536/13B	14/07/85	14:22	1.03	24.0
538/11A	25/07/85	14:05	1.28	49.0
539/01A	27/07/85	13:44	1.16	42.1
544/11A	31/08/85	14:13	1.00	28.8
546/08B	11/09/85	13:56	1.29	33.2
547/08A	17/09/85	14:34	1.00	15.7
549/05B	28/09/85	14:17	1.56	0.0
551/14A	11/10/85	13:38	1.34	6.6
554/08B	25/10/85	14:31	1.34	0.0

Image id	Date	Time (GMT)	ε	% clouds
578/05B	13/02/86	14:54	1.10	5.3
581/07B	29/02/86	14:15	0.94	9.5
583/01A	02/03/86	13:32	1.28	10.1
583/13B	07/03/86	14:19	1.03	4.5
586/03A	19/03/86	13:51	0.93	20.5
588/10B	02/04/86	14:43	1.12	1.2
589/01B	04/04/86	14:22	1.12	6.2
593/14A	01/05/86	14:34	0.97	0.3
601/09A	15/06/86	13:15	1.01	5.0
602/02B	18/06/86	14:23	0.72	5.3
614/11A	08/09/86	14:50	0.47	17.8
616/04A	12/09/86	14:07	0.78	1.2
617/03A	18/09/86	14:43	0.50	3.3
617/05A	19/09/86	14:32	0.82	20.8
622/03B	03/10/86	13:42	1.06	24.0

Image id	Date	Time (GMT)	ε	% clouds
646/12A	30/01/87	14:12	0.70	8.9
647/01A	31/01/87	14:01	0.96	20.8
654/10A	12/03/87	08:50	1.19	22.8
663/07B	28/04/87	15:11	1.27	11.0
664/12A	06/05/87	08:57	1.09	24.6
664/13A	06/05/87	13:45	0.91	7.4
664/13B	06/05/87	15:26	0.72	3.3
665/01A	07/05/87	08:35	1.04	16.3
665/02B	07/05/87	15:15	0.80	4.5
667/08A	20/05/87	15:35	0.75	0.9
675/12A	04/07/87	14:53	0.62	19.6
685/12A	27/08/87	15:14	0.19	16.9
688/13A	13/09/87	08:36	0.32	7.1
690/08A	22/09/87	08:40	0.11	11.6
692/03B	01/10/87	08:45	1.40	2.7

Image id	Date	Time (GMT)	ε	% clouds
727/13A	04/04/88	15:36	0.64	1.5
728/01B	05/04/88	15:25	0.51	7.4
728/11A	09/04/88	14:42	1.03	14.5
729/08A	13/04/88	15:39	0.78	3.3
734/06B	10/05/88	15:48	0.77	10.4
735/11B	18/05/88	08:45	0.76	7.4
736/02A	19/05/88	15:50	0.59	26.1
740/06B	05/06/88	08:53	0.89	7.1
754/03A	07/08/88	16:25	0.92	14.2

APPENDIX 2

Constituent	Period (hours)	Related to constituent
Z_0	---	
Mm	661.309	
MSf	354.367	
Q_1	26.868	
O_1	25.819	
P_1	24.066	K_1
K_1	23.934	
J_1	23.098	
$2N_2$	12.905	N_2
μ_2	12.872	
N_2	12.658	
Nu_2	12.626	N_2
M_2	12.421	
L_2	12.192	
T_2	12.016	S_2
S_2	12.000	
K_2	11.967	S_2
$2SM_2$	11.607	
M_3	8.280	
MK_3	8.177	
MN_4	6.269	
M_4	6.210	
SN_4	6.160	
MS_4	6.103	
$2MN_6$	4.166	
M_6	4.140	
$2MS_6$	4.092	
$2SM_6$	4.046	

The 27 tidal constituents used in the harmonic analysis of east-west component of currents. Due to the length of the timeseries 5 inseparable constituents were inferred from the equilibrium tide; these constituents are indicated in column 3.

APPENDIX 3

Results of the regression analyses of the high frequency variation in beam attenuation. The symbol ns denotes values which are not significant.

A.3.1 Results for LB3 3 mab for the winter deployment using displacement in Eq. 7.8.

Period	k_0	k_1	k_2	k_3	R^2 (%)
n = 1 m = 1					
171190 - 201190	1.26E+00	1.00E-01 ns	-7.40E-03 ns	-4.97E-02	17.5
201190 - 231190	9.90E-01	7.27E-01	-8.41E-03 ns	-4.60E-02	53.5
231190 - 261190	9.97E-01	1.57E-01	-4.90E-03	1.46E-02	44.1
261190 - 291190	1.02E+00	2.43E-01	-1.00E-02	4.85E-03 ns	54.4
291190 - 021290	1.16E+00	3.45E-01	7.59E-03 ns	-1.74E-03 ns	16.2
021290 - 051290	1.69E+00	7.89E-01	-2.94E-02 ns	-8.18E-02	35.7
051290 - 081290	1.75E+00	5.04E-01	1.12E-02	-9.39E-02	68.9
081290 - 111290	1.39E+00	1.36E+00	6.04E-02	-8.95E-02	75.1
111290 - 141290	1.95E+00	1.00E+00	-3.56E-02	-1.11E-01	65.3
141290 - 171290	8.27E-01 ns	4.43E+00	3.14E-01 ns	-1.88E-01	48.0
Mean	1.3034	0.9655	0.0297	-0.0642	47.87
n = 1 m = 2					
171190 - 201190	1.27E+00	1.01E-01 ns	1.08E-03 ns	-4.96E-02	19.3
201190 - 231190	9.82E-01	7.31E-01	1.02E-03	-4.59E-02	55.7
231190 - 261190	9.82E-01	1.59E-01	3.21E-04	1.42E-02	47.2
261190 - 291190	1.00E+00	2.59E-01	9.78E-04	4.41E-03 ns	50.3
291190 - 021290	1.18E+00	3.42E-01	-1.05E-03 ns	-1.20E-03 ns	16.0
021290 - 051290	1.62E+00	7.88E-01	-2.53E-03 ns	-8.06E-02	35.3
051290 - 081290	1.77E+00	5.07E-01	7.84E-04	-9.43E-02	69.5
081290 - 111290	1.62E+00	1.36E+00	3.11E-03	-8.27E-02	70.9
111290 - 141290	1.84E+00	1.11E+00	2.50E-03	-1.11E-01	61.0
141290 - 171290	1.16E+00	4.41E+00	6.98E-02 ns	-1.91E-01	47.9
Mean	1.3424	0.9767	0.0076	-0.0638	47.31
n = 1 m = 3					
171190 - 201190	1.27E+00	8.93E-02 ns	1.15E-04 ns	-4.98E-02	21.2
201190 - 231190	9.75E-01	7.36E-01	1.02E-04	-4.52E-02	57.0
231190 - 261190	9.76E-01	1.59E-01	2.25E-05	1.40E-02	48.2
261190 - 291190	9.92E-01	2.73E-01	1.03E-04	4.13E-03 ns	47.6
291190 - 021290	1.18E+00	3.39E-01	-9.71E-04 ns	-9.13E-04 ns	16.7
021290 - 051290	1.60E+00	7.89E-01	2.62E-04 ns	-7.98E-02	35.1
051290 - 081290	1.79E+00	5.07E-01	5.55E-05	-9.46E-02	69.6
081290 - 111290	1.69E+00	1.38E+00	1.79E-04	-7.91E-02	66.0
111290 - 141290	1.79E+00	1.19E+00	1.94E-04	-1.11E-01	58.4
141290 - 171290	1.28E+00	4.42E+00	1.79E-02 ns	-1.95E-01	47.5
Mean	1.3543	0.9882	0.0018	-0.0637	46.73
n = 2 m = 1					
171190 - 201190	1.27E+00	1.53E-01 ns	-7.53E-03 ns	-4.98E-02	17.5
201190 - 231190	1.07E+00	1.22E+00	-9.25E-03 ns	-4.54E-02	58.7
231190 - 261190	1.01E+00	3.15E-01	-5.04E-03	1.46E-02	44.2
261190 - 291190	1.04E+00	4.61E-01	-9.93E-03	4.70E-03 ns	55.4
291190 - 021290	1.21E+00	4.68E-01	7.61E-03 ns	-2.19E-03 ns	19.1
021290 - 051290	1.81E+00	9.45E-01	-3.01E-02 ns	-8.16E-02	37.3
051290 - 081290	1.81E+00	6.77E-01	1.21E-02	-9.35E-02	69.3
081290 - 111290	1.54E+00	2.42E+00	5.98E-02	-9.01E-02	73.0
111290 - 141290	2.02E+00	2.21E+00	-3.43E-02	-1.12E-01	67.7
141290 - 171290	1.48E+00	7.87E+00	2.31E-01 ns	-1.92E-01	54.4
Mean	1.4260	1.6739	0.0214	-0.0647	49.66
n = 2 m = 2					
171190 - 201190	1.28E+00	1.55E-01 ns	1.08E-03 ns	-4.96E-02	19.4
201190 - 231190	1.06E+00	1.23E+00	1.08E-03	-4.53E-02	61.0
231190 - 261190	9.97E-01	3.19E-01	3.29E-04	1.42E-02	47.3
261190 - 291190	1.03E+00	4.90E-01	9.71E-04	4.26E-03 ns	51.5
291190 - 021290	1.23E+00	4.65E-01	-9.90E-04 ns	-1.66E-03 ns	18.9
021290 - 051290	1.74E+00	9.43E-01	-2.64E-03 ns	-8.05E-02	36.9
051290 - 081290	1.84E+00	6.83E-01	8.40E-04	-9.39E-02	70.0
081290 - 111290	1.76E+00	2.44E+00	3.09E-03	-8.35E-02	69.1
111290 - 141290	1.93E+00	2.43E+00	2.41E-03	-1.12E-01	63.8
141290 - 171290	1.73E+00	7.86E+00	4.96E-02 ns	-1.95E-01	54.2
Mean	1.4597	1.7015	0.0056	-0.0643	49.21

Period	k_0	k_1	k_2	k_3	R^2 (%)
n = 2 m = 3					
171190 - 201190	1.28E+00	1.41E-01 ns	1.15E-04 ns	-4.98E-02	21.2
201190 - 231190	1.06E+00	1.24E+00	1.08E-04	-4.46E-02	62.4
231190 - 261190	9.91E-01	3.18E-01	2.29E-05	1.40E-02	48.3
261190 - 291190	1.02E+00	5.15E-01	1.02E-04	3.98E-03 ns	48.9
291190 - 021290	1.23E+00	4.61E-01	-9.36E-04 ns	-1.38E-03 ns	19.5
021290 - 051290	1.72E+00	9.43E-01	2.76E-04 ns	-7.96E-02	36.7
051290 - 081290	1.85E+00	6.81E-01	5.91E-05	-9.42E-02	70.1
081290 - 111290	1.84E+00	2.49E+00	1.78E-04	-8.00E-02	64.4
111290 - 141290	1.90E+00	2.58E+00	1.88E-04	-1.12E-01	61.4
141290 - 171290	1.82E+00	7.89E+00	1.22E-02 ns	-1.98E-01	53.9
Mean	1.4711	1.7259	0.0012	-0.0642	48.68
n = 3 m = 1					
171190 - 201190	1.27E+00	2.76E-01 ns	-7.63E-03 ns	-4.98E-02	17.6
201190 - 231190	1.11E+00	2.24E+00	-9.99E-03	-4.47E-02	60.8
231190 - 261190	1.02E+00	6.27E-01	-5.07E-03	1.47E-02	41.9
261190 - 291190	1.05E+00	9.33E-01	-1.03E-02	4.80E-03 ns	54.4
291190 - 021290	1.23E+00	7.24E-01	7.59E-03 ns	-2.39E-03 ns	20.7
021290 - 051290	1.86E+00	1.22E+00	-3.14E-02 ns	-8.11E-02	38.0
051290 - 081290	1.84E+00	9.65E-01	1.22E-02	-9.30E-02	69.2
081290 - 111290	1.59E+00	4.57E+00	5.99E-02	-8.96E-02	70.2
111290 - 141290	2.06E+00	5.19E+00	-3.37E-02	-1.12E-01	69.1
141290 - 171290	1.80E+00	1.63E+01	1.49E-01 ns	-1.95E-01	59.7
Mean	1.4830	3.3045	0.0131	-0.0648	50.16
n = 3 m = 2					
171190 - 201190	1.28E+00	2.79E-01 ns	1.09E-03 ns	-4.97E-02	19.5
201190 - 231190	1.10E+00	2.26E+00	1.14E-03	-4.45E-02	63.2
231190 - 261190	1.00E+00	6.38E-01	3.32E-04	1.43E-02	45.0
261190 - 291190	1.04E+00	9.94E-01	1.02E-03	4.36E-03 ns	50.4
291190 - 021290	1.25E+00	7.18E-01	-9.45E-04 ns	-1.87E-03 ns	20.6
021290 - 051290	1.79E+00	1.22E+00	-2.92E-03 ns	-8.01E-02	37.5
051290 - 081290	1.87E+00	9.74E-01	8.51E-04	-9.34E-02	69.9
081290 - 111290	1.82E+00	4.64E+00	3.10E-03	-8.30E-02	66.6
111290 - 141290	1.97E+00	5.67E+00	2.37E-03	-1.12E-01	65.3
141290 - 171290	1.97E+00	1.64E+01	2.93E-02 ns	-1.97E-01	59.5
Mean	1.5090	3.3793	0.0035	-0.0643	49.75
n = 3 m = 3					
171190 - 201190	1.28E+00	2.57E-01 ns	1.15E-04 ns	-4.98E-02	21.3
201190 - 231190	1.09E+00	2.28E+00	1.12E-04	-4.37E-02	64.7
231190 - 261190	9.98E-01	6.36E-01	2.31E-05	1.41E-02	46.0
261190 - 291190	1.03E+00	1.04E+00	1.10E-04	4.09E-03 ns	47.6
291190 - 021290	1.25E+00	7.13E-01	-9.06E-04 ns	-1.59E-03 ns	21.1
021290 - 051290	1.77E+00	1.22E+00	3.27E-04 ns	-7.93E-02	37.4
051290 - 081290	1.88E+00	9.69E-01	5.96E-05	-9.37E-02	69.9
081290 - 111290	1.89E+00	4.76E+00	1.78E-04	-7.95E-02	61.9
111290 - 141290	1.94E+00	6.01E+00	1.86E-04	-1.12E-01	63.0
141290 - 171290	2.03E+00	1.65E+01	6.49E-03 ns	-1.99E-01	59.4
Mean	1.5158	3.4385	0.0007	-0.0640	49.23

A.3.2 Results for LB3 3 mab for the winter deployment using salinity in Eq. 7.9.

Period	k_0'	k_1'	k_2'	k_3'	R^2 (%)
n = 1 m = 1					
171190 - 201190	6.24E+01	9.13E-02 ns	-3.93E-03 ns	-1.83E+00	60.0
201190 - 231190	5.34E+01	6.71E-01	-5.95E-03 ns	-1.57E+00	65.1
231190 - 261190	-1.25E+01	1.70E-01	1.77E-03 ns	3.99E-01	56.8
261190 - 291190	-1.28E+00 ns	2.47E-01	-1.01E-02	6.82E-02 ns	52.2
291190 - 021290	3.41E+01	3.97E-01	-1.11E-02 ns	-9.79E-01	62.1
021290 - 051290	9.01E+01	7.54E-01	-2.34E-02 ns	-2.65E+00	57.1
051290 - 081290	1.18E+02	5.35E-01	3.49E-03 ns	-3.48E+00	77.6
081290 - 111290	7.63E+01	1.39E+00	5.38E-02	-2.25E+00	71.3
111290 - 141290	6.03E+01	1.06E+00	-9.64E-03 ns	-1.76E+00	77.2
141290 - 171290	9.75E+01	3.38E+00	1.94E-01 ns	-2.90E+00	45.6
Mean	57.832	0.8695	0.0189	-1.6952	62.50
n = 1 m = 2					
171190 - 201190	6.21E+01	8.90E-02 ns	3.23E-04 ns	-1.82E+00	60.1
201190 - 231190	5.25E+01	6.72E-01	5.12E-04 ns	-1.54E+00	65.2
231190 - 261190	-1.22E+01	1.70E-01	7.55E-05 ns	3.89E-01	56.2
261190 - 291190	4.28E-01 ns	2.64E-01	9.25E-04	1.69E-02 ns	48.2
291190 - 021290	3.41E+01	3.94E-01	-4.09E-03 ns	-9.79E-01	62.7
021290 - 051290	9.05E+01	7.49E-01	-3.20E-03 ns	-2.66E+00	57.1
051290 - 081290	1.18E+02	5.31E-01	1.88E-04 ns	-3.48E+00	77.6
081290 - 111290	7.07E+01	1.39E+00	2.77E-03	-2.07E+00	67.3
111290 - 141290	6.17E+01	1.11E+00	4.60E-04 ns	-1.81E+00	76.7
141290 - 171290	9.90E+01	3.37E+00	3.54E-02 ns	-2.94E+00	45.2
Mean	57.683	0.8739	0.0033	-1.6893	61.63
n = 1 m = 3					
171190 - 201190	6.18E+01	8.56E-02 ns	2.81E-05 ns	-1.81E+00	60.1
201190 - 231190	5.18E+01	6.74E-01	4.13E-05 ns	-1.52E+00	65.0
231190 - 261190	-1.17E+01	1.71E-01	3.14E-06 ns	3.76E-01	55.9
261190 - 291190	1.69E+00 ns	2.78E-01	8.97E-05 ns	-2.08E-02 ns	45.8
291190 - 021290	3.39E+01	3.93E-01	1.42E-03 ns	-9.72E-01	63.2
021290 - 051290	9.08E+01	7.45E-01	5.38E-04 ns	-2.67E+00	57.1
051290 - 081290	1.18E+02	5.26E-01	9.16E-06 ns	-3.49E+00	77.5
081290 - 111290	7.03E+01	1.41E+00	1.60E-04	-2.06E+00	63.5
111290 - 141290	6.25E+01	1.14E+00	2.31E-05 ns	-1.83E+00	76.5
141290 - 171290	9.96E+01	3.37E+00	7.45E-03 ns	-2.95E+00	44.8
Mean	57.869	0.8793	0.0010	-1.6947	60.94
n = 2 m = 1					
171190 - 201190	6.24E+01	1.24E-01 ns	-3.99E-03 ns	-1.83E+00	60.0
201190 - 231190	5.27E+01	1.13E+00	-6.76E-03 ns	-1.54E+00	69.6
231190 - 261190	-1.26E+01	3.43E-01	1.66E-03 ns	4.01E-01	57.2
261190 - 291190	-1.30E+00 ns	4.68E-01	-1.00E-02	6.94E-02 ns	53.3
291190 - 021290	3.43E+01	5.33E-01	-1.15E-02 ns	-9.83E-01	65.3
021290 - 051290	8.91E+01	8.63E-01	-2.37E-02 ns	-2.62E+00	57.6
051290 - 081290	1.17E+02	7.08E-01	4.34E-03 ns	-3.46E+00	77.9
081290 - 111290	7.69E+01	2.48E+00	5.32E-02	-2.26E+00	69.1
111290 - 141290	6.05E+01	2.29E+00	-8.46E-03 ns	-1.77E+00	79.4
141290 - 171290	9.98E+01	5.68E+00	1.82E-01 ns	-2.96E+00	50.0
Mean	57.88	1.4619	0.0177	-1.6953	63.94
n = 2 m = 2					
171190 - 201190	6.21E+01	1.21E-01 ns	3.27E-04 ns	-1.82E+00	60.1
201190 - 231190	5.16E+01	1.13E+00	5.84E-04 ns	-1.51E+00	69.8
231190 - 261190	-1.22E+01	3.46E-01	6.93E-05 ns	3.91E-01	56.7
261190 - 291190	3.62E-01 ns	5.00E-01	9.23E-04	1.96E-02 ns	49.5
291190 - 021290	3.43E+01	5.30E-01	-4.11E-03 ns	-9.82E-01	65.9
021290 - 051290	8.95E+01	8.58E-01	-3.24E-03 ns	-2.63E+00	57.5
051290 - 081290	1.17E+02	7.02E-01	2.43E-04 ns	-3.46E+00	77.8
081290 - 111290	7.12E+01	2.49E+00	2.75E-03	-2.09E+00	65.4
111290 - 141290	6.18E+01	2.38E+00	3.87E-04 ns	-1.81E+00	78.9
141290 - 171290	1.01E+02	5.68E+00	3.34E-02 ns	-2.99E+00	49.6
Mean	57.66	1.4737	0.0031	-1.6881	63.12

Period	k_0	k_1	k_2	k_3	R^2 (%)
n = 2 m = 3					
171190 - 201190	6.18E+01	1.16E-01 ns	2.85E-05 ns	-1.81E+00	60.1
201190 - 231190	5.08E+01	1.14E+00	4.80E-05 ns	-1.49E+00	69.6
231190 - 261190	-1.18E+01	3.48E-01	2.85E-06 ns	3.79E-01	56.4
261190 - 291190	1.59E+00 ns	5.25E-01	9.06E-05 ns	-1.70E-02 ns	47.2
291190 - 021290	3.40E+01	5.28E-01	1.40E-03 ns	-9.75E-01	66.3
021290 - 051290	8.98E+01	8.53E-01	5.43E-04 ns	-2.64E+00	57.5
051290 - 081290	1.17E+02	6.94E-01	1.27E-05 ns	-3.47E+00	77.7
081290 - 111290	7.09E+01	2.54E+00	1.58E-04	-2.08E+00	61.7
111290 - 141290	6.25E+01	2.43E+00	1.83E-05 ns	-1.83E+00	78.8
141290 - 171290	1.02E+02	5.68E+00	7.09E-03 ns	-3.01E+00	49.3
Mean	57.86	1.4854	0.0010	-1.6943	62.46
n = 3 m = 1					
171190 - 201190	6.24E+01	1.89E-01 ns	-3.99E-03 ns	-1.82E+00	60.0
201190 - 231190	5.20E+01	2.08E+00	-7.49E-03 ns	-1.52E+00	71.6
231190 - 261190	-1.26E+01	6.93E-01	1.64E-03 ns	4.03E-01	54.8
261190 - 291190	-1.59E+00 ns	9.49E-01	-1.04E-02	7.82E-02 ns	52.3
291190 - 021290	3.42E+01	8.13E-01	-1.16E-02 ns	-9.80E-01	66.7
021290 - 051290	8.81E+01	1.08E+00	-2.48E-02 ns	-2.58E+00	57.3
051290 - 081290	1.16E+02	9.83E-01	4.39E-03 ns	-3.43E+00	77.3
081290 - 111290	7.59E+01	4.66E+00	5.33E-02	-2.23E+00	66.1
111290 - 141290	6.04E+01	5.27E+00	-8.21E-03 ns	-1.76E+00	80.3
141290 - 171290	1.02E+02	1.08E+01	1.71E-01 ns	-3.01E+00	52.5
Mean	57.681	2.7517	0.0163	-1.6849	63.89
n = 3 m = 2					
171190 - 201190	6.20E+01	1.84E-01 ns	3.27E-04 ns	-1.81E+00	60.0
201190 - 231190	5.08E+01	2.09E+00	6.43E-04 ns	-1.49E+00	71.7
231190 - 261190	-1.23E+01	6.99E-01	6.77E-05 ns	3.93E-01	54.3
261190 - 291190	5.60E-02 ns	1.01E+00	9.86E-04	2.90E-02 ns	48.4
291190 - 021290	3.42E+01	8.08E-01	-4.10E-03 ns	-9.79E-01	67.2
021290 - 051290	8.85E+01	1.07E+00	-3.46E-03 ns	-2.60E+00	57.2
051290 - 081290	1.16E+02	9.75E-01	2.48E-04 ns	-3.43E+00	77.2
081290 - 111290	7.02E+01	4.72E+00	2.76E-03	-2.06E+00	62.7
111290 - 141290	6.17E+01	5.47E+00	3.83E-04 ns	-1.80E+00	79.9
141290 - 171290	1.03E+02	1.08E+01	3.16E-02 ns	-3.05E+00	52.3
Mean	57.416	2.7826	0.0029	-1.6797	63.09
n = 3 m = 3					
171190 - 201190	6.18E+01	1.76E-01 ns	2.86E-05 ns	-1.81E+00	60.1
201190 - 231190	4.99E+01	2.10E+00	5.31E-05 ns	-1.46E+00	71.5
231190 - 261190	-1.19E+01	7.04E-01	2.77E-06 ns	3.81E-01	54.0
261190 - 291190	1.29E+00 ns	1.06E+00	9.95E-05	-7.70E-03 ns	45.8
291190 - 021290	3.40E+01	8.06E-01	1.37E-03 ns	-9.72E-01	67.6
021290 - 051290	8.89E+01	1.06E+00	5.84E-04 ns	-2.61E+00	57.2
051290 - 081290	1.16E+02	9.62E-01	1.28E-05 ns	-3.44E+00	77.1
081290 - 111290	6.98E+01	4.84E+00	1.59E-04	-2.04E+00	59.1
111290 - 141290	6.23E+01	5.57E+00	1.90E-05 ns	-1.82E+00	79.8
141290 - 171290	1.04E+02	1.08E+01	6.79E-03 ns	-3.06E+00	51.9
Mean	57.609	2.8078	0.0009	-1.6839	62.41

A.3.3 Results for LB3 surface for the winter deployment using displacement in Eq. 7.8.

Period	k_0	k_1	k_2	k_3	R^2 (%)
n = 1 m = 1					
171190 - 201190	1.09E+00	-3.46E-01	1.36E-03 ns	-3.39E-02	20.1
201190 - 231190	8.32E-01	1.67E-01 ns	4.37E-02	-1.14E-01	33.0
231190 - 261190	8.11E-01	-1.53E-01 ns	8.66E-03 ns	-3.99E-02	2.4
261190 - 291190	1.83E+00	4.27E-02 ns	-2.61E-02	-7.32E-02	41.3
291190 - 021290	1.32E+00	6.50E-03 ns	4.56E-02 ns	-3.75E-03 ns	0.0
021290 - 051290	1.39E+00	-1.57E-01	-7.62E-03 ns	-1.67E-02	22.8
051290 - 081290	1.44E+00	-2.94E-01 ns	3.06E-02	-4.10E-02	38.3
081290 - 111290	1.01E+00	-2.13E-02 ns	9.96E-02	-8.91E-02	79.5
111290 - 141290	1.70E+00	-3.79E-01	-7.22E-03 ns	-1.05E-01	56.4
141290 - 171290	1.39E+00	4.55E-02 ns	-3.67E-02 ns	-3.12E-02	30.7
171290 - 201290	1.19E+00	-1.17E-01 ns	3.30E-02	-2.99E-02	55.8
201290 - 231290	1.23E+00	-1.52E-01 ns	1.36E-02	1.99E-02	25.0
231290 - 261290	1.33E+00	-3.03E-01	7.57E-03 ns	-7.37E-02	49.3
261290 - 291290	1.88E+00	-6.17E-01	3.22E-02 ns	-1.98E-01	66.8
291290 - 010191	3.82E+00	-4.11E-01 ns	-8.32E-02	-2.84E-01	80.5
010191 - 040191	6.28E+00	4.90E-01 ns	-9.17E-02 ns	-3.21E-01	33.7
040191 - 070191	3.18E+00	-4.23E-01 ns	2.90E-01	-3.89E-01	74.0
070191 - 100191	3.41E+00	2.16E+00 ns	6.77E-02 ns	-2.12E-01	16.5
100191 - 130191	2.86E+00	-7.37E-01 ns	8.22E-02	-1.08E-01	46.7
130191 - 160191	3.49E+00	-2.33E-01 ns	-4.43E-02 ns	6.10E-02	10.2
160191 - 190191	3.35E+00	-5.44E-01	-8.19E-02	-8.41E-02	36.0
190191 - 220191	1.56E+00	-2.66E-01	1.07E-01	-3.48E-03 ns	90.6
220191 - 250191	1.39E+00	1.34E-01 ns	4.21E-02	-3.32E-02	35.3
250191 - 280191	1.30E+00	-6.64E-02 ns	5.59E-02	-1.30E-02 ns	21.2
280191 - 310191	1.69E+00	-2.40E-01	1.32E-02 ns	3.73E-02	21.1
310191 - 030291	1.85E+00	-1.64E-01	2.97E-02 ns	1.36E-02 ns	7.6
030291 - 060291	1.75E+00	-3.65E-01	2.37E-02	-2.35E-03 ns	23.4
Mean	2.0138	-0.1090	0.0240	-0.0802	37.71
n = 1 m = 2					
171190 - 201190	1.12E+00	-3.57E-01	3.31E-04 ns	-3.34E-02	20.4
201190 - 231190	9.83E-01	1.60E-01 ns	1.79E-03 ns	-1.15E-01	28.5
231190 - 261190	8.73E-01	-1.53E-01 ns	3.90E-05 ns	-3.92E-02 ns	1.4
261190 - 291190	1.81E+00	3.92E-02 ns	-3.73E-03	-7.28E-02	42.5
291190 - 021290	1.34E+00	2.40E-03 ns	1.73E-02 ns	-3.90E-03 ns	0.1
021290 - 051290	1.38E+00	-1.58E-01	-8.95E-04 ns	-1.66E-02	22.6
051290 - 081290	1.54E+00	-3.11E-01	1.90E-03	-4.19E-02	38.3
081290 - 111290	1.36E+00	6.30E-03 ns	5.37E-03	-7.94E-02	78.8
111290 - 141290	1.70E+00	-4.06E-01	8.52E-04 ns	-1.05E-01	57.1
141290 - 171290	1.36E+00	4.51E-02 ns	-1.04E-02	-3.01E-02	32.8
171290 - 201290	1.26E+00	-1.19E-01 ns	2.50E-03	-3.12E-02	52.1
201290 - 231290	1.28E+00	-1.58E-01 ns	6.83E-04	1.96E-02	21.4
231290 - 261290	1.40E+00	-3.33E-01	1.35E-04 ns	-7.33E-02	48.1
261290 - 291290	2.07E+00	-6.20E-01	1.30E-03 ns	-1.98E-01	66.7
291290 - 010191	3.44E+00	-4.06E-01 ns	-4.34E-03	-2.85E-01	80.1
010191 - 040191	5.70E+00	4.91E-01 ns	-3.52E-03 ns	-3.19E-01	33.9
040191 - 070191	4.70E+00	-3.47E-01 ns	1.11E-02	-3.74E-01	72.3
070191 - 100191	3.74E+00	2.22E+00	2.98E-03 ns	-2.16E-01	15.6
100191 - 130191	3.18E+00	-9.71E-01	4.60E-03	-1.10E-01	36.6
130191 - 160191	3.40E+00	-2.28E-01 ns	-3.96E-03 ns	5.90E-02	9.1
160191 - 190191	3.04E+00	-5.35E-01 ns	-4.09E-03	-8.52E-02	30.0
190191 - 220191	1.70E+00	-2.43E-01	1.05E-02	-3.81E-03 ns	86.7
220191 - 250191	1.44E+00	1.21E-01 ns	6.75E-03	-3.22E-02	37.2
250191 - 280191	1.37E+00	-5.75E-02 ns	7.79E-03	-1.19E-02 ns	19.1
280191 - 310191	1.73E+00	-2.44E-01	8.13E-04 ns	3.62E-02	19.7
310191 - 030291	1.88E+00	-1.63E-01 ns	3.39E-03 ns	1.31E-02 ns	6.0
030291 - 060291	1.79E+00	-3.72E-01	2.49E-03 ns	-2.85E-03 ns	21.7
Mean	2.0958	-0.1147	0.0019	-0.0797	36.25

Period	k_0	k_1	k_2	k_3	R^2 (%)
n = 1 m = 3					
171190 - 201190	1.13E+00	-3.68E-01	4.88E-05 ns	-3.33E-02	21.2
201190 - 231190	1.03E+00	1.51E-01 ns	4.64E-05 ns	-1.16E-01	27.1
231190 - 261190	8.88E-01	-1.53E-01 ns	1.78E-05 ns	-3.93E-02 ns	1.7
261190 - 291190	1.80E+00	4.09E-02 ns	5.63E-04	-7.23E-02	43.7
291190 - 021290	1.35E+00	-4.80E-03 ns	6.20E-03	-3.77E-03 ns	2.6
021290 - 051290	1.38E+00	-1.59E-01	1.49E-04 ns	-1.67E-02	22.6
051290 - 081290	1.58E+00	-3.26E-01	1.25E-04	-4.26E-02	36.7
081290 - 111290	1.48E+00	4.23E-02 ns	3.16E-04	-7.36E-02	72.6
111290 - 141290	1.70E+00	-4.07E-01	8.26E-05 ns	-1.04E-01	57.3
141290 - 171290	1.35E+00	4.41E-02 ns	-3.16E-03	-2.90E-02	34.8
171290 - 201290	1.28E+00	-1.23E-01 ns	1.88E-04	-3.18E-02	46.5
201290 - 231290	1.31E+00	-1.67E-01 ns	3.68E-05	1.94E-02	18.0
231290 - 261290	1.43E+00	-3.56E-01	1.89E-06 ns	-7.33E-02	47.9
261290 - 291290	2.14E+00	-6.24E-01	6.74E-05 ns	-1.97E-01	66.6
291290 - 010191	3.31E+00	-3.97E-01 ns	2.80E-04	-2.85E-01	79.7
010191 - 040191	5.51E+00	4.94E-01 ns	1.71E-04 ns	-3.17E-01	34.1
040191 - 070191	5.30E+00	-3.13E-01 ns	4.77E-04	-3.71E-01	66.9
070191 - 100191	3.85E+00	2.26E+00	1.62E-04 ns	-2.20E-01	15.0
100191 - 130191	3.31E+00	-1.14E+00	2.76E-04	-1.11E-01	30.7
130191 - 160191	3.36E+00	-2.42E-01 ns	2.61E-04 ns	5.84E-02	8.0
160191 - 190191	2.94E+00	-5.26E-01 ns	2.33E-04	-8.58E-02	26.6
190191 - 220191	1.74E+00	-2.22E-01	1.11E-03	-3.30E-03 ns	80.1
220191 - 250191	1.45E+00	1.18E-01 ns	1.13E-03	-3.15E-02	37.5
250191 - 280191	1.39E+00	-3.99E-02 ns	1.14E-03	-9.24E-03 ns	15.7
280191 - 310191	1.74E+00	-2.47E-01	4.98E-05 ns	3.56E-02	19.2
310191 - 030291	1.89E+00	-1.64E-01 ns	3.96E-04 ns	1.29E-02 ns	5.4
030291 - 060291	1.79E+00	-3.77E-01	3.06E-04 ns	-3.14E-03 ns	20.9
Mean	2.1270	-0.1187	0.0004	-0.0793	34.78
n = 2 m = 1					
171190 - 201190	1.04E+00	-4.47E-01	7.29E-04 ns	-3.40E-02	19.5
201190 - 231190	8.50E-01	2.73E-01 ns	4.37E-02	-1.13E-01	33.1
231190 - 261190	8.01E-01	-3.69E-01 ns	8.66E-03 ns	-3.97E-02 ns	2.6
261190 - 291190	1.84E+00	7.19E-02 ns	-2.59E-02	-7.32E-02	41.3
291190 - 021290	1.33E+00	1.00E-03 ns	4.57E-02 ns	-3.77E-03 ns	0.0
021290 - 051290	1.37E+00	-1.71E-01	-7.33E-03 ns	-1.67E-02	23.3
051290 - 081290	1.40E+00	-3.58E-01 ns	3.01E-02	-4.16E-02	38.0
081290 - 111290	1.01E+00	-4.67E-02 ns	9.96E-02	-8.91E-02	79.5
111290 - 141290	1.66E+00	-6.39E-01	-7.64E-03 ns	-1.05E-01	56.2
141290 - 171290	1.40E+00	3.93E-02 ns	-3.69E-02 ns	-3.10E-02	30.6
171290 - 201290	1.18E+00	-1.78E-01	3.28E-02	-3.00E-02	56.6
201290 - 231290	1.21E+00	-2.14E-01 ns	1.34E-02	1.97E-02	25.1
231290 - 261290	1.30E+00	-5.36E-01	7.19E-03 ns	-7.37E-02	49.7
261290 - 291290	1.81E+00	-9.91E-01	3.17E-02 ns	-1.97E-01	66.6
291290 - 010191	3.75E+00	-4.60E-01 ns	-8.37E-02	-2.84E-01	80.4
010191 - 040191	6.32E+00	6.31E-01 ns	-9.01E-02 ns	-3.21E-01	33.8
040191 - 070191	3.18E+00	-8.47E-01 ns	2.89E-01	-3.88E-01	74.2
070191 - 100191	3.61E+00	4.40E+00	6.89E-02 ns	-2.12E-01	16.8
100191 - 130191	2.82E+00	-1.52E+00 ns	7.91E-02	-1.09E-01	47.1
130191 - 160191	3.46E+00	-3.15E-01 ns	-4.36E-02 ns	6.09E-02	10.1
160191 - 190191	3.24E+00	-5.70E-01 ns	-8.10E-02	-8.52E-02	35.2
190191 - 220191	1.52E+00	-3.21E-01	1.07E-01	-3.61E-03 ns	90.4
220191 - 250191	1.40E+00	2.98E-01 ns	4.11E-02	-3.32E-02	36.4
250191 - 280191	1.29E+00	-8.64E-02 ns	5.59E-02	-1.29E-02 ns	21.1
280191 - 310191	1.65E+00	-2.22E-01 ns	1.32E-02 ns	3.67E-02	19.0
310191 - 030291	1.83E+00	-1.84E-01 ns	3.00E-02 ns	1.41E-02 ns	6.3
030291 - 060291	1.69E+00	-4.28E-01	2.67E-02	-3.09E-03 ns	16.7
Mean	1.9986	-0.1181	0.0240	-0.0803	37.39

Period	k_0	k_1	k_2	k_3	R^2 (%)
n = 2 m = 2					
171190 - 201190	1.07E+00	-4.67E-01	3.83E-04 ns	-3.35E-02	19.9
201190 - 231190	9.98E-01	2.68E-01 ns	1.79E-03 ns	-1.15E-01	28.6
231190 - 261190	8.62E-01	-3.69E-01 ns	4.09E-05 ns	-3.90E-02 ns	1.6
261190 - 291190	1.81E+00	7.04E-02 ns	-3.71E-03	-7.28E-02	42.6
291190 - 021290	1.34E+00	-5.10E-03 ns	1.73E-02 ns	-3.93E-03 ns	0.1
021290 - 051290	1.35E+00	-1.73E-01	-8.53E-04 ns	-1.67E-02	23.1
051290 - 081290	1.49E+00	-3.78E-01 ns	1.86E-03	-4.25E-02	38.1
081290 - 111290	1.36E+00	2.12E-02 ns	5.37E-03	-7.94E-02	78.8
111290 - 141290	1.66E+00	-6.92E-01	8.99E-04 ns	-1.05E-01	57.0
141290 - 171290	1.37E+00	3.89E-02 ns	-1.05E-02	-3.00E-02	32.6
171290 - 201290	1.25E+00	-1.85E-01	2.49E-03	-3.13E-02	53.0
201290 - 231290	1.26E+00	-2.23E-01 ns	6.67E-04	1.94E-02	21.5
231290 - 261290	1.37E+00	-5.89E-01	1.19E-04 ns	-7.34E-02	48.6
261290 - 291290	2.00E+00	-9.98E-01	1.28E-03 ns	-1.97E-01	66.5
291290 - 010191	3.38E+00	-4.52E-01 ns	-4.37E-03	-2.85E-01	80.0
010191 - 040191	5.75E+00	6.36E-01 ns	-3.47E-03 ns	-3.19E-01	34.0
040191 - 070191	4.71E+00	-7.62E-01 ns	1.11E-02	-3.74E-01	72.5
070191 - 100191	3.95E+00	4.51E+00	3.04E-03 ns	-2.17E-01	15.9
100191 - 130191	3.12E+00	-2.08E+00	4.31E-03	-1.12E-01	37.9
130191 - 160191	3.37E+00	-3.21E-01 ns	-3.91E-03 ns	5.89E-02	9.1
160191 - 190191	2.94E+00	-5.75E-01 ns	-4.05E-03	-8.63E-02	29.4
190191 - 220191	1.66E+00	-2.91E-01	1.06E-02	-3.92E-03 ns	86.5
220191 - 250191	1.44E+00	2.75E-01 ns	6.60E-03	-3.23E-02	38.2
250191 - 280191	1.36E+00	-6.62E-02 ns	7.77E-03	-1.18E-02 ns	19.0
280191 - 310191	1.68E+00	-2.29E-01 ns	7.88E-04 ns	3.56E-02	17.5
310191 - 030291	1.86E+00	-1.82E-01 ns	3.42E-03 ns	1.36E-02 ns	4.8
030291 - 060291	1.72E+00	-4.38E-01	2.93E-03 ns	-3.54E-03 ns	15.0
Mean	2.0789	-0.1354	0.0019	-0.0799	35.99
n = 2 m = 3					
171190 - 201190	1.08E+00	-4.84E-01	5.28E-05 ns	-3.34E-02	20.8
201190 - 231190	1.04E+00	2.57E-01 ns	4.67E-05 ns	-1.16E-01	27.2
231190 - 261190	8.77E-01	-3.67E-01 ns	1.76E-05 ns	-3.91E-02 ns	1.8
261190 - 291190	1.80E+00	7.70E-02 ns	5.61E-04	-7.23E-02	43.7
291190 - 021290	1.36E+00	-1.35E-02 ns	6.21E-03	-3.80E-03 ns	2.6
021290 - 051290	1.35E+00	-1.74E-01	1.44E-04 ns	-1.67E-02	23.1
051290 - 081290	1.54E+00	-4.01E-01	1.22E-04	-4.32E-02	36.5
081290 - 111290	1.48E+00	9.43E-02 ns	3.16E-04	-7.36E-02	72.6
111290 - 141290	1.66E+00	-6.95E-01	8.69E-05 ns	-1.05E-01	57.2
141290 - 171290	1.36E+00	3.69E-02 ns	-3.17E-03	-2.88E-02	34.6
171290 - 201290	1.27E+00	-1.91E-01 ns	1.87E-04	-3.19E-02	47.5
201290 - 231290	1.29E+00	-2.37E-01 ns	3.55E-05	1.92E-02	18.2
231290 - 261290	1.39E+00	-6.30E-01	2.68E-06 ns	-7.34E-02	48.4
261290 - 291290	2.07E+00	-1.01E+00	6.65E-05 ns	-1.96E-01	66.5
291290 - 010191	3.24E+00	-4.41E-01 ns	2.82E-04	-2.85E-01	79.6
010191 - 040191	5.56E+00	6.45E-01 ns	1.70E-04 ns	-3.17E-01	34.2
040191 - 070191	5.31E+00	-7.61E-01 ns	4.76E-04	-3.71E-01	67.1
070191 - 100191	4.06E+00	4.58E+00	1.66E-04 ns	-2.20E-01	15.3
100191 - 130191	3.24E+00	-2.46E+00	2.51E-04	-1.13E-01	32.6
130191 - 160191	3.33E+00	-3.50E-01 ns	2.57E-04 ns	5.84E-02	8.0
160191 - 190191	2.85E+00	-5.72E-01 ns	2.32E-04	-8.68E-02	26.0
190191 - 220191	1.71E+00	-2.61E-01	1.12E-03	-3.41E-03 ns	79.9
220191 - 250191	1.46E+00	2.70E-01 ns	1.11E-03	-3.16E-02	38.4
250191 - 280191	1.38E+00	-3.05E-02 ns	1.14E-03	-9.10E-03 ns	15.5
280191 - 310191	1.69E+00	-2.34E-01 ns	4.56E-05 ns	3.50E-02	17.1
310191 - 030291	1.87E+00	-1.83E-01 ns	3.93E-04 ns	1.34E-02 ns	4.1
030291 - 060291	1.73E+00	-4.46E-01	3.74E-04 ns	-3.81E-03 ns	14.1
Mean	2.1111	-0.1474	0.0004	-0.0796	34.54

Period	k_0	k_1	k_2	k_3	R^2 (%)
n = 3 m = 1					
171190 - 201190	1.02E+00	-6.49E-01	3.48E-04 ns	-3.40E-02	19.1
201190 - 231190	8.53E-01	5.16E-01 ns	4.36E-02	-1.13E-01	33.2
231190 - 261190	7.94E-01	-8.54E-01 ns	8.76E-03 ns	-3.97E-02 ns	2.6
261190 - 291190	1.84E+00	1.05E-01 ns	-2.60E-02	-7.32E-02	41.3
291190 - 021290	1.33E+00	-1.64E-02 ns	4.59E-02 ns	-3.82E-03 ns	0.0
021290 - 051290	1.36E+00	-2.02E-01	-7.01E-03 ns	-1.68E-02	23.4
051290 - 081290	1.37E+00	-4.21E-01 ns	3.04E-02	-4.19E-02	37.2
081290 - 111290	1.01E+00	-1.04E-01 ns	9.96E-02	-8.92E-02	79.5
111290 - 141290	1.64E+00	-1.12E+00	-7.34E-03 ns	-1.05E-01	55.9
141290 - 171290	1.40E+00	2.26E-02 ns	-3.69E-02 ns	-3.10E-02	30.5
171290 - 201290	1.17E+00	-2.89E-01	3.27E-02	-3.00E-02	57.3
201290 - 231290	1.20E+00	-3.24E-01 ns	1.33E-02	1.96E-02	25.0
231290 - 261290	1.29E+00	-9.63E-01	7.17E-03 ns	-7.36E-02	49.6
261290 - 291290	1.78E+00	-1.69E+00	3.15E-02 ns	-1.96E-01	66.2
291290 - 010191	3.73E+00	-5.62E-01 ns	-8.40E-02	-2.84E-01	80.3
010191 - 040191	6.33E+00	8.47E-01 ns	-8.89E-02 ns	-3.21E-01	33.9
040191 - 070191	3.16E+00	-1.36E+00 ns	2.88E-01	-3.89E-01	74.3
070191 - 100191	3.67E+00	9.30E+00 ns	7.13E-02 ns	-2.13E-01	16.3
100191 - 130191	2.79E+00	-3.13E+00 ns	7.81E-02	-1.09E-01	47.1
130191 - 160191	3.44E+00	-5.11E-01 ns	-4.29E-02 ns	6.08E-02	10.2
160191 - 190191	3.20E+00	-6.62E-01 ns	-8.05E-02	-8.54E-02	34.7
190191 - 220191	1.50E+00	-4.07E-01	1.07E-01	-3.73E-03 ns	90.1
220191 - 250191	1.40E+00	6.45E-01 ns	4.05E-02	-3.34E-02	37.4
250191 - 280191	1.29E+00	-1.04E-01 ns	5.56E-02	-1.28E-02 ns	20.9
280191 - 310191	1.63E+00	-2.04E-01 ns	1.33E-02 ns	3.64E-02	17.5
310191 - 030291	1.82E+00	-1.98E-01 ns	3.01E-02 ns	1.44E-02 ns	5.1
030291 - 060291	1.66E+00	-4.60E-01 ns	2.96E-02	-3.62E-03 ns	11.6
Mean	1.988	-0.1035	0.0242	-0.0804	37.04
n = 3 m = 2					
171190 - 201190	1.05E+00	-6.86E-01	4.14E-04 ns	-3.36E-02	19.6
201190 - 231190	1.00E+00	5.17E-01 ns	1.79E-03 ns	-1.15E-01	28.7
231190 - 261190	8.56E-01	-8.39E-01 ns	4.80E-05 ns	-3.90E-02 ns	1.6
261190 - 291190	1.81E+00	1.08E-01 ns	-3.72E-03	-7.29E-02	42.5
291190 - 021290	1.35E+00	-2.41E-02 ns	1.74E-02 ns	-3.97E-03 ns	0.2
021290 - 051290	1.34E+00	-2.04E-01	-7.92E-04 ns	-1.67E-02	23.2
051290 - 081290	1.47E+00	-4.50E-01 ns	1.88E-03	-4.28E-02	37.2
081290 - 111290	1.36E+00	4.76E-02 ns	5.37E-03	-7.94E-02	78.9
111290 - 141290	1.64E+00	-1.22E+00	8.72E-04 ns	-1.05E-01	56.6
141290 - 171290	1.37E+00	2.22E-02 ns	-1.05E-02	-2.99E-02	32.5
171290 - 201290	1.24E+00	-3.02E-01	2.48E-03	-3.13E-02	53.8
201290 - 231290	1.25E+00	-3.40E-01 ns	6.60E-04	1.93E-02	21.4
231290 - 261290	1.35E+00	-1.06E+00	1.20E-04 ns	-7.33E-02	48.5
261290 - 291290	1.97E+00	-1.71E+00	1.27E-03 ns	-1.96E-01	66.2
291290 - 010191	3.35E+00	-5.53E-01 ns	-4.39E-03	-2.85E-01	79.9
010191 - 040191	5.77E+00	8.57E-01 ns	-3.44E-03 ns	-3.19E-01	34.1
040191 - 070191	4.69E+00	-1.25E+00 ns	1.11E-02	-3.75E-01	72.6
070191 - 100191	4.02E+00	9.52E+00 ns	3.17E-03 ns	-2.18E-01	15.4
100191 - 130191	3.08E+00	-4.43E+00	4.19E-03	-1.12E-01	38.2
130191 - 160191	3.36E+00	-5.35E-01 ns	-3.84E-03 ns	5.89E-02	9.2
160191 - 190191	2.90E+00	-6.80E-01 ns	-4.03E-03	-8.65E-02	28.9
190191 - 220191	1.64E+00	-3.64E-01	1.06E-02	-4.04E-03 ns	86.2
220191 - 250191	1.45E+00	6.03E-01 ns	6.49E-03	-3.25E-02	39.1
250191 - 280191	1.36E+00	-6.11E-02 ns	7.71E-03	-1.16E-02 ns	18.9
280191 - 310191	1.66E+00	-2.14E-01 ns	8.08E-04 ns	3.53E-02	16.0
310191 - 030291	1.85E+00	-1.95E-01 ns	3.47E-03 ns	1.38E-02 ns	3.6
030291 - 060291	1.69E+00	-4.77E-01 ns	3.33E-03	-4.05E-03 ns	9.7
Mean	2.0596	-0.1452	0.0019	-0.0800	35.66

Period	k_0	k_1	k_2	k_3	R^2 (%)
n = 3 m = 3					
171190 - 201190	1.06E+00	-7.14E-01	5.51E-05 ns	-3.35E-02	20.5
201190 - 231190	1.05E+00	5.01E-01 ns	4.71E-05 ns	-1.16E-01	27.3
231190 - 261190	8.71E-01	-8.23E-01 ns	1.71E-05 ns	-3.91E-02 ns	1.8
261190 - 291190	1.81E+00	1.22E-01 ns	5.62E-04	-7.23E-02	43.7
291190 - 021290	1.36E+00	-3.42E-02 ns	6.23E-03	-3.85E-03 ns	2.6
021290 - 051290	1.34E+00	-2.05E-01	1.33E-04 ns	-1.67E-02	23.2
051290 - 081290	1.51E+00	-4.85E-01 ns	1.23E-04	-4.36E-02	35.7
081290 - 111290	1.49E+00	1.93E-01 ns	3.16E-04	-7.36E-02	72.6
111290 - 141290	1.64E+00	-1.22E+00	8.41E-05 ns	-1.05E-01	56.8
141290 - 171290	1.36E+00	1.85E-02 ns	-3.17E-03	-2.87E-02	34.5
171290 - 201290	1.26E+00	-3.13E-01	1.87E-04	-3.19E-02	48.4
201290 - 231290	1.28E+00	-3.64E-01 ns	3.50E-05	1.91E-02	18.1
231290 - 261290	1.38E+00	-1.13E+00	2.61E-06 ns	-7.33E-02	48.3
261290 - 291290	2.03E+00	-1.72E+00	6.63E-05 ns	-1.96E-01	66.1
291290 - 010191	3.22E+00	-5.35E-01 ns	2.83E-04	-2.85E-01	79.5
010191 - 040191	5.59E+00	8.71E-01 ns	1.69E-04 ns	-3.17E-01	34.3
040191 - 070191	5.30E+00	-1.30E+00 ns	4.74E-04	-3.72E-01	67.2
070191 - 100191	4.14E+00	9.65E+00 ns	1.74E-04 ns	-2.21E-01	14.8
100191 - 130191	3.20E+00	-5.26E+00	2.43E-04	-1.13E-01	33.3
130191 - 160191	3.32E+00	-5.91E-01 ns	2.51E-04 ns	5.84E-02	8.1
160191 - 190191	2.81E+00	-6.82E-01 ns	2.30E-04	-8.71E-02	25.6
190191 - 220191	1.69E+00	-3.19E-01 ns	1.12E-03	-3.52E-03 ns	79.6
220191 - 250191	1.46E+00	5.96E-01 ns	1.09E-03	-3.18E-02	39.4
250191 - 280191	1.38E+00	9.00E-03 ns	1.13E-03	-8.91E-03 ns	15.5
280191 - 310191	1.67E+00	-2.21E-01 ns	4.76E-05 ns	3.46E-02	15.6
310191 - 030291	1.86E+00	-1.96E-01 ns	4.09E-04 ns	1.36E-02 ns	2.9
030291 - 060291	1.70E+00	-4.91E-01 ns	4.31E-04 ns	-4.33E-03 ns	8.7
Mean	2.1030	-0.1720	0.0004	-0.0800	34.23

A.3.4 Results for LB3 surface for the winter deployment using salinity in Eq. 7.9.

Period	k_0'	k_1'	k_2'	k_3'	R^2 (%)
n = 1 m = 1					
171190 - 201190	4.97E+01	-2.68E-01	2.52E-02	-1.46E+00	70.0
201190 - 231190	5.96E+01	-9.12E-02 ns	2.08E-02	-1.76E+00	92.1
231190 - 261190	2.94E+01	-6.30E-02 ns	3.42E-03 ns	-8.50E-01	88.5
261190 - 291190	3.51E+01	-3.29E-01	5.40E-02	-1.03E+00	65.3
291190 - 021290	2.25E+01	-1.83E-01	5.99E-02	-6.51E-01	90.2
021290 - 051290	1.58E+01	-1.91E-01	-9.91E-03 ns	-4.31E-01	24.8
051290 - 081290	7.06E+01	-2.96E-01	2.74E-02	-2.08E+00	53.4
081290 - 111290	6.29E+01	7.20E-02 ns	1.03E-01	-1.86E+00	75.4
111290 - 141290	4.09E+01	-2.62E-01 ns	4.42E-02	-1.20E+00	57.0
141290 - 171290	1.28E+01	6.37E-03 ns	-3.60E-02 ns	-3.48E-01	35.2
171290 - 201290	1.63E+01	-4.04E-02 ns	3.87E-02	-4.58E-01	52.5
201290 - 231290	1.51E+01	-1.50E-01 ns	1.58E-02	-4.19E-01	24.3
231290 - 261290	-2.42E+01	-3.16E-01 ns	8.00E-05 ns	7.69E-01	11.6
261290 - 291290	1.97E+02	3.23E-01 ns	-4.99E-02	-5.80E+00	64.2
291290 - 010191	1.61E+02	-8.42E-01	1.15E-01	-4.76E+00	92.3
010191 - 040191	3.88E+02	-5.06E-01 ns	-2.16E-03 ns	-1.15E+01	71.7
040191 - 070191	3.53E+02	-5.41E-01 ns	2.58E-01	-1.04E+01	72.8
070191 - 100191	2.67E+02	1.55E+00 ns	9.08E-02	-7.88E+00	27.4
100191 - 130191	4.64E+01	-8.48E-01 ns	1.27E-01	-1.31E+00	40.5
130191 - 160191	-4.90E+01	-2.49E-01 ns	-5.64E-02 ns	1.58E+00	21.7
160191 - 190191	7.61E+01	-3.17E-01 ns	-3.93E-02	-2.17E+00	59.5
190191 - 220191	5.85E-01 ns	-2.73E-01	1.06E-01	2.90E-02 ns	90.6
220191 - 250191	1.93E+01	1.56E-01 ns	4.74E-02	-5.31E-01 ns	21.3
250191 - 280191	-4.52E+00 ns	-3.51E-02 ns	4.24E-02	1.73E-01 ns	18.9
280191 - 310191	-4.33E+01	-2.88E-01	1.14E-02 ns	1.33E+00	33.2
310191 - 030291	-3.64E+00 ns	-1.62E-01 ns	2.91E-02 ns	1.63E-01 ns	5.5
030291 - 060291	-6.42E+00 ns	-4.12E-01	2.92E-02	2.41E-01 ns	24.5
Mean	66.963	-0.16872	0.0391	-1.9468	51.27
n = 1 m = 2					
171190 - 201190	4.98E+01	-2.64E-01	1.57E-03	-1.46E+00	68.5
201190 - 231190	6.06E+01	-9.21E-02 ns	1.63E-03	-1.79E+00	92.0
231190 - 261190	2.95E+01	-6.31E-02 ns	5.37E-05 ns	-8.52E-01	88.3
261190 - 291190	3.68E+01	-3.55E-01	7.57E-03	-1.09E+00	66.8
291190 - 021290	2.23E+01	-1.81E-01	1.51E-02	-6.41E-01	90.3
021290 - 051290	1.59E+01	-1.93E-01	-1.36E-03 ns	-4.35E-01	24.7
051290 - 081290	6.98E+01	-3.20E-01	1.60E-03	-2.05E+00	51.8
081290 - 111290	4.95E+01	7.81E-02 ns	5.44E-03	-1.45E+00	73.7
111290 - 141290	3.69E+01	-3.30E-01 ns	2.82E-03	-1.07E+00	50.0
141290 - 171290	1.24E+01	7.23E-03 ns	-9.82E-03	-3.37E-01	36.8
171290 - 201290	1.64E+01	-4.55E-02 ns	2.87E-03	-4.59E-01	46.3
201290 - 231290	1.44E+01	-1.56E-01 ns	7.99E-04	-3.98E-01	19.9
231290 - 261290	-2.53E+01	-3.38E-01 ns	1.47E-04 ns	8.02E-01	11.9
261290 - 291290	1.99E+02	3.38E-01 ns	2.29E-03	-5.85E+00	65.0
291290 - 010191	1.61E+02	-8.38E-01	6.37E-03	-4.74E+00	92.6
010191 - 040191	3.88E+02	-5.07E-01 ns	-1.76E-04 ns	-1.15E+01	71.7
040191 - 070191	3.52E+02	-4.75E-01 ns	1.00E-02	-1.04E+01	72.7
070191 - 100191	2.69E+02	1.62E+00 ns	4.20E-03	-7.94E+00	26.2
100191 - 130191	2.18E+01 ns	-1.03E+00	6.10E-03	-5.61E-01 ns	25.3
130191 - 160191	-4.78E+01	-2.40E-01 ns	-5.47E-03 ns	1.54E+00	20.5
160191 - 190191	7.85E+01	-3.04E-01 ns	1.78E-03	-2.25E+00	57.8
190191 - 220191	-2.77E-01 ns	-2.54E-01	1.05E-02	5.87E-02 ns	86.6
220191 - 250191	1.84E+01	1.40E-01 ns	7.60E-03	-5.03E-01 ns	23.9
250191 - 280191	-5.28E+00 ns	-2.83E-02 ns	5.84E-03	1.97E-01 ns	17.6
280191 - 310191	-4.28E+01	-2.92E-01	7.26E-04 ns	1.32E+00	32.1
310191 - 030291	-3.27E+00 ns	-1.62E-01 ns	3.34E-03 ns	1.53E-01 ns	4.1
030291 - 060291	-5.96E+00 ns	-4.12E-01	3.28E-03	2.29E-01 ns	22.9
Mean	65.604	-0.1740	0.0031	-1.9065	49.63

Period	k_0'	k_1'	k_2'	k_3'	R^2 (%)
n = 1 m = 3					
171190 - 201190	4.93E+01	-2.63E-01	1.11E-04	-1.44E+00	67.0
201190 - 231190	6.13E+01	-9.62E-02 ns	1.40E-04	-1.81E+00	92.0
231190 - 261190	2.95E+01	-6.30E-02 ns	1.57E-05 ns	-8.52E-01	88.5
261190 - 291190	3.71E+01	-3.78E-01	1.02E-03	-1.09E+00	66.1
291190 - 021290	2.21E+01	-1.82E-01	4.21E-03	-6.34E-01	90.0
021290 - 051290	1.60E+01	-1.95E-01	2.36E-04 ns	-4.39E-01	24.7
051290 - 081290	7.00E+01	-3.38E-01	1.01E-04	-2.05E+00	49.8
081290 - 111290	4.18E+01	1.01E-01 ns	3.19E-04	-1.22E+00	67.1
111290 - 141290	3.42E+01	-3.80E-01	2.03E-04	-9.90E-01	46.5
141290 - 171290	1.20E+01	7.65E-03 ns	-2.93E-03	-3.24E-01	38.4
171290 - 201290	1.60E+01	-5.57E-02 ns	2.11E-04	-4.46E-01	38.3
201290 - 231290	1.37E+01	-1.65E-01 ns	4.34E-05	-3.76E-01	15.6
231290 - 261290	-2.61E+01	-3.52E-01 ns	1.41E-05 ns	8.27E-01	12.6
261290 - 291290	2.00E+02	3.53E-01 ns	1.31E-04	-5.90E+00	65.7
291290 - 010191	1.60E+02	-8.37E-01	4.36E-04	-4.71E+00	92.7
010191 - 040191	3.88E+02	-5.07E-01 ns	1.25E-05 ns	-1.15E+01	71.7
040191 - 070191	3.60E+02	-4.48E-01 ns	4.33E-04	-1.06E+01	68.6
070191 - 100191	2.71E+02	1.67E+00 ns	2.39E-04 ns	-7.98E+00	25.3
100191 - 130191	3.35E+00 ns	-1.12E+00	2.98E-04	-1.70E-03 ns	18.0
130191 - 160191	-4.67E+01	-2.50E-01 ns	4.47E-04 ns	1.50E+00	18.8
160191 - 190191	7.99E+01	-2.96E-01 ns	9.24E-05 ns	-2.29E+00	56.9
190191 - 220191	-3.73E+00 ns	-2.50E-01	1.09E-03	1.63E-01 ns	80.2
220191 - 250191	1.76E+01 ns	1.34E-01 ns	1.28E-03	-4.80E-01 ns	24.7
250191 - 280191	-7.09E+00 ns	-1.61E-02 ns	8.56E-04	2.52E-01 ns	15.8
280191 - 310191	-4.25E+01	-2.94E-01	4.69E-05 ns	1.31E+00	31.8
310191 - 030291	-3.17E+00 ns	-1.62E-01 ns	4.00E-04 ns	1.50E-01 ns	3.5
030291 - 060291	-5.54E+00 ns	-4.15E-01	4.16E-04 ns	2.16E-01 ns	21.9
Mean	64.741	-0.1777	0.0004	-1.8783	47.86
n = 2 m = 1					
171190 - 201190	4.98E+01	-3.50E-01	2.47E-02	-1.46E+00	69.7
201190 - 231190	5.97E+01	-1.48E-01 ns	2.08E-02	-1.76E+00	92.1
231190 - 261190	2.94E+01	-1.07E-01 ns	3.43E-03 ns	-8.50E-01	88.4
261190 - 291190	3.50E+01	-5.18E-01	5.33E-02	-1.03E+00	65.3
291190 - 021290	2.26E+01	-2.27E-01	6.16E-02	-6.54E-01	90.7
021290 - 051290	1.59E+01	-2.10E-01	-9.73E-03 ns	-4.37E-01	25.8
051290 - 081290	7.13E+01	-3.72E-01	2.67E-02	-2.10E+00	53.4
081290 - 111290	6.30E+01	1.49E-01 ns	1.03E-01	-1.87E+00	75.4
111290 - 141290	4.09E+01	-3.91E-01 ns	4.43E-02	-1.20E+00	56.6
141290 - 171290	1.28E+01	6.80E-03 ns	-3.60E-02 ns	-3.48E-01	35.2
171290 - 201290	1.61E+01	-7.67E-02 ns	3.85E-02	-4.54E-01	52.8
201290 - 231290	1.49E+01	-2.13E-01 ns	1.55E-02	-4.15E-01	24.4
231290 - 261290	-2.41E+01	-5.48E-01 ns	-2.04E-04 ns	7.64E-01	11.8
261290 - 291290	1.98E+02	5.89E-01 ns	-5.01E-02	-5.83E+00	64.3
291290 - 010191	1.62E+02	-1.06E+00	1.14E-01	-4.79E+00	92.5
010191 - 040191	3.87E+02	-4.69E-01 ns	-2.74E-03 ns	-1.15E+01	71.6
040191 - 070191	3.52E+02	-9.74E-01 ns	2.57E-01	-1.04E+01	73.0
070191 - 100191	2.66E+02	3.02E+00 ns	9.18E-02	-7.84E+00	27.3
100191 - 130191	4.71E+01	-1.72E+00 ns	1.24E-01	-1.34E+00	40.9
130191 - 160191	-4.91E+01	-3.66E-01 ns	-5.55E-02 ns	1.58E+00	21.8
160191 - 190191	7.66E+01	-3.03E-01 ns	-3.85E-02	-2.19E+00	59.1
190191 - 220191	1.04E+00 ns	-3.25E-01	1.07E-01	1.42E-02 ns	90.4
220191 - 250191	1.91E+01	3.22E-01 ns	4.66E-02	-5.25E-01 ns	22.3
250191 - 280191	-4.63E+00 ns	-3.06E-02 ns	4.21E-02	1.76E-01 ns	18.9
280191 - 310191	-4.25E+01	-2.80E-01	1.12E-02 ns	1.31E+00	30.6
310191 - 030291	-4.07E+00 ns	-1.82E-01 ns	2.94E-02 ns	1.75E-01 ns	4.3
030291 - 060291	-5.74E+00 ns	-4.98E-01	3.20E-02	2.19E-01 ns	17.6
Mean	67.041	-0.1956	0.0390	-1.9539	50.97

Period	k_0'	k_1'	k_2'	k_3'	R^2 (%)
n = 2 m = 2					
171190 - 201190	4.99E+01	-3.45E-01	1.53E-03	-1.46E+00	68.2
201190 - 231190	6.07E+01	-1.49E-01 ns	1.63E-03	-1.79E+00	92.1
231190 - 261190	2.95E+01	-1.06E-01 ns	5.30E-05 ns	-8.52E-01	88.3
261190 - 291190	3.69E+01	-5.71E-01	7.54E-03	-1.09E+00	66.9
291190 - 021290	2.24E+01	-2.24E-01	1.55E-02	-6.44E-01	90.8
021290 - 051290	1.60E+01	-2.12E-01	-1.34E-03 ns	-4.41E-01	25.7
051290 - 081290	7.06E+01	-4.03E-01	1.55E-03	-2.07E+00	51.9
081290 - 111290	4.97E+01	1.75E-01 ns	5.44E-03	-1.45E+00	73.7
111290 - 141290	3.69E+01	-5.20E-01 ns	2.81E-03	-1.07E+00	49.6
141290 - 171290	1.24E+01	7.40E-03 ns	-9.82E-03	-3.37E-01	36.8
171290 - 201290	1.62E+01	-8.76E-02 ns	2.85E-03	-4.54E-01	46.7
201290 - 231290	1.43E+01	-2.22E-01 ns	7.81E-04	-3.94E-01	20.0
231290 - 261290	-2.51E+01	-5.84E-01 ns	1.58E-04 ns	7.96E-01	12.1
261290 - 291290	2.00E+02	6.16E-01 ns	2.30E-03	-5.89E+00	65.2
291290 - 010191	1.61E+02	-1.05E+00	6.30E-03	-4.77E+00	92.8
010191 - 040191	3.87E+02	-4.70E-01 ns	-1.92E-04 ns	-1.15E+01	71.6
040191 - 070191	3.52E+02	-8.94E-01 ns	1.00E-02	-1.04E+01	72.9
070191 - 100191	2.68E+02	3.15E+00 ns	4.25E-03	-7.90E+00	26.1
100191 - 130191	2.38E+01 ns	-2.18E+00	5.94E-03	-6.23E-01 ns	26.5
130191 - 160191	-4.79E+01	-3.65E-01 ns	-5.38E-03 ns	1.54E+00	20.5
160191 - 190191	7.89E+01	-2.97E-01 ns	1.75E-03 ns	-2.26E+00	57.4
190191 - 220191	1.89E-01 ns	-3.01E-01	1.05E-02	4.36E-02 ns	86.4
220191 - 250191	1.82E+01	2.94E-01 ns	7.47E-03	-4.99E-01 ns	24.8
250191 - 280191	-5.39E+00 ns	-1.56E-02 ns	5.79E-03	2.01E-01 ns	17.5
280191 - 310191	-4.20E+01	-2.86E-01	6.88E-04 ns	1.29E+00	29.5
310191 - 030291	-3.69E+00 ns	-1.80E-01 ns	3.37E-03 ns	1.64E-01 ns	2.8
030291 - 060291	-5.44E+00 ns	-4.98E-01	3.74E-03	2.11E-01 ns	16.1
Mean	65.743	-0.2118	0.0032	-1.9129	49.37
n = 2 m = 3					
171190 - 201190	4.94E+01	-3.47E-01	1.08E-04	-1.45E+00	66.8
201190 - 231190	6.14E+01	-1.55E-01 ns	1.40E-04	-1.81E+00	92.0
231190 - 261190	2.95E+01	-1.05E-01 ns	1.57E-05 ns	-8.52E-01	88.5
261190 - 291190	3.73E+01	-6.18E-01	1.03E-03	-1.10E+00	66.5
291190 - 021290	2.21E+01	-2.24E-01	4.30E-03	-6.36E-01	90.5
021290 - 051290	1.62E+01	-2.15E-01	2.36E-04 ns	-4.45E-01	25.8
051290 - 081290	7.08E+01	-4.30E-01	9.69E-05	-2.08E+00	49.9
081290 - 111290	4.20E+01	2.22E-01 ns	3.19E-04	-1.22E+00	67.2
111290 - 141290	3.42E+01	-6.18E-01 ns	2.01E-04	-9.90E-01	46.1
141290 - 171290	1.20E+01	6.70E-03 ns	-2.93E-03	-3.24E-01	38.4
171290 - 201290	1.58E+01	-1.02E-01 ns	2.09E-04	-4.41E-01	38.7
201290 - 231290	1.36E+01	-2.37E-01 ns	4.20E-05	-3.72E-01	15.8
231290 - 261290	-2.59E+01	-6.09E-01	1.47E-05 ns	8.20E-01	12.9
261290 - 291290	2.01E+02	6.45E-01 ns	1.31E-04	-5.93E+00	65.8
291290 - 010191	1.60E+02	-1.05E+00	4.31E-04	-4.73E+00	92.9
010191 - 040191	3.87E+02	-4.71E-01 ns	1.31E-05 ns	-1.14E+01	71.6
040191 - 070191	3.60E+02	-8.95E-01 ns	4.31E-04	-1.06E+01	68.8
070191 - 100191	2.70E+02	3.23E+00 ns	2.42E-04 ns	-7.95E+00	25.2
100191 - 130191	6.18E+00 ns	-2.41E+00	2.90E-04	-8.93E-02 ns	19.6
130191 - 160191	-4.70E+01	-3.92E-01 ns	4.38E-04 ns	1.51E+00	18.9
160191 - 190191	8.02E+01	-2.92E-01 ns	9.07E-05 ns	-2.30E+00	56.5
190191 - 220191	-3.21E+00 ns	-2.91E-01	1.10E-03	1.46E-01 ns	79.9
220191 - 250191	1.75E+01 ns	2.85E-01 ns	1.26E-03	-4.76E-01 ns	25.6
250191 - 280191	-7.20E+00 ns	8.20E-03 ns	8.47E-04	2.55E-01 ns	15.8
280191 - 310191	-4.17E+01	-2.89E-01	4.08E-05 ns	1.28E+00	29.2
310191 - 030291	-3.59E+00 ns	-1.81E-01 ns	3.97E-04 ns	1.62E-01 ns	2.2
030291 - 060291	-5.09E+00 ns	-5.02E-01	4.87E-04	2.01E-01 ns	15.1
Mean	64.907	-0.2236	0.0004	-1.8823	47.64

Period	k_0'	k_1'	k_2'	k_3'	R^2 (%)
n = 3 m = 1					
171190 - 201190	4.98E+01	-5.03E-01	2.45E-02	-1.46E+00	69.4
201190 - 231190	5.97E+01	-2.41E-01 ns	2.08E-02	-1.76E+00	92.1
231190 - 261190	2.94E+01	-2.10E-01 ns	3.45E-03 ns	-8.50E-01	88.4
261190 - 291190	3.48E+01	-8.77E-01	5.26E-02	-1.03E+00	65.2
291190 - 021290	2.26E+01	-2.92E-01	6.20E-02	-6.53E-01	90.8
021290 - 051290	1.60E+01	-2.48E-01	-9.37E-03 ns	-4.39E-01	25.9
051290 - 081290	7.17E+01	-4.51E-01 ns	2.69E-02	-2.11E+00	52.7
081290 - 111290	6.30E+01	2.99E-01 ns	1.03E-01	-1.87E+00	75.4
111290 - 141290	4.09E+01	-6.09E-01 ns	4.49E-02	-1.20E+00	56.3
141290 - 171290	1.28E+01	1.30E-03 ns	-3.60E-02 ns	-3.48E-01	35.2
171290 - 201290	1.60E+01	-1.47E-01 ns	3.82E-02	-4.50E-01	53.1
201290 - 231290	1.49E+01	-3.25E-01 ns	1.54E-02	-4.13E-01	24.3
231290 - 261290	-2.39E+01	-9.75E-01 ns	-1.51E-04 ns	7.59E-01	11.7
261290 - 291290	1.98E+02	1.08E+00 ns	-5.01E-02	-5.83E+00	64.3
291290 - 010191	1.62E+02	-1.40E+00	1.13E-01	-4.80E+00	92.5
010191 - 040191	3.86E+02	-4.17E-01 ns	-2.54E-03 ns	-1.14E+01	71.4
040191 - 070191	3.53E+02	-1.50E+00 ns	2.56E-01	-1.04E+01	73.1
070191 - 100191	2.67E+02	6.11E+00 ns	9.37E-02	-7.87E+00	26.9
100191 - 130191	4.71E+01	-3.50E+00 ns	1.23E-01	-1.34E+00	40.8
130191 - 160191	-4.93E+01	-6.35E-01 ns	-5.44E-02 ns	1.58E+00	21.9
160191 - 190191	7.68E+01	-3.16E-01 ns	-3.82E-02	-2.19E+00	58.8
190191 - 220191	1.92E+00 ns	-4.05E-01	1.07E-01	-1.25E-02 ns	90.1
220191 - 250191	1.90E+01	6.68E-01 ns	4.61E-02	-5.23E-01 ns	23.2
250191 - 280191	-4.74E+00 ns	-5.40E-03 ns	4.17E-02	1.79E-01 ns	18.8
280191 - 310191	-4.19E+01	-2.70E-01 ns	1.14E-02 ns	1.29E+00	28.5
310191 - 030291	-4.24E+00 ns	-1.93E-01 ns	2.95E-02 ns	1.79E-01 ns	3.1
030291 - 060291	-4.06E+00 ns	-5.65E-01	3.42E-02	1.68E-01 ns	11.9
Mean	67.196	-0.2195	0.0391	-1.9553	50.59
n = 3 m = 2					
171190 - 201190	4.99E+01	-4.96E-01	1.51E-03	-1.46E+00	67.9
201190 - 231190	6.07E+01	-2.41E-01 ns	1.63E-03	-1.79E+00	92.1
231190 - 261190	2.95E+01	-2.00E-01 ns	5.14E-05 ns	-8.52E-01	88.3
261190 - 291190	3.68E+01	-9.78E-01	7.48E-03	-1.09E+00	66.9
291190 - 021290	2.23E+01	-2.88E-01	1.55E-02	-6.43E-01	90.9
021290 - 051290	1.61E+01	-2.50E-01	-1.28E-03 ns	-4.42E-01	25.8
051290 - 081290	7.10E+01	-4.95E-01	1.56E-03	-2.09E+00	51.1
081290 - 111290	4.97E+01	3.66E-01 ns	5.44E-03	-1.46E+00	73.7
111290 - 141290	3.69E+01	-8.61E-01 ns	2.85E-03	-1.07E+00	49.1
141290 - 171290	1.24E+01	1.30E-03 ns	-9.82E-03	-3.37E-01	36.8
171290 - 201290	1.60E+01	-1.67E-01 ns	2.83E-03	-4.50E-01	47.1
201290 - 231290	1.42E+01	-3.41E-01 ns	7.73E-04	-3.92E-01	19.9
231290 - 261290	-2.49E+01	-1.04E+00 ns	1.54E-04 ns	7.90E-01	12.0
261290 - 291290	2.00E+02	1.14E+00 ns	2.30E-03	-5.89E+00	65.2
291290 - 010191	1.62E+02	-1.39E+00	6.23E-03	-4.78E+00	92.8
010191 - 040191	3.86E+02	-4.19E-01 ns	-1.86E-04 ns	-1.14E+01	71.4
040191 - 070191	3.53E+02	-1.40E+00 ns	9.98E-03	-1.04E+01	72.9
070191 - 100191	2.69E+02	6.37E+00 ns	4.34E-03	-7.93E+00	25.7
100191 - 130191	2.46E+01 ns	-4.64E+00	5.88E-03	-6.49E-01 ns	26.9
130191 - 160191	-4.81E+01	-6.49E-01 ns	-5.28E-03 ns	1.55E+00	20.7
160191 - 190191	7.91E+01	-3.15E-01 ns	1.73E-03 ns	-2.27E+00	57.2
190191 - 220191	1.07E+00 ns	-3.70E-01	1.06E-02	1.68E-02 ns	86.1
220191 - 250191	1.82E+01	6.17E-01 ns	7.40E-03	-4.98E-01 ns	25.5
250191 - 280191	-5.50E+00 ns	2.55E-02 ns	5.73E-03	2.04E-01 ns	17.5
280191 - 310191	-4.14E+01	-2.78E-01 ns	6.99E-04 ns	1.27E+00	27.4
310191 - 030291	-3.86E+00 ns	-1.91E-01 ns	3.42E-03 ns	1.69E-01 ns	1.6
030291 - 060291	-3.86E+00 ns	-5.67E-01 ns	4.07E-03	1.63E-01 ns	10.5
Mean	65.957	-0.2613	0.0032	-1.9159	49.00

Period	k_0'	k_1'	k_2'	k_3'	R^2 (%)
n = 3 m = 3					
171190 - 201190	4.94E+01	-5.02E-01	1.07E-04	-1.45E+00	66.6
201190 - 231190	6.14E+01	-2.50E-01 ns	1.40E-04	-1.81E+00	92.0
231190 - 261190	2.95E+01	-1.89E-01 ns	1.56E-05 ns	-8.52E-01	88.5
261190 - 291190	3.72E+01	-1.07E+00	1.02E-03	-1.10E+00	66.5
291190 - 021290	2.21E+01	-2.87E-01	4.31E-03	-6.36E-01	90.5
021290 - 051290	1.62E+01	-2.53E-01	2.24E-04 ns	-4.46E-01	25.9
051290 - 081290	7.13E+01	-5.35E-01	9.74E-05	-2.09E+00	49.1
081290 - 111290	4.20E+01	4.58E-01 ns	3.19E-04	-1.22E+00	67.2
111290 - 141290	3.42E+01	-1.05E+00 ns	2.05E-04	-9.89E-01	45.7
141290 - 171290	1.20E+01	-1.40E-03 ns	-2.93E-03	-3.24E-01	38.4
171290 - 201290	1.56E+01	-1.89E-01 ns	2.08E-04	-4.37E-01	39.2
201290 - 231290	1.35E+01	-3.67E-01 ns	4.13E-05	-3.70E-01	15.8
231290 - 261290	-2.57E+01	-1.09E+00 ns	1.44E-05 ns	8.14E-01	12.7
261290 - 291290	2.01E+02	1.20E+00 ns	1.31E-04	-5.94E+00	65.8
291290 - 010191	1.61E+02	-1.38E+00	4.26E-04	-4.74E+00	92.8
010191 - 040191	3.86E+02	-4.20E-01 ns	1.29E-05 ns	-1.14E+01	71.4
040191 - 070191	3.60E+02	-1.44E+00 ns	4.30E-04	-1.06E+01	68.9
070191 - 100191	2.71E+02	6.53E+00 ns	2.48E-04 ns	-7.99E+00	24.8
100191 - 130191	7.58E+00 ns	-5.17E+00	2.88E-04	-1.33E-01 ns	20.2
130191 - 160191	-4.72E+01	-7.04E-01 ns	4.28E-04 ns	1.52E+00	19.2
160191 - 190191	8.04E+01	-3.12E-01 ns	9.00E-05 ns	-2.31E+00	56.3
190191 - 220191	-2.28E+00 ns	-3.50E-01 ns	1.11E-03	1.18E-01 ns	79.6
220191 - 250191	1.75E+01 ns	6.03E-01 ns	1.25E-03	-4.76E-01 ns	26.4
250191 - 280191	-7.27E+00 ns	7.14E-02 ns	8.37E-04	2.57E-01 ns	15.9
280191 - 310191	-4.10E+01	-2.84E-01 ns	4.17E-05 ns	1.26E+00	27.1
310191 - 030291	-3.76E+00 ns	-1.92E-01 ns	4.12E-04 ns	1.66E-01 ns	1.0
030291 - 060291	-3.54E+00 ns	-5.75E-01	5.37E-04	1.54E-01 ns	9.5
Mean	65.116	-0.2870	0.0004	-1.8898	47.30

A.3.5 Results for LB2 surface for the winter deployment using displacement in Eq. 7.8.

Period	k_0	k_1	k_2	k_3	R^2 (%)
n = 1 m = 1					
171190 - 201190	8.24E-01	7.77E-02 ns	3.06E-02	-6.89E-02	34.5
201190 - 231190	7.27E-01	3.17E-01 ns	2.21E-02	-2.36E-02	13.1
231190 - 261190	1.31E+00	-2.33E-01 ns	-3.71E-02 ns	-1.48E-01	19.3
261190 - 291190	1.91E+00	-2.21E-01 ns	3.21E-02	3.27E-02	33.5
291190 - 021290	1.23E+00	-1.59E-01 ns	8.01E-02	-2.86E-02	21.0
021290 - 051290	1.53E+00	-1.24E-01 ns	-1.92E-02 ns	-5.25E-02	68.7
051290 - 081290	1.92E+00	-7.97E-01 ns	5.57E-02	-1.10E-01	30.7
081290 - 111290	2.24E+00	-3.31E-01 ns	1.35E-01	-3.08E-01	67.1
111290 - 141290	2.01E+00	-3.76E-01 ns	6.98E-02	-1.56E-01	70.7
141290 - 171290	2.13E+00	-1.09E+00	4.33E-02 ns	-1.18E-01	63.8
171290 - 201290	1.91E+00	-6.83E-01	2.87E-02	-1.14E-01	81.1
201290 - 231290	1.27E+00	-2.14E-02 ns	1.88E-02	-5.31E-02	34.7
231290 - 261290	1.25E+00	-2.41E-01 ns	2.25E-02	-1.00E-02 ns	9.0
261290 - 291290	4.51E+00	-1.20E+00	-1.11E-01	-1.50E-01	47.3
291290 - 010191	3.03E+00	8.71E-02 ns	3.41E-02 ns	-1.13E-01	46.4
010191 - 040191	5.57E+00	1.13E+00 ns	8.37E-02 ns	-2.58E-01	22.4
040191 - 070191	3.67E+00	2.30E-01 ns	3.36E-01	-8.85E-02 ns	57.4
070191 - 100191	3.72E+00	1.73E+00 ns	1.88E-01	-1.21E-01 ns	16.7
100191 - 130191	2.12E+00	1.72E-01 ns	1.78E-01	-4.93E-02	79.5
130191 - 160191	3.57E+00	6.40E-01 ns	1.08E-02 ns	9.44E-03 ns	0.0
160191 - 190191	4.39E+00	-8.22E-01	-9.72E-02	-1.73E-01	42.0
190191 - 220191	1.58E+00	-3.93E-01	1.61E-01	-7.79E-02	90.4
220191 - 250191	1.57E+00	-3.77E-01	5.87E-02	3.10E-04 ns	17.7
250191 - 280191	1.45E+00	-6.36E-01	3.58E-02	5.53E-03 ns	31.6
280191 - 310191	1.84E+00	-4.70E-01	-1.65E-02 ns	-9.79E-03 ns	10.0
310191 - 030291	2.66E+00	-8.08E-01	8.30E-03 ns	-1.95E-01	40.0
030291 - 060291	2.17E+00	-9.84E-01	1.41E-01	-2.07E-01	65.7
Mean	2.3004	-0.2068	0.0553	-0.0957	41.27
n = 1 m = 2					
171190 - 201190	9.66E-01	6.82E-02 ns	1.40E-03 ns	-6.70E-02	30.9
201190 - 231190	8.02E-01	3.13E-01 ns	9.32E-04 ns	-2.44E-02	7.8
231190 - 261190	1.19E+00	-2.34E-01 ns	-2.28E-03 ns	-1.51E-01	19.6
261190 - 291190	1.96E+00	-2.32E-01 ns	3.75E-03	3.31E-02	32.3
291190 - 021290	1.29E+00	-1.62E-01 ns	2.38E-02	-2.82E-02	24.3
021290 - 051290	1.49E+00	-1.27E-01 ns	-2.17E-03 ns	-5.23E-02	68.2
051290 - 081290	2.12E+00	-8.40E-01	3.29E-03	-1.11E-01	29.9
081290 - 111290	2.71E+00	-2.97E-01 ns	7.33E-03	-2.95E-01	67.4
111290 - 141290	2.12E+00	-3.95E-01 ns	5.81E-03	-1.57E-01	69.4
141290 - 171290	2.18E+00	-1.09E+00	8.51E-03 ns	-1.19E-01	63.8
171290 - 201290	1.98E+00	-6.93E-01	1.91E-03	-1.15E-01	79.9
201290 - 231290	1.35E+00	-3.12E-02 ns	9.24E-04	-5.36E-02	32.3
231290 - 261290	1.41E+00	-2.85E-01 ns	7.16E-04 ns	-9.11E-03 ns	4.9
261290 - 291290	3.85E+00	-1.19E+00	-4.51E-03	-1.50E-01	47.1
291290 - 010191	3.14E+00	9.38E-02 ns	2.17E-03	-1.12E-01	47.2
010191 - 040191	6.09E+00	1.13E+00 ns	3.21E-03 ns	-2.59E-01	22.5
040191 - 070191	5.37E+00	3.14E-01 ns	1.32E-02	-7.26E-02 ns	58.8
070191 - 100191	4.53E+00	1.86E+00 ns	9.40E-03	-1.33E-01 ns	15.7
100191 - 130191	2.56E+00	1.81E-02 ns	1.28E-02	-4.88E-02	78.9
130191 - 160191	3.56E+00	6.17E-01 ns	3.28E-03 ns	1.01E-02 ns	0.0
160191 - 190191	3.99E+00	-8.13E-01 ns	-4.16E-03	-1.73E-01	36.5
190191 - 220191	1.79E+00	-3.58E-01	1.58E-02	-7.84E-02	86.1
220191 - 250191	1.64E+00	-3.86E-01	8.77E-03	1.22E-03 ns	17.5
250191 - 280191	1.49E+00	-6.30E-01	4.97E-03	6.25E-03 ns	31.0
280191 - 310191	1.85E+00	-4.79E-01	-3.33E-03	-1.15E-02 ns	13.8
310191 - 030291	2.69E+00	-8.12E-01	-3.04E-03 ns	-1.95E-01	40.1
030291 - 060291	2.31E+00	-9.39E-01	1.99E-02	-2.06E-01	67.1
Mean	2.4603	-0.2066	0.0049	-0.0952	40.48

Period	k_0	k_1	k_2	k_3	R^2 (%)
n = 1 m = 3					
171190 - 201190	1.02E+00	5.68E-02 ns	6.82E-05 ns	-6.61E-02	28.9
201190 - 231190	8.29E-01	3.08E-01 ns	1.47E-05 ns	-2.48E-02	6.0
231190 - 261190	1.15E+00	-2.30E-01 ns	1.54E-04 ns	-1.52E-01	19.6
261190 - 291190	1.98E+00	-2.46E-01 ns	4.67E-04	3.33E-02	30.7
291190 - 021290	1.31E+00	-1.69E-01 ns	7.54E-03	-2.78E-02	26.6
021290 - 051290	1.48E+00	-1.27E-01 ns	2.58E-04 ns	-5.19E-02	67.8
051290 - 081290	2.20E+00	-8.76E-01	2.07E-04	-1.12E-01	28.6
081290 - 111290	2.87E+00	-2.51E-01 ns	4.37E-04	-2.87E-01	65.3
111290 - 141290	2.17E+00	-4.24E-01 ns	5.31E-04	-1.57E-01	68.9
141290 - 171290	2.20E+00	-1.09E+00	2.04E-03 ns	-1.19E-01	63.8
171290 - 201290	2.00E+00	-6.98E-01	1.37E-04	-1.15E-01	79.1
201290 - 231290	1.38E+00	-4.56E-02 ns	4.69E-05 ns	-5.39E-02	30.0
231290 - 261290	1.47E+00	-3.26E-01 ns	2.38E-05 ns	-8.72E-03 ns	2.2
261290 - 291290	3.62E+00	-1.17E+00	2.35E-04	-1.50E-01	46.6
291290 - 010191	3.18E+00	9.89E-02 ns	1.68E-04	-1.11E-01	48.1
010191 - 040191	6.26E+00	1.13E+00 ns	1.58E-04 ns	-2.62E-01	22.7
040191 - 070191	6.02E+00	3.52E-01 ns	5.88E-04	-6.97E-02 ns	56.7
070191 - 100191	4.81E+00	1.94E+00 ns	5.70E-04	-1.45E-01 ns	14.6
100191 - 130191	2.80E+00	-2.10E-01 ns	9.33E-04	-4.79E-02 ns	72.5
130191 - 160191	3.57E+00	5.90E-01 ns	6.46E-04 ns	1.17E-02 ns	0.0
160191 - 190191	3.88E+00	-8.07E-01 ns	2.10E-04 ns	-1.72E-01	34.1
190191 - 220191	1.86E+00	-3.27E-01 ns	1.66E-03	-7.76E-02	79.7
220191 - 250191	1.65E+00	-3.83E-01	1.37E-03	1.73E-03 ns	15.3
250191 - 280191	1.51E+00	-6.18E-01	7.19E-04	8.06E-03 ns	29.8
280191 - 310191	1.85E+00	-4.82E-01	5.07E-04	-1.19E-02 ns	16.6
310191 - 030291	2.69E+00	-8.15E-01	-9.99E-04 ns	-1.94E-01	40.1
030291 - 060291	2.34E+00	-9.28E-01	2.88E-03	-2.06E-01	67.4
Mean	2.522	-0.2129	0.0008	-0.0951	39.32
n = 2 m = 1					
171190 - 201190	8.33E-01	1.09E-01 ns	3.08E-02	-6.89E-02	34.6
201190 - 231190	7.61E-01	5.10E-01	2.20E-02	-2.31E-02	14.3
231190 - 261190	1.32E+00	-8.13E-01 ns	-3.71E-02 ns	-1.48E-01	19.7
261190 - 291190	1.91E+00	-4.82E-01	3.03E-02	3.29E-02	36.3
291190 - 021290	1.21E+00	-1.98E-01 ns	8.16E-02	-2.87E-02	21.5
021290 - 051290	1.51E+00	-1.47E-01	-1.90E-02 ns	-5.25E-02	69.1
051290 - 081290	1.85E+00	-1.11E+00	5.26E-02	-1.11E-01	31.6
081290 - 111290	2.20E+00	-5.15E-01 ns	1.35E-01	-3.08E-01	67.0
111290 - 141290	1.96E+00	-5.70E-01 ns	6.99E-02	-1.56E-01	70.4
141290 - 171290	1.96E+00	-1.46E+00	4.90E-02 ns	-1.21E-01	64.2
171290 - 201290	1.81E+00	-8.78E-01	2.91E-02	-1.15E-01	81.2
201290 - 231290	1.27E+00	-6.37E-02 ns	1.86E-02	-5.31E-02	34.7
231290 - 261290	1.25E+00	-6.02E-01 ns	2.11E-02	-1.03E-02 ns	10.8
261290 - 291290	4.38E+00	-1.99E+00	-1.11E-01	-1.48E-01	47.3
291290 - 010191	3.01E+00	2.02E-01 ns	3.53E-02 ns	-1.13E-01	46.7
010191 - 040191	5.75E+00	1.17E+00 ns	8.57E-02 ns	-2.57E-01	22.1
040191 - 070191	3.69E+00	4.02E-01 ns	3.36E-01	-8.86E-02 ns	57.4
070191 - 100191	3.88E+00	3.40E+00 ns	1.89E-01	-1.21E-01 ns	16.7
110191 - 130191	2.11E+00	4.72E-01 ns	1.80E-01	-4.90E-02	79.6
130191 - 160191	3.66E+00	8.85E-01 ns	8.64E-03 ns	9.74E-03 ns	0.0
160191 - 190191	4.29E+00	-1.14E+00	-9.54E-02	-1.75E-01	43.3
190191 - 220191	1.53E+00	-5.48E-01	1.61E-01	-7.80E-02	90.8
220191 - 250191	1.52E+00	-5.41E-01	5.80E-02	0.00E+00 ns	15.8
250191 - 280191	1.37E+00	-9.92E-01	3.84E-02	4.69E-03 ns	30.6
280191 - 310191	1.77E+00	-5.29E-01	-1.73E-02 ns	-1.06E-02 ns	8.6
310191 - 030291	2.57E+00	-9.79E-01	9.71E-03 ns	-1.92E-01	39.4
030291 - 060291	2.05E+00	-1.48E+00	1.44E-01	-2.08E-01	65.4
Mean	2.2750	-0.2921	0.0558	-0.0959	41.45

Period	k_0	k_1	k_2	k_3	R^2 (%)
n = 2 m = 2					
171190 - 201190	9.75E-01	9.03E-02 ns	1.41E-03 ns	-6.70E-02	30.9
201190 - 231190	8.34E-01	5.08E-01	9.35E-04 ns	-2.39E-02	9.1
231190 - 261190	1.19E+00	-8.06E-01 ns	-2.27E-03 ns	-1.50E-01	20.0
261190 - 291190	1.95E+00	-5.05E-01	3.56E-03	3.32E-02	35.5
291190 - 021290	1.26E+00	-2.01E-01 ns	2.42E-02	-2.84E-02	24.9
021290 - 051290	1.48E+00	-1.50E-01	-2.16E-03 ns	-5.23E-02	68.6
051290 - 081290	2.03E+00	-1.17E+00	3.10E-03	-1.13E-01	30.9
081290 - 111290	2.67E+00	-4.29E-01 ns	7.32E-03	-2.95E-01	67.3
111290 - 141290	2.07E+00	-6.02E-01 ns	5.82E-03	-1.57E-01	69.1
141290 - 171290	2.02E+00	-1.46E+00	9.40E-03 ns	-1.22E-01	64.2
171290 - 201290	1.87E+00	-8.92E-01	1.98E-03	-1.16E-01	80.0
201290 - 231290	1.35E+00	-7.90E-02 ns	9.06E-04	-5.36E-02	32.4
231290 - 261290	1.40E+00	-6.81E-01 ns	6.58E-04 ns	-9.41E-03 ns	7.1
261290 - 291290	3.71E+00	-1.96E+00	-4.54E-03	-1.48E-01	47.0
291290 - 010191	3.13E+00	2.12E-01 ns	2.23E-03	-1.12E-01	47.5
010191 - 040191	6.30E+00	1.16E+00 ns	3.26E-03 ns	-2.59E-01	22.2
040191 - 070191	5.40E+00	5.11E-01 ns	1.32E-02	-7.27E-02 ns	58.8
070191 - 100191	4.71E+00	3.64E+00 ns	9.46E-03	-1.33E-01 ns	15.6
100191 - 130191	2.57E+00	3.44E-02 ns	1.28E-02	-4.88E-02	78.9
130191 - 160191	3.65E+00	8.46E-01 ns	3.16E-03 ns	1.03E-02 ns	0.0
160191 - 190191	3.90E+00	-1.15E+00	-4.08E-03	-1.74E-01	38.0
190191 - 220191	1.75E+00	-5.03E-01	1.58E-02	-7.84E-02	86.5
220191 - 250191	1.59E+00	-5.60E-01	8.68E-03	9.00E-04 ns	15.5
250191 - 280191	1.41E+00	-9.77E-01	5.28E-03	5.57E-03 ns	29.7
280191 - 310191	1.78E+00	-5.46E-01	-3.45E-03	-1.24E-02 ns	12.6
310191 - 030291	2.60E+00	-9.84E-01	-3.05E-03 ns	-1.93E-01	39.4
030291 - 060291	2.20E+00	-1.43E+00	2.03E-02	-2.06E-01	67.0
Mean	2.437	-0.2994	0.0050	-0.0953	40.69
n = 2 m = 3					
171190 - 201190	1.03E+00	6.77E-02 ns	6.85E-05 ns	-6.61E-02	28.9
201190 - 231190	8.61E-01	5.01E-01	1.51E-05 ns	-2.44E-02	7.3
231190 - 261190	1.15E+00	-7.96E-01 ns	1.54E-04 ns	-1.52E-01	20.0
261190 - 291190	1.97E+00	-5.29E-01	4.46E-04	3.33E-02	34.2
291190 - 021290	1.28E+00	-2.09E-01 ns	7.63E-03	-2.79E-02	27.1
021290 - 051290	1.46E+00	-1.50E-01	2.59E-04 ns	-5.19E-02	68.3
051290 - 081290	2.11E+00	-1.22E+00	1.94E-04	-1.14E-01	29.7
081290 - 111290	2.83E+00	-3.35E-01 ns	4.37E-04	-2.87E-01	65.2
111290 - 141290	2.12E+00	-6.59E-01 ns	5.31E-04	-1.57E-01	68.6
141290 - 171290	2.04E+00	-1.46E+00	2.19E-03 ns	-1.22E-01	64.1
171290 - 201290	1.89E+00	-8.99E-01	1.44E-04	-1.16E-01	79.3
201290 - 231290	1.39E+00	-1.03E-01 ns	4.53E-05 ns	-5.40E-02	30.2
231290 - 261290	1.46E+00	-7.51E-01 ns	2.10E-05 ns	-9.06E-03 ns	4.7
261290 - 291290	3.48E+00	-1.93E+00	2.36E-04	-1.49E-01	46.5
291290 - 010191	3.17E+00	2.20E-01 ns	1.73E-04	-1.11E-01	48.4
010191 - 040191	6.48E+00	1.15E+00 ns	1.60E-04 ns	-2.61E-01	22.4
040191 - 070191	6.05E+00	5.24E-01 ns	5.89E-04	-6.98E-02 ns	56.8
070191 - 100191	5.00E+00	3.81E+00 ns	5.73E-04	-1.45E-01 ns	14.5
100191 - 130191	2.79E+00	-5.17E-01 ns	9.26E-04	-4.83E-02 ns	72.6
130191 - 160191	3.65E+00	8.06E-01 ns	6.43E-04 ns	1.19E-02 ns	0.0
160191 - 190191	3.79E+00	-1.15E+00	2.05E-04 ns	-1.74E-01	35.6
190191 - 220191	1.82E+00	-4.58E-01	1.66E-03	-7.77E-02	80.0
220191 - 250191	1.60E+00	-5.52E-01	1.35E-03	1.39E-03 ns	13.4
250191 - 280191	1.43E+00	-9.50E-01	7.54E-04	7.61E-03 ns	28.3
280191 - 310191	1.78E+00	-5.54E-01	5.24E-04	-1.28E-02 ns	15.6
310191 - 030291	2.60E+00	-9.89E-01	-1.06E-03 ns	-1.92E-01	39.5
030291 - 060291	2.23E+00	-1.43E+00	2.94E-03	-2.06E-01	67.4
Mean	2.499	-0.3171	0.0008	-0.0953	39.58

Period	k_0	k_1	k_2	k_3	R^2 (%)
n = 3 m = 1					
171190 - 201190	8.40E-01	1.39E-01 ns	3.08E-02	-6.88E-02	34.5
201190 - 231190	7.75E-01	8.71E-01	2.19E-02	-2.28E-02	15.0
231190 - 261190	1.31E+00	-2.22E+00 ns	-3.68E-02 ns	-1.48E-01	20.0
261190 - 291190	1.91E+00	-9.88E-01	2.89E-02	3.32E-02	38.8
291190 - 021290	1.20E+00	-2.62E-01 ns	8.21E-02	-2.88E-02	21.8
021290 - 051290	1.50E+00	-1.84E-01	-1.87E-02 ns	-5.25E-02	69.4
051290 - 081290	1.79E+00	-1.49E+00	5.21E-02	-1.12E-01	31.5
081290 - 111290	2.19E+00	-1.03E+00 ns	1.35E-01	-3.08E-01	67.0
111290 - 141290	1.93E+00	-8.58E-01 ns	7.09E-02	-1.56E-01	70.2
141290 - 171290	1.89E+00	-2.10E+00	5.25E-02 ns	-1.23E-01	63.0
171290 - 201290	1.76E+00	-1.21E+00	2.97E-02	-1.16E-01	80.5
201290 - 231290	1.27E+00	-1.39E-01 ns	1.83E-02	-5.32E-02	34.8
231290 - 261290	1.26E+00	-1.32E+00 ns	2.03E-02	-1.04E-02 ns	12.4
261290 - 291290	4.32E+00	-3.48E+00	-1.12E-01	-1.47E-01	46.6
291290 - 010191	3.00E+00	3.65E-01 ns	3.64E-02 ns	-1.12E-01	47.1
010191 - 040191	5.82E+00	1.35E+00 ns	8.68E-02 ns	-2.57E-01	21.9
040191 - 070191	3.71E+00	4.83E-01 ns	3.36E-01	-8.84E-02 ns	57.4
070191 - 100191	3.93E+00	7.07E+00 ns	1.91E-01	-1.22E-01 ns	16.4
100191 - 130191	2.10E+00	1.34E+00 ns	1.82E-01	-4.87E-02	79.8
130191 - 160191	3.71E+00	1.28E+00 ns	7.66E-03 ns	1.01E-02 ns	0.0
160191 - 190191	4.23E+00	-1.58E+00	-9.37E-02	-1.75E-01	44.2
190191 - 220191	1.51E+00	-7.93E-01	1.62E-01	-7.81E-02	90.9
220191 - 250191	1.50E+00	-8.47E-01 ns	5.72E-02	-2.00E-05 ns	14.4
250191 - 280191	1.33E+00	-1.62E+00	3.96E-02	4.61E-03 ns	27.9
280191 - 310191	1.74E+00	-6.02E-01	-1.75E-02 ns	-1.11E-02 ns	6.6
310191 - 030291	2.53E+00	-1.15E+00	9.67E-03 ns	-1.91E-01	38.6
030291 - 060291	1.98E+00	-2.12E+00	1.49E-01	-2.08E-01	64.3
Mean	2.261	-0.4109	0.0563	-0.0960	41.30
n = 3 m = 2					
171190 - 201190	9.82E-01	1.04E-01 ns	1.41E-03 ns	-6.70E-02	30.8
201190 - 231190	8.48E-01	8.72E-01	9.33E-04 ns	-2.36E-02	9.9
231190 - 261190	1.19E+00	-2.18E+00 ns	-2.25E-03 ns	-1.50E-01	20.3
261190 - 291190	1.95E+00	-1.03E+00	3.42E-03	3.34E-02	38.2
291190 - 021290	1.25E+00	-2.66E-01 ns	2.43E-02	-2.84E-02	25.1
021290 - 051290	1.47E+00	-1.87E-01	-2.12E-03 ns	-5.23E-02	68.9
051290 - 081290	1.97E+00	-1.57E+00	3.06E-03	-1.13E-01	30.8
081290 - 111290	2.66E+00	-8.31E-01 ns	7.32E-03	-2.95E-01	67.3
111290 - 141290	2.05E+00	-9.25E-01 ns	5.91E-03	-1.57E-01	68.9
141290 - 171290	1.95E+00	-2.10E+00	9.95E-03 ns	-1.23E-01	62.9
171290 - 201290	1.83E+00	-1.24E+00	2.04E-03	-1.17E-01	79.3
201290 - 231290	1.35E+00	-1.66E-01 ns	8.89E-04	-5.36E-02	32.5
231290 - 261290	1.40E+00	-1.47E+00	6.25E-04 ns	-9.54E-03 ns	8.9
261290 - 291290	3.65E+00	-3.42E+00	-4.55E-03	-1.47E-01	46.3
291290 - 010191	3.12E+00	3.82E-01 ns	2.30E-03	-1.12E-01	47.9
010191 - 040191	6.37E+00	1.34E+00 ns	3.29E-03 ns	-2.59E-01	22.0
040191 - 070191	5.43E+00	6.41E-01 ns	1.33E-02	-7.25E-02 ns	58.8
070191 - 100191	4.78E+00	7.58E+00 ns	9.56E-03	-1.34E-01 ns	15.4
100191 - 130191	2.56E+00	1.64E-01 ns	1.28E-02	-4.87E-02	78.9
130191 - 160191	3.69E+00	1.21E+00 ns	3.14E-03 ns	1.05E-02 ns	0.0
160191 - 190191	3.85E+00	-1.62E+00	-3.99E-03	-1.75E-01	39.0
190191 - 220191	1.73E+00	-7.28E-01	1.59E-02	-7.86E-02	86.6
220191 - 250191	1.57E+00	-8.81E-01 ns	8.55E-03	8.60E-04 ns	14.1
250191 - 280191	1.38E+00	-1.58E+00	5.41E-03	5.61E-03 ns	26.9
280191 - 310191	1.75E+00	-6.29E-01	-3.50E-03	-1.29E-02 ns	10.8
310191 - 030291	2.55E+00	-1.16E+00	-2.94E-03 ns	-1.91E-01	38.6
030291 - 060291	2.13E+00	-2.06E+00	2.10E-02	-2.07E-01	66.0
Mean	2.424	-0.4352	0.0050	-0.0954	40.56

Period	k_0	k_1	k_2	k_3	R^2 (%)
n = 3 m = 3					
171190 - 201190	1.03E+00	6.24E-02 ns	6.75E-05 ns	-6.61E-02	28.9
201190 - 231190	8.74E-01	8.62E-01	1.54E-05 ns	-2.41E-02	8.1
231190 - 261190	1.14E+00	-2.16E+00 ns	1.52E-04 ns	-1.51E-01	20.3
261190 - 291190	1.96E+00	-1.07E+00	4.30E-04	3.36E-02	37.1
291190 - 021290	1.27E+00	-2.74E-01 ns	7.65E-03	-2.79E-02	27.4
021290 - 051290	1.46E+00	-1.88E-01	2.53E-04 ns	-5.20E-02	68.6
051290 - 081290	2.05E+00	-1.64E+00	1.92E-04	-1.15E-01	29.6
081290 - 111290	2.82E+00	-6.45E-01 ns	4.37E-04	-2.87E-01	65.2
111290 - 141290	2.09E+00	-1.04E+00 ns	5.38E-04	-1.57E-01	68.3
141290 - 171290	1.97E+00	-2.10E+00	2.29E-03 ns	-1.24E-01	62.8
171290 - 201290	1.85E+00	-1.25E+00	1.51E-04	-1.17E-01	78.6
201290 - 231290	1.39E+00	-2.07E-01 ns	4.40E-05 ns	-5.40E-02	30.3
231290 - 261290	1.45E+00	-1.59E+00	1.96E-05 ns	-9.21E-03 ns	6.6
261290 - 291290	3.42E+00	-3.36E+00	2.37E-04	-1.47E-01	45.8
291290 - 010191	3.16E+00	3.95E-01 ns	1.77E-04	-1.10E-01	48.8
010191 - 040191	6.56E+00	1.32E+00 ns	1.60E-04 ns	-2.61E-01	22.1
040191 - 070191	6.09E+00	6.23E-01 ns	5.89E-04	-6.96E-02 ns	56.7
070191 - 100191	5.07E+00	7.93E+00 ns	5.80E-04	-1.46E-01 ns	14.3
100191 - 130191	2.78E+00	-1.14E+00 ns	9.24E-04	-4.84E-02 ns	72.6
130191 - 160191	3.69E+00	1.15E+00 ns	6.51E-04 ns	1.22E-02 ns	0.0
160191 - 190191	3.75E+00	-1.63E+00	1.99E-04 ns	-1.74E-01	36.7
190191 - 220191	1.80E+00	-6.60E-01	1.67E-03	-7.78E-02	80.1
220191 - 250191	1.59E+00	-8.63E-01 ns	1.33E-03	1.32E-03 ns	12.0
250191 - 280191	1.39E+00	-1.53E+00	7.66E-04	7.77E-03 ns	25.3
280191 - 310191	1.75E+00	-6.41E-01	5.31E-04	-1.33E-02 ns	13.7
310191 - 030291	2.55E+00	-1.17E+00	-1.02E-03 ns	-1.91E-01	38.7
030291 - 060291	2.17E+00	-2.07E+00	3.04E-03	-2.07E-01	66.5
Mean	2.4861	-0.4772	-0.0008	-0.0954	39.45

A.3.6 Results for LB2 surface for the winter deployment using salinity in Eq. 7.9.

Period	k_0'	k_1'	k_2'	k_3'	R^2 (%)
n = 1 m = 1					
171190 - 201190	6.79E+01	1.76E-01 ns	6.09E-02	-2.01E+00	63.4
201190 - 231190	1.25E+01	2.64E-01 ns	1.75E-02 ns	-3.53E-01	23.7
231190 - 261190	4.99E+01	-6.28E-02 ns	-4.76E-02	-1.44E+00	63.3
261190 - 291190	-7.72E+00	-1.14E-01 ns	1.08E-02 ns	2.99E-01	28.6
291190 - 021290	1.47E+01	-2.56E-01	7.24E-02	-4.14E-01	51.2
021290 - 051290	4.39E+01	-2.23E-01	-2.33E-02 ns	-1.27E+00	66.5
051290 - 081290	1.82E+02	-8.05E-01	4.73E-02	-5.40E+00	45.6
081290 - 111290	2.08E+02	-2.38E-02 ns	1.44E-01	-6.20E+00	52.2
111290 - 141290	4.69E+01	-2.34E-01 ns	1.28E-01	-1.37E+00	53.6
141290 - 171290	3.82E+01	-1.24E+00	3.69E-02 ns	-1.10E+00	53.9
171290 - 201290	6.25E+01	-3.67E-01	5.27E-02	-1.84E+00	79.6
201290 - 231290	1.01E+01 ns	-4.70E-02 ns	2.36E-02	-2.67E-01 ns	7.7
231290 - 261290	-4.99E+01	-3.46E-01 ns	9.89E-03 ns	1.54E+00	39.7
261290 - 291290	7.86E+01	-7.58E-01 ns	-1.59E-01	-2.20E+00	27.7
291290 - 010191	5.94E+01	-6.59E-02 ns	1.07E-01	-1.71E+00	43.1
010191 - 040191	1.95E+02	6.39E-01 ns	1.54E-01 ns	-5.71E+00	17.5
040191 - 070191	3.78E+01 ns	2.23E-01 ns	3.31E-01	-1.02E+00 ns	56.5
070191 - 100191	1.71E+02	1.33E+00 ns	2.02E-01	-5.01E+00	20.0
100191 - 130191	4.28E+00 ns	1.76E-01 ns	1.82E-01	-6.56E-02 ns	78.0
130191 - 160191	-6.26E+01	5.82E-01 ns	-1.11E-02 ns	1.99E+00	14.0
160191 - 190191	1.40E+02	-4.07E-01 ns	-1.62E-02 ns	-4.06E+00	69.5
190191 - 220191	7.99E+01	-7.68E-02 ns	1.86E-01	-2.33E+00	87.8
220191 - 250191	-2.98E+00 ns	-3.88E-01	5.87E-02	1.35E-01 ns	17.9
250191 - 280191	4.79E+00 ns	-6.51E-01	4.23E-02	-9.94E-02 ns	31.4
280191 - 310191	1.61E+01 ns	-4.53E-01	-1.64E-02 ns	-4.23E-01 ns	11.1
310191 - 030291	1.37E+02	-9.09E-01	3.05E-03 ns	-3.98E+00	56.1
030291 - 060291	2.41E+02	-6.40E-01	9.70E-02	-7.06E+00	81.2
Mean	65.862	-0.1732	0.0627	-1.9025	45.96
n = 1 m = 2					
171190 - 201190	6.88E+01	1.90E-01 ns	3.93E-03	-2.03E+00	60.3
201190 - 231190	1.34E+01	2.60E-01 ns	8.98E-04 ns	-3.79E-01	21.1
231190 - 261190	4.91E+01	-6.47E-02 ns	2.44E-03	-1.42E+00	61.5
261190 - 291190	-8.62E+00	-1.14E-01 ns	5.61E-04 ns	3.28E-01	28.0
291190 - 021290	1.44E+01	-2.55E-01	1.95E-02	-4.02E-01	52.2
021290 - 051290	4.40E+01	-2.28E-01	-3.07E-03 ns	-1.27E+00	66.1
051290 - 081290	1.81E+02	-8.65E-01	2.50E-03	-5.37E+00	43.9
081290 - 111290	1.89E+02	-1.48E-02 ns	7.63E-03	-5.61E+00	51.2
111290 - 141290	4.09E+01	-3.04E-01 ns	9.81E-03	-1.18E+00	46.5
141290 - 171290	3.85E+01	-1.24E+00	7.55E-03 ns	-1.10E+00	53.9
171290 - 201290	6.19E+01	-3.90E-01	3.54E-03	-1.82E+00	75.9
201290 - 231290	9.08E+00 ns	-5.66E-02 ns	1.18E-03	-2.34E-01 ns	4.4
231290 - 261290	-5.17E+01	-3.86E-01	1.79E-04 ns	1.60E+00	38.4
261290 - 291290	8.06E+01	-7.27E-01 ns	-6.62E-03	-2.29E+00	27.9
291290 - 010191	5.97E+01	-6.04E-02 ns	6.10E-03	-1.70E+00	45.4
010191 - 040191	1.99E+02	6.28E-01 ns	5.63E-03 ns	-5.80E+00	17.6
040191 - 070191	3.64E+01 ns	3.06E-01 ns	1.31E-02	-9.29E-01 ns	58.2
070191 - 100191	1.80E+02	1.45E+00 ns	1.02E-02	-5.23E+00	19.0
100191 - 130191	-2.65E+00 ns	4.99E-02 ns	1.26E-02	1.57E-01 ns	77.4
130191 - 160191	-6.16E+01	5.60E-01 ns	1.48E-03 ns	1.96E+00	14.0
160191 - 190191	1.43E+02	-3.96E-01 ns	2.20E-04 ns	-4.15E+00	69.2
190191 - 220191	7.81E+01	-4.63E-02 ns	1.82E-02	-2.27E+00	82.7
220191 - 250191	-3.97E+00 ns	-3.99E-01	8.77E-03	1.67E-01 ns	17.7
250191 - 280191	4.12E+00 ns	-6.44E-01	5.88E-03	-7.78E-02 ns	30.6
280191 - 310191	1.76E+01 ns	-4.61E-01	-3.33E-03	-4.66E-01 ns	15.0
310191 - 030291	1.37E+02	-9.11E-01	-2.39E-03 ns	-3.98E+00	56.1
030291 - 060291	2.39E+02	-6.02E-01	1.40E-02	-7.00E+00	82.0
Mean	65.039	-0.1749	0.0052	-1.8702	45.04

Period	k_0'	k_1'	k_2'	k_3'	R^2 (%)
n = 1 m = 3					
171190 - 201190	6.78E+01	1.94E-01 ns	2.84E-04	-2.00E+00	56.3
201190 - 231190	1.37E+01	2.55E-01 ns	3.48E-05 ns	-3.87E-01	19.7
231190 - 261190	4.87E+01	-6.11E-02 ns	1.49E-04	-1.42E+00	60.4
261190 - 291190	-9.62E+00	-1.09E-01 ns	2.67E-05 ns	3.59E-01	27.9
291190 - 021290	1.41E+01	-2.57E-01	5.68E-03	-3.92E-01	52.3
021290 - 051290	4.38E+01	-2.29E-01	4.25E-04 ns	-1.27E+00	65.7
051290 - 081290	1.82E+02	-9.08E-01	1.43E-04 ns	-5.39E+00	42.4
081290 - 111290	1.79E+02	1.52E-02 ns	4.51E-04	-5.29E+00	48.5
111290 - 141290	3.53E+01	-3.87E-01 ns	8.16E-04	-1.01E+00	41.7
141290 - 171290	3.87E+01	-1.24E+00	1.88E-03 ns	-1.11E+00	53.9
171290 - 201290	6.11E+01	-4.07E-01	2.50E-04	-1.80E+00	73.4
201290 - 231290	8.04E+00 ns	-6.97E-02 ns	6.41E-05 ns	-2.01E-01 ns	1.5
231290 - 261290	-5.33E+01	-4.18E-01	2.67E-06 ns	1.65E+00	38.2
261290 - 291290	8.23E+01	-6.96E-01 ns	3.51E-04	-2.34E+00	27.6
291290 - 010191	5.91E+01	-5.66E-02 ns	4.30E-04	-1.68E+00	47.0
010191 - 040191	2.02E+02	6.13E-01 ns	2.65E-04 ns	-5.89E+00	17.6
040191 - 070191	4.39E+01 ns	3.40E-01 ns	5.82E-04	-1.13E+00 ns	56.3
070191 - 100191	1.87E+02	1.53E+00 ns	6.22E-04	-5.44E+00	17.8
100191 - 130191	-2.14E+01 ns	-6.51E-02 ns	8.31E-04	7.26E-01 ns	72.4
130191 - 160191	-6.13E+01	5.30E-01 ns	4.99E-04 ns	1.95E+00	14.6
160191 - 190191	1.44E+02	-3.96E-01 ns	5.68E-05 ns	-4.18E+00	69.4
190191 - 220191	7.18E+01	-3.93E-02 ns	1.90E-03	-2.08E+00	74.9
220191 - 250191	-4.69E+00 ns	-3.97E-01	1.37E-03	1.88E-01 ns	15.7
250191 - 280191	2.01E+00 ns	-6.31E-01	8.35E-04	-1.50E-02 ns	28.9
280191 - 310191	1.81E+01 ns	-4.64E-01	5.08E-04	-4.81E-01 ns	17.8
310191 - 030291	1.37E+02	-9.13E-01	-6.39E-04 ns	-3.97E+00	56.1
030291 - 060291	2.39E+02	-5.88E-01	2.04E-03	-6.99E+00	82.2
Mean	64.01	-0.1798	0.0007	-1.8368	43.71
n = 2 m = 1					
171190 - 201190	6.78E+01	2.29E-01 ns	6.12E-02	-2.01E+00	63.3
201190 - 231190	1.24E+01	4.26E-01 ns	1.75E-02	-3.47E-01	24.6
231190 - 261190	4.98E+01	-3.80E-01 ns	-4.76E-02	-1.44E+00	63.4
261190 - 291190	-7.22E+00	-3.18E-01 ns	1.06E-02 ns	2.84E-01	30.3
291190 - 021290	1.48E+01	-3.14E-01	7.48E-02	-4.17E-01	52.2
021290 - 051290	4.42E+01	-2.59E-01	-2.32E-02 ns	-1.28E+00	67.7
051290 - 081290	1.84E+02	-1.15E+00	4.38E-02	-5.45E+00	46.7
081290 - 111290	2.09E+02	1.33E-01 ns	1.44E-01	-6.21E+00	52.2
111290 - 141290	4.69E+01	-2.62E-01 ns	1.29E-01	-1.37E+00	53.4
141290 - 171290	3.84E+01	-1.58E+00	4.21E-02 ns	-1.11E+00	52.4
171290 - 201290	6.28E+01	-4.54E-01	5.31E-02	-1.85E+00	79.4
201290 - 231290	1.00E+01 ns	-7.43E-02 ns	2.35E-02	-2.66E-01 ns	7.7
231290 - 261290	-5.01E+01	-7.52E-01	8.54E-03 ns	1.54E+00	41.8
261290 - 291290	7.69E+01	-1.30E+00 ns	-1.59E-01	-2.15E+00	27.8
291290 - 010191	5.92E+01	-6.90E-03 ns	1.07E-01	-1.70E+00	43.0
010191 - 040191	1.96E+02	6.33E-01 ns	1.54E-01 ns	-5.72E+00	17.3
040191 - 070191	3.79E+01 ns	3.90E-01 ns	3.31E-01	-1.02E+00 ns	56.5
070191 - 100191	1.71E+02	2.50E+00 ns	2.03E-01	-4.99E+00	19.9
100191 - 130191	3.72E+00 ns	5.08E-01 ns	1.83E-01	-4.90E-02 ns	78.1
130191 - 160191	-6.23E+01	7.74E-01 ns	-1.28E-02 ns	1.98E+00	13.7
160191 - 190191	1.40E+02	-6.48E-01 ns	-1.53E-02 ns	-4.05E+00	70.2
190191 - 220191	7.89E+01	-1.56E-01 ns	1.86E-01	-2.30E+00	87.9
220191 - 250191	-1.05E+00 ns	-5.49E-01	5.81E-02	7.66E-02 ns	15.9
250191 - 280191	4.69E+00 ns	-1.01E+00	4.45E-02	-9.89E-02 ns	30.5
280191 - 310191	1.68E+01 ns	-5.08E-01	-1.70E-02 ns	-4.46E-01 ns	9.8
310191 - 030291	1.35E+02	-1.06E+00	4.94E-03 ns	-3.91E+00	54.8
030291 - 060291	2.42E+02	-7.67E-01	1.01E-01	-7.10E+00	80.4
Mean	65.983	-0.2206	0.0632	-1.9038	45.96

Period	k_0'	k_1'	k_2'	k_3'	R^2 (%)
n = 2 m = 2					
171190 - 201190	6.88E+01	2.50E-01 ns	3.96E-03	-2.03E+00	60.3
201190 - 231190	1.33E+01	4.21E-01 ns	9.01E-04 ns	-3.73E-01	22.0
231190 - 261190	4.90E+01	-3.77E-01 ns	2.44E-03	-1.42E+00	61.6
261190 - 291190	-8.00E+00	-3.22E-01 ns	6.18E-04 ns	3.09E-01	29.7
291190 - 021290	1.45E+01	-3.11E-01	2.00E-02	-4.05E-01	53.2
021290 - 051290	4.43E+01	-2.64E-01	-3.09E-03 ns	-1.28E+00	67.3
051290 - 081290	1.83E+02	-1.23E+00	2.28E-03	-5.43E+00	45.2
081290 - 111290	1.90E+02	1.71E-01 ns	7.62E-03	-5.63E+00	51.2
111290 - 141290	4.09E+01	-3.90E-01 ns	9.87E-03	-1.18E+00	46.2
141290 - 171290	3.87E+01	-1.58E+00	8.21E-03 ns	-1.12E+00	52.3
171290 - 201290	6.21E+01	-4.86E-01	3.59E-03	-1.83E+00	75.7
201290 - 231290	9.03E+00 ns	-8.91E-02 ns	1.17E-03	-2.33E-01 ns	4.5
231290 - 261290	-5.19E+01	-8.20E-01	1.24E-04 ns	1.60E+00	40.8
261290 - 291290	7.90E+01	-1.24E+00 ns	-6.62E-03	-2.24E+00	28.0
291290 - 010191	5.95E+01	2.80E-03 ns	6.12E-03	-1.70E+00	45.3
010191 - 040191	2.00E+02	6.10E-01 ns	5.65E-03 ns	-5.82E+00	17.4
040191 - 070191	3.66E+01 ns	4.99E-01 ns	1.31E-02	-9.32E-01 ns	58.2
070191 - 100191	1.79E+02	2.73E+00 ns	1.03E-02	-5.22E+00	18.8
100191 - 130191	-2.82E+00 ns	1.28E-01 ns	1.26E-02	1.62E-01 ns	77.4
130191 - 160191	-6.13E+01	7.31E-01 ns	1.41E-03 ns	1.95E+00	13.6
160191 - 190191	1.43E+02	-6.46E-01 ns	2.66E-04 ns	-4.13E+00	70.0
190191 - 220191	7.71E+01	-1.16E-01 ns	1.82E-02	-2.24E+00	82.8
220191 - 250191	-2.01E+00 ns	-5.70E-01	8.67E-03	1.07E-01 ns	15.6
250191 - 280191	3.88E+00 ns	-9.99E-01	6.12E-03	-7.31E-02 ns	29.4
280191 - 310191	1.83E+01 ns	-5.24E-01	-3.44E-03	-4.89E-01 ns	13.9
310191 - 030291	1.35E+02	-1.07E+00	-2.34E-03 ns	-3.91E+00	54.8
030291 - 060291	2.40E+02	-7.24E-01	1.47E-02	-7.03E+00	81.2
Mean	65.147	-0.2302	0.00528	-1.8736	45.05
n = 2 m = 3					
171190 - 201190	6.77E+01	2.49E-01 ns	2.85E-04	-2.00E+00	56.2
201190 - 231190	1.36E+01	4.14E-01 ns	3.48E-05 ns	-3.81E-01	20.5
231190 - 261190	4.87E+01	-3.71E-01 ns	1.48E-04	-1.41E+00	60.5
261190 - 291190	-8.89E+00	-3.17E-01 ns	8.20E-06 ns	3.37E-01	29.6
291190 - 021290	1.42E+01	-3.12E-01	5.80E-03	-3.95E-01	53.2
021290 - 051290	4.41E+01	-2.66E-01	4.34E-04 ns	-1.28E+00	66.9
051290 - 081290	1.84E+02	-1.30E+00	1.27E-04 ns	-5.46E+00	43.9
081290 - 111290	1.79E+02	2.33E-01 ns	4.50E-04	-5.31E+00	48.6
111290 - 141290	3.52E+01	-5.53E-01 ns	8.19E-04	-1.01E+00	41.4
141290 - 171290	3.88E+01	-1.58E+00	1.94E-03 ns	-1.12E+00	52.3
171290 - 201290	6.14E+01	-5.09E-01	2.55E-04	-1.81E+00	73.3
201290 - 231290	7.99E+00 ns	-1.11E-01 ns	6.32E-05 ns	-2.00E-01 ns	1.6
231290 - 261290	-5.34E+01	-8.74E-01	5.19E-06 ns	1.65E+00	40.7
261290 - 291290	8.07E+01	-1.19E+00 ns	3.50E-04	-2.30E+00	27.7
291290 - 010191	5.88E+01	9.20E-03 ns	4.31E-04	-1.67E+00	47.0
010191 - 040191	2.03E+02	5.84E-01 ns	2.66E-04 ns	-5.91E+00	17.4
040191 - 070191	4.41E+01 ns	5.10E-01 ns	5.83E-04	-1.14E+00 ns	56.3
070191 - 100191	1.86E+02	2.88E+00 ns	6.25E-04	-5.42E+00	17.6
100191 - 130191	-2.10E+01 ns	-1.72E-01 ns	8.30E-04	7.17E-01 ns	72.4
130191 - 160191	-6.11E+01	6.84E-01 ns	5.02E-04 ns	1.94E+00	14.2
160191 - 190191	1.44E+02	-6.50E-01 ns	6.00E-05 ns	-4.16E+00	70.2
190191 - 220191	7.10E+01	-9.99E-02 ns	1.90E-03	-2.05E+00	74.9
220191 - 250191	-2.71E+00 ns	-5.64E-01	1.35E-03	1.28E-01 ns	13.6
250191 - 280191	1.60E+00 ns	-9.70E-01	8.59E-04	-5.00E-03 ns	27.5
280191 - 310191	1.88E+01 ns	-5.31E-01	5.25E-04	-5.04E-01 ns	16.9
310191 - 030291	1.35E+02	-1.07E+00	-6.88E-04 ns	-3.91E+00	54.8
030291 - 060291	2.39E+02	-7.13E-01	2.14E-03	-7.01E+00	81.6
Mean	64.059	-0.2441	0.0007	-1.8401	43.73

Period	k_0'	k_1'	k_2'	k_3'	R^2 (%)
n = 3 m = 1					
171190 - 201190	6.78E+01	3.22E-01 ns	6.14E-02	-2.01E+00	63.2
201190 - 231190	1.22E+01	7.23E-01	1.75E-02	-3.43E-01	25.0
231190 - 261190	4.97E+01	-1.18E+00 ns	-4.75E-02	-1.44E+00	63.5
261190 - 291190	-6.95E+00	-7.16E-01	1.01E-02 ns	2.76E-01	32.1
291190 - 021290	1.48E+01	-4.01E-01	7.53E-02	-4.17E-01	52.3
021290 - 051290	4.43E+01	-3.17E-01	-2.28E-02 ns	-1.28E+00	68.3
051290 - 081290	1.85E+02	-1.57E+00	4.30E-02	-5.49E+00	46.7
081290 - 111290	2.09E+02	3.12E-01 ns	1.44E-01	-6.22E+00	52.2
111290 - 141290	4.70E+01	-2.27E-01 ns	1.31E-01	-1.38E+00	53.3
141290 - 171290	3.82E+01	-2.18E+00	4.47E-02 ns	-1.11E+00	49.5
171290 - 201290	6.31E+01	-6.14E-01	5.36E-02	-1.86E+00	79.1
201290 - 231290	1.00E+01 ns	-1.33E-01 ns	2.34E-02	-2.66E-01 ns	7.8
231290 - 261290	-5.01E+01	-1.56E+00	7.78E-03 ns	1.54E+00	43.4
261290 - 291290	7.70E+01	-2.33E+00 ns	-1.59E-01	-2.15E+00	27.7
291290 - 010191	5.89E+01	7.77E-02 ns	1.08E-01	-1.69E+00	43.0
010191 - 040191	1.96E+02	7.39E-01 ns	1.55E-01 ns	-5.74E+00	17.3
040191 - 070191	3.79E+01 ns	4.79E-01 ns	3.32E-01	-1.02E+00 ns	56.5
070191 - 100191	1.72E+02	4.99E+00 ns	2.05E-01	-5.02E+00	19.7
100191 - 130191	3.21E+00 ns	1.44E+00 ns	1.85E-01	-3.41E-02 ns	78.3
130191 - 160191	-6.23E+01	1.06E+00 ns	-1.32E-02 ns	1.98E+00	13.2
160191 - 190191	1.40E+02	-9.49E-01	-1.43E-02 ns	-4.04E+00	70.7
190191 - 220191	7.84E+01	-2.82E-01 ns	1.86E-01	-2.28E+00	88.0
220191 - 250191	-2.00E-01 ns	-8.54E-01 ns	5.72E-02	5.07E-02 ns	14.5
250191 - 280191	4.25E+00 ns	-1.65E+00	4.53E-02	-8.71E-02 ns	27.8
280191 - 310191	1.76E+01 ns	-5.76E-01	-1.73E-02 ns	-4.69E-01 ns	8.0
310191 - 030291	1.34E+02	-1.26E+00	4.87E-03 ns	-3.89E+00	53.9
030291 - 060291	2.45E+02	-8.80E-01 ns	1.05E-01	-7.18E+00	79.7
Mean	66.141	-0.2791	0.0637	-1.9100	45.73
n = 3 m = 2					
171190 - 201190	6.87E+01	3.54E-01 ns	3.97E-03	-2.03E+00	60.2
201190 - 231190	1.32E+01	7.15E-01 ns	9.00E-04 ns	-3.69E-01	22.4
231190 - 261190	4.89E+01	-1.17E+00 ns	2.43E-03	-1.42E+00	61.7
261190 - 291190	-7.64E+00	-7.27E-01	6.18E-04 ns	2.98E-01	31.6
291190 - 021290	1.44E+01	-3.97E-01	2.01E-02	-4.05E-01	53.3
021290 - 051290	4.45E+01	-3.23E-01	-3.03E-03 ns	-1.29E+00	67.9
051290 - 081290	1.84E+02	-1.68E+00	2.22E-03	-5.48E+00	45.2
081290 - 111290	1.90E+02	4.08E-01 ns	7.62E-03	-5.64E+00	51.2
111290 - 141290	4.09E+01	-4.86E-01 ns	9.98E-03	-1.18E+00	46.0
141290 - 171290	3.85E+01	-2.18E+00	8.45E-03 ns	-1.11E+00	49.4
171290 - 201290	6.25E+01	-6.64E-01	3.64E-03	-1.84E+00	75.5
201290 - 231290	9.00E+00 ns	-1.59E-01 ns	1.16E-03	-2.32E-01 ns	4.5
231290 - 261290	-5.18E+01	-1.68E+00	9.65E-05 ns	1.60E+00	42.6
261290 - 291290	7.92E+01	-2.20E+00 ns	-6.62E-03	-2.25E+00	27.8
291290 - 010191	5.92E+01	9.47E-02 ns	6.14E-03	-1.69E+00	45.4
010191 - 040191	2.00E+02	7.02E-01 ns	5.67E-03 ns	-5.83E+00	17.4
040191 - 070191	3.65E+01 ns	6.37E-01 ns	1.31E-02	-9.30E-01 ns	58.2
070191 - 100191	1.80E+02	5.47E+00 ns	1.03E-02	-5.25E+00	18.6
100191 - 130191	-3.08E+00 ns	3.84E-01 ns	1.26E-02	1.69E-01 ns	77.4
130191 - 160191	-6.12E+01	9.82E-01 ns	1.44E-03 ns	1.95E+00	13.2
160191 - 190191	1.42E+02	-9.57E-01	3.17E-04 ns	-4.12E+00	70.5
190191 - 220191	7.66E+01	-2.22E-01 ns	1.82E-02	-2.22E+00	82.9
220191 - 250191	-1.12E+00 ns	-8.92E-01 ns	8.54E-03	7.99E-02 ns	14.2
250191 - 280191	3.35E+00 ns	-1.62E+00	6.19E-03	-5.86E-02 ns	26.6
280191 - 310191	1.90E+01 ns	-6.02E-01	-3.49E-03	-5.12E-01 ns	12.2
310191 - 030291	1.34E+02	-1.26E+00	-2.23E-03 ns	-3.89E+00	53.9
030291 - 060291	2.42E+02	-8.28E-01 ns	1.51E-02	-7.09E+00	80.7
Mean	65.245	-0.3074	0.0053	-1.8792	44.83

Period	k_0'	k_1'	k_2'	k_3'	R^2 (%)
n = 3 m = 3					
171190 - 201190	6.77E+01	3.43E-01 ns	2.85E-04	-2.00E+00	56.0
201190 - 231190	1.34E+01	7.06E-01 ns	3.48E-05 ns	-3.77E-01	21.0
231190 - 261190	4.86E+01	-1.17E+00 ns	1.48E-04	-1.41E+00	60.7
261190 - 291190	-8.44E+00	-7.22E-01	2.00E-07 ns	3.23E-01	31.4
291190 - 021290	1.41E+01	-3.97E-01	5.81E-03	-3.94E-01	53.3
021290 - 051290	4.42E+01	-3.25E-01	4.25E-04 ns	-1.28E+00	67.5
051290 - 081290	1.86E+02	-1.78E+00	1.24E-04 ns	-5.51E+00	44.0
081290 - 111290	1.79E+02	5.30E-01 ns	4.50E-04	-5.32E+00	48.6
111290 - 141290	3.52E+01	-8.17E-01 ns	8.27E-04	-1.01E+00	41.1
141290 - 171290	3.87E+01	-2.18E+00	1.94E-03 ns	-1.12E+00	49.4
171290 - 201290	6.17E+01	-6.97E-01	2.60E-04	-1.82E+00	73.0
201290 - 231290	7.95E+00 ns	-1.98E-01 ns	6.23E-05 ns	-1.99E-01 ns	1.7
231290 - 261290	-5.33E+01	-1.78E+00	6.36E-06 ns	1.64E+00	42.6
261290 - 291290	8.10E+01	-2.08E+00 ns	3.50E-04	-2.31E+00	27.5
291290 - 010191	5.85E+01	1.05E-01 ns	4.33E-04	-1.67E+00	47.0
010191 - 040191	2.04E+02	6.62E-01 ns	2.66E-04 ns	-5.92E+00	17.4
040191 - 070191	4.41E+01 ns	6.15E-01 ns	5.84E-04	-1.14E+00 ns	56.3
070191 - 100191	1.88E+02	5.79E+00 ns	6.31E-04	-5.46E+00	17.4
100191 - 130191	-2.09E+01 ns	-3.73E-01 ns	8.30E-04	7.13E-01 ns	72.4
130191 - 160191	-6.10E+01	9.06E-01 ns	5.15E-04 ns	1.94E+00	13.8
160191 - 190191	1.43E+02	-9.67E-01	6.34E-05 ns	-4.15E+00	70.7
190191 - 220191	7.05E+01	-1.90E-01 ns	1.90E-03	-2.04E+00	75.0
220191 - 250191	-1.80E+00 ns	-8.77E-01 ns	1.32E-03	1.01E-01 ns	12.1
250191 - 280191	9.98E-01 ns	-1.56E+00	8.62E-04	1.17E-02 ns	24.5
280191 - 310191	1.95E+01 ns	-6.14E-01	5.32E-04	-5.26E-01 ns	15.2
310191 - 030291	1.34E+02	-1.26E+00	-6.52E-04 ns	-3.89E+00	53.9
030291 - 060291	2.42E+02	-8.23E-01 ns	2.21E-03	-7.07E+00	81.0
Mean	64.323	-0.3390	0.0007	-1.8477	43.50

A.3.7 Results for LB3 32 mab for the summer deployment using displacement in Eq. 7.8.

Period	k_0	k_1	k_2	k_3	R^2 (%)
n = 1 m = 1					
140690 - 170690	5.82E-01	4.54E-02	8.88E-03	3.35E-03	40.8
170690 - 200690	5.41E-01	-2.42E-02 ns	2.12E-02	5.81E-03	29.6
200690 - 230690	8.36E-01	-8.99E-02	3.98E-03 ns	1.67E-02	73.2
230690 - 260690	9.60E-01	-1.09E-01	6.03E-03	1.68E-02	58.4
260690 - 290690	1.06E+00	-1.69E-01	-3.91E-03 ns	-2.28E-03 ns	36.8
290690 - 020790	9.32E-01	1.86E-02 ns	1.01E-03 ns	-1.96E-02	47.9
020790 - 050790	9.40E-01	4.22E-02 ns	-8.58E-03	-4.47E-03 ns	38.0
050790 - 080790	8.18E-01	-4.02E-02	3.44E-03 ns	2.89E-04 ns	4.2
080790 - 110790	8.79E-01	6.72E-03 ns	-1.05E-02	-1.06E-02	40.0
110790 - 140790	8.51E-01	-5.02E-02	-1.52E-03 ns	-8.66E-03	40.2
140790 - 170790	8.09E-01	7.36E-02 ns	5.13E-03 ns	-2.14E-02	24.5
170790 - 200790	7.27E-01	-3.56E-02 ns	1.95E-02	-8.70E-05 ns	20.2
200790 - 230790	8.34E-01	-3.01E-03 ns	-1.75E-03 ns	1.80E-03 ns	0.0
230790 - 260790	9.84E-01	-8.02E-02	-2.13E-03 ns	-2.16E-03 ns	24.9
Mean	0.840	-0.0296	0.0029	-0.0018	34.19
n = 1 m = 2					
140690 - 170690	5.92E-01	4.49E-02	1.57E-03	3.37E-03	38.1
170690 - 200690	6.10E-01	-2.68E-02 ns	1.56E-03	5.86E-03	30.0
200690 - 230690	8.50E-01	-9.04E-02	2.04E-04 ns	1.65E-02	72.5
230690 - 260690	9.72E-01	-1.10E-01	4.91E-04	1.67E-02	58.7
260690 - 290690	1.05E+00	-1.69E-01	3.83E-04 ns	-2.27E-03 ns	36.5
290690 - 020790	9.31E-01	2.02E-02 ns	2.20E-04 ns	-1.95E-02	48.2
020790 - 050790	9.19E-01	4.22E-02 ns	5.99E-04	-2.98E-03 ns	36.9
050790 - 080790	8.28E-01	-3.98E-02	2.73E-04 ns	1.73E-04 ns	4.7
080790 - 110790	8.47E-01	7.58E-03 ns	8.39E-04	-1.06E-02	40.6
110790 - 140790	8.51E-01	-4.98E-02	3.22E-04 ns	-8.58E-03	40.6
140790 - 170790	8.15E-01	7.36E-02 ns	6.64E-04 ns	-2.13E-02	24.4
170790 - 200790	7.49E-01	-3.49E-02 ns	3.73E-03	8.70E-05 ns	18.7
200790 - 230790	8.30E-01	-3.15E-03 ns	1.36E-04 ns	1.78E-03 ns	0.0
230790 - 260790	9.82E-01	-8.00E-02	-3.65E-04 ns	-2.21E-03 ns	24.9
Mean	0.8447	-0.0297	0.0008	-0.0016	33.91
n = 1 m = 3					
140690 - 170690	5.96E-01	4.54E-02	2.97E-04	3.41E-03	34.5
170690 - 200690	6.34E-01	-2.89E-02 ns	1.45E-04	5.89E-03	29.8
200690 - 230690	8.54E-01	-9.09E-02	7.20E-07 ns	1.65E-02	72.4
230690 - 260690	9.78E-01	-1.10E-01	3.87E-05	1.65E-02	58.3
260690 - 290690	1.05E+00	-1.69E-01	4.53E-05 ns	-2.24E-03 ns	36.4
290690 - 020790	9.32E-01	2.01E-02 ns	2.98E-05 ns	-1.95E-02	48.5
020790 - 050790	9.08E-01	4.04E-02 ns	4.03E-05	-2.60E-03 ns	29.5
050790 - 080790	8.31E-01	-3.94E-02	2.73E-05 ns	5.70E-05 ns	5.1
080790 - 110790	8.36E-01	8.55E-03 ns	8.36E-05	-1.06E-02	41.0
110790 - 140790	8.50E-01	-4.94E-02	5.43E-05 ns	-8.52E-03	40.8
140790 - 170790	8.17E-01	7.35E-02 ns	5.80E-05 ns	-2.11E-02	24.4
170790 - 200790	7.58E-01	-3.39E-02 ns	8.13E-04	2.06E-04 ns	16.3
200790 - 230790	8.29E-01	-3.16E-03 ns	1.30E-05 ns	1.79E-03 ns	0.0
230790 - 260790	9.80E-01	-7.95E-02	6.41E-05 ns	-2.22E-03 ns	24.8
Mean	0.8466	-0.0297	0.0001	-0.0016	32.99
n = 2 m = 1					
140690 - 170690	5.90E-01	5.63E-02	8.78E-03	3.33E-03	38.8
170690 - 200690	5.39E-01	-4.84E-02 ns	2.15E-02	5.77E-03	30.3
200690 - 230690	8.20E-01	-9.43E-02	4.12E-03 ns	1.66E-02	73.4
230690 - 260690	9.42E-01	-1.13E-01	6.07E-03	1.66E-02	59.7
260690 - 290690	1.03E+00	-1.84E-01	-4.71E-03 ns	-2.48E-03 ns	38.7
290690 - 020790	9.36E-01	1.78E-02 ns	9.43E-04 ns	-1.96E-02	47.8
020790 - 050790	9.47E-01	5.69E-02 ns	-8.62E-03	-4.39E-03 ns	37.5
050790 - 080790	8.13E-01	-6.12E-02	3.64E-03 ns	2.68E-04 ns	7.0
080790 - 110790	8.81E-01	4.51E-03 ns	-1.06E-02	-1.06E-02	39.9
110790 - 140790	8.42E-01	-4.88E-02	-1.61E-03 ns	-8.66E-03	39.1
140790 - 170790	8.26E-01	6.15E-02 ns	4.98E-03 ns	-2.14E-02	23.7
170790 - 200790	7.23E-01	-4.65E-02 ns	1.93E-02	-9.30E-05 ns	20.9
200790 - 230790	8.35E-01	-6.28E-03 ns	-1.81E-03 ns	1.80E-03 ns	0.0
230790 - 260790	9.74E-01	-7.87E-02	-3.18E-03 ns	-2.18E-03 ns	29.7
Mean	0.8356	-0.0346	0.0028	-0.0018	34.75

Period	k_0	k_1	k_2	k_3	R^2 (%)
n = 2 m = 2					
140690 - 170690	6.00E-01	5.57E-02	1.55E-03	3.36E-03	36.1
170690 - 200690	6.08E-01	-5.19E-02 ns	1.59E-03	5.81E-03	30.8
200690 - 230690	8.34E-01	-9.45E-02	2.07E-04 ns	1.64E-02	72.6
230690 - 260690	9.54E-01	-1.14E-01	4.93E-04	1.65E-02	60.0
260690 - 290690	1.02E+00	-1.83E-01	4.50E-04 ns	-2.47E-03 ns	38.3
290690 - 020790	9.35E-01	2.09E-02 ns	2.16E-04 ns	-1.95E-02	48.1
020790 - 050790	9.25E-01	5.49E-02 ns	6.01E-04	-2.90E-03 ns	36.4
050790 - 080790	8.23E-01	-6.08E-02	2.89E-04 ns	1.46E-04 ns	7.5
080790 - 110790	8.49E-01	5.35E-03 ns	8.42E-04	-1.06E-02	40.5
110790 - 140790	8.41E-01	-4.84E-02	3.35E-04 ns	-8.57E-03	39.6
140790 - 170790	8.32E-01	6.16E-02 ns	6.00E-04 ns	-2.12E-02	23.6
170790 - 200790	7.45E-01	-4.56E-02 ns	3.69E-03	7.80E-05 ns	19.4
200790 - 230790	8.31E-01	-6.16E-03 ns	1.44E-04 ns	1.78E-03 ns	0.0
230790 - 260790	9.70E-01	-7.85E-02	-5.76E-04 ns	-2.26E-03 ns	29.6
Mean	0.8405	-0.0346	0.0007	-0.0017	34.46
n = 2 m = 3					
140690 - 170690	6.04E-01	5.66E-02	2.93E-04	3.40E-03	32.6
170690 - 200690	6.32E-01	-5.45E-02 ns	1.48E-04	5.85E-03	30.6
200690 - 230690	8.38E-01	-9.51E-02	4.10E-07 ns	1.64E-02	72.5
230690 - 260690	9.60E-01	-1.14E-01	3.88E-05	1.63E-02	59.5
260690 - 290690	1.02E+00	-1.83E-01	5.27E-05 ns	-2.42E-03 ns	38.1
290690 - 020790	9.36E-01	2.11E-02 ns	2.96E-05 ns	-1.95E-02	48.3
020790 - 050790	9.14E-01	4.81E-02 ns	4.04E-05	-2.52E-03 ns	28.9
050790 - 080790	8.27E-01	-6.05E-02	2.88E-05 ns	2.60E-05 ns	7.9
080790 - 110790	8.38E-01	6.31E-03 ns	8.37E-05	-1.06E-02	40.9
110790 - 140790	8.40E-01	-4.80E-02	5.65E-05 ns	-8.51E-03	39.8
140790 - 170790	8.34E-01	6.14E-02 ns	3.30E-05 ns	-2.11E-02	23.6
170790 - 200790	7.53E-01	-4.46E-02 ns	8.03E-04	1.94E-04 ns	17.0
200790 - 230790	8.30E-01	-6.09E-03 ns	1.44E-05 ns	1.78E-03 ns	0.0
230790 - 260790	9.68E-01	-7.80E-02	1.12E-04 ns	-2.30E-03 ns	29.5
Mean	0.8424	-0.0350	0.0001	-0.0016	33.51
n = 3 m = 1					
140690 - 170690	5.92E-01	7.78E-02	8.75E-03	3.32E-03	37.3
170690 - 200690	5.36E-01	-8.48E-02 ns	2.18E-02	5.74E-03	30.9
200690 - 230690	8.12E-01	-1.03E-01	4.36E-03 ns	1.66E-02	72.5
230690 - 260690	9.33E-01	-1.24E-01	6.14E-03	1.65E-02	59.8
260690 - 290690	1.02E+00	-2.02E-01	-4.97E-03 ns	-2.47E-03 ns	35.4
290690 - 020790	9.37E-01	3.02E-02 ns	9.56E-04 ns	-1.96E-02	47.8
020790 - 050790	9.49E-01	7.56E-02 ns	-8.63E-03	-4.36E-03 ns	37.1
050790 - 080790	8.10E-01	-9.23E-02	3.84E-03 ns	2.36E-04 ns	8.8
080790 - 110790	8.82E-01	2.45E-03 ns	-1.06E-02	-1.06E-02	39.9
110790 - 140790	8.38E-01	-5.07E-02	-1.70E-03 ns	-8.66E-03	38.0
140790 - 170790	8.33E-01	5.00E-02 ns	4.90E-03 ns	-2.14E-02	23.2
170790 - 200790	7.21E-01	-6.44E-02 ns	1.91E-02	-9.50E-05 ns	21.2
200790 - 230790	8.35E-01	-8.03E-03 ns	-1.87E-03 ns	1.79E-03 ns	0.0
230790 - 260790	9.68E-01	-7.90E-02	-3.60E-03 ns	-2.20E-03 ns	30.2
Mean	0.8333	-0.0409	0.0027	-0.0018	34.44
n = 3 m = 2					
140690 - 170690	6.03E-01	7.69E-02	1.54E-03	3.35E-03	34.6
170690 - 200690	6.06E-01	-9.00E-02 ns	1.61E-03	5.78E-03	31.4
200690 - 230690	8.26E-01	-1.03E-01	2.28E-04 ns	1.64E-02	71.7
230690 - 260690	9.46E-01	-1.24E-01	4.97E-04	1.64E-02	60.1
260690 - 290690	1.01E+00	-2.00E-01	4.56E-04 ns	-2.47E-03 ns	34.8
290690 - 020790	9.35E-01	3.60E-02 ns	2.19E-04 ns	-1.95E-02	48.1
020790 - 050790	9.28E-01	6.83E-02 ns	6.01E-04	-2.87E-03 ns	36.0
050790 - 080790	8.21E-01	-9.22E-02	3.05E-04 ns	1.08E-04 ns	9.4
080790 - 110790	8.50E-01	3.34E-03 ns	8.45E-04	-1.06E-02	40.5
110790 - 140790	8.37E-01	-5.04E-02	3.49E-04 ns	-8.57E-03	38.5
140790 - 170790	8.39E-01	5.01E-02 ns	5.57E-04 ns	-2.12E-02	23.1
170790 - 200790	7.43E-01	-6.30E-02 ns	3.66E-03	7.40E-05 ns	19.7
200790 - 230790	8.31E-01	-7.69E-03 ns	1.52E-04 ns	1.77E-03 ns	0.0
230790 - 260790	9.64E-01	-7.88E-02	-6.53E-04 ns	-2.29E-03 ns	30.0
Mean	0.8385	-0.0410	0.0007	-0.0017	34.14

Period	k_0	k_1	k_2	k_3	R^2 (%)
n = 3 m = 3					
140690 - 170690	6.07E-01	7.89E-02	2.92E-04	3.39E-03	31.1
170690 - 200690	6.30E-01	-9.36E-02 ns	1.50E-04	5.82E-03	31.3
200690 - 230690	8.31E-01	-1.04E-01	1.25E-06 ns	1.64E-02	71.5
230690 - 260690	9.51E-01	-1.24E-01	3.91E-05	1.62E-02	59.6
260690 - 290690	1.00E+00	-1.99E-01	5.21E-05 ns	-2.43E-03 ns	34.5
290690 - 020790	9.36E-01	3.66E-02 ns	2.99E-05 ns	-1.95E-02	48.3
020790 - 050790	9.17E-01	4.80E-02 ns	4.04E-05	-2.49E-03 ns	28.5
050790 - 080790	8.25E-01	-9.20E-02	3.05E-05 ns	-2.00E-05 ns	9.9
080790 - 110790	8.39E-01	4.37E-03 ns	8.40E-05	-1.06E-02	40.8
110790 - 140790	8.36E-01	-4.99E-02	5.87E-05 ns	-8.50E-03	38.7
140790 - 170790	8.41E-01	4.99E-02 ns	1.40E-05 ns	-2.11E-02	23.1
170790 - 200790	7.51E-01	-6.18E-02 ns	7.95E-04	1.87E-04 ns	17.2
200790 - 230790	8.30E-01	-7.53E-03 ns	1.57E-05 ns	1.77E-03 ns	0.0
230790 - 260790	9.62E-01	-7.82E-02	1.30E-04 ns	-2.34E-03 ns	29.9
Mean	0.8397	-0.0423	0.0001	-0.0017	33.17

A.3.8 Results for LB3 32 mab for the summer deployment using salinity in Eq. 7.9.

Period	k_0'	k_1'	k_2'	k_3'	R^2 (%)
n = 1 m = 1					
140690 - 170690	-3.49E+00	4.04E-02	9.00E-03	1.22E-01	37.6
170690 - 200690	-9.94E+00	1.13E-02 ns	1.96E-02	3.13E-01	33.2
200690 - 230690	-1.54E+01	-3.12E-02 ns	7.58E-03	4.82E-01	66.6
230690 - 260690	-1.40E+01	-8.73E-02	6.25E-03	4.48E-01	64.2
260690 - 290690	3.12E+00	-1.61E-01	-3.83E-03 ns	-6.17E-02 ns	37.4
290690 - 020790	2.06E+01	1.23E-02 ns	-1.25E-03 ns	-5.89E-01	50.1
020790 - 050790	2.26E+00 ns	4.08E-02 ns	-8.45E-03	-3.96E-02 ns	35.9
050790 - 080790	-8.50E-01 ns	-3.48E-02 ns	2.23E-03 ns	5.03E-02 ns	7.9
080790 - 110790	7.92E+00	1.22E-02 ns	2.74E-03 ns	-2.15E-01	52.2
110790 - 140790	8.67E+00	-3.59E-02 ns	2.56E-04 ns	-2.37E-01	47.6
140790 - 170790	2.06E+01	1.17E-01 ns	-7.31E-03 ns	-6.00E-01	22.9
170790 - 200790	-1.12E+00 ns	-3.52E-02 ns	2.07E-02	5.57E-02 ns	24.5
200790 - 230790	-1.61E+00 ns	-3.39E-03 ns	-1.28E-03 ns	7.35E-02	6.1
230790 - 260790	2.78E+00	-6.62E-02	-2.64E-03 ns	-5.37E-02 ns	20.7
Mean	1.3957	-0.0158	0.0031	-0.0180	36.21
n = 1 m = 2					
140690 - 170690	-3.62E+00	3.96E-02	1.62E-03	1.26E-01	35.3
170690 - 200690	-9.76E+00	8.54E-03 ns	1.43E-03	3.10E-01	33.2
200690 - 230690	-1.49E+01	-3.29E-02 ns	5.90E-04 ns	4.70E-01	65.1
230690 - 260690	-1.39E+01	-8.82E-02	5.09E-04	4.45E-01	64.5
260690 - 290690	3.09E+00	-1.61E-01	3.70E-04 ns	-6.13E-02 ns	37.1
290690 - 020790	2.04E+01	1.48E-02 ns	1.07E-05 ns	-5.83E-01	49.9
020790 - 050790	1.21E+00 ns	4.11E-02 ns	6.20E-04	-8.61E-03 ns	35.8
050790 - 080790	-7.75E-01 ns	-3.47E-02 ns	1.69E-04 ns	4.83E-02 ns	8.0
080790 - 110790	7.90E+00	1.16E-02 ns	1.76E-04 ns	-2.14E-01	52.1
110790 - 140790	8.61E+00	-3.58E-02 ns	8.16E-05 ns	-2.35E-01	47.6
140790 - 170790	2.05E+01	1.16E-01 ns	-2.07E-03 ns	-5.95E-01	23.0
170790 - 200790	-1.19E+00 ns	-3.47E-02 ns	4.03E-03	5.86E-02	23.5
200790 - 230790	-1.62E+00 ns	-3.44E-03 ns	2.75E-05 ns	7.38E-02	5.9
230790 - 260790	2.80E+00	-6.62E-02	-5.82E-04 ns	-5.43E-02 ns	20.8
Mean	1.3389	-0.0161	0.0005	-0.0157	35.84
n = 1 m = 3					
140690 - 170690	-3.75E+00	3.98E-02	3.15E-04	1.30E-01	32.1
170690 - 200690	-9.68E+00	6.55E-03 ns	1.33E-04	3.08E-01	32.8
200690 - 230690	-1.47E+01	-3.43E-02 ns	4.54E-05 ns	4.62E-01	64.2
230690 - 260690	-1.37E+01	-8.85E-02	4.03E-05	4.39E-01	64.1
260690 - 290690	3.06E+00	-1.61E-01	4.31E-05 ns	-6.04E-02 ns	37.0
290690 - 020790	2.03E+01	1.57E-02 ns	9.85E-06 ns	-5.80E-01	50.0
020790 - 050790	1.31E+00 ns	3.96E-02 ns	4.16E-05	-1.21E-02 ns	28.7
050790 - 080790	-7.07E-01 ns	-3.47E-02 ns	1.63E-05 ns	4.63E-02 ns	8.0
080790 - 110790	7.88E+00	1.12E-02 ns	1.45E-05 ns	-2.13E-01	52.0
110790 - 140790	8.57E+00	-3.56E-02 ns	2.05E-05 ns	-2.34E-01	47.7
140790 - 170790	2.04E+01	1.15E-01 ns	-6.40E-04 ns	-5.92E-01	23.1
170790 - 200790	-1.24E+00 ns	-3.38E-02 ns	8.89E-04	6.02E-02	21.2
200790 - 230790	-1.64E+00 ns	-3.34E-03 ns	1.05E-05 ns	7.44E-02	6.0
230790 - 260790	2.81E+00	-6.59E-02	1.38E-04 ns	-5.49E-02 ns	20.8
Mean	1.3509	-0.0164	0.0001	-0.0162	34.84
n = 2 m = 1					
140690 - 170690	-3.47E+00	4.86E-02	8.93E-03	1.21E-01	35.6
170690 - 200690	-9.51E+00	-3.47E-03 ns	1.98E-02	3.00E-01	33.1
200690 - 230690	-1.54E+01	-2.86E-02 ns	7.64E-03	4.82E-01	66.3
230690 - 260690	-1.38E+01	-9.05E-02	6.27E-03	4.42E-01	64.9
260690 - 290690	3.00E+00	-1.75E-01	-4.62E-03 ns	-5.89E-02 ns	38.9
290690 - 020790	2.06E+01	1.23E-02 ns	-1.29E-03 ns	-5.89E-01	50.0
020790 - 050790	2.21E+00 ns	5.55E-02 ns	-8.50E-03	-3.81E-02 ns	35.4
050790 - 080790	-7.39E-01 ns	-5.41E-02	2.50E-03 ns	4.68E-02 ns	10.2
080790 - 110790	7.91E+00	7.06E-03 ns	2.61E-03 ns	-2.14E-01	52.0
110790 - 140790	8.69E+00	-3.35E-02 ns	1.97E-04 ns	-2.38E-01	46.8
140790 - 170790	2.03E+01	1.08E-01 ns	-7.68E-03 ns	-5.88E-01	21.4
170790 - 200790	-1.08E+00 ns	-4.47E-02 ns	2.05E-02	5.42E-02 ns	25.0
200790 - 230790	-1.61E+00 ns	-7.53E-03 ns	-1.34E-03 ns	7.36E-02	6.2
230790 - 260790	2.77E+00	-6.41E-02	-3.64E-03 ns	-5.38E-02 ns	22.9
Mean	1.4194	-0.0193	0.0030	-0.0186	36.34

Period	k_0'	k_1'	k_2'	k_3'	R^2 (%)
n = 2 m = 2					
140690 - 170690	-3.60E+00	4.76E-02	1.60E-03	1.25E-01	33.4
170690 - 200690	-9.33E+00	-7.14E-03 ns	1.46E-03	2.97E-01	33.2
200690 - 230690	-1.49E+01	-3.01E-02 ns	5.94E-04 ns	4.70E-01	64.8
230690 - 260690	-1.37E+01	-9.11E-02	5.10E-04	4.39E-01	65.2
260690 - 290690	2.97E+00	-1.74E-01	4.38E-04 ns	-5.85E-02 ns	38.4
290690 - 020790	2.04E+01	1.65E-02 ns	8.80E-06 ns	-5.83E-01	49.9
020790 - 050790	1.16E+00 ns	5.46E-02 ns	6.23E-04	-6.97E-03 ns	35.2
050790 - 080790	-6.49E-01 ns	-5.41E-02	1.91E-04 ns	4.44E-02 ns	10.3
080790 - 110790	7.89E+00	6.46E-03 ns	1.67E-04 ns	-2.14E-01	51.9
110790 - 140790	8.63E+00	-3.35E-02 ns	9.02E-05 ns	-2.36E-01	46.9
140790 - 170790	2.01E+01	1.07E-01 ns	-2.21E-03 ns	-5.83E-01	21.5
170790 - 200790	-1.15E+00 ns	-4.39E-02 ns	3.98E-03	5.71E-02	23.9
200790 - 230790	-1.62E+00 ns	-7.31E-03 ns	3.68E-05 ns	7.39E-02	6.1
230790 - 260790	2.80E+00	-6.41E-02	-7.90E-04 ns	-5.47E-02 ns	23.1
Mean	1.3572	-0.0195	0.0005	-0.0164	35.99
n = 2 m = 3					
140690 - 170690	-3.73E+00	4.81E-02	3.13E-04	1.29E-01	30.3
170690 - 200690	-9.24E+00	-9.61E-03 ns	1.35E-04	2.95E-01	32.8
200690 - 230690	-1.47E+01	-3.14E-02 ns	4.55E-05 ns	4.62E-01	63.9
230690 - 260690	-1.35E+01	-9.13E-02	4.03E-05	4.34E-01	64.8
260690 - 290690	2.94E+00	-1.74E-01	5.09E-05 ns	-5.75E-02 ns	38.2
290690 - 020790	2.03E+01	1.83E-02 ns	9.82E-06 ns	-5.80E-01	49.9
020790 - 050790	1.27E+00 ns	4.78E-02 ns	4.18E-05	-1.06E-02 ns	28.1
050790 - 080790	-5.69E-01 ns	-5.42E-02	1.86E-05 ns	4.20E-02 ns	10.3
080790 - 110790	7.86E+00	6.02E-03 ns	1.39E-05 ns	-2.13E-01	51.8
110790 - 140790	8.59E+00	-3.33E-02 ns	2.19E-05 ns	-2.35E-01	47.0
140790 - 170790	2.00E+01	1.05E-01 ns	-6.87E-04 ns	-5.79E-01	21.5
170790 - 200790	-1.19E+00 ns	-4.29E-02 ns	8.79E-04	5.87E-02	21.7
200790 - 230790	-1.64E+00 ns	-7.11E-03 ns	8.89E-06 ns	7.45E-02	6.1
230790 - 260790	2.82E+00	-6.38E-02	1.86E-04 ns	-5.54E-02 ns	23.1
Mean	1.3722	-0.0202	0.0001	-0.0168	34.96
n = 3 m = 1					
140690 - 170690	-3.49E+00	6.55E-02	8.92E-03	1.22E-01	34.2
170690 - 200690	-9.18E+00	-2.52E-02 ns	2.01E-02	2.90E-01	33.3
200690 - 230690	-1.55E+01	-2.51E-02 ns	7.77E-03	4.85E-01	66.0
230690 - 260690	-1.38E+01	-9.83E-02	6.33E-03	4.40E-01	64.9
260690 - 290690	3.02E+00	-1.91E-01	-4.85E-03 ns	-6.01E-02 ns	35.6
290690 - 020790	2.06E+01	2.45E-02 ns	-1.26E-03 ns	-5.89E-01	50.0
020790 - 050790	2.20E+00 ns	7.45E-02 ns	-8.52E-03	-3.76E-02 ns	35.1
050790 - 080790	-6.79E-01 ns	-8.27E-02	2.73E-03 ns	4.50E-02 ns	11.8
080790 - 110790	7.91E+00	1.42E-03 ns	2.46E-03 ns	-2.14E-01	51.9
110790 - 140790	8.72E+00	-3.38E-02 ns	1.47E-04 ns	-2.39E-01	46.2
140790 - 170790	2.00E+01	9.87E-02 ns	-8.02E-03 ns	-5.78E-01	20.2
170790 - 200790	-1.04E+00 ns	-6.08E-02 ns	2.04E-02	5.30E-02 ns	25.1
200790 - 230790	-1.62E+00 ns	-1.02E-02 ns	-1.43E-03 ns	7.38E-02	6.3
230790 - 260790	2.81E+00	-6.21E-02	-3.98E-03 ns	-5.51E-02 ns	22.1
Mean	1.4251	-0.0232	0.0029	-0.0189	35.91
n = 3 m = 2					
140690 - 170690	-3.61E+00	6.40E-02	1.61E-03	1.26E-01	32.0
170690 - 200690	-9.00E+00	-3.06E-02 ns	1.48E-03	2.87E-01	33.4
200690 - 230690	-1.50E+01	-2.62E-02 ns	6.07E-04 ns	4.72E-01	64.4
230690 - 260690	-1.37E+01	-9.89E-02	5.14E-04	4.37E-01	65.2
260690 - 290690	3.01E+00	-1.89E-01	4.41E-04 ns	-6.00E-02 ns	35.0
290690 - 020790	2.04E+01	3.17E-02 ns	1.27E-05 ns	-5.83E-01	49.9
020790 - 050790	1.15E+00 ns	7.02E-02 ns	6.24E-04	-6.52E-03 ns	34.9
050790 - 080790	-5.77E-01 ns	-8.31E-02	2.11E-04 ns	4.21E-02 ns	11.9
080790 - 110790	7.89E+00	7.60E-04 ns	1.58E-04 ns	-2.13E-01	51.8
110790 - 140790	8.66E+00	-3.39E-02 ns	9.76E-05 ns	-2.37E-01	46.3
140790 - 170790	1.98E+01	9.72E-02 ns	-2.33E-03 ns	-5.73E-01	20.3
170790 - 200790	-1.11E+00 ns	-5.93E-02 ns	3.95E-03	5.59E-02 ns	23.9
200790 - 230790	-1.63E+00 ns	-9.77E-03 ns	4.76E-05 ns	7.41E-02	6.2
230790 - 260790	2.84E+00	-6.22E-02	-8.67E-04 ns	-5.61E-02 ns	22.2
Mean	1.3659	-0.0235	0.0005	-0.0168	35.53

Period	k_0'	k_1'	k_2'	k_3'	R^2 (%)
n = 3 m = 3					
140690 - 170690	-3.74E+00	6.50E-02	3.14E-04	1.30E-01	28.9
170690 - 200690	-8.91E+00	-3.40E-02 ns	1.37E-04	2.85E-01	33.1
200690 - 230690	-1.48E+01	-2.74E-02 ns	4.68E-05 ns	4.65E-01	63.5
230690 - 260690	-1.35E+01	-9.90E-02	4.06E-05	4.31E-01	64.8
260690 - 290690	2.98E+00	-1.88E-01	5.00E-05 ns	-5.91E-02 ns	34.8
290690 - 020790	2.03E+01	3.50E-02 ns	1.02E-05 ns	-5.80E-01	50.0
020790 - 050790	1.26E+00 ns	4.92E-02 ns	4.18E-05	-1.03E-02 ns	27.8
050790 - 080790	-4.84E-01 ns	-8.34E-02	2.07E-05 ns	3.94E-02 ns	12.0
080790 - 110790	7.87E+00	2.90E-04 ns	1.31E-05 ns	-2.13E-01	51.8
110790 - 140790	8.62E+00	-3.37E-02 ns	2.31E-05 ns	-2.35E-01	46.4
140790 - 170790	1.96E+01	9.54E-02 ns	-7.31E-04 ns	-5.69E-01	20.4
170790 - 200790	-1.15E+00 ns	-5.80E-02 ns	8.70E-04	5.74E-02 ns	21.7
200790 - 230790	-1.65E+00 ns	-9.48E-03 ns	7.31E-06 ns	7.46E-02	6.2
230790 - 260790	2.86E+00	-6.19E-02	2.04E-04 ns	-5.69E-02 ns	22.3
Mean	1.3754	-0.0250	0.0001	-0.0172	34.55